University of Zagreb

UNIVERSITY OF ZAGREB
FACULTY OF VETERINARY MEDICINE

Željka Anzulović Šanta

APPLICABILITY OF PULMONARY FUNCTION TESTS IN MOUSE MODELS OF RESTRICTIVE AND OBSTRUCTIVE RESPIRATORY DISEASES

DOCTORAL DISSERTATION

Zagreb, 2024

University of Zagreb

SVEUČILIŠTE U ZAGREBU
VETERINARSKI FAKULTET

Željka Anzulović Šanta

PRIMJENJIVOST TEHNIKA MJERENJA PLUĆNIH FUNKCIJA U MODELIMA RESTRIKTIVNIH I OPSTRUKTIVNIH PLUĆNIH BOLESTI U MIŠEVA

DOKTORISKI RAD

Zagreb, 2024

Sveučilište u Zagrebu

UNIVERSITY OF ZAGREB
FACULTY OF VETERINARY MEDICINE

Željka Anzulović Šanta

APPLICABILITY OF PULMONARY FUNCTION TESTS IN MOUSE MODELS OF RESTRICTIVE AND OBSTRUCTIVE RESPIRATORY DISEASES

DOCTORAL THESIS

Supervisor:
Prof. Frane Božić, PhD, DVM

Zagreb, 2024

Sveučilište u Zagrebu

SVEUČILIŠTE U ZAGREBU
VETERINARSKI FAKULTET

Željka Anzulović Šanta

PRIMJENJIVOST TEHNIKA MJERENJA PLUĆNIH FUNKCIJA U MODELIMA RESTRIKTIVNIH I OPSTRUKTIVNIH PLUĆNIH BOLESTI U MIŠEVA

DOKTORSKI RAD

Mentor:

Prof. dr. sc. Frane Božić, dr. med vet.

Zagreb, 2024

Sveučilište u Zagrebu

VETERINARSKI FAKULTET

IZJAVA

Ja, _____ (ime i prezime studenta), potvrđujem da je moj doktorski rad izvorni rezultat mojega rada te da se u njegovoj izradi nisam koristio/-la drugim izvorima do onih navedenih u radu.

_____

(potpis studenta)

Zagreb, 2024

The doctoral dissertation was submitted to the Faculty Council of the Faculty of Veterinary Medicine, the University of Zagreb, to acquire a Ph.D. degree in the area of Veterinary Science. The work presented in this doctoral dissertation was performed at Fidelta Ltd. (Selvita Ltd.) under the supervision of full prof. Frane Božić, PhD from the Department of Pharmacology and Toxicology, Faculty of Veterinary Medicine, University of Zagreb.

INFORMATION ON SUPERVISOR

Full prof. Frane Božić, PhD, DVM, currently serves as a Professor of Veterinary Pharmacology at the Veterinary Faculty, University of Zagreb. Born in 1964 in Zadar, prof. Božić completed his primary and secondary education with an Associate degree in Education - Science and Mathematics. He graduated in 1992 from the Faculty of Veterinary Medicine in Zagreb and earned his master's degree in 1996 from the Faculty of Science and Mathematics in Zagreb. His master's thesis focused on "Intraepithelial T-lymphocytes in the reaction against intestinal worms (Trichinella spiralis)." He received his PhD in 2000 at the same faculty with a dissertation on the "Immunomodulating effect of levamisole in oral vaccination of rejected piglets with a live vaccine against colibacillosis."

Prof. Božić began his career in 1992 as a research trainee at the Department of Parasitology, working on the project MZT RH 3-03-301 ("Trichinosis: immunology and immunopathology of zoonosis") and later served as an assistant, senior assistant, assistant professor, associate professor, and full professor at the Department of Pharmacology and Toxicology of the Faculty of Veterinary Medicine in Zagreb. He has been teaching at both undergraduate and postgraduate levels at his home faculty since his appointment. Prof. Božić was also a scholarship holder of the Italian Government at the World Trichinosis Referral Center in Rome during 2000/2001.

He has actively participated in the implementation of eleven scientific projects as a researcher and published more than one hundred bibliographic units. His contributions to the field have been recognized numerous times, including the first prize at the Ninth International EAVPT Congress in Lisbon in 2003 for his oral presentation. Prof. Božić academic and research endeavors are complemented by his role as an expert in "One Health", he has served on numerous committees at his Faculty, was a member and deputy president of the Council of the Biomedical Area at the University, and has been involved with the State Committee for Drug Registration. He also served as the head of the Department for Veterinary Public Health and Food Safety and is currently the head of the Department of Pharmacology and Toxicology.

Before the accession of the Republic of Croatia to the EU, Prof. Božić was an observer in the Committee for Veterinary Medicines (CVMP) at the European Medical Agency

(EMA), then deputy representative, and is currently the representative of the Republic of Croatia in the CVMP in his third term. He is a member of the Croatian Immunological, Toxicological, Pharmacological, and Veterinary Society.

List of publications:

- OSTER, E., N. ČUDINA, H. PAVASOVIĆ, A. PREVENDAR CRNIĆ, F. BOŽIĆ, C. FADEL, M. GIORGI (2023): Intoxication of dogs and cats with common stimulating, hallucinogenic and dissociative recreational drugs. Veterinary and Animal Science 19, 100288. DOI:10.1016/j.vas.2023.100288

- KOVAČEVIĆ, Z., S. MUGOŠA, M. LALIĆ-POPOVIĆ, S. STOJANOVIĆ, N. TEŠIN, D. MARIĆ, N. TODOROVIĆ, F. BOŽIĆ (2023): Veterinary compounding: the impact of different gelling agents on the rheological characteristics and release kinetics from meloxicam oral gels in the treatment of cats. Veterinarski arhiv 93, 695-708. doi.DOI:10.24099/vet.arhiv.2279

- ANZULOVIĆ ŠANTA, Ž., A. OGNJENOVIĆ, M. ANTOLIĆ, S. ČUŽIĆ, I. GLOJNARIĆ, B. HRVAČIĆ, F. BOŽIĆ (2023): Retrospective assessment of nintedanib in the mice model of pulmonary fibrosis: alignment with patient outcomes in idiopathic pulmonary fibrosis. Veterinarska Stanica 54, 395-406. DOI:10.46419/vs.54.4.4

- MARIC, K., P. SOSTARIC, H. VALPOTIC, J. SURAN, M. LIPAR, F. BOZIC, A. PREVENDAR CRNIC, D. BROZIC (2017): Activity of salivary enzymes and level of salivary urea in gingivitis of dogs. Book of Abstracts 7th International Congress "Veterinary Science and Profession" 27/12/2021 European Medicines Agency Page 1/5 (BRKLJACA BOTTEGARO, N., N. ZDOLEC, Z. VRBANAC, (ur.). Zagreb: Faculty of Veterinary Medicine, University of Zagreb, 2017. 136-136 (presented as a poster).

- BOZIC, F. (2017): Koncept "One Health": vaznost racionalne primjene antimikrobnih lijekova. 7th International Congress "Veterinary Science and Profession" Book of Abstracts (BRKLJACA BOTTEGARO, N., DOLCE, N., VRBANAC, Z. (ur.). Zagreb: Faculty of Veterinary Medicine, University of Zagreb, 2017.178-178 (invited lecture).

- SURAN, J., K. MILOSEVIC, M. GALOVIC, T. MASEK, D. BROZIC, K. MATANOVIC, L. RADIN, J. ALADROVIC, B. SEOL MARTINEC, B. RADIC, S. RADIC, M. BENIC, A. KOSTELIC, F. BOZIC, G. BACIC, N. MACESIC (2017): Intramammary propolis solution (Apimast) for subclinical mastitis treatment in dairy cows. Book of Abstracts 7th International Congress "Veterinary Science and Profession" (BRKLJACA BOTTEGARO, N., N. ZDOLEC, Z. VRBANAC (ur.). Zagreb: Faculty of Veterinary Medicine, University of Zagreb, 2017. 66-66. (lecture).

ACKNOWLEDGEMENTS

First, I would like to express my gratitude to Fidelta Ltd. (Selvita Ltd.) for providing me with financial, technical, and scientific opportunities making my journey toward obtaining a doctoral degree possible. A special thanks to my dear Boška Hrvačić, PhD, DVM for recognizing me as a candidate for postgraduate studies and guiding me toward this goal with her expertise, knowledge, and support. I am also grateful for the opportunities to develop through my work and present my research at various international conferences and in everyday interactions with clients.

I want to extend my thanks to my mentor, Prof. Frane Božić, PhD, DVM for the assistance provided throughout my doctoral studies, the publication of my work, and the completion of this thesis.

Special appreciation goes to all my colleagues at Fidelta/Selvita who contributed to this research in any way and provided immense support. I would like to particularly highlight Snježana Čužić,MD, PhD, Anja Ognjenović, DVM, and Maja Antolić, DVM, for their significant scientific contributions, as well as Milka Horvatinčić, Leonardo Barišić, Viktorija Pogačić, Magdalena Brajdić, and Sonja Vidović Iviš, who made substantial technical contributions to these studies.

Also, immense thanks to my colleagues, Anamarija Markota, PhD and Katarina Špiranec Spes, PhD. Each of your pieces of advice was of immeasurable value, and without your support and the right words at the right time, everything would have been much more challenging. Thank you for your patience and understanding. I appreciate Hrvoje Brzica, PhD who always found time to help and provide helpful advice.

In my expressions of gratitude, as well as in my heart, Ana Beck, PhD, DVM and Relja Beck, PhD, DVM hold a special place. Their selflessness in providing help, love, support, a desire to teach, and contribute to my personal and professional development is immeasurable. You will always be my role models, both personally and professionally.

A big thank you to all my friends who were with me during this process. There were many of you, and I hope you recognize yourselves. I want to highlight Ana and Andrea, my dear true friends, who push me forward and help me find strength when it's most demanding.

Thank you to my parents for their unconditional support and love. I appreciate them for giving me courage and strength and teaching me the values of hard work, respect for others, and gratitude for the opportunities provided to me. I'm grateful that they endeavoured to guide me positively during my upbringing while giving me the freedom to choose and follow my own path independently. I also express gratitude to the rest of my family, brothers, and their families, as well as my Oremović family, for endless love and support and for believing in me.

In memory of my Ljubica, you will always have a special place in my heart. Until the last moment, you believed in me and eagerly anticipated each of my achievements. It is profoundly regrettable that we won't have the opportunity to celebrate this accomplishment together.

Last but not least, to my husband Nikola, my faithful companion, a safe harbour, and a light in the darkest moments, thank you!

ABSTRACT

Applicability of Pulmonary Function Tests in Mouse Models of Restrictive and Obstructive Respiratory Diseases

Pulmonary function tests (PFTs), routinely conducted in clinics, serve as the initial diagnostic step for respiratory diseases, yet their potential contribution to translational medicine remains underrated. These surveys aimed to assess the relevance of PFTs in enhancing the preclinical phase of drug development for restrictive and obstructive respiratory diseases, such as idiopathic pulmonary disease (IPF) and asthma. Asthma and IPF, as chronic conditions, impact a significant number of individuals across various age groups. Current treatment options, including pirfenidone and nintedanib for IPF and corticosteroids for asthma, are insufficient in resolving these diseases, necessitating the exploration of more effective therapies. One strategy to advance the development of new treatments involves refining existing models by introducing analytical techniques routinely used in clinics.

Therefore, the research aimed to establish a platform for the development of novel therapies for both restrictive and obstructive pulmonary diseases. It was performed by assessing the applicability of PFTs in preclinical mouse models of bleomycin (BLM)-induced pulmonary fibrosis and ovalbumin (OVA)-induced asthma.

A retrospective analysis of "gold standard" treatments in mouse models was conducted, including PFT measurements and standard readouts like clinical signs, histological and immunohistological assessment, total and differential cell influx, and cytokine levels in bronchoalveolar lavage fluid. The specific goal was to confirm the improvement of key functional parameters, such as forced vital capacity, forced expiratory volume, and the Tiffeneau index, and correlate these findings with other readouts.

The results confirmed the restrictive or obstructive pattern and the effect of standard treatments in the evaluated disease models. The confirmation of PFT results aligning with standard treatment outcomes in animal models and their correlation with clinical findings affirmed the translational value of applying these techniques in preclinical drug research.

The utilization of PFTs is anticipated to significantly enhance the translational value of these two mouse models, thereby increasing the likelihood of successful therapy development. These findings contribute by establishing PFT values in the BLM lung fibrosis and OVA acute asthma models as the threshold for the successful development of novel therapeutic entities.

Keywords: pulmonary function tests, preclinical mouse models, idiopathic pulmonary fibrosis, acute allergic asthma, translational medicine

PROŠIRENI SAŽETAK

Primjenjivost tehnika mjerenja plućnih funkcija u modelima restriktivnih i opstruktivnih plućnih bolesti u miševa

UVOD: Disertacija se bavi istraživanjem primjenjivosti testova plućne funkcije (eng. pulmonary function testing (PFT)) u prekliničkim modelima restriktivnih i opstruktivnih respiratornih bolesti, poput idiopatske plućne fibroze (IPF) i alergijske astme. Te kronične bolesti značajno utječu na populaciju, a trenutačne terapijske opcije poput pirfenidona i nintedaniba za IPF te kortikosteroida za astmu nedostatne su za potpuno rješavanje problema.

Najvažniji klinički alat u dijagnostici i razlikovanju restriktivnih od opstruktivnih bolesti pluća su PFT-ovi. Koriste se za procjenu funkcionalnosti dišnog sustava, opsega zahvaćenosti respiratorne površine te kao sustav za praćenje napredovanja bolesti i/ili djelovanja terapije. Mjerenje plućnih funkcija uključuje korištenje više različitih uređaja i testova. Osnovni parametri koji se koriste u interpretaciji plućnih funkcija su vitalni kapacitet (VC), koji se često izražava i kao forsirani vitalni kapacitet (FVC), forsirani ekspiratorni volumen u prvoj sekundi ekspirija (FEV1), odnos FEV1/FVC, takozvani Tiffeneau index te ukupni plućni kapacitet (eng. total lung capacity (TLC)).

Karakteristike IPF-a, restriktivnog poremećaja, očituju se smanjenjem parametara funkcije pluća: parametara protoka zraka, volumena i kapaciteta pluća. Astma, opstruktivna bolest, za razliku od IPF-a se odlikuje: povećanjem rezidualnog volumena pluća (RV) i TLC zbog zraka zarobljenog u promijenjenim dijelovima pluća dok se parametar FVC smanjuje ili ostaje nepromijenjen. Promjene parametara protoka zraka jednake su kao i u IPF-u. U praćenju razvoja astme Tiffeneau-ov index je ključan za razlučivanje napredovanja bolesti i učinka lijeka. Povećana osjetljivost dišnih putova (eng. airway hyperresponsivness (AHR)) je klinička karakteristika astme i u ljudi i u miševa.

U istraživanju etiologije obiju bolesti i razvoja novih terapija, životinjski modeli su neizostavan dio procesa. Omogućavaju kontrolirano proučavanje patofizioloških mehanizama nastanka bolesti kao i procjenu učinkovitosti i toksičnosti potencijalnih terapeutika. Idealno oponašanje svih značajki ljudskih oblika restriktivnih i opstruktivnih plućnih bolesti nažalost

nije moguće postići. No, model miša omogućava uspostavu najvažnijih značajki IPF-a i astme ljudi.

Bleomicinom (BLM) uzrokovana plućna fibroza miševa je, unatoč nedostatcima, do sada najkorišteniji model za razvoj terapije IPF-a u ljudi. Mišji model koji bi objektivnije prikazao bolest još uvijek nije uspostavljen zbog dubioznosti etiologije same bolesti. Izazovi postavke validnog modela plućne fibroze u miša su primarno odabir agensa kojim će se potaknuti razvoj i tijek promjena na plućima u tipu IPF-a kod ljudi. Odabirom doze i načina primjene u osjetljivom soju miša potrebno je postići karakterističan tip i obim oštećenja pluća, koja pritom ne bi smjela biti pogubna za životinju. K tome, u modelu s već razvijenim fibrotičnim promjenama u plućima, valja odrediti vremenski okvir dostatan za učestalu aplikaciju i djelovanje terapeutika do trenutka spontane rezolucije oštećenja.

Testiranjem antifibrotičnih spojeva u terapijskim postavkama protokola (u fibrotičnoj fazi bolesti), povećava se translacijska vrijednost BLM modela i takav protokol više odgovara primjeni u ljudi. Dokaz uspješne primjene BLM mišjeg modela u razvoju lijeka su nintedanib i pirfenidon, jedina dva klinički odobrena lijeka za tretiranje navedene bolesti ljudi. O važnosti djelovanja terapije na poboljšanje plućnih funkcija govori podatak kako je Food and Drug Administration agencija odobrenje navedenih terapija temeljila na rezultatima poboljšanja parametra FVC ljudi, unatoč poznatim nuspojavama. Upravo zato iznenađuje nedovoljna zastupljenost primjene PFT-a u mišjim modelima.

U zadnjih 25 godina umnogome su rasvijetljeni patofiziološki mehanizmi astme te su otkriveni lijekovi s različitim terapijskim ciljem djelovanja, najvećim djelom izravno upotrebom životinjskih modela. Višestrukom sistemskom senzibilizacijom te izravnom bronhoprovokacijom antigenom uspješno se razvija akutna astma u miševa. Izazov takvog modela miša je, u što kraćem vremenu i sa što manjom količinom antigena, postići oštećenja karakteristična za bolest na kojima će se uspješno testirati nova potencijalna terapija. Ovalbumin (OVA) kao antigen, je najčešće korišten agens u modelima akutne astme miševa zbog robusnosti odgovora organizma i razvoja oštećenja karakterističnih za astmu. Terapija kortikosteroidima je najčešće korištena i opisana u astmi.

Suočeni s podatcima o razlici uspješnosti ispitivanih lijekova u pretkliničkim i kliničkim ispitivanjima, razna svjetska respiratorna društva izdaju izvještaj sa smjernicama za poboljšanje

životinjskih modela s ciljem bolje translacije. Navode kako su mišji modeli značajni u istraživanju lijekova, no potrebno je pomno planiranje pokusa, uvrštavanje terapija koje su „zlatni standardi“ u liječenju pacijenata te uvođenje dodatnih analiza uz do sada najčešće korištenu patohistološku obradu pluća. PFT navode kao analizu s visokim potencijalom koja nije dovoljno zastupljena u pretkliničkim modelima.

Mjerenje i interpretacija plućnih funkcija miševa predstavlja tehnički izazov zbog anatomskih razlika, osobito u veličini pluća, između čovjeka i miša. Stoga ne iznenađuje kako su istraživanja u kojima je opisana primjena navedenih sustava PFT-ova u modelima astme i plućne fibroze miševa oskudna. Ključni članak u kojem su opisani parametri PFT-a u kontekstu restriktivnih i opstruktivnih plućnih bolesti potječe iz 2010. godine (VANOIRBEEK et al.). Služi kao temeljna referenca za razumijevanje kako PFT parametri variraju u različitim bolestima pluća, pružajući vrijedne uvide u karakteristike plućne funkcije koje se mogu očekivati u stanjima poput IPF-a i astme. Međutim, unatoč detaljnom opisu PFT parametara, u literaturi nedostaju podaci o vrijednostima PFT-a prilikom primjene specifičnih terapija za ove bolesti. Taj nedostatak informacija naglašava potrebu za dodatnim istraživanjima koja će ispuniti ovu prazninu i pružiti sveobuhvatniji uvid u učinke terapije na plućnu funkciju u kontekstu restriktivnih i opstruktivnih plućnih oboljenja te boljeg probira molekula u pretkliničkim istraživanjima.

HIPOTEZA: Pretpostavka je da će retrospektivna evaluacija dostupnih tretmana u životinjskim modelima, tzv. "zlatnih standarda", pokazati slične učinke kao i kod ljudi. Cilj je istraživanja korištenje klinički relevantnih analiza poput PFT-a na modelima miševa s plućnom fibrozom uzrokovanom BLM-om I akutnom astmom uzrokovanom OVA-om kako bi se poboljšale vrijednosti parametara plućne funkcije. Određivanjem granica unutar kojih je liječenje ovih bolesti "zlatnim standardima" najučinkovitije poboljšat će se primjenjivost postojećih modela korištenih u ovom istraživanju te omogućiti bolji probir novih molekula i njihovo daljnje kliničko istraživanje u budućim studijama.

MATERIJAL I METODE: U modelu BLM-izazvane plućne fibroze, BLM je primjenjen intranazalno (*i.n.*), u dozi od 1 mg/kg, miševima u dvije testne skupine i skupini pozitivne kontrole. U ovom modelu su ljekovite tvari primjenjene peroralno (*p.o.*), dvaput dnevno, s razmakom od 7.5 sati između dnevnih aplikacija, u terapijskom načinu, počevši od sedmog dana nakon administracije BLM. Nintedanib je primijenjen u dozi od 60 mg/kg, a pirfenidone

u dozi od 100 mg/kg. Mjerenje plućnih funkcija provedeno je 21. dana istraživanja. Nakon provedenog mjerenja PFT-a, životinje su eutanazirane prekomjernom dozom anestetika te su pluća miša uzorkovana za daljnju patohistološku obradu. Ocjenjivanje lezija pluća provedeno je prema Matsuse modificiranom Ashcroft sustavu bodovanja 1-5. Imunohistokemijska analiza pluća je napravljena označavanjem protutijelima specifičnim za kolagen i miofibroblaste. U svrhu provođenja analize, histološka stakalca rezova pluća skenirana su sustavom AxioScan.Z1, Zeiss© te su označeni segmenti kompjuterski obrađeni automatiziranom kvantificiranom metodom za digitalnu patologiju (Calopix, TRIBVN©).

Model astme je postavljen intraperitonealnom senzibilizacijom OVA dva puta (dan 0 i 14) u dozi od 10 μg po mišu, a izravna provokacija dišnih puteva (dan 20-23) potaknuta je intranazalnom primjenom OVA u dozi od 50 μg po mišu jednom dnevno, kroz 4 dana. Opisani režim doziranja OVA primjenjen je pozitivnoj kontrolnoj skupini i skupinama kod kojih su bile aplicirane farmakološke kontrole deksametazona u dozi od 3 mg/kg i flutikazon propionata u dozi 2 mg/kg. Navedena terapija primjenjena je pola sata prije prve *i.n.* administracije te nadalje prije svake sljedeće administracije OVA. Mjerenje je provedeno 24 sata nakon zadnje administracije OVA. U ovom modelu, plućne funkcije bile su mjere na PFT i Resistance and Compliance (RC) sustavu u svrhu validacije parametara prije i nakon metakolinske bronhoprovokacije te u svrhu mjerenja odgovora preosjetljivosti dišnih putova na navedene metakolinske doze. Nakon mjerenja, životinje su eutanizirane te su uzorkovani bronholaveolarni ispirci i pluća. Histološki preparati obojani su periodic-acid Schiff (PAS) metodom te su se ocjenjivali prisustvo upale i oštećenja bronhoalveolarnog epitela te metaplazija vrčastih stanica ocjenom od 0 do 12.

U oba modela, na dan završetka pokusa i uzorkovanja, provelo se mjerenje plućnih funkcija invazivnom tehnikom. Korištena su dva sustava: Buxco® PFT, sličan spirometriji kod ljudi, za mjerenje parametara plućnih funkcija; te Buxco® FinePointe RC, sličan provokaciji preosjetljivosti dišnih putova kod ljudi, za mjerenje povećane osjetljivosti dišnih putova. Sustavi su specijalizirani za primjenu u *in vivo* istraživanjima na glodavcima te omogućavaju direktan pristup plućima postavljanjem tubusa za mjerenje direktno u traheju miša. Zbog potrebe za obavljanjem zahvata traheotomije prije postavljanja tubusa, oba sustava su invazivne tehnike te su korištena samo terminalno, na kraju pokusa. Prije samog zahvata, miš je anesteziran kombinacijom ksilazina/ketamina prema smjernicama organizacije za dobrobit

životinja. Nakon postignute duboke anestezije, okolno tkivo dušnika tupo je isprepariranо, transverzalni mali rez napravljen je između kranijalnih prstena dušnika, u koji je bio umetnut plastični tubus sa zaobljenim metalnim vrhom. Prije provođenja mjerenja, sustavi su kalibrirani te je svaka životinja zavedena u softverskom programu stroja (Fine Pointe Buxco®) pod određenim brojem i s dodatnom pripadnosti po grupama. Miš je položen u izolirano plastično kućište i spojen sa sustavom za mjerenje preko trahealnog tubusa; životinja je tijekom čitavog procesa mjerenja bila priključena na mehanički ventilator, što je omogućavalo minimalni utjecaj svjesnih voljnih radnji na rezultate tijekom izvođenja testova. PFT sustavom su, u strogo kontroliranim uvjetima, na temelju promjena protoka, volumena i tlaka zraka u plućima miša, izmjereni određeni parametri plućnih funkcija kroz četiri različita testa: procjena funkcionalnog rezidualnog kapaciteta (forsirani respiratorni kapacitet FRC); testiranje tlaka i volumena zraka (inspiratorni kapacitet (IC), VC, popustljivost prsnog koša (Cchord), ekspiracijski rezervni volumen (ERV), TLC, RV, krivulja tlaka i volumena zraka (P-V)); testiranje volumena i protoka zraka (FVC, FEV100ms, PEF i MMEF, FEV100/FVC te F-V krivulje) te procjena parametara plućne mehanike (otpornost (Ri) i dinamička popustljivost (Cdyn) dišnih puteva). RC sustav, na temelju promjena plućnog tlaka i zračnog protoka, mjerio je vrijednosti parametara Ri i Cdyn dišnih putova kao odgovor na postepeno povećanje doze udahnutog bronhoprovokatora metakolina (0,625, 2,5, 5,0 i 12,5 mg/mL). Tekući metakolin životinja je udahnula u obliku aerosola korištenjem nebulizatora, dodatka sustavu koji korištenjem ultrazvučnih valova pretvara tekućinu u aerosol. U modelu OVA izazvane akutne astme, životinje su nakon izloženosti najvećim dozama metakolina bile podvrgnute PFT testiranju volumena i protoka zraka.

Za dodatnu potvrdu razvoja bolesti i učinka terapije, nakon PFT-a, provedene su analize bronhoalveolarnog ispirka (BALF) u modelu astme i tkiva pluća eutanaziranih miševa. Analizirane su stanice BALF-a i mjerene razine citokina IL-4, IL-5, IL-13 i protutijela IgE klase. Pluća su pripremljena i obrađena za patohistološke i imunohistokemijske studije radi detaljnije analize patoloških promjena. Statistička analiza izvršena je korištenjem GraphPad©Prism, uspoređujući sve grupe s kontrolnom skupinom za procjenu bolesti i terapijskog učinka, pri čemu je značajnost postavljena na $p<0.05$.

REZULTATI I RASPRAVA: U ovom istraživanju je ispitana primjenjivost PFT-ova u modelima miševa s restriktivnim i opstruktivnim plućnim bolestima, koristeći se obrascima

IPF-a i alergijske astme. Analiza PFT parametara poput PEF, MMEF, FEV100, TLC, FVC i Tiffeneau indeksa omogućila je razlikovanje između restriktivnih i opstruktivnih obrazaca plućne funkcije, dok je korelacija između PFT rezultata i histoloških nalaza pružila uvid u strukturne promjene u plućima koje prate funkcionalne abnormalnosti. Retrospektivna analiza nintedaniba, pirfenidona, deksametazona i flutikazon propionate, terapije korištene u liječenju bolesti, bila je usmjerena na evaluaciju njihove učinkovitosti u pretkliničkim modelima, s ciljem utvrđivanja vrijednsti PFT parametera.

Model plućne fibroze uzrokovane BLM je uspješno reproducirao karakteristike IPF-a, uključujući povećanu smrtnost, promjene u plućnim funkcijama te prisutnost histopatoloških lezija u tkivu pluća. Kliničko praćenje miševa tretiranih BLM-om pokazalo je značajan gubitak tjelesne mase, a neki su ispunili kriterije za eutanaziju zbog vidljivih znakova bolesti. Liječenje nintedanibom i pirfenidonom rezultiralo je smanjenjem broja eutanaziranih životinja i stabilizacijom tjelesne mase.

Histološke analize potvrdile su razvoj fibrotičnih lezija karakterističnih za plućnu fibrozu potaknutu BLM-om, uključujući intraalveolarne fibroze, fokalno guste fibroze i hiperplaziju epitela. Analize su potvrdile prisutnost plućne fibroze 21. dana nakon primjene BLM-a putem povećane ocjene Ashcroft sustava bodovanja, imunohistokemijskog dokaza prisutnosti kolagena i miofibroblasta u pregledanim rezovima pluća. Kako je dokazano uništavanje arhitekture pluća, funkcionalna oštećenja su logična posljedica.

Restriktivan uzorak plućne funkcije kod miševa tretiranih BLM, 21. dan nakon primjene, potvrđen je smanjenjem karakterističnih parametara PFT-a poput FVC, FEV100, TLC, PEF, MMEF, F-V i P-V oblika krivulje. F-V vrijednosti pokazuju manje područje ispod krivulje (eng. area under the curve (AUC)) kod životinja tretiranih BLM-om, što utječe na značajno niže vrijednosti parametara sile prisilnog izdisaja poput FVC, FEV100, PEF i MMEF. Parametri poput FVC i FEV100, kao parametri od interesa u modelima plućne fibroze uzrokovane BLM-om, smanjeni su za približno 30 % u usporedbi sa zdravim, ne tretiranim miševima. P-V krivulja pokazala je tipičan lijevi i prema dolje pomak fibrotičnih pluća s povećanim opružanjem koje utječe na značajno smanjenje TLC, IC i VC, ali nije zabilježen utjecaj na RV parametar.

Kako Cdyn parametar uvelike određuje rad disanja, razumna je pretpostavka da su drugi parametri poput FRC, IC, VC i TLC značajno smanjeni u kontrolnih životinja. Nije uočen učinak na parametre RV i Ri unutar svih testiranih skupina, budući da u ovom modelu upalna komponenta nije dominantna, a znakovi opstrukcije nisu dokazani. Odsutnost opstrukcije u ovom modelu potvrđuje i značajno povećanje FEV100/FVC indeksa kod životinja s razvijenim fibrotičnim promjenama.

Ovi rezultati potvrđuju da je korišteni model plućne fibroze uzorkovane BLM, rezultirao obimom patoloških promjena u željenoj mjeri 21. dan studije, pokazujući restriktivan uzorak plućne funkcionalnosti. Međutim, kako bi se potvrdilo da su PFT-ovi važan alat u procesima pretkliničkog otkrivanja lijekova, utjecaj na plućnu funkcionalnost procijenjen je kod životinja tretiranih "zlatnim standardima" nintedanibom i pirfenidonom.

Nintedanib tretman je značajno poboljšao FVC, FEV100 i TLC vrijednosti, karakteristične parametre restriktivnih plućnih funkcionalnih poremećaja. F-V krivulja je pokazala FVC vrijednost sličnu zdravoj skupini i FEV100 vrijednost značajno poboljšanu u odnosu na oboljele životinje. Međutim, PEF i MMEF parametri nisu bili poboljšani, jer je vršna točka F-V krivulje bila slična bolesnoj skupini s polaganim spuštanjem do postizanja određene FVC vrijednosti. Pirfenidon je uzrokovao poboljšanje parametara FVC, FEV100 i TLC. Zapravo, također je značajno poboljšao PEF i MMEF jer F-V krivulja pokazuje rast najviše točke i brži pad do FVC vrijednosti, slično kao u skupini tretiranoj nintedanibom. Promatrajući P-V krivulju, u skupini tretiranoj nintedanibom nagib je postavljen više prema gore i desno u odnosu na zdravu skupinu. Nasuprot tome, nagib krivulje u skupini tretiranoj pirfenidonom bio je više prema oboljeloj skupini, što je utjecalo na značajno poboljšanje uočeno samo u parametrima VC i Te mjerenim u ovom testnom slijedu. Kako je očekivano na temelju nagiba krivulje, nintedanib je postigao značajnost u TLC, IC, VC, i Cchord parametrima u usporedbi s oboljelom izazvanom skupinom. Osim toga, nintedanib je značajno poboljšao parametre poput FEV100/FVC i Cdyn, dočim pirfenidon nije poboljšao ove parametre, kao ni Cchord, TLC i IC.

Analiza korelacije FVC, FEV100 i ocjena Ashcroft bodovanja potvrdile su vezu između histoloških i funkcionalnih promjena. Rezultati ove studije ukazuju na povezanost fibrotičnih promjena i funkcionalnih oštećenja, kao i terapijski učinak nintedaniba i pirfenidona u modelu

fibroze pluća. Pritom se funkcionalni parametri mogu smatrati valjanim za dokazivanje translacijske vrijednosti PFT tehnike u prekliničkom modelu plućne fibroze.

Provedeno istraživanje na modelu akutne astme uzrokovane OVA-om potvrdilo je glavna obilježja bolesti; to je ozbiljna, difuzna upala plućnoga tkiva, s oštećenjem bronhalnoga i alveolarnoga epitela, metaplazijom vrčastih stanica u velikim i terminalnim dišnim putovima, opstrukcijom dišnih putova i povećanom reaktivnosti dišnih putova te infiltracijom eozinofila i povećanjem karakterističnih citokina i IgE. U navedenom modelu nije zabilježena smrtnost niti ozbiljni klinički znakovi.

Promjene plućnih funkcija 24 sata nakon četvrte i.n. primjene OVA, potvrđene su Buxco® PFT sustavom. Sustavno senzibiliziranje na OVA rezultiralo je smanjenjem F-V površine ispod krivulje u obje OVA/OVA Ctrls skupine kao posljedica tipičnog konkavnog obrasca ograničenja protoka zraka, odnosno opstruktivnog poremećaja disanja. Ove promjene bile su popraćene značajnim smanjenjem FVC, FEV100, PEF i MMEF vrijednosti, smanjenjem FEV100/FVC vrijednosti u usporedbi sa zdravim miševima iz kontrolne skupine.

Najvažniji simptom i objektivna potvrda astme, AHR, evaluiran je u ovom modelu mjerenjem vrijednosti Ri i Cdyn kao odgovora na povećanje doza Mch. Uz to, normalni nalazi spirometrije mogu se uočiti kod pacijenata s astmom, pa se provodi AHR mjerenje kako bi se procijenila prisutnost upale. Rezultati su pokazali da se bazalni Ri nije promijenio u OVA/OVA Ctrls skupinama u usporedbi s miševima koji nisu senzibilizirani i tretirani izazivačkom primjenom OVA-om. Međutim, nagib krivulje odgovora na Mch značajno se povećao u OVA/OVA Ctrls *p.o.* skupini, počevši od najniže doze, dok je značajnost bila vidljiva u OVA/OVA Ctrls *i.n.* skupini pri dvije najviše doze Mch. Značajniji pad primijećen je u OVA/OVA Ctrls *p.o.* skupini, pokazujući značajnu promjenu od početne razine u usporedbi sa zdravom skupinom. U OVA/OVA Ctrls *i.n.* značajnost nije bila vidljiva na početnoj razini, već od najniže doze Mch.

Nakon konstrikcije uzrokovane bronhijalnom primjenom Mch u AHR testu, ponovo je testiran volumen i protok zraka kod nekoliko životinja po skupini. Rezultati su pokazali značajno smanjenje varijabli protoka, što je utjecalo na smanjenje AUC zdrave skupine i obje OVA/OVA kontrolne skupine. Dakle, uočene su promjene u vrijednostima parametara između tih kontrolnih bolesnih skupina i zdravih životinja. Zaključno, korišteni model astme potaknut

OVA-om, uključujući četiri lokalne izazivačke aplikacije, uzrokovao je funkcionalne promjene u plućima, ukazujući na opstruktivni poremećaj funkcionalnosti pluća prije izlaganja bronhoskonstriktoru, kao i nakon izlaganja, ali u manjoj mjeri.

Analize BALF-a otkrile su povećanu infiltraciju pluća upalnim stanicama, poglavito eozinofilima. Povećane razine IL-4, poticatelja hipersekrecije sluzi i sinteze IgE-a, zabilježene su u OVA/OVA Ctrls *p.o.* kontrolnoj skupini. IL-5, poticatelj eozinofilne upale, nije bio značajno povećan. IL-13, čimbenik AHR, pokazao je povećanje koje nije bilo statističi značajno. IgE je bio značajno povećan u OVA/OVA Ctrls p.o. skupini.

Liječenje deksametazonom i flutikazon propionatom utjecalo je na vrijednosti parametara plućnih funkcija poboljšavajući glavne parametre opstrukcije, FEV100 i FEV100/FVC. Parametar FEV100 značajno je poboljšan u oba referentna standarda u usporedbi s odgovarajućim kontrolnim skupinama. Kako je parametar FVC značajno poboljšan u oba standarda u usporedbi s odgovarajućim kontrolama, vrijednosti FEV100/FVC su poboljšane, ali nisu dosegle statistički značajne vrijednosti. Testiranjem protoka i volumena zraka utvrđeno je poboljšanje PEF i MMEF parametara. To je utjecalo na F-V krivulju, koja je bila slična krivulji zdrave skupine. Testiranje tlaka i volumena zraka pokazalo je značajnu razliku samo u Cchord, IC i VC parametrima, što je i očekivano, budući da ovaj test nije specifičan za opstruktivni poremećaj.

Testiranjem plućne mehanike nije utvrđena poremetnja Ri i Cdyn parametara. Ipak, u Mch bronhijalnom izazovu AHR testa, Ri i Cdyn vrijednosti pokazale su prisutnost upale u kontrolnim OVA skupinama, odsutnost u zdravoj skupini i poboljšanje promjena u skupinama tretiranim referentnim glukokortikoidima, deksametazonom i flutikazon propionatom. Nagib krivulje Ri za obje tretirane skupine bio je usmjeren prema dolje, bliže krivulji zdravih životinja. Rezultati Cdyn parametra su pokazali također značajan pad u obje skupine.

Slično kontrolnim skupinama, mjerenja PFT-a nakon izlaganja najvećoj dozi Mch su rezultirala značajno nižim AUC-om, što je utjecalo na značajno niže vrijednosti parametara protoka zraka od parametara F-V krivulje izmjerene prije izlaganje Mch.

Rezultati BALF analiza su pokazali značajni učinak deksametazona i flutikazona na smanjenje staničnih infiltrata u plućima, histoloških procjena upale i oštećenja epitela te

metaplazije vrčastih stanica. Nadalje, deksametazon je značajno utjecao na snižavanje koncentracije citokina i IgE. Histološki nalazi su korelirali s parametrima opstrukcije plućnih funkcija, što potvrđuje valjanost translacijske vrijednosti PFT tehnike u prekliničkom modelu alergijske astme.

Unatoč jasnim dokazima o primjenjivosti PFT u navedenim modelima pretkliničkog istraživanja, navedene su također i ograničenja zapažena u istraživanju. Jedno od glavnih ograničenja je korištenje animalnih modela, koji iako dobro rekapituliraju neke aspekte ljudskih bolesti, ne mogu u potpunosti odraziti kompleksnost i heterogenost bolesti kod ljudi. Osim toga, invazivna priroda PFT-a u eksperimentalnim modelima ograničava mogućnost longitudinalnih studija na istim jedinkama. Unatoč ograničenjima, ova teza pruža vrijedan uvid u korištenje PFT-a u prekliničkim modelima, omogućavajući bolje razumijevanje mehanizama bolesti i evaluaciju terapijskih intervencija.

Retrospektivna analiza učinkovitosti nintedaniba, pirfenidona, deksametazona i flutikazona u ovom istraživanju potvrđuje relevantnost istraživanih modela bolesti u miševa te naglašava važnost integracije PFT-a u prekliničkim studijama kako bi se omogućilo točnije praćenje učinkovitosti terapeutskih intervencija i bolje razumijevanje mehanizama djelovanja testiranih lijekova.

ZAKLJUČAK: Korištenje PFT-a u prekliničkim modelima miševa s plućnom fibrozom uzrokovanom BLM-om i s akutnom astmom uzrokovanom OVA-om povećava translacijsku vrijednost ovih modela, čime se povećava vjerojatnost razvoja uspješne terapije. Ovi nalazi doprinose uspostavi referentnih vrijednosti PFT-a u BLM modelu plućne fibroze i OVA modelu akutne astme kao polazišta za uspješan razvoj novih terapijskih mogućnosti.

Ključne riječi: testovi plućne funkcije, pretklinički mišji modeli, idiopatska plućna fibroza, akutna alergijska astma, translacijska medicina

ABBREVIATIONS

ADEM	absorption, distribution, excretion, and metabolism
AEC	alveolar epithelial cells
AHR	airway hyperreactivity
ANOVA	analysis of variances
ATS	American Thoracic Society
AUC	area under the curve
BC	before Christ
BALF	bronchoalveolar lavage fluid
bid	twice a day
BLM	bleomycin
BrdU	5-bromo-29-deoxyuridine
BSA	bovine serum albumin
Cchord	chord compliance
CCL	chemokine c-c motif ligand
Cdyn	dynamic compliance
CMC	carboxymethyl cellulose
COL1A1	alpha-1 type I collagen
CT	computed tomography
CTGF	connective tissue growth factor
ctrl	control
CXCL	c-x-c motif chemokine
CYP	cytochrome
D	day
DC	dendritic cell
DNA	deoxyribonucleic acid
ECM	extracellular matrix
ELISA	enzyme-linked immunosorbent assay
EMT	epithelial-mesenchymal transition
ERS	European Respiratory Society
ERV	expiratory reserve volume
FEF	forced expiratory flow
FEV	flow expiratory volume
FGF	fibroblast growth factor
FOT	forced oscillation technique
FRC	functional residual capacity
F-V	flow volume
FVC	forced vital capacity
GCP	good clinical practice
GLP	good laboratory practice
GMP	good manufacturing practice
h	hours
HRCT	high-resolution computed tomography
HRP	horseradish peroxidase
i.n.	intranasal
i.p.	intraperitoneal
i.t.	intratracheal

IC	inspiratory capacity
IFN	interferon
IgE	immunoglobulin e
IHC	immunohistochemical
IL	interleukin
ILC	innate lymphoid cells
IND	investigational new drug
IPF	idiopathic pulmonary fibrosis
IU	international unit
LPF	low-power fields
Mch	methacholine
MMEF	maximal mid-expiratory flow
MMP	matrix metalloprotease
ms	millisecond
MΦ	macrophage
n	total number
NA	not applied
NDA	new drug application
NKT	natural killer t cells
nm	nanometers
No	number
OVA	ovalbumin
p.o.	peroral
PAS	periodic acid-schiff
PBS	phosphate-buffered saline
PDGF	platelet-derived growth factor
PEEP	positive end-expiratory pressure
PEF	peak expiratory flow
P_{ehn}	enhanced pause
PFTs	pulmonary function tests
PGD	prostaglandin D
PI3K	phosphatidylinositol 3-kinase
P-V	pressure-volume
qd	once daily
RC	resistance and compliance
Ri	resistance
ROS	reactive oxygen species
RT	room temperature
RV	residual volume
s.c.	subcutaneously
sem	standard error of the mean
sICAM	soluble intercellular adhesion molecule
SMA	smooth muscle actin
SPF	specific pathogen-free
Te	expiration time
TGF	transforming growth factor
Th	t helper
Ti	inspiration time

TLC	total lung capacity
TNF	tumor necrosis factor
TSLP	thymic stromal lymphopoietin
TV	tidal volume
UIP	usual interstitial pneumonitis
UPR	unfolded protein response
vs.	*versus*
VC	vital capacity
VEGF	vascular endothelial growth factor

TABLE OF CONTENTS:

1 INTRODUCTION 1

1.1 A RESTRICTIVE PULMONARY DISORDER 2

1.2 AN OBSTRUCTIVE PULMONARY DISORDER 3

1.3 PULMONARY FUNCTION TESTS 4

1.3.1 Spirometry 4

1.3.2 Bronchial Provocation Test 4

2 LITERATURE OVERVIEW 8

2.1 MOUSE MODEL OF BLEOMYCIN-INDUCED PULMONARY FIBROSIS 16

2.1.1 Mechanisms and Phases of Bleomycin-Induced Pulmonary Fibrosis in Mouse Models 16

2.1.2 Pathogenesis of Idiopathic Pulmonary Fibrosis 18

2.1.3 Available Treatment in Idiopathic Pulmonary Functions 20

2.1.4 Literature Review on Models and PFT Utility Advancements, Challenges, and Recommendations 21

2.2 MOUSE MODEL OF OVALBUMIN-INDUCED ASTHMA 28

2.2.1 Mechanisms and Phases of Ovalbumin-Induced Asthma in Mouse Models 30

2.2.2 Pathogenesis of Allergic Asthma 31

2.2.3 Literature Review on Evaluating Murine Models Through Pathogenesis and PFT 33

3 DISSERTATION GUIDELINES 44

3.1 OBJECTIVES 45

3.2 HYPOTHESIS 46

4 MATERIAL AND METHODS 47

4.1 ANIMALS 48

4.1.1 Animals Husbandry 48

4.1.2 Animal Welfare and Euthanasia Criteria 48

4.2 ANIMAL MODELS 49

4.2.1 Model of Bleomycin-Induced Pulmonary Fibrosis 49

4.2.1.1 Experimental Groups 49

4.2.1.2 Bleomycin Preparation, Challenge, and Anesthesia 50

4.2.1.3 Treatment Preparation and Administration Regimen 51

4.2.1.4 Sampling Procedures 51

4.2.2 Model of Ovalbumin-Induced Asthma 52

4.2.2.1 Experimental Groups 52

4.2.2.2 Ovalbumin Preparation, Sensitization, Challenge, and Anesthesia 53

4.2.2.3 Treatment Preparation and Administration Regimen 54
4.2.2.4 Sampling Procedures 55
4.3 PULMONARY FUNCTION TESTING 56
4.3.1 Buxco® Pulmonary Function Test 56
4.3.1.1 Anesthesia and Tracheostomy Procedures 56
4.3.1.2 System Set-up 56
4.3.1.3 Test Sequences 57
4.3.2 Buxco® FinePointe Resistance and Compliance 58
4.3.2.1 Animal Preparation and Methacholine Delivery 58
4.3.2.2 System Set-up 59
4.4 BRONCHOALVEOLAR LAVAGE SAMPLING 60
4.4.1 Euthanasia and BAL Procedure 60
4.4.2 Cells Count Analysis 60
4.4.3 Measurement of IL-4, IL-5 and IL-13 in the BALF Supernatant 60
4.4.4 Measurement of IgE in the BALF Supernatant 61
4.5 HISTOLOGY 63
4.5.1 Lung Tissue Fixation and Paraffin Blocks Preparation 63
4.5.2 Histology Slides Preparation 63
4.5.3 Histology Procedures and Assessments in a Model of Bleomycin-Induced Pulmonary Fibrosis 64
4.5.3.1 Crossman's Trichrome for Muscle and Collagen Staining 64
4.5.3.2 Matsuse Modification of the Ashcroft Score 64
4.5.4 Histology Procedures and Assessments in a Model of Ovalbumin-Induced Asthma 65
4.5.4.1 The Periodic Acid-Schiff Staining Method 65
4.5.4.2 Histological Assessment of General Pulmonary Inflammation, Epithelial Damage, and Goblet Cell Metaplasia 65
4.6 IMMUNOHISTOCHEMISTRY 67
4.6.1 Collagen Type 1 Presence in the Lungs 67
4.6.2 Myofibroblast Presence in the Lungs 68
4.6.3 Digital Quantification of Immunohistochemically Stained Slides 68
4.7 STATISTICAL ANALYSIS 69
5 RESULTS 70
5.1 RESPIRATORY MODELS' EUTHANASIA CRITERIA OUTCOMES 71
5.1.1 Model of Bleomycin-Induced Pulmonary Fibrosis 71
5.1.2 Model of Ovalbumin-Induced Asthma 71
5.2 BODY WEIGHT RESULTS 72
5.2.1 Model of Bleomycin-Induced Pulmonary Fibrosis 72

5.2.2 Model of Ovalbumin-Induced Asthma 73
5.3 PULMONARY FUNCTION TESTING RESULTS 75
5.3.1 Model of Bleomycin-Induced Pulmonary Fibrosis 75
5.3.1.1 Sequence 1. Boyle's Law Functional Residual Capacity Test 75
5.3.1.2 Sequence 2. Quasistatic Pressure Volume Test 76
5.3.1.3 Sequence 3. Fast Flow Volume Maneuver Test 79
5.3.1.4 Sequence 4. Resistance And Compliance Test 82
5.3.2 Model of Ovalbumin-Induced Asthma 84
5.3.2.1 Sequence 1. Boyle's Law Functional Residual Capacity Test 85
5.3.2.2 Sequence 2. Quasistatic Pressure Volume Test 86
5.3.2.3 Sequence 3. Fast Flow Volume Maneuver Test 90
5.3.2.4 Sequence 4. Resistance and Compliance Test 94
5.4 AIRWAY HYPERRESPONSIVENESS TEST 97
5.4.1 Model of Ovalbumin-Induced Asthma 97
5.5 PULMONARY FUNCTION TESTING POST MCH CHALLENGE 100
5.6 BRONCHOALVEOLAR LAVAGE CELL COUNT 105
5.7 IMMUNOGLOBULIN E AND CYTOKINE ANALYSES IN THE BALF 108
5.8 HISTOLOGY RESULTS 110
5.8.1 Model of Bleomycin-Induced Pulmonary Fibrosis 110
5.8.2 Model of Ovalbumin-Induced Asthma 113
5.8.3 Goblet Cell Metaplasia in Large and Terminal Airways 116
5.9 IMMUNOHISTOCHEMISTRY RESULTS 118
5.9.1 Results of Collagen Type 1 Presence in the Lungs 119
5.9.2 Results of Myofibroblast Presence in the Lungs 122
5.10 CORRELATION ANALYSES 125
6 DISCUSSION 127
6.1 A RESTRICTIVE PULMONARY DISORDER 128
6.2 AN OBSTRUCTIVE PULMONARY DISORDER 133
7 CONCLUSIONS 144
8 REFERENCES 146
9 APPENDICES 157
10 BIOGRAPHY 170

LIST OF FIGURES

Figure 1 A schematic diagram of the activities involved in the drug discovery and development process 6
Figure 2 A volume-time spirogram of static lung volumes and capacities 11
Figure 3 A schematic view of the flow-volume curve changes over expected – healthy person results. 12
Figure 4 A schematic image of bleomycin-induced pulmonary fibrosis phases in mice after single intratracheal administration at D0. 17
Figure 5 A schematic view of idiopathic pulmonary fibrosis (IPF) pathogenesis 20
Figure 6 A schematic image of allergic asthma immune mechanism. 32
Figure 7 BLM-induced pulmonary fibrosis model scheme 50
Figure 8 OVA-induced asthma model scheme 53
Figure 9 Buxco© Pulmonary Function Test 58
Figure 10 Buxco® FinePointe Resistance and Compliance system 59
Figure 11 Body weight values over days in the BLM-induced pulmonary fibrosis model 72
Figure 12 Body weight values over days in the OVA-induced asthma model 74
Figure 13 PFT sequence 1. Functional residual capacity parameter 75
Figure 14 PFT sequence 2: TLC, RV, IC, VC, Te, and Cchord parameters 77
Figure 15 PFT sequence 2: A pressure-volume curve 78
Figure 16 PFT sequence 3: A pressure-volume curve 79
Figure 17 PFT sequence 3: FVC, FEV100, PEF and MMEF parameters 80
Figure 18 Tiffeneau index 81
Figure 19 PFT sequence 4: Resistance and compliance parameters 82
Figure 20 PFT sequence 1. Functional residual capacity parameter 85
Figure 21 PFT sequence 2. A pressure-volume curve 86
Figure 22 PFT sequence 2: Cchord and Te parameters 87
Figure 23 PFT sequence 2: TLC, RV, VC, and IC parameters 88
Figure 24 PFT sequence 3: A pressure-volume curve 90
Figure 25 PFT sequence 3: FVC, FEV100, PEF and MMEF parameters 92
Figure 26 Tiffeneau index 93
Figure 27 PFT sequence 4: Resistance and compliance parameters 95
Figure 28 AHR test resistance and compliance curves 98
Figure 29 A pre and post-Mch exposure flow-volume curve of Ctrl groups 101
Figure 30 PFT sequence 3: A flow-volume curve measured post-Mch exposure 102
Figure 31 Graphical presentation of bronchoalveolar lavage fluid cell count analysis in the OVA-induced asthma model 106
Figure 32 Graphical presentation and statistical analyses of IgE and cytokines concentrations measured in the BALF of animals in the OVA-induced asthma model 109
Figure 33 Graphical presentation of the fibrotic score and statistical analyses results 110
Figure 34 PBS Ctrls group fibrotic changes in lungs stained by Crossman's Trichrome 111
Figure 35 BLM Ctrls group fibrotic changes in lungs stained by Crossman's Trichrome staining 111
Figure 36 BLM/Nintedanib 60 mg/kg *p.o. bid* group fibrotic changes in lungs stained by Crossman's Trichrome staining 112
Figure 37 BLM/Pirfenidone 100 mg/kg *p.o. bid* group fibrotic changes in lungs stained by Crossman's Trichrome staining 112
Figure 38 Graphical presentation and statistical analyses of general pulmonary inflammation and/or epithelial damage score results in the OVA-induced asthma model 115

Figure 39 Graphical presentation and statistical analysis of goblet cell metaplasia in large and terminal airways score results in the OVA-induced asthma model 116
Figure 40 Goblet cell metaplasia in large airways (PAS staining 20x). 117
Figure 41 *De novo* collagen type I deposition in the lungs of BLM Ctrls animal 118
Figure 42 Graphical quantification of immunohistochemically stained collagen type 1 in the lungs 119
Figure 43 PBS Ctrls group COL1A1 IHC stained lung sample..... 120
Figure 44 BLM Ctrls group COL1A1 IHC stained lung sample 120
Figure 45 BLM/Nintedanib 60 mg/kg *p.o. bid* group COL1A1 IHC stained lung sample.... 121
Figure 46 BLM/Pirfenidone 100 mg/kg *p.o. bid* group COL1A1 IHC stained lung sample. 121
Figure 47 Graphical quantification of immunohistochemically stained myofibroblasts in the lungs 122
Figure 48 PBS Ctrls group αSMA IHC stained lung sample..... 123
Figure 49 BLM Ctrls group αSMA IHC stained lung sample 123
Figure 50 BLM/Nintedanib 60 mg/kg *p.o. bid* group αSMA IHC stained lung sample..... 124
Figure 51 BLM/Pirfenidone 100 mg/kg *p.o. bid* group αSMA IHC stained lung sample..... 124
Figure 52 Spearman correlation between the modified Ashcroft score and PFT parameters evaluated in the model of bleomycin-induced pulmonary fibrosis 125
Figure 53 Spearman correlation between the total histology score of general pulmonary inflammation and epithelial damage of bronchi and alveoli and PFT parameters evaluated in the model of ovalbumin-induced asthma 126

LIST OF TABLES

Table 1 Three main criteria for animal model validation and factors to be considered in animal studies conducting processes 15
Table 2 Overview of lung function parameters in the BLM-fibrosis and OVA-asthma models reported in VANOIRBEEK et al., 2010. 43
Table 3 Bleomycin-induced pulmonary fibrosis experiment design 49
Table 4 Ovalbumin-induced asthma experiment design 52
Table 5 Matsuse modification of Ashcroft score 65
Table 6 General pulmonary inflammation and/or epithelial damage scoring criteria 66
Table 7 Goblet cell metaplasia scoring criteria 66
Table 8 Euthanasia list and number of mice that survived *per* group 71
Table 9 Overview of lung function parameters values measured in the BLM-induced pulmonary fibrosis model using the DSI's Buxco® Pulmonary function testing system 83
Table 10 Overview of lung function parameters values measured in the OVA-induced asthma model using the DSI's Buxco® Pulmonary function testing system 96
Table 11 Resistance changes to increasing methacholine levels and statistical analysis results 99
Table 12 Dynamic compliance changes to increasing methacholine levels and statistical analysis results 99
Table 13 Statistical analysis of fast flow volume maneuver parameter values before and after methacholine challenge 103

LIST OF APPENDICES

Appendix 1 Body weight (g) raw data in the BLM-induced lung fibrosis model 158
Appendix 2 Raw data body weight (g) in the OVA-induced asthma model 159
Appendix 3 PFTs parameters in the BLM-induced lung fibrosis model 160
Appendix 4 P-V curve values in the BLM-induced lung fibrosis model 161
Appendix 5 F-V curve values in the BLM-induced lung fibrosis model 161
Appendix 6 PFTs parameters in the OVA-induced asthma model 162
Appendix 7 P-V curve valued in the model of OVA-induced asthma model 163
Appendix 8 F-V curve values in the OVA-induced asthma model 163
Appendix 9 Airway hyperresponsiveness test parameters 164
Appendix 10 F-V curve and parameters data post-Mch challenge 165
Appendix 11 Total and differential cell count in BALF 166
Appendix 12 Immunoglobulin E and cytokines analysis in the BALF (pg/mL) 167
Appendix 13 Histology and immunohistochemical results in the BLM-induced pulmonary fibrosis model 168
Appendix 14 Histology score and goblet cell metaplasia in the OVA-induced asthma model 169

1 INTRODUCTION

Respiratory diseases, according to the report from the FORUM OF INTERNATIONAL RESPIRATORY SOCIETIES (2017), make up five of the 30 most common causes of death. Collectively, over 1 billion individuals are estimated to suffer from acute or chronic respiratory conditions. This high prevalence is unsurprising, given the lung's constant exposure to air pollution, tobacco smoke, various chemical particles, and infections. Respiratory disorders can be categorized into obstructive, restrictive, or mixed abnormalities, representing combinations of both (PELLEGRINO et al., 2005).

1.1 A RESTRICTIVE PULMONARY DISORDER

Restrictive pulmonary disorder, characterized by lung stiffness and reduced compliance, is exemplified in patients with pulmonary fibrosis (GILDEA and MCCARTHY, 2010). Idiopathic pulmonary fibrosis (IPF), a type of interstitial lung disease, presents a typical restrictive pathophysiology (MOORE et al., 2013). This chronic and ultimately fatal lung disease leads to mortality within 2-3 years of diagnosis. The global incidence of IPF, estimated between 2.8 and 9.3 cases per 100,000 individuals annually, has shown an increasing trend over time (BARRATT et al., 2018).

IPF is characterized by usual interstitial pneumonitis (UIP) and progressive interstitial fibrosis, resulting from the formation of fibroblastic foci and excessive deposition of disorganized collagen and extracellular matrix (ECM) (MOELLER et al., 2008, WILSON and WYNN, 2009, BARRAT et al., 2018). Clinical features include chronic exertional dyspnea, cough, inspiratory crackles, and finger clubbing, predominantly affecting individuals over 50, particularly men and cigarette smokers (RAGHU et al., 2011).

The exact cause of IPF remains elusive, though there are implications of genetic predisposition and exposure to environmental factors like cigarette smoke and occupational hazards (WILSON and WYNN, 2009, KING JR. et al., 2011, RAGHU et al., 2011, SGALLA et al., 2018). Pathogenesis theories suggest the involvement of inflammatory stimuli leading to immunopathology and abnormal wound healing responses (WILSON and WYNN, 2009). Early and precise IPF diagnosis relies on multidisciplinary approaches and imaging techniques such as high-resolution computed tomography (HRCT) (RAGHU et al., 2015). Treatment options, including oxygen supplementation, nintedanib, and pirfenidone, aim to alleviate symptoms and slow disease progression (RAGHU et al., 2011, RAGHU et al., 2018, SGALLA et al., 2018, RAGHU et al., 2022). While the approvals of nintedanib and pirfenidone offer hope, ongoing research endeavours seek more effective therapeutic interventions for IPF.

1.2 AN OBSTRUCTIVE PULMONARY DISORDER

The obstructive pulmonary disorder is characterized by reduced airflow and increased lung volumes with air trapping, commonly associated with heightened airway hyperreactivity (AHR) observed in asthma patients.

Asthma, a heterogeneous airway disease, is characterized by variable and often reversible airflow limitations typical of obstructive pulmonary disorders (GILDEA and MCCARTHY, 2010, BOONPIYATHAD et al., 2019). Its multifactorial nature involves various clinical phenotypes influenced by both genetic and environmental factors, including allergic asthma, non-allergic asthma, and asthma with comorbidities such as obesity (GINA, 2023).

With an estimated global prevalence of up to 262 million individuals, asthma has been on the rise over the past three decades, affecting individuals of all ages and ethnic backgrounds and ranking among the most common chronic diseases worldwide (FIRS, 2017, GINA, 2023).

A hallmark of asthma is AHR, an exaggerated airway response to nonspecific stimuli, leading to chronic inflammation and airway remodelling. Allergic asthma, the most common phenotype, involves immune-mediated reactions to aeroallergens, triggering persistent inflammation and symptoms (BOONPIYATHAD et al., 2019).

Diagnosing asthma requires assessing multiple domains, including symptoms, airway obstruction, AHR, and inflammation. Additional tests such as blood biomarkers and bronchial provocation tests aid in confirming diagnosis and assessing disease severity (REDDEL et al., 2009, GAN, 2022, GINA, 2023).

Treatment recommendations for asthma typically involve inhaled corticosteroids and long-acting β2-adrenergic agonists. However, individualized treatment strategies are essential due to the disease's heterogeneity and varying responses to standard therapy (ROWE et al., 2004, SAGAR et al., 2015, BONNIAUD et al., 2018).

1.3 PULMONARY FUNCTION TESTS

Pulmonary function tests (PFTs) are important tools in investigating and monitoring respiratory disease patients. Although they do not provide a diagnosis *per se*, different patterns of dysfunction can be observed in various diseases (RANU et al., 2011). According to the Cleveland Clinic's definition, it is a generic term indicating a battery of studies or maneuvers that may be performed using standardized equipment to measure lung function. Usually, it includes simple screening spirometry, lung volume measurements, and the measurements of carbon monoxide diffusing capacity or arterial blood gases (GILDEA and MCCARTHY, 2010).

1.3.1 Spirometry

Spirometry stands as the foremost and commonly employed PFT. Widely utilized in clinical practice, it serves as the initial assessment in gauging lung function and plays a fundamental role in evaluating overall respiratory health. Its widespread adoption began in the 1970s, coinciding with the introduction of standardized testing equipment, patient maneuvers, and testing techniques. This advancement was facilitated by the evolution of the computer industry, leading to the miniaturization and simplification of the requisite tools. The previous need for large, highly controlled equipment has been supplanted by high-quality, compact tools suitable for medical facilities and patients' homes (GILDEA and MCCARTHY, 2010; GRAHAM et al., 2019).

As an initial diagnostic tool for individuals presenting with respiratory symptoms, spirometry, when combined with other diagnostic modalities such as blood biomarkers of inflammation and radiographic imaging, provides an initial assessment of the type of pulmonary defect. Subsequently, it is a valuable tool for monitoring disease progression and assessing treatment response (ALHAMED et al., 2001, MELTZER and NOBLE, 2008, RAGHU et al., 2011, ALVARADO-VAZQUEZ et al., 2020).

1.3.2 Bronchial Provocation Test

Another crucial PFT to be included in this survey, vital for both human and preclinical pulmonary investigations, is the assessment of AHR through bronchial provocation testing.

A defining characteristic of asthma, AHR refers to the airway's propensity to narrow in response to bronchoconstrictor challenges. If the bronchial smooth muscle's response to incremental doses of a bronchoconstrictor increases, it leads to a heightened maximal response,

known as AHR (O'BYRNE and INMAN, 2003, COCKCROFT and DAVIS, 2006, WALKER et al., 2013).

The earliest observations of AHR in asthma patients date back to 1921 when Alexander and Paddock administered the cholinergic agonist pilocarpine subcutaneously (*s.c.*) to an asthmatic patient, resulting in what they termed "asthmatic breathing." This observation was later confirmed by WEISS and colleagues (1932), who measured changes in vital capacity (VC) after intravenous administration of histamine (O'BYRNE and INMAN, 2003).

According to the American Thoracic Society and European Respiratory Society (ATS/ERS) guidelines, methacholine (Mch) challenge tests for AHR are highly effective in diagnosing obstructive diseases and quantifying the severity, condition, and treatment response of airway dysfunction (REDDEL et al., 2009).

Bronchial provocation tests, utilized for measuring AHR, employ both "indirect" and "direct" challenge methods. Indirect stimulation methods encompass exercises, hyperventilation, exposure to cold air, among others. On the other hand, direct challenges involve substances like histamine and Mch. A non-selective muscarinic receptor agonist in the parasympathetic nervous system, Mch, acts directly on the airway's smooth muscle *via* H1 muscarine receptors. The Mch challenge test is notable for its quick execution, safety, and good reproducibility when conducted by a well-trained technician (O'BYRNE and INMAN, 2003, COCKCROFT and DAVIS, 2006, REDDEL et al., 2009).

There's a critical need to link basic scientific findings with practical clinical solutions due to the ineffective treatments available for conditions such as asthma and IPF, compounded by the high failure rates in drug development. MOHS and GREIG (2017) highlight that only about one in eight compounds entering clinical development in the pharmaceutical industry ultimately secure marketing approval. Their schematic diagram shown in Figure 1 outlines the lengthy and costly journey of drug development, spanning over 12 years with an average cost of $2.6 billion. This process involves stages from target identification through preclinical and clinical development to regulatory approval by bodies like the Food and Drug Administration. Despite substantial investments, many candidates fail to meet desired outcomes during clinical trials, leading to setbacks in delivering new treatments. Efforts to address these challenges require enhancing research methodologies, fostering interdisciplinary collaboration, and optimizing the drug development pipeline.

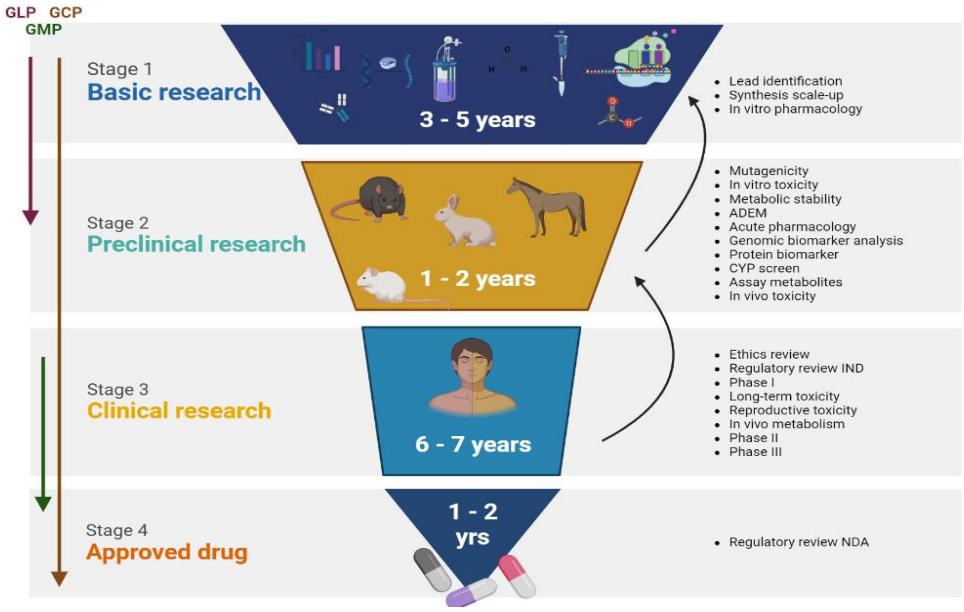

Figure 1 A schematic diagram of the activities involved in the drug discovery and development process

At the left are shown icons presenting new molecular or biological entities that are considered for development through specific activities in four stages of development: basic research, preclinical development (among all, including the studies of in vivo experimental models, absorption, distribution, excretion and metabolism (ADEM), screening for activity at cytochrome P450 (CYP) liver enzymes), clinical trials and regulatory filings for Investigational New Drug (IND) and New Drug Application (NDA). At the top are the timelines for quality assurance guides governing the process: good laboratory practice (GLP), good manufacturing practice (GMP), and good clinical practice (GCP). A modified image from MOHS and GREIG, 2017, created on BioRender.com.

Abbreviations: ADEM-absorption, distribution, excretion and metabolism, CYP-cytochrome, IND-Investigational New Drug, NDA-New Drug Application, GLP-good laboratory practice, GMP-good manufacturing practice, GCP-good clinical practice

In preclinical research, animal models play a crucial role in translating drug findings from bench to bedside (DENAYER et al., 2014). These models are developed to enhance our understanding of disease pathophysiology, validate potential therapeutic targets, and facilitate the development of novel treatments. However, it's important to acknowledge that, while valuable, animal models are not perfect replicas of human diseases (MOURATIS and AIDINIS, 2011). They may not fully capture all aspects of the clinical condition due to factors such as incomplete knowledge of disease triggers and limitations inherent to animal models.

One significant challenge in using animal models is replicating the characteristics of chronic diseases, particularly in conditions like IPF, where disease progression in humans is slow and irreversible (MOELLER et al., 2008). These limitations have led to increased scrutiny and questioning of the utility of animal models in drug development (MCGONIGLE and RUGGERI, 2014, ROBINSON et al., 2019). Despite these criticisms, animal models continue to make invaluable contributions to human research.

Rather than dismissing animal models altogether, it is essential to invest additional resources and efforts into improving existing models and developing new ones (MCGONIGLE and RUGGERI, 2014). This study aimed to explore how PFTs could enhance the translational value of animal models of respiratory diseases. While PFTs are routinely used in clinical practice, their application in preclinical animal models of pulmonary diseases is limited.

To address this gap, a back-translational approach was adopted in this research. The study evaluated the effects of "gold standard" treatments, such as nintedanib and pirfenidone for IPF and dexamethasone and fluticasone propionate for asthma, on PFT values in animal disease models. By using PFTs as an endpoint of interest, the study aimed to assess the efficacy of these treatments in preclinical settings, thus enhancing the translational relevance of the research.

2 LITERATURE OVERVIEW

While commonly employed in clinical settings, PFTs are less frequently utilized within preclinical animal models of lung diseases. This underuse stems, in part, from the significant methodological challenges associated with adapting these tests for small animal models, particularly mice.

Despite differences in size and structural variances, the fundamental principles of ventilation, airflow, lung volumes, and gas exchange are largely consistent across mammalian species (COSTA, 1985, GOMES et al., 2000, BATES and IRWIN, 2003). HOYMANN (2012) further supports this notion, suggesting that while not identical, the respiratory mechanisms in mice share essential similarities with those of other mammals.

The challenge of conducting PFTs in mice primarily lies in their small size, which demands highly sensitive and fast-responsive measurement systems and instrumentation. Additionally, certain PFTs in humans involve forced maneuvers that are performed voluntarily, a feat not possible with mice. This necessitates the development of innovative systems capable of circumventing these technical hurdles to obtain reliable pulmonary function measurements in murine models (COSTA, 1985, BONNARDEL et al., 2019).

Historically, reports on mouse lung function measurements were sparse before the late 1980s, primarily focusing on adapting human-centric tests for small experimental animals. These early efforts were hampered by the need for highly sensitive instruments, limiting the scope of dynamic lung function data available (COSTA, 1985). A pivotal moment came with the work of Martin and colleagues in 1988, who introduced precise methods for measuring resistance and compliance in mice, setting a new standard for invasive PFTs by employing miniaturized technologies originally designed for larger animals and humans (BATES and IRVIN, 2003).

In preclinical research, PFTs can be categorized into three main approaches: ex-vivo, in-vivo invasive, and in-vivo noninvasive. The in-vivo methods, particularly favoured for their applicability in both anesthetized and conscious mice, are further divided into invasive and noninvasive categories (HOYT et al., 2007). Noninvasive PFTs, conducted with conscious mice within a plethysmograph, offer a suitable option for long-term screening despite their limited capacity for in-depth mechanical lung function characterization. The quest for enhanced experimental control and measurement precision has led to the predominance of invasive

techniques, which, despite sacrificing noninvasiveness, offer superior sensitivity and specificity (BATES and IRVIN, 2003, HOYT et al., 2007).

The invasive approach necessitates deep anesthesia to inhibit spontaneous breathing and instrumentation prior to pulmonary function assessment. Regarded as the gold standard for lung function determination in mice, this method allows for high-precision measurements and direct lung examination. Its main advantage lies in the direct access to the lungs *via* an endotracheal tube, eliminating upper airway influences. Controlled mechanical ventilation ensures consistent tidal volume and respiratory rate, facilitating repeatable techniques under stable conditions. While highly accurate, the invasive method's drawbacks include the requirement for general anesthesia and a surgical procedure for endotracheal tube placement, limiting the assessment to a single session and altering the animal's natural breathing pattern due to anesthesia's depressant effects. Furthermore, this method demands more extensive operator training, more time for procedure execution, and incurs higher costs due to the need for specialized mechanical ventilation and measurement equipment (BATES and IRVIN, 2003, HOYT et al., 2007, HOYMANN, 2012).

Currently, two invasive systems are available for measuring pulmonary function in laboratory animals: the Buxco® PFT (DSI, USA) and the FlexiVent® (SCIREQ, Canada), both of which directly measure pulmonary function using a reprogrammed ventilator and specific maneuvers. This research employs the Buxco® PFT system, offering a detailed exploration of its application and advantages in assessing pulmonary function within murine models (VANOIRBEEK et al., 2010, DE ANDRADE CASTRO and RUSSO, 2019).

To fully evaluate the utility of PFTs in assessing respiratory health, it's crucial to understand the key parameters these tests measure and how they relate to lung function. Lung volumes and capacities, which describe the amount of air moved in and out of the lungs during breathing cycles, are fundamental to this understanding. Illustrated in Figure 2, a volume-time spirogram provides a visual representation of static lung volumes and capacities during both inspiration and expiration phases, as well as parameters measured at rest, including those obtained through forced maneuvers**.**

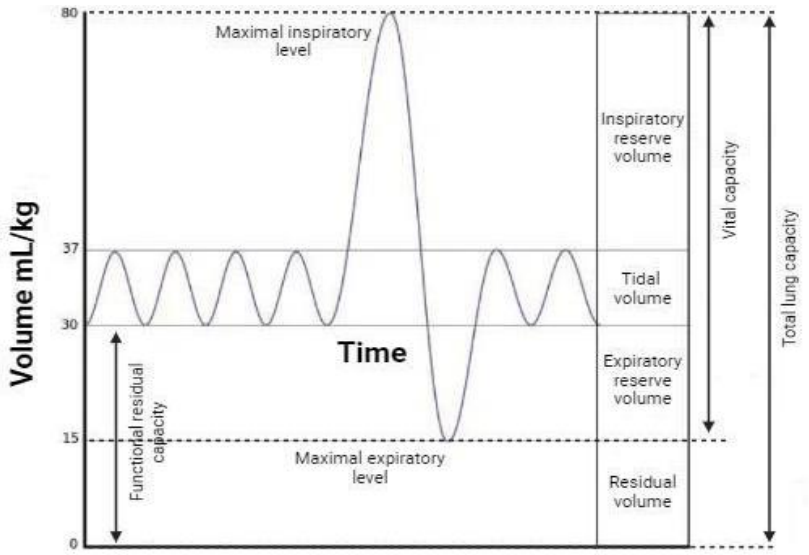

Figure 2 A volume-time spirogram of static lung volumes and capacities
The graph shows curves of inspiration and expiration and parameters measured during the resting period, including force maneuvers. A modified image from QUANJER et al., 1993, created on BioRender.com.

Their standardization guidelines and definitions are corroborated by WANGER et al. in 2005 in the ATS/ERS task force document as follows:

- "Functional residual capacity (FRC) is the volume of gas present in the lung at end-expiration during tidal breathing;
- Expiratory reserve volume (ERV) is the volume of gas that can be maximally exhaled from the end-expiratory level during tidal breathing (i.e., from the FRC);
- The maximum volume of gas that can be inspired from FRC is referred to as the inspired capacity (IC);
- Inspiratory reserve volume is the maximum volume of gas that can be inhaled from the end-inspiratory level during tidal breathing;
- Reserve volume (RV) refers to the volume of gas remaining in the lung after maximal exhalation (regardless of the lung volume at which exhalation was started);
- The volume of gas inhaled or exhaled during the respiratory cycle is called tidal volume (TV);
- Total lung capacity (TLC) refers to the volume of gas in the lungs after a maximal inspiration or the sum of all volume compartments.
- Vital capacity (VC) is the volume change at the mouth between the positions of total inspiration and complete expiration.".

Respiratory disorders, however, present in various forms and impact these lung volumes and capacities in distinct ways, altering the patterns observed in PFTs. These altered patterns play a crucial role in diagnosing and characterizing different respiratory conditions, as depicted in Figure 3. Understanding these parameters and their interrelations is key to leveraging PFTs effectively in preclinical and clinical practice and research.

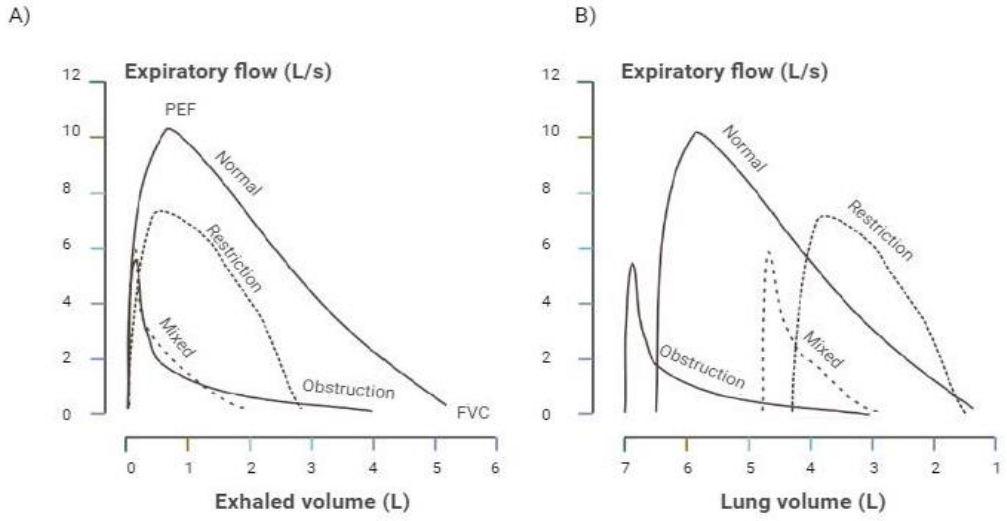

Figure 3 A schematic view of the flow-volume curve changes over expected – healthy person results.

Characteristic changes of the F-V curve to a convex-shaped curve in the restrictive and concave-shaped curve in obstructive disorder patients are presented in a graph of expiratory flow in A) the exhaled volume and the B) total lung volume (A modified image from QUANJER et al., 1993, created on BioRender.com).

Abbreviations: PEF peak expiratory flow, MMEF-maximal mid-expiratory flow, FVC-forced vital capacity, F-V-flow volume;

Restrictive pulmonary disorders are marked by lung tissue stiffness, resulting in decreased flow parameters as peak expiratory flow (PEF) and maximal mid-expiratory flow (MMEF) and reduced lung volumes, including forced expiratory volume at 1 second (FEV1) and RV, along with TLC. The forced vital capacity (FVC), reduced alongside FEV1, often yields a normal or elevated FEV1/FVC ratio, called the Tiffeneau index, a key feature of restrictive disorders. Additionally, a convex shape of the flow-volume (F-V) curve and a downward and rightward shift of the static expiratory pressure-volume (P-V) curve are typical PFT findings in this disorder (QUANJER et al., 1993, ALHAMAD et al., 2001, PELLEGRINO et al., 2005, GILDEA and MCCARTHY, 2010).

In contrast, obstructive pulmonary disorder arises from airway narrowing, leading to a disproportionate reduction of FEV1 compared to the maximal volume exhaled from the lung,

FVC. This condition typically exhibits a decreased FEV1/FVC ratio, a crucial indicator of asthma and a predictor of disease progression and treatment efficacy. The air trapping within the lungs often results in normal or increased TLC and elevated RV. Similarly, airflow parameters such as MMEF and PEF demonstrate a reduction trend similar to those in restrictive disorders. The decreased expiratory flow parameters, particularly in the MMEF, between 25 and 75% of FVC, contribute to the characteristic concave shape of the F-V curve in obstructive disorders (PELLEGRINO et al., 2005, REDDEL et al., 2009, GILDEA and MCCARTHY, 2010; GINA, 2023).

Evaluation of PFT in surveys reported in this thesis was performed using the Buxco® PFT to measure lung volumes and capacities in both models and the bronchial provocation test in the model of ovalbumin (OVA)-induced asthma using the Buxco® FinePointe Resistance and Compliance (RC) system.

As corroborated by VANOIRBEEK et al. (2010), the Buxco® PFT enables three semiautomatic maneuvers to measure Boyle's law functional residual capacity, quasistatic P-V curve, and fast F-V curve; and forced oscillation technique (FOT) to measure resistance (Ri) and compliance (Cdyn). The system provides clinically relevant parameters, such as FEV1 (in mice in 100 ms), VC, FVC, Tiffeneau index, RV, and TLC by measuring standard and maximal P-V and F-V curves, as well as lung mechanistic parameters Ri and Cdyn (VANOIRBEEK et al., 2010, BONNARDEL et al., 2019, DE ANDRADE CASTRO and RUSSO, 2019). Each maneuver protocol was described by VANOIRBEEK and his colleagues (2010) as follows:

"To measure FRC, ventilation was stopped at the end of expiration with an immediate closure of a valve located proximally to the endotracheal tube. Spontaneous breathing maneuvers against a closed valve with consequent pressure changes at the mouth and in the bodybox were then recorded to calculate the functional residual capacity or FRC (Boyle's law). To measure the TLC, RV, IC, and VC, a quasistatic pressure volume maneuver was performed, which inflates the lungs to a standard pressure of +30 cm H2O and then slowly exhales until a negative pressure of -30 cm H2O is reached. The quasistatic compliance was defined as the volume/pressure ratio at 50 % of the expiration (cord compliance (Cchord) 50). With the fast flow volume maneuver, lungs were first inflated to +30 cm H2O (TLC) and immediately afterward connected to a highly negative pressure in order to enforce expiration until RV at –30 cm H2O. Forced expiratory flows (PEF and FEF), times of expiration and inspiration (Te,

Ti), and forced expiratory volumes (FEV100 and FEV200) were recorded during this maneuver."

The bronchial provocation test in mice relies on the same principles as in humans. To measure AHR, animals are exposed to increasing bronchoconstriction challenge agent concentrations, administered *via* systemic route or as an aerosol. The changes in Ri and Cdyn are plotted against challenge concentration, resulting in a curve presenting parameter change over the challenge concentration increase (COCKCROFT and DAVIS, 2006, VANOIRBEEK et al., 2010).

Animal models are a valuable tool for developing new and more effective therapies, as they allow for the experimental manipulation of various controlled variables to investigate the pathogenesis of respiratory diseases and test potential treatments. They have been integral to biomedical research since ancient times, with their use dating back to the 4th century BC (DENAYER et al., 2014). Models vary in design, focusing on factors such as species, strain, disease trigger or challenge, challenge dose, and environmental conditions (BARRIOS, 2008). Among the various animal species used, mice are the most commonly employed due to their lower cost, faster reproduction rates, and the ability for multiple genetic manipulations (MOURATIS and AIDINIS, 2011, IVETIĆ TKALČEVIĆ et al., 2014). However, establishing characteristic lesions in a short period in these models poses a challenge, requiring the application of the appropriate challenge agent at a non-lethal but effective dose and administration route, with sufficient time for therapeutic intervention evaluation (SCOTTON and CHAMBERS, 2010).

The work of DENAYER et al. (2014) emphasizes the importance of validating animal models to bridge the translational gap between preclinical and clinical research endeavours. To facilitate this validation process, the authors reported several critical factors to consider when conducting animal studies, as outlined in Table 1.

Table 1 Three main criteria for animal model validation and factors to be considered in animal studies conducting processes

Criteria are listed in the paper published by DENAYER et al. (2014).

Main criteria for animal model validation		
Face validity	Predictive validity	Target validity
to achieve as many as possible similarities in biology and symptoms of disease in the animal models	demonstration of similar effects of known treatment in animal models	disease model should be developed by targeting the same disease pathways as in humans
Animal studies conducting factors to be considered		
Time course of the treatment	often, treatment in animal models is not initiated at the right moment, most often before the disease pathology is achieved, which is not in line with a clinical situation	
Animal characteristics and background	a careful selection of proper species and strains of animals, which will have the best expression of wanted immunological characteristics	
Subjective endpoint	many outcomes are evaluated by subjective interpretation, and to avoid bias, the experimental groups should be blinded, and the scorer should not be aware of the animals' treatment	
Reproducibility of experimental animal results	to standardize procedures as much as possible	
Group size	to ensure the most informative group size by conducting the 3R rule: replacement, reduction, and refinement	
Reporting	the importance of reporting both negative and positive animal studies outcomes	

Tailoring the model requires certain knowledge of disease pathogenesis and animal models' characteristics. Further, relevant findings from the literature were elaborated on to evaluate the PFT applicability in these models.

2.1 MOUSE MODEL OF BLEOMYCIN-INDUCED PULMONARY FIBROSIS

The bleomycin (BLM) animal model stands out as the most commonly utilized method for inducing experimental pulmonary fibrosis in animals and is considered a standard agent for this purpose. It has been shown to induce lung fibrosis *via* different administration routes in various experimental animals, including mice, rats, hamsters, rabbits, guinea pigs, dogs, and primates. The earliest description of BLM-induced pulmonary fibrosis dates back to its use in dogs in 1971, followed by reports in mice (1974), hamsters (1978), and rats (1979) (MOELLER et al., 2008).

Originally isolated from the fungus *Streptomyces verticillatus*, BLM was developed in the 1960s as a chemotherapeutic antibiotic for treating cancers such as lymphoma and squamous cell carcinomas. Patients undergoing intrapleural administration in oncology settings reported lung fibrosis as a side effect, which is attributed to the physiological absence of BLM hydrolase. This enzyme deactivates BLM in lung tissue, thus mitigating its harmful effects. Additionally, BLM interferes with the cell cycle by causing damage to both single and double-stranded DNA in rapidly dividing cancer cells. This genetic damage, coupled with an overproduction of reactive oxygen species (ROS), initiates inflammation in adjacent tissue. Such an inflammatory cascade results in pulmonary toxicity, stimulates fibroblast activity, and ultimately leads to fibrosis, as documented by MOELLER et al. (2008) and YANAGIHARA et al. (2020).

Mice are the preferred species for preclinical testing using the BLM model, as recommended by the ATS. Studies have shown that the response to BLM varies depending on strain and sex in mice, with male C57BL/6 mice exhibiting greater suitability than BALB/c mice. This difference is attributed to variations in BLM hydrolase production across strains and differential expression patterns of cytokines and proteases (DEGRYSE and LAWSON, 2011, YANAGIHARA et al., 2020). The intratracheal (*i.t.*) route of administration, at doses of 0.025–0.05 U/mouse (approximately equivalent to 1 mg/kg), is commonly employed in this model (SCOTTON and CHAMBERS, 2010).

2.1.1 Mechanisms and Phases of Bleomycin-Induced Pulmonary Fibrosis in Mouse Models

The mechanism underlying BLM activity in mouse models of lung fibrosis involves a combination of oxidative tissue damage, a relative deficiency of the deactivating enzyme BLM

hydrolase, genetic susceptibility of the mouse, and elaboration of inflammatory cytokines (REINERT et al., 2013).

Single *i.t.* administration of BLM in mice induces alveolar epithelial injury, triggering inflammatory and fibrotic reactions within a short period (Figure 4). Initially, an exaggerated inflammatory response resembling acute lung injury occurs, characterized by the overproduction of free radicals. This reaction is initiated by BLM binding to iron, forming a complex that generates ROS through oxygen reduction. These ROS induce lung inflammation, releasing pro-inflammatory cytokines such as interleukin (IL)-1, IL-6, tumor necrosis factor (TNF)-α, and interferon (IFN)-γ from activated alveolar macrophages and neutrophils. The peak of this inflammatory phase typically occurs around day 14 post-BLM instillation. Subsequently, a fibrotic reaction ensues, marked by increased expression of profibrotic markers, including transforming growth factor (TGF)-β1, connective tissue growth factor (CTGF), and alpha-1 type I collagen (COL1A1). The transition from inflammation to fibrosis occurs around day nine after BLM administration, with maximal fibrotic responses observed on days 21–28. Histologically, fibrosis becomes evident by day 14, characterized by the expansion of the myofibroblast population, augmented ECM deposition, and heightened levels of profibrotic cytokines such as TGF-β1 (Figure 4). The peak fibrotic response is typically observed on days 21-28. However, many standard outcome parameters in the model become highly variable subsequently, and fibrosis may spontaneously resolve at a later stage (IZBICKI et al., 2002, MOELLER et al., 2008, SCOTTON and CHAMBERS, 2010, REINERT et al., 2013, YANAGIHARA et al., 2020).

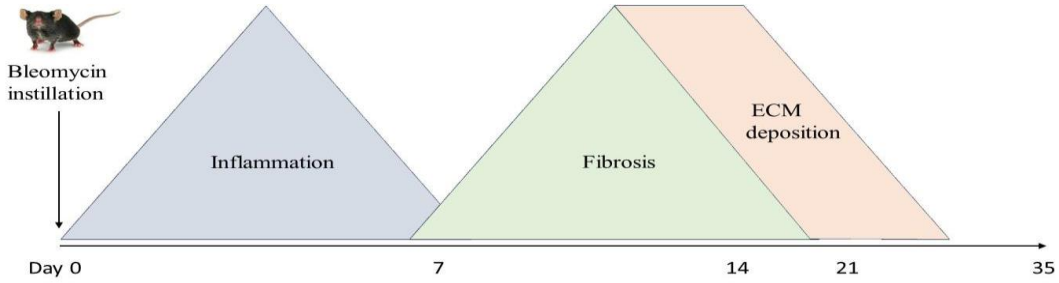

Figure 4 A schematic image of bleomycin-induced pulmonary fibrosis phases in mice after single intratracheal administration at D0.
Two phases of the model are present: inflammatory and fibrotic. Acute inflammation lasts approximately seven days, followed by fibrogenic changes with extracellular matrix deposition up to 28 to 35 days. These fibrogenic changes with ECM deposition resolve after 35 days. (A modified image from YANAGIHARA et al., 2020).

Abbreviations: ECM-extracellular matrix

The resolution of BLM-induced fibrosis after a certain period continues to be a subject of various research endeavours. It has been postulated that nitric oxide synthases, enzymes catalysing nitric oxide production known to protect endothelial cells from oxidant-mediated injury, may influence resolution. However, CHUNG et al. (2003) found that both C57BL/6 and nitric oxide synthase knockout mice resolved fibrosis, suggesting a multifaceted healing process influenced by genetic and environmental factors.

Although the BLM-induced pulmonary fibrosis model in mice presents several advantages, including its well-characterized nature, clinical relevance, and widespread accessibility, it does not fully replicate all critical features of UIP observed in human IPF. The model falls short in reproducing fibrotic lung remodelling with temporal heterogeneity, hyperplastic areas of fibrosis lined by type alveolar epithelial cells (AEC) cells, fibroblastic foci, and minor inflammation. Moreover, it fails to mimic the slow, irreversible progression of fibrotic changes characteristic of IPF due to the self-limiting response to BLM in mice. Despite these limitations, significant histological IPF hallmarks, such as intra-alveolar buds, mural collagen incorporation, and alveolar space obliteration, are present in the animal model (MOELLER et al., 2008, DEGRYSE and LAWSON, 2011, MOORE et al., 2013). Nevertheless, as JENKINS et al. (2017) have concluded, while it does not offer an exact replication of IPF, the mouse BLM model of pulmonary fibrosis remains a crucial experimental tool for investigating disease pathogenesis and advancing preclinical drug development efforts.

2.1.2 Pathogenesis of Idiopathic Pulmonary Fibrosis

SGALLA et al., in their review paper on IPF pathogenesis from 2018, have summarized the processes that have been reported to have a crucial contribution to disease development. The schematic view of IPF pathogenesis is presented in Figure 5B. Lungs of IPF patients are susceptible to disordered responses to sustained micro-injuries due to dysfunctional aging and/or genetically related alveolar epithelium. In the IPF-affected lungs, the ability to re-establish normality by replacing damaged AEC I with AEC II cells is seriously impaired, activating another protective pathway called unfolded protein response (UPR).

In a healthy lung (Figure 5A), after injury and loss of AEC I, alveolar integrity is restored through a process involving the proliferation and differentiation of AEC II and stem cells. Chemokines such as TGF-β1, platelet-derived growth factor (PDGF), vascular endothelial growth factor (VEGF), and fibroblast growth factor (FGF) play crucial roles in this process by orchestrating activities like coagulation cascade, new vessel formation, fibroblast activation and

migration, collagen synthesis, and proper alignment. However, if injuries persist or if typical tissue restoration is not possible (Figure 5B), increased levels of IL-1 and TNF-α drive tissue remodelling in wound healing activities (SGALLA et al., 2018).

The activation of profibrotic mediators, including TGF-β1, PDGF, c-x-c motif chemokine (CXCL)12, and chemokine c-c motif ligand (CCL)2, drives this pathway, with TGF-β1 playing a central role in IPF pathogenesis. TGF-β1 promotes epithelial cell apoptosis, epithelial-mesenchymal transition (EMT), epithelial cell migration, and the production of other profibrotic mediators. It also recruits circulating fibrocytes and activates and transforms fibroblasts into myofibroblasts. Additionally, TGF-β1 induces the production of VEGF, CTGF, and other proangiogenic factors through various pathways. Another TGF-β1-driven pathway in IPF pathogenesis is the Wnt-β-catenin signalling, a deregulated embryological pathway involved in EMT and fibrogenesis, leading to apoptosis resistance and cell proliferation.

The EMT process, influenced by TGF-β1, causes epithelial cells to express genes associated with mesenchymal cells. As a result, AECs detach from the basement membrane, migrate, and down-regulate their typical markers. These transitional cells typically express α smooth muscle actin (SMA), a characteristic of myofibroblasts. The loss of AECs and disruption of the basement membrane leads to increased vascular permeability and the formation of a provisional matrix. While angiogenesis aids in tissue repair, failed re-endothelization, often associated with decreased endothelial progenitor cells in IPF patients, triggers a profibrotic effect *via* VEGF chemokine. Additionally, activation of the coagulation cascade at this stage increases plasminogen activation inhibitors, reducing ECM degradation and inducing fibroblast differentiation into myofibroblasts.

Circulating fibrocytes, pulmonary fibroblasts, and myofibroblasts play pivotal roles in IPF pathogenesis. The activated epithelial and endothelial cells create an abnormal biochemical environment that promotes these cells' recruitment, activation, differentiation, trans-differentiation, and proliferation. Fibrocytes, recruited by TGF-β1 from damaged tissue or activated AECs, differentiate into fibroblasts and myofibroblasts, contributing to IPF by secreting profibrotic cytokines and producing ECM. Persistently exposed to profibrotic mediators, particularly TGF-β1, fibroblasts generate ECM and undergo trans-differentiation into myofibroblasts. These cells form fibroblast foci, clusters of active fibroblasts, and myofibroblasts in the local microenvironment, positioned close to hyperplastic AEC2s. This

proximity enhances aberrant crosstalk and magnifies the effects of TGF-β1, PDGF, and Wnt pathways, amplifying the profibrotic environment (Figure 5B).

Increased trans-differentiation rate to myofibroblasts, their resistance to apoptosis, excessive matrix production, and an imbalance between collagen deposition and degradation lead to uncontrolled accumulation of scar tissue in the alveolar space. Myofibroblasts, secreting αSMA, undergo irreversible contraction, reorganizing collagen fibrils and leading to a stiffer ECM (WILSON and WYNN, 2009, KING JR. et al., 2011, SGALLA et al., 2018).

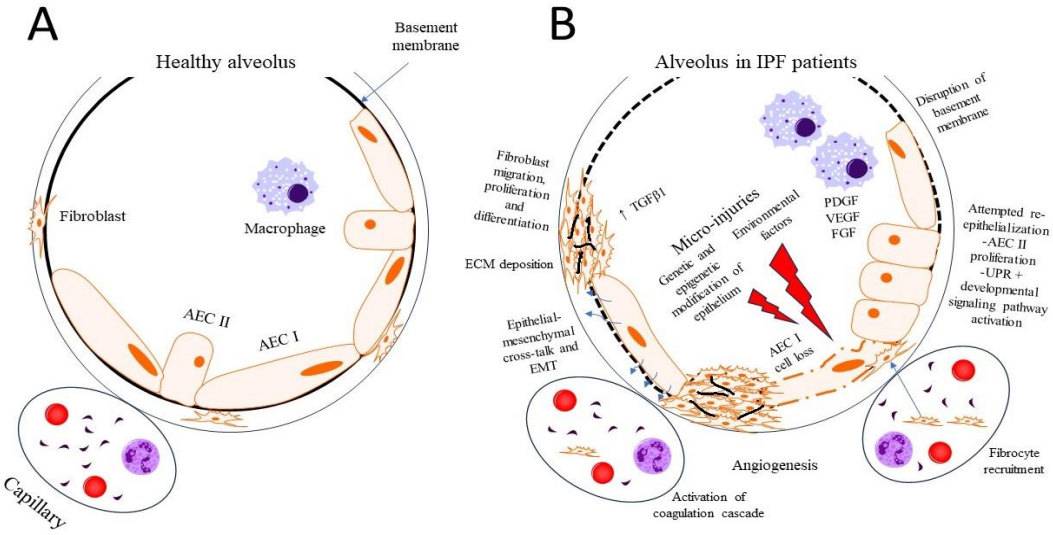

Figure 5 A schematic view of idiopathic pulmonary fibrosis (IPF) pathogenesis
The picture on the left represents normal alveolar tissue of healthy lungs. In contrast, the image on the right represents alveolar tissue and pathogenesis mechanisms in the lung's alveoli affected by IPF (A modified image from SGALLA et al., 2018, created on BioRender.com).

Abbreviations: AEC-alveolar epithelial cell, ECM-extracellular matrix, EMT-epithelial-mesenchymal transition, UPR- unfolded protein response, TGF β1-transforming growth factor beta 1, PDGF-platelet-derived growth factor, VEGF-vascular endothelial growth factor, FGF-fibroblast growth factor

2.1.3 Available Treatment in Idiopathic Pulmonary Functions

A quite recent advancements in IPF treatment have brought hope, with medications like pirfenidone and nintedanib demonstrating significant efficacy in slowing disease progression.

Pirfenidone, an orally available pyridine compound, possesses both anti-inflammatory and antifibrotic properties, supported by multiple placebo-controlled randomized clinical trials (KING JR. et al., 2014, LOVEMAN et al., 2015).

Similarly, nintedanib, a potent inhibitor of tyrosine kinase receptors, has exhibited antifibrotic effects in clinical studies, resulting in reduced lung function decline and fewer acute exacerbations of IPF (RICHELDI et al., 2014, WOLLIN et al., 2015).

However, a systematic review by LOVEMAN et al. (2015) comparing pirfenidone and nintedanib suggests that nintedanib may be more effective in slowing FVC decline. Despite these findings, the individualized treatment approach advocated by international guidelines highlights the importance of considering factors such as side effect tolerance (RAGHU et al., 2015, BARRAT et al., 2018, RAGHU et al., 2022).

Although several molecules, including Interferon-γ 1b, Omipalisib/GSK212645, GLPG1690, PBI-4050, Pentraxin-2, and Pamrevlumab, have shown promise in clinical trials, no single treatment apart from nintedanib and pirfenidone has yet been approved for IPF patients. This underscores the ongoing efforts of scientists to discover effective therapies for this debilitating condition (SOMOGYI et al., 2019).

2.1.4 Literature Review on Models and PFT Utility Advancements, Challenges, and Recommendations

The model's primary criticism lies in the spontaneous resolution of BLM-induced lung inflammation and fibrosis in mice (SCOTTON and CHAMBERS, 2010). To address this issue, DEGRYSE and LAWSON (2011) proposed repeated BLM lung injury. The significant decrease in AEC death two weeks post-BLM administration in the single challenge model formed the basis for establishing the repeated injury model. It was administered every two weeks at a dose of 0.04 units per 100 µL saline *i.t.* for eight doses, with lungs harvested two weeks post-last administration. This regimen resulted in significant lung fibrosis and architectural distortion, with hyperplastic AECs lining fibrosis areas and fibroblast foci. Despite improvements over the single-dose BLM model, the repetitive model requires a significant time commitment and fails to reproduce the complete UIP pattern. Nevertheless, the authors contend that this modification substantially enhances the animal model for IPF investigation.

Contrary to previous suggestions, PENG et al. (2013) demonstrated that a single BLM instillation effectively reproduces specific pathogenic molecular changes relevant to IPF. Investigating both single and repetitive BLM-induced fibrosis mouse models, they employed C57Bl6 male mice instilled *i.t.* with 2 IU/kg BLM per mouse, once or every other week, for eight doses. Interestingly, both challenge regimens significantly increased bronchoalveolar lavage fluid (BALF) inflammatory cells and hydroxyproline levels, Ashcroft score, and immunohistochemical (IHC) analysis of COL1A1 and αSMA compared to the saline control group on all respective days. This finding contradicts the assumption that repetitive BLM administration is necessary for effective modelling.

Furthermore, lung function measurements using the FlexiVent® system failed to differentiate between groups, likely due to its poor sensitivity in small animals. Genomic profiling of lung tissue revealed three temporal phases of BLM-challenge response: inflammation (days 1–2), active fibrosis (days 7–14), and late fibrosis (days 21–35), with saline-treated samples clustering separately. Interestingly, during the inflammation phase, alterations primarily involved immune response and wound healing genes. In the active fibrosis phase, up-regulation of matrix metalloprotease (MMP) genes, collagen genes, Wnt signalling genes, phosphatidylinositol 3-kinase (PI3K) activity-related genes, and genes associated with alternative macrophage activation and other fibrosis-related pathways was observed. Positive regulators of TGFβ signalling were upregulated, while negative regulators were down-regulated during the fibrosis phases.

In their conclusion, the authors acknowledged that the molecular changes during the inflammation phase did not correlate with those observed in IPF patients, highlighting the translation issue of candidate therapies tested in prophylactic BLM models. However, they found that the single challenge model induced molecular changes similar to those expressed in IPF patients during the "active" disease stage, particularly in genes associated with mitosis and ECM signalling.

In accordance with their validation of the timing for treatment initiation, understanding the progression of pathological changes in C57Bl/6 mice following the BLM challenge is vital for research planning. This timeline has been meticulously explored by IZBICKI et al. (2002) and MOORE and HOGABOAM (2008). Their investigations involved administering BLM *i.t.* to C57Bl/6 male mice at doses ranging from approximately 2.4 to 4 IU/kg and monitoring changes on days 3, 6, 14, and 21 post-administration. They concluded that signs of fibrosis in this model typically appear on days 3 and 6, progressing to day 14, with peak responses generally observed between days 21 and 28. These conclusions were drawn based on observed BALF inflammatory cell increases, hydroxyproline level alterations, and histopathological assessments.

Despite the well-documented phases and timing of the BLM model, a significant number of tested molecules have been administered during the inflammatory phase. MOELLER and colleagues (2008) conducted a meta-analysis of publications from 1980 to 2006, identifying 240 articles, with the majority focusing on preventive rather than therapeutic regimens. Similarly, KOLB et al. (2020) evaluated 976 publications from 2008 to 2019,

revealing a similar trend, with the vast majority investigating preventive therapies. Both studies emphasized the necessity to administer tested molecules during the established fibrosis phase, a point reiterated by SCOTTON and CHAMBERS (2010) and DENAYER et al. (2014).

In response to the discrepancy between successful preclinical development and poor translatability to patient care, the ATS convened an official workshop in 2017. The resulting workshop report, titled "Use of Animal Models for the Preclinical Assessment of Potential Therapies for Pulmonary Fibrosis" (JENKINS et al., 2017), aimed to provide recommendations to enhance the translation of preclinical models into clinical practice.

The workshop focused on three main themes: animal selection, practical considerations of fibrosis modelling, and fibrotic endpoints for evaluation. Recommendations included using mice as the primary animal model for preclinical testing, with rats employed for confirmation if necessary. The timing of treatment initiation was emphasized, suggesting that treatment should commence no earlier than 7-10 days post-BLM to ensure the peak of the acute inflammatory phase has subsided.

Additionally, the workshop recommended employing an integrated approach to drug development, incorporating relevant animal models and appropriate ex vivo/in vitro approaches. While PFTs were recognized as a potential endpoint for assessing fibrotic changes and therapeutic response, their technical challenges hinder widespread adoption in preclinical models.

Furthermore, the workshop highlighted the importance of publishing negative results to prevent unnecessary duplication of effort and reduce animal experimentation. Although PFTs and other endpoints, such as imaging and blood biomarkers, show promise in increasing the translational value of preclinical models, their routine use remains limited.

Lastly, the report provided valuable data on the employment of pirfenidone and nintedanib in animal models, underscoring the need for further investigation into their efficacy and safety in preclinical settings.

While PFTs have been utilized in numerous published research studies as an additional measure, their utility in the mouse model of respiratory fibrosis has been thoroughly elucidated in only a handful of papers.

One such study by FERNANDEZ et al. (2016) focused on utilizing the FlexiVent® system in C57BL/6 female mice to induce BLM-induced fibrosis. Their investigation aimed to correlate clinically relevant blood biomarkers with lung function and histology in this preclinical model. Initiated by a single *i.t.* BLM instillation (3 IU/kg), pulmonary fibrosis progression was monitored at various intervals post-BLM administration (7, 14, 28, or 56 days). Significant declines in lung function were observed on day 14, correlating with histological findings, while later time points indicated some improvement in lung function despite continued fibrosis. Notably, an increase in blood biomarker soluble intercellular adhesion molecule-1 (sICAM-1) correlated with declining lung function, suggesting ongoing lung injury and fibrosis in this model.

Another study conducted by GILHODES et al. (2017) also incorporated PFTs in the preclinical fibrosis model. Their focus was on establishing an automated analysis of pulmonary fibrosis induced by BLM in mice. Recognizing the limitations of traditional histological scoring, they developed automated software for image analysis to achieve a more quantitative assessment of lung fibrosis.

The establishment of automated analysis as a quantitative endpoint measure of pulmonary fibrosis in the BLM mouse model included correlating it with Ashcroft scoring, in vivo micro-computed tomography (CT), and PFT. Pulmonary fibrosis was induced by single *i.t.* instillation of varying doses of BLM. On day 14 post-BLM instillation, both PFT and micro-CT were performed, followed by lung harvesting for histopathology score and automated histological image analysis. The analysis confirmed a dose-dependent statistically significant increase in Ashcroft score and lung tissue density over saline control lungs on day 14 post-BLM challenge, which was consistent with micro-CT analysis.

PFT measurements were conducted using the FlexiVent® system, reporting impaired lung function parameters such as Cdyn and FVC, with a dose-dependent trend observed. Correlation analysis of tissue density and high-frequency density indexes with Ashcroft score, micro-CT, and PFT in the BLM mice model yielded statistically significant results across all observed readouts.

However, these publications, despite including PFT measurements in their research, were not aimed at directly investigating this technique as part of their methodology. Therefore,

to the best of my knowledge, only the following publications have focused their research on validating PFT in preclinical mouse models of fibrosis.

In 2011, MANALI et al. published a paper evaluating murine lung's static and dynamic mechanics after *i.t.* BLM instillation. They aimed to systematically assess the functional alterations induced in murine lungs by the fibrogenic agent BLM. Additionally, they aimed to compare the effectiveness of the FOT with quasistatic P-V curves in mice following BLM exposure.

This study involved both C57BL/6 and BALB/c male mice receiving a single *i.t.* application of BLM at a dose of 2 mg/kg. BALB/c mice, known for their resistance to BLM, were used as a negative control. The FlexiVent® system was employed for PFT measurements on days 7 (early, inflammatory phase) and 21 (late, fibrotic phase) post-challenge. Biochemical and morphological assays supplemented these tests to characterize the different stages of the model from a structural perspective.

Functional assessment was performed using the FOT, dynamic lung impedance to airflow measurement, and quasistatic P-V curve analysis. The FOT technique measured parameters such as airway resistance, tissue damping, and elastance coefficient. Quasistatic measurement provided the P-V curve, and the area under the curve was calculated. Results obtained on day seven post-BLM instillation in both C57BL/6 and BALB/c mice indicated an acute inflammatory response, as evidenced by an increased lung injury score.

In contrast to BALB/c mice, C57BL/6 mice exhibited a robust fibrotic response on day 21, characterized by a significant increase in lung fibrosis score, tissue volume density, and lung collagen content. Consistent with histological changes, lung tissue elastance and damping also significantly increased in C57BL/6 mice on day 21. No significant changes were observed in the BALB/c strain using the FOT on either testing day. The administration of BLM led to an upward and leftward shift of the P-V curve in C57BL/6 mice as early as day 7, with further increases observed on day 21. In BALB/c mice, although no effects were noted in histology or FOT analysis, the P-V area was significantly higher on day 21.

A strong correlation was observed between functional measurements of tissue elastance and fibrosis analysis, including histology score, tissue volume density, and lung collagen content. However, the correlation between the P-V area and histology result was insignificant. Based on these findings, the authors concluded that both techniques are valuable tools for

evaluating lung function impairment in the mouse model of BLM-induced fibrosis. They suggested that the quasistatic P-V curve is more sensitive than FOT in detecting pulmonary functional impairments in both evaluated phases. However, lung elastance measured by FOT strongly correlates with histology score and soluble collagen content in the lungs.

Another study describing the impact of nintedanib treatment on the FVC parameter in the BLM-induced lung fibrosis model emerged partly from this thesis research, detailing changes on day 21 and from additional studies describing the effect on day 14 (ANZULOVIĆ ŠANTA et al., 2023). The obtained findings correlated with the Ashcroft score, emphasizing the assessment of this particular PFT parameter in model evaluation.

In the realm of pulmonary research, a seminal paper stands out as a cornerstone in the evaluation of PFT methodologies in preclinical models of respiratory diseases. Published in 2010 by VANOIRBEEK et al., this groundbreaking study offers a comprehensive assessment of both noninvasive (unrestrained plethysmography) and invasive (forced maneuvers and FOT) pulmonary function techniques to assess the models. The study found that while noninvasive tests had limitations, invasive methods could effectively quantify changes in lung function relevant to human clinical variables. The study provides measurements of various parameters using both the FlexiVent® and Buxco® systems across multiple mouse models, including those induced with BLM-triggered fibrosis. VANOIRBEEK and his team embarked on a pioneering journey, evaluating cutting-edge technologies for pulmonary measurements across four distinct laboratory models of respiratory ailments: asthma, emphysema, and fibrosis.

The study highlights the significance of invasive PFT techniques in animal research, demonstrating their effectiveness in detecting lung function changes relevant to human diseases. Such validation is essential for exploring the pathophysiology of respiratory conditions and evaluating new treatments. Moreover, the research provides a detailed functional assessment across various respiratory disease models, delivering a nuanced perspective on the respiratory system's response to different pathologies and enriching our understanding of potential disease mechanisms and interventions.

In this pivotal study, male BALB/c mice served as the subjects across all models. The induction of lung fibrosis was meticulously executed through a single administration of BLM at a precise dose of 0.1 IU per mouse, equivalent to approximately 2.5-3 mg/kg. The researchers

conducted PFTs on day 21 post-BLM *i.t.* instillation, aiming to capture the comprehensive physiological alterations induced by the fibrogenic agent.

Initially, noninvasive measurements using whole-body plethysmography were performed on the subjects, followed by invasive measurements subsequent to tracheotomy. While the noninvasive assessments provided limited insights into the functional impairment of fibrotic lungs, with only minor alterations in breathing patterns detected, the invasive Buxco® system yielded significant and noteworthy results when employed on day 21 in the BLM-induced fibrosis model.

Utilizing the Buxco® system, the researchers uncovered substantial changes in various parameters such as IC, VC, Cchord, Te, FEV200, and PEF compared to the control group consisting of BLM-free animals. Additionally, characteristic alterations in P-V and F-V curves were meticulously observed and documented.

In the specific context of the BLM model of fibrosis, this study's findings are particularly noteworthy. The study demonstrates that mice with induced fibrosis exhibit a restrictive pulmonary function pattern, characterized by a significant reduction in compliance and an increase in lung elastance, which mirrors the physiological changes observed in human pulmonary fibrosis. These findings not only validate the BLM model as a representation of fibrotic lung disease but also highlight the utility of invasive PFTs in capturing the functional impairments associated with lung fibrosis.

Moreover, the research contributes to the standardization of PFT application in mouse models, detailing the procedures and showcasing the reproducibility of these tests in capturing disease-specific pulmonary function changes. This standardization is a crucial step forward, ensuring that results from different studies are comparable and that the most accurate and reliable data inform preclinical and clinical research decisions.

Overall, this study marks a significant advancement in preclinical respiratory research, offering a robust framework for employing PFTs in animal models to better understand and treat human respiratory diseases.

The detailed parameter values obtained from the Buxco® system are meticulously outlined in the study and presented in Table 2, providing a thorough list of parameters and their directional changes across various respiratory diseases.

2.2 MOUSE MODEL OF OVALBUMIN-INDUCED ASTHMA

Asthma, a multifactorial disease with a complex pathophysiology and multiple subtypes, presents a challenge when it comes to developing an effective disease model in preclinical research. Nevertheless, various models have contributed to understanding the mechanisms underlying asthma and differentiating between endotypes over the past three decades (EPSTEIN, 2004). While asthma predominantly affects humans, cases have also been observed spontaneously in cats and horses. However, practical and ethical constraints limit the use of asthmatic cats and horses as models for asthma research, consequently requiring the development of various animal models of asthma over the years (NIALS and UDDIN, 2008).

Despite scientists' efforts to develop a standard model, it is widely acknowledged that such a model does not exist. This is due to the existence of numerous models with variations in strain, sensitization method, route, and challenge duration (KUMAR et al., 2008). However, all models follow a similar principle of disease induction, involving sensitization and challenge. These models can be categorized as acute or chronic, depending on the number of challenges. Chronic models necessitate repeated exposure to low allergen levels over a period of up to 12 weeks, while acute models involve fewer challenges over a shorter duration, often requiring multiple sensitizations *via* systemic allergen administration with adjuvants. Various allergens such as OVA, house dust mites, fungi, cockroach extracts, parasite antigens, cotton dust, and latex have been employed in asthma protocols to induce asthma-related pathophysiological characteristics (AUN et al., 2017).

Despite the availability of various allergens, OVA-challenged mouse models are the most widely utilized for preclinical evaluations of potential asthma therapeutics (KIM et al., 2019).

Throughout the history of asthma animal models, various species have been employed, including Drosophila, rats, guinea pigs, cats, dogs, swine, cattle, sheep, horses, and primates. Guinea pigs were particularly prominent in asthma research due to their strong response to allergens and the development of pathophysiological processes similar to humans. However, limitations such as a low number of reactive reagents and limited genetic knowledge restricted the widespread use of this model (SAGAR et al., 2015, AUN et al., 2017).

Mice, chosen as the primary species for asthma modelling, were first employed in 1994 and have since remained the most utilized model (EPSTEIN et al., 2017). However, the

selection of mouse strain is crucial. The BALB/c strain is favoured for antigen challenge models due to its pronounced t helper (Th)2 response and asthma-biased immunological pathway. Although successful asthma models have been developed using other strains, such as C57BL/6 and A/J, BALB/c females are the most commonly employed (NIALS and UDIN, 2008). It is noted that allergen-induced asthma models are influenced not only by genetic background but also by gender and environmental factors, with female mice reportedly developing more severe allergic inflammation than males (EPSTEIN et al., 2017).

Mouse models of acute OVA-induced asthma have significantly contributed to elucidating the role of T cells and Th2 cytokines in disease pathogenesis, facilitating the evaluation of molecules targeting these immunological components (SAGAR et al., 2015).

The sensitization phase initiates with the production of OVA-specific immunoglobulin (Ig)E by B cells, which subsequently binds to high-affinity receptors on mast cells and basophils. Upon direct airway administration of OVA, effector cells like mast cells and basophils become activated, initiating an immediate hypersensitivity reaction characterized by bronchospasm, edema, and mucous secretion in the lower airways. Sequential phases involve cytokines and chemokines orchestrating inflammation, with IL-5 recruiting eosinophils that contribute to the later-phase response (AUN et al., 2017).

While mouse models offer valuable insights, it's essential to acknowledge their limitations. Mice cannot spontaneously develop asthma, and notable anatomical, physiological, and pathological disparities exist between human and mouse airways and lungs. These distinctions encompass lung size, airway branching pattern, division of the lungs, lymphoid tissue distribution, epithelial cell composition, mast cell and IgE involvement, and eosinophil concentrations in BALF (SAGAR et al., 2015, EPSTEIN et al., 2017). Additionally, in acute challenge models, key asthma features are shortly present, with airway inflammation and hyperresponsiveness resolving within weeks after the final allergen challenge, lacking the chronic inflammation and airway remodelling aspects of asthma (NIALS and UDDIN, 2008).

Nonetheless, despite these limitations, EPSTEIN et al. (2017) contend that treatment studies on OVA-induced BALB/c mice can still be predictive, underscoring the ongoing significance of mouse models in asthma research. They advocate for enhancements such as precise phenotypic distinctions, identification of drug pathways, utilization of multiple models,

and appropriate experimental controls to augment the translational value of mouse models and align them more closely with human disease research.

In conclusion, although mouse models of asthma have greatly enhanced our understanding of the disease, ongoing efforts are crucial to refine these models and overcome their limitations. This will ultimately improve their translational value and relevance to human asthma. However, to achieve these refinements, it is essential to understand both the model characteristics and the disease's pathogenesis.

2.2.1 Mechanisms and Phases of Ovalbumin-Induced Asthma in Mouse Models

In line with the literature recommendations (KIM et al., 2019), this survey employs the OVA model in BALB/c mice. Therefore, the following text will corroborate the OVA origin, characteristics, and model expectations. Derived from chicken eggs, OVA is a cost-effective allergen, provoking a robust response upon systemic sensitization and direct airway challenge when paired with an adjuvant. The presence of an adjuvant, commonly aluminium hydroxide, promotes the development of a Th2 phenotype of the immune system upon exposure to the OVA antigen (DAUBEUF and FROSSARD, 2013).

The acute sensitization protocol entails multiple systemic administrations of OVA, usually ranging from 10 to 50 μg, along with aluminium hydroxide, ranging from one to 40 mg, administered at intervals of seven to 14 days (KUMAR et al., 2008). Traditionally, the sensitization antigen-adjuvant solution was administered intraperitoneally (*i.p.*), but in recent years, there has been a transition to *s.c.* injection due to its comparable effectiveness and decreased invasiveness (AUN et al., 2017).

Following sensitization, mice undergo allergen challenge to induce airway inflammation. This challenge can be administered by inhaling aerosolized OVA, *i.t.* or *i.n.* instillation, with the dose and frequency of challenges varying based on the route of administration. Typically, short-term challenges involve one or several administrations over four to eight consecutive days, with the intranasal (*i.n.*) route often preferred for its reduced invasiveness and practicality (KUMAR et al., 2008, AUN et al., 2017).

During the sensitization phase, B cells produce OVA-specific IgE, which binds to high-affinity receptors on mast cells and basophils. Upon direct airway exposure to OVA, effector cells like mast cells and basophils become activated, triggering an immediate hypersensitivity reaction characterized by bronchospasm, edema, and mucous secretion in the lower airways.

This immediate response is followed by a later phase mediated by cytokines and chemokines, leading to edema and recruitment of eosinophils by the IL-5 cytokine (AUN et al., 2017).

Mouse models of acute OVA-induced asthma have played a significant role in elucidating the involvement of T cells and Th2 cytokines, such as IL-4, IL-5, and IL-13, in the pathogenesis of the disease. Furthermore, these models have demonstrated their translational relevance by facilitating the evaluation of numerous molecules targeting these immunological components (SAGAR et al., 2015).

2.2.2 Pathogenesis of Allergic Asthma

Allergic asthma, most commonly beginning in childhood, involves exacerbation phases—acute or sub-acute deteriorations in symptoms and lung function, known as acute asthma (REDDEL et al., 2009; FERGESON et al., 2017; GINA, 2023). Acute asthma, more frequent in children, signifies poor disease management in both children and adults, often spurred by factors like viral infections and allergens (RAMSAHAI et al., 2019). BOONPIYATHAD et al. (2019) detail asthma's underlying mechanisms (Figure 6), highlighting the complex immune responses within the lungs, aiming to mirror these in animal studies.

The airway epithelium is a crucial barrier in organ defense. Damage to this layer prompts the release of cytokines like thymic stromal lymphopoietin (TSLP), IL-25, and IL-33, weakening the tight junctions of airway epithelial cells and promoting Th2 cytokine production.

Dendritic cells (DCs) are key in starting allergen-specific T-cell responses, activated directly by allergens or through interactions with innate immune cells. Upon allergen contact, DCs present the allergen to T lymphocytes, leading to Th2 cell activation, with natural killer T cells (NKT) also modulating DCs' response.

Th2 cells, by releasing cytokines IL-4, IL-5, and IL-13, play a vital role in allergic asthma management: IL-4 drives Th2 cell differentiation; IL-5 supports eosinophil maturation and release; and IL-13 promotes B cell and endothelial cell proliferation, leading to IgE production. Allergen-reactive Th2 cell induction requires initial sensitization and reactivation upon later allergen encounters, involving complex interplays among various cell types in the lungs and lymph nodes.

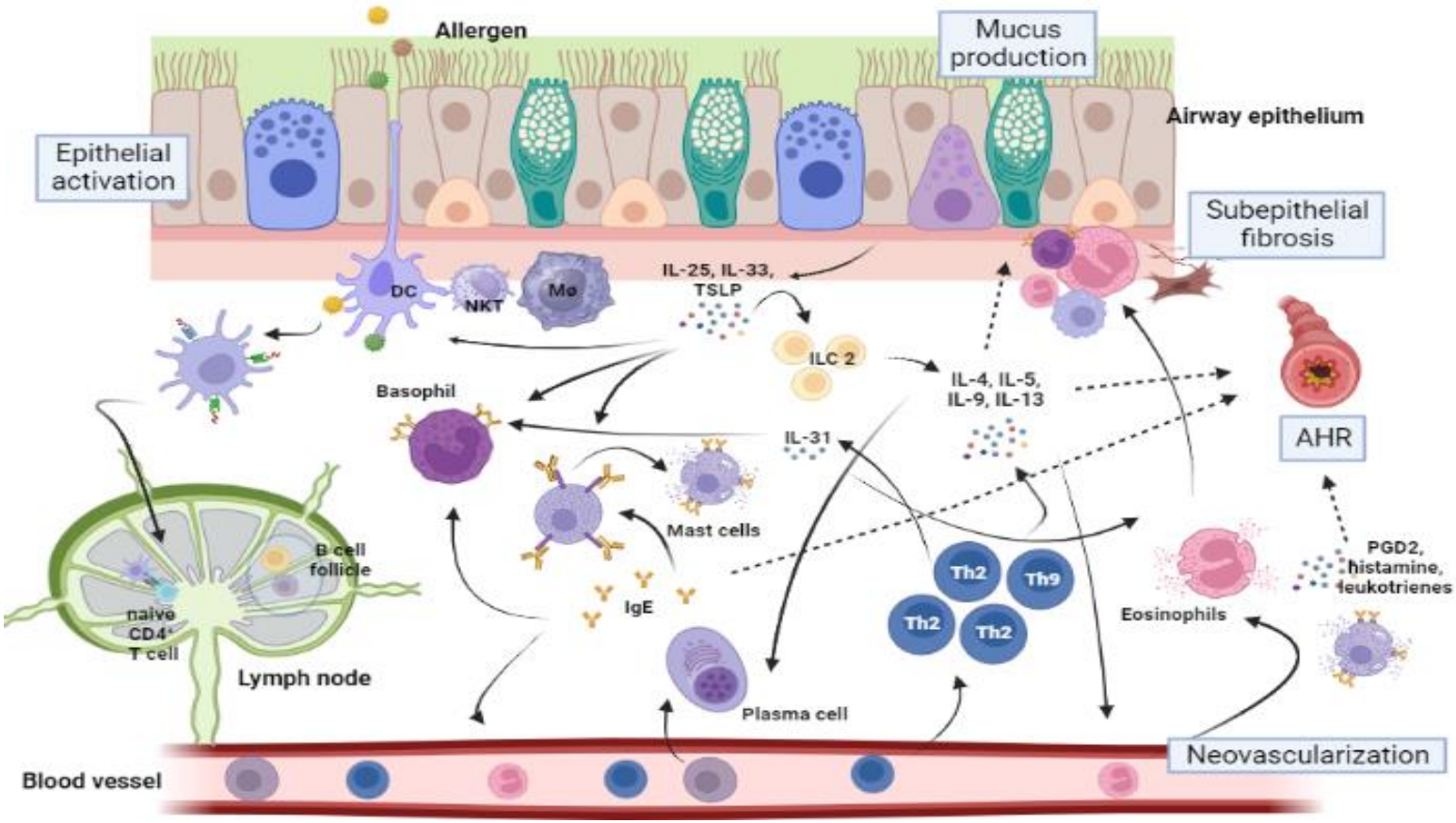

Figure 6 A schematic image of allergic asthma immune mechanism.
Complex cell interactions and various pathways are activated by allergen sensitization and reactivation exposure (A modified image from BOONPIYATHAD et al., 2019, created in BioRender.com).

Abbreviations: MΦ-macrophage, NKT-natural killer T cell, DC-dendritic cell, IL-interleukin, IgE-immunoglobulin E, TSLP-thymic stromal lymphopoietin, ILC-innate lymphoid cell, PGD2-prostaglandin D2, AHR- airway hyperresponsiveness.

Additionally, IL-31 and IL-31R also play a significant role in activating basophils and eosinophils. Type 2 cytokines, including IL-4, IL-5, IL-9, and IL-13, are produced by type 2 innate lymphoid cells (ILC2s) and Th9 cells (which produce IL-9). Apart from their involvement in the inflammatory mechanism of asthma, these cells and their cytokines have been implicated in steroid resistance.

Allergic inflammation is directly affects by IgE influencing central effector cells such as eosinophils, mast cells, and basophils. Activated B cells IL-4 and IL-13 secrete IgE antibodies, responsible for the early phase of allergic reactions. Alongside T cells, IgE significantly contributes to AHR.

Upon stimulation by Th2 cytokines, eosinophils become activated, undergo degranulation, and release cytokines and leukotrienes, contributing to asthma development. Additionally, the authors of this report suggest that eosinophils may play a role in airway remodeling through the production of TGF-β. Basophils have also been implicated in eosinophilic asthma, as increased numbers have been observed in the sputum of asthma patients.

Mast cells are another critical cell type in the mechanism of allergic asthma. Stimulated by IgE and ILs such as IL-33, mast cells release histamine, prostaglandin D (PGD)2, and Th2 cytokines like IL-13 upon activation. These interactions significantly impact smooth muscle function, mucus hypersecretion, and tissue remodelling (Figure 6).

2.2.3 Literature Review on Evaluating Murine Models Through Pathogenesis and PFT

The term "asthma" has evolved over centuries, with its earliest descriptions dating back to ancient Greece. Modern understanding of the disease emerged in the mid-nineteenth century, with advancements in defining its pathological mechanisms and treatment approaches (MCFADDEN JR, 2004). Asthma is characterized by chronic inflammation and structural changes in the airways, resulting in persistent symptoms and reduced lung function controlled by corticosteroids (ROWE et al., 2004, BOONPIYATHAD et al., 2019.

In 2017, EPSTEIN and colleagues authored an overarching article examining the utility of mouse asthma models in discovering and developing novel drugs. Given the prevalence of the OVA asthma model induced in BALB/c mice, the authors provided a more in-depth description of its utilization. Acknowledging the variations, complexities, and challenges

inherent in asthma mouse models, the authors thoroughly assessed the parameters influencing the predictive value of these models in drug discovery endeavours.

An intriguing revelation presented in this review was that the molecules deemed unsuccessful in further development were not necessarily ineffective but somewhat lacked superior efficacy compared to existing standard therapeutics. To mitigate the likelihood of drug development setbacks using mouse asthma models, the authors proposed a pragmatic approach aimed at fostering more dependable and predictive investigations. This approach was distilled into several guiding principles: developing models reflective of asthmatic phenotypes; elucidating the relevant pathways targeted by the drug under investigation; employing multiple models when the mode of action is unclear to delineate involved pathways; implementing appropriate experimental controls; and customizing the model to align with the type of treatment being evaluated.

Selecting a reliable and predictive mouse model becomes more efficient once the appropriate phenotype, pathway, and target are clearly defined. Following these guidelines, experimental designs must incorporate proper control substances. For instance, new drug candidates or tools should be benchmarked against drugs currently on or soon to be on the market, such as inhaled and/or oral steroids, which represent the current standard anti-inflammatory therapy for asthmatics. This step is crucial to ensure that the efficacy of the tested drug is compared to the established effectiveness of existing therapeutics. Successful development of novel medications hinges on their ability to improve symptoms and enhance the quality of life for patients with significant unmet medical needs. However, they should also surpass commercially available drugs, ideally demonstrating superior efficacy and safety profiles.

Another crucial consideration in treatment planning is the timing of therapy initiation in the mouse OVA model. It has been noted that asthma treatment in mice is often initiated at the induction stage rather than when the disease is established. This report advocates for the use of more "clinically relevant" models, where treatment evaluation occurs when lung inflammation is established in OVA-sensitized and challenged mice. Furthermore, this approach emphasizes tailoring the model to the type of treatment. As elucidated in the report, the selection of biomarkers to monitor drug effects in mice and patients should be carefully chosen once the target and target population have been defined.

The study described offers a comprehensive overview of the significance of OVA models for in vivo modelling of human asthma and underscores its considerable translational value for the advancement of novel therapies. In contrast, FEHRENBACH and colleagues (2017) placed greater emphasis on airway remodelling in asthma, recognizing its direct influence on respiratory functionality.

Their definition of airway remodelling is as follows: "It is generally quite broadly defined as any change in composition, distribution, thickness, mass, or volume, and/or several structural components observed in the airway wall of patients relative to healthy individuals."

Asthma patients manifest the findings of airway remodelling in various tissues, including epithelial shedding, goblet cell hyperplasia, basal membrane thickening in the airway epithelium, subepithelial fibrosis in the peribronchial interstitial tissue, hyperplasia and/or hypertrophy of airway smooth muscle cells, increased neurite sprouting in nerve tissue, and changes such as barrier dysfunction and angiogenesis in bronchial vasculature. These structural changes are a response to chronic injury and/or inflammation, leading to persistently altered airway wall structures and function. Therefore, these alterations are defined as pathological airway remodelling.

This review article aims to address several significant aspects. Among them, the following are considered important for further findings in this thesis: what are reliable quantitative approaches to assess airway remodelling, and what can we learn from different animal models to study airway remodelling?

According to these authors, the initial approach to assessing airway remodelling in patients and animal models involves obtaining an unbiased set of representative tissue samples, such as animal lungs and human biopsies. Collected samples must undergo histologic analysis of two-dimensional sections through light, fluorescence, or electron microscopy to provide clear insight into the structural tissue changes.

Previous reports indicate that in asthma patients, a combination of infiltrating cells such as Th cells, eosinophils, neutrophils, and mast cells under the direction of various defined signalling pathways interact with resident cells of the airways, resulting in airway remodelling in chronic conditions. With extensive utilization of mouse models of asthma, it is known that with allergen sensitization, mice develop an adaptive Th2 cell-dominated immune response. Short-term allergen aerosol inhalation or local application of an allergen-containing solution

directs allergic airway inflammation to the airways. This results in allergic airway inflammation with infiltration of eosinophils and Th2 cells, increased mucus production, and AHR, displaying key hallmarks of human allergic asthma.

In their report, FEHRENBACH and colleagues (2017) advocate for long-term OVA exposure models (12 weeks exposure) to mimic airway remodelling processes in mice. However, other articles suggest that repeated OVA exposure in sensitized mice over shorter durations can also induce asthma-related changes.

TRIFILIEFF et al. (2000) published research on inflammatory and remodelling events in murine models, using OVA sensitization and aerosol challenge to study AHR, lung inflammation kinetics, and remodelling. They employed male BALB/c mice in acute and chronic protocols, sensitized with OVA *i.p.* on days 0 and 14 and challenged with nebulized OVA or phosphate-buffered saline (PBS) for 20 min once on day 21 (acute) or daily from day 21 to 25 (chronic protocol). BAL samples were collected for inflammatory cell assessment, protein concentration, cellular fibronectin content, and cytokine levels at various time points. AHR was measured using barometric and whole-body plethysmography, and tissue samples were analysed for cellular proliferation and mucus secretion. The resistance was expressed as an enhanced pause (P_{enh}).

In addition, an extra group for inflammation evaluation was included in the survey presented in this paper. This group was challenged by chronic protocol and treated with an *i.p.* injection of dexamethasone in a dose of 3 mg/kg, one hour before each challenge and sampled three or seven days post-last challenge.

The experiments revealed BAL neutrophil and eosinophil infiltration induced by both acute and chronic protocols. In the acute group, eosinophilia peaked at day three and lasted until day 14, while neutrophil levels peaked on day one and resolved by day three. In the chronic protocol, eosinophilia was more pronounced and present from the first time point, with a 4 to 5-fold increase in eosinophil count observed on day three post-last challenge compared to the acute group. Neutrophils were observed from the first time point in the chronic protocol but significantly increased only at the next time point (six hours post-last challenge).

Other components evaluated in BALF included protein content, which increased from day one, peaked at day three and resolved by day seven in the chronic protocol while remaining

unaffected by the acute challenge. IL-4 and IL-5 levels increased at the first time point and six hours post-challenge in both protocols, with no detection of IFN-γ in the BAL.

Serum IgE levels peaked on day nine following initial sensitization, with a rapid increase following the boost on day 14. Repeated OVA challenges induced a further significant increase in total serum IgE, starting on the first day post-challenge with a peak three days after. Levels began returning to basal values after 14 and 21 days post-last challenge.

Lung remodelling was evaluated by measuring BAL cellular fibronectin content and 5-bromo-29-deoxyuridine (BrdU)-positive epithelial and alveolar cells. After repeated OVA exposures, the chronic protocol showed more pronounced increases in cellular fibronectin content and BrdU-positive cells, indicating greater ECM component production and cellular proliferation.

A similar trend was observed in AHR measurements, with increased P_{enh} responses to Mch levels more pronounced following repeated challenges than the acute protocol.

Dexamethasone treatment was administered three days post-last challenge and fully inhibited AHR in both protocols. Notably, in the acute protocol, it reduced BALF eosinophil and neutrophil numbers, while in the chronic protocol, it decreased BALF eosinophil and lymphocyte numbers, BALF protein levels, and total serum IgE. Additionally, BALF IL-4 and IL-5 levels were reduced in both protocols.

Epithelial cell proliferation was observed on day seven post-last challenge, and dexamethasone significantly reduced allergen-induced epithelial cell proliferation in both protocols. However, the chronic protocol only showed the effect on alveolar cell proliferation. Although epithelial mucus secretory phenotypes induced by the OVA challenge were attenuated in both protocols, complete inhibition was not achieved.

In the article's discussion section, the authors assert that they have characterized an allergen-driven lung inflammation murine model that demonstrates associations between airway inflammation and some remodelling features typically observed in asthmatics. They suggest that the repeated challenge model closely mirrors the pattern of inflammation observed in patients. In conclusion, they propose that the murine model described in the paper could be valuable for evaluating the initial events leading to a comprehensive understanding of asthmatic airway remodelling in patients.

In 2019, KIM and colleagues published a study examining the effects of short-term repetitive OVA challenges on airway inflammation, AHR, histological features, IgE levels, and inflammatory and epithelial cytokines. They aimed to investigate whether different allergen challenge routes could replicate various pathophysiological asthma patterns, reflecting the heterogeneous phenotypes observed in human asthma.

To explore this hypothesis, they utilized female BALB/c mice sensitized *i.p.* on days one and eight with 20 μg OVA in 1 mg aluminium hydroxide. Subsequently, on days 15, 16, and 17 post-sensitizations, mice were subjected to OVA challenge either *via* aerosol exposure or *i.n.* instillation.

Assessment of AHR was conducted 24 hours post-last challenge, while tissue sampling for other evaluated parameters was performed 48 hours post-last challenge.

Results from BALF analysis showed significantly higher total and eosinophil cell counts in both OVA inhalation and *i.n.* OVA groups compared to control groups, along with elevated serum IgE levels. Histological analysis revealed typical features of allergic asthma in both OVA-challenged groups, including eosinophilic infiltration in pulmonary vessels and alveolar ducts, increased mucus production, and elevated numbers of PAS-positive cells per mm basement membrane.

Cytokines IL-4, IL-5, and IL-13, associated with the Th2 response, were identified as crucial in the airway remodelling observed in asthma. Development of AHR was significantly increased in both groups challenged with OVA compared to controls, with a notably higher elevation of IL-13 observed in the group inhaling OVA. This increase in AHR was consistent with the observed resistance to Mch administration.

Elevated levels of epithelial cytokines IL-25 and IL-33 were also detected in BALF and lung tissue of OVA-challenged groups, with a significant upregulation of IL-25 observed in the inhaled OVA group compared to *i.n.* instillation.

Despite more pronounced results in the inhaled OVA group, the authors concluded that both routes of repeated challenges exhibited typical asthma hallmarks, including upregulated Th2 and epithelial cytokines and altered AHR in response to increasing doses of Mch.

A pivotal indicator in evaluating mouse models of asthma, AHR, is frequently cited as a primary outcome measure, as highlighted by LUNDBLAD (2012). This report delves into the techniques for measuring AHR and the factors influencing its interpretation.

In human asthma, AHR is a cardinal feature alongside characteristic signs like cough and airway inflammatory infiltration. However, in animal models, AHR serves as an objective confirmation, yet variables affecting its outcomes are often insufficiently described.

Two main measurement techniques, the FOT and unrestrained plethysmography, are employed for AHR assessment in mouse models. While FOT is invasive and considered the gold standard, unrestrained plethysmography is favoured for its simplicity and repeatability. However, the differences between these techniques in principles and mathematical models can significantly impact result interpretation.

Time is another critical variable in AHR interpretation, as its localization changes over several weeks. An experiment involving OVA-sensitized mice revealed varying AHR profiles at different time points, emphasizing the dynamic nature of AHR over time.

The primary bronchoprovocation agent, Mch, is commonly used due to its solubility and ability to diffuse across barriers. However, considerations such as route of administration and diffusion across epithelial barriers must be accounted for.

The impact of lung volumes and ventilation patterns on respiratory mechanics parameters cannot be overlooked. Standardizing parameters like positive end-expiratory pressure (PEEP) and ventilation pattern is crucial for obtaining reliable measurements.

In conclusion to this review article, the author believes that if all of these variables are carefully implemented in the AHR interpretation, valuable results will be obtained, and assessing AHR in mice models of asthma will continue to be a vital endpoint readout.

READER et al. (2003) conducted a study evaluating inflammatory markers in blood and BALF, along with AHR, in a mouse model of repeated OVA challenge.

Male BALB/c mice were sensitized *i.p.* with OVA and aluminium hydroxide on days zero and seven, followed by OVA exposure *via* inhalation on days 14, 17, and 20. AHR was assessed 48 hours after the last exposure using increasing doses of Mch. Subsequently, blood, BALF, and lung samples were collected for analysis.

The results demonstrated that allergen sensitization and nebulized challenge induced asthma-like changes, including airflow obstruction, AHR, and eosinophilic and lymphocytic inflammatory infiltrates. Additionally, sensitized and challenged animals exhibited heightened AHR to increasing concentrations of nebulized Mch, elevated levels of eosinophils and leukocytes in BALF, and increased serum IgE compared to non-challenged controls.

Several articles were encountered during the literature review on utilizing AHR in murine asthma models. However, a study conducted by WALKER et al. (2013) stood out due to its insights into relevant aspects of this research. This study aimed to address clinically relevant components of disease and asthma control assessments, focusing on murine changes significant to this disorder and its translational potential.

In clinical practice, asthma management is based on four key domains: symptoms, airway inflammation, airway obstruction, and AHR. While symptoms serve as a crucial tool for disease control in patients, translating this aspect to mice poses challenges, as their inability to communicate symptoms complicates the assessment process.

Biomarkers such as exhaled nitric oxide, sputum, and serum eosinophils help identify allergic asthma phenotypes but are deemed less relevant for assessing asthma control. While inflammation, assessed directly through bronchoscopy and biopsy, is not routinely conducted in patients, such assessments are more readily available in mice, allowing for comprehensive immunological and histological evaluations. However, the authors emphasize the importance of complementing immunological outcomes with lung mechanics assessments.

Lung function measurements and AHR serve as crucial indicators and predictors of asthma progression in patients. Thus, optimizing these methods for use in mice would be advantageous. Despite the pros and cons outlined for invasive AHR techniques, they are regarded as providing reproducible, consistent, and meaningful data, making them the standard for assessing murine lung mechanics. Although the FOT has gained prominence in animal models, it is not commonly utilized in clinical settings. Alongside method recommendations, standardizing protocols and reports for murine lung mechanics measures is deemed the most impactful suggestion.

Commonly reported AHR parameters in mice, Ri and Cdyn, are derived from the equation of motion, incorporating transpulmonary pressure, airflow, and TV measurements. The exact relationship between Ri and Cdyn with lung structure is not fully elucidated.

However, the authors suggest that Ri is directly linked to airway luminal diameter, while Cdyn is inversely related to the degree of airway closure.

The article highlights the need to standardize AHR methodologies due to their significant impact on lung mechanics and animal health. Mechanical ventilation parameters like PEEP, breathing frequency, and TV influence lung Cdyn and airway Ri. Research indicates that PEEP helps maintain airway pressure during the passive part of breathing out. This process increases the amount of gas in the lungs at the end of a breath compared to what would be there without PEEP. In animals like mice, which have very flexible chest walls, PEEP is particularly important because it helps prevent the airways from closing off at the end of a breath, which is a natural tendency without this supportive pressure.

Introducing PEEP can restore lung volumes close to conscious levels, counteracting anesthesia's negative effects on respiratory mechanics.

The guideline recommends planning Mch concentrations based on achieving a 50% increase in baseline Ri, which serves as a physiologically relevant midpoint for the resistance curve.

The Ri curve is constructed by plotting baseline values and post-exposure responses to escalating Mch doses on the ordinate and abscissa, respectively. Interpretation hinges on curve shifts and slope changes: a leftward shift signifies heightened sensitivity, while slope alterations indicate reactivity. Reactivity denotes airway constriction in response to a constrictor stimulus, while sensitivity pertains to reactions to lower doses. The article suggests that changes in the dose-response curve slope in mice hold considerable translational significance.

In human bronchoprovocation tests, exposure to increasing constrictor concentrations is similar; however, FEV1 measurements follow each exposure. While FEV1 values cannot directly correlate with Ri in mice, the translational relevance of AHR measurements remains undeniable.

Assessing airway obstruction in asthma patients involves lung function tests like spirometry, which measure parameters like FEV1 and the Tiffeneau index to describe airflow limitations. These tests are routinely used in clinical settings. However, a different approach is necessary in mice due to the absence of voluntary maneuvers. Instead, a negative pressure expiration technique is employed to simulate a forced expiratory maneuver.

In a manner reminiscent of the previous section discussing literature findings on PFT in the BLM-induced fibrosis model in mice, the study led by VANOIRBEEK and colleagues (2010) emerges as a pivotal investigation in evaluating pulmonary function and AHR using the FlexiVent® and Buxco® systems in the OVA asthma model. This study, which focused on male BALB/c mice aged seven weeks, involved sensitizing the mice to OVA every other day from day one to day 13, administering a total of seven *i.p.* injections of OVA at a concentration of 10 µg in 0.5 mL saline. Subsequently, the mice underwent whole-body exposure to nebulized OVA challenge from day 33 to day 40, at a concentration of 6-10 mg/mL daily. Invasive pulmonary function measurements were conducted 24 hours after the final challenge, followed by AHR assessments using increasing Mch concentrations and fast flow expiration maneuvers utilizing the Buxco® system. Following the measurements, BALF and lung samples were collected for analysis, with untreated and age-matched mice serving as the control group.

Analysis of BALF revealed a pronounced eosinophilic inflammation, and lung histopathology was characterized by severe peribronhovascular neutrophilic and eosinophilic inflammation, which extended to the distal bronchioles. Pulmonary function parameter values pre- and post-Mch exposure are presented in Table 2. The study highlighted specific findings from the PFTs that reflect the characteristics of asthma. In a significant study on asthma model, researchers found a marked increase in respiratory Ri when subjected to a Mch challenge, highlighting the AHR characteristic of asthma. This response was consistently observed across invasive measurement techniques utilized in the study, reinforcing its validity. Interestingly, at the outset, the models did not display the kind of airflow obstruction or limitation typically seen in chronic human asthma cases, suggesting that employed acute mouse models may not fully capture the structural airway changes associated with long-term asthma.

Upon Mch challenge, the OVA-asthma model revealed a pronounced decrease in lung Cdyn and a rise in airway Ri, indicating bronchoconstriction and heightened airway Ri responses that are symbolic of asthma. Significant reductions in FEVs and FEFs, such as the FEV200 and PEF, after the Mch provocation further evidenced this. These reductions mirror the decrease in FEV1 seen in asthmatic humans, underscoring substantial airway constriction in response to the challenge.

The study did not measure FEV1 directly due to the differences in lung physiology and measurement techniques between mice and humans. However, the observed decrease in the FEV200/FVC ratio and related measures post-challenge implied a reduction in the Tiffeneau

index, akin to the diminished FEV1/FVC ratio noted in asthmatic patients, signifying airflow obstruction.

Moreover, the analysis of F-V loops following the Mch challenge unveiled patterns of expiratory flow limitation towards the end of expiration in asthmatic mice, aligning with the airflow limitation associated with asthma due to bronchoconstriction. These findings collectively contribute to a deeper understanding of asthma's physiological manifestations and underscore the utility of these models in studying the disease's pathophysiology and potential therapeutic interventions.

Table 2 Overview of lung function parameters in the BLM-fibrosis and OVA-asthma models reported in VANOIRBEEK et al., 2010.

BALB/c mice values were measured using the Buxco® system in control animals and animals in BLM and OVA models of fibrosis and asthma. Values are expressed as mean ± sem. Parameters values measured in the system's first three sequences are listed in the table. In the OVA asthma model, the fast flow volume test sequence parameters were measured post-exposure to methacholine and listed in the table. *p<0.05 decrease and **p<0.05 increase compared to the untreated control mice

Buxco® system test	Parameter (unit)	Control (n=7)	BLM fibrosis (n=10)	OVA asthma pre-Mch (n=7)	OVA asthma post-Mch (n=7)
Boyle's Law FRC	FRC (mL)	0.28 ± 0.07	0.28 ± 0.12	0.22 ± 0.07	/
Quasistatic pressure volume	IC (mL)	1.03 ± 0.10	0.79 ± 0.11*	0.88 ± 0.22	/
	VC (mL)	1.17 ± 0.09	0.91 ± 0.17*	0.96 ± 0.19	/
	TLC (mL)	1.31 ± 0.16	1.07 ± 0.20	1.10 ± 0.24	/
	ERV (mL)	0.13 ± 0.09	0.12 ± 0.07	0.08 ± 0.06	/
	RV (mL)	0.15 ± 0.14	0.16 ± 0.11	0.14 ± 0.09	/
	Cchord (mL/cm H2O)	0.07 ± 0.01	0.05 ± 0.01*	0.06 ± 0.01	/
	Ti (sec)	1.48 ± 0.19	1.16 ± 0.15	1.33 ± 0.35	/
	Te (sec)	0.90 ± 0.07	0.67 ± 0.09*	0.77 ± 0.12	/
Fast flow volume	IC (mL)	0.97 ± 0.08	0.76 ± 0.13*	0.86 ± 0.24	0.68 ± 0.23*
	FVC (mL)	1.12 ± 0.10	0.89 ± 0.17	0.92 ± 0.22	0.69 ± 0.25*
	Ti (sec)	1.34 ± 0.09	1.13 ± 0.17	1.24 ± 0.39	1.00 ± 0.30
	Te (sec)	0.19 ± 0.04	0.16 ± 0.04	0.18 ± 0.05	0.23 ± 0.07
	ERV (mL)	0.14 ± 0.04	0.13 ± 0.05	0.07 ± 0.06	0.01 ± 0.05
	FEV100 (mL/sec)	1.05 ± 0.09	0.83 ± 0.16	0.85 ± 0.17	0.60 ± 0.17*
	FEV200 (mL/sec)	1.12 ± 0.09	0.89 ± 0.17*	0.92 ± 0.20	0.67 ± 0.22*
	PEF (mL/sec)	16.31 ± 3.24	20.87 ± 2.46**	18.68 ± 2.09	16.70± 3.02

Abbreviations: FRC-forced residual capacity, IC-inspiratory capacity, VC-vital capacity, TLC-total lung capacity, ERV-expiratory reserve volume, RV-residual volume, Cchord-chord compliance, Ti-inspiration time, Te-expiration time, FVC-forced vital capacity, FEV-forced expiratory volume, PEF-peak expiratory flow.

3 DISSERTATION GUIDELINES

3.1 OBJECTIVES

The study aimed to establish baseline lung function values in mouse models using standard human treatments for IPF (nintedanib, pirfenidone) and asthma (dexamethasone, fluticasone). This foundation seeks to accelerate the development of new treatments for human pulmonary diseases through PFT evaluation in two specific mouse models of respiratory conditions by encompassing specific goals for each:

A) Model of Bleomycin-Induced Pulmonary Fibrosis

1. Initiating fibrosis between day 7 (D7) and day 21 (D21) through a single BLM dose on day 0 (D0).
2. Observing characteristic fibrotic lesions in the control group by D21 post-BLM.
3. Administering pirfenidone and nintedanib orally to test groups from D7, aiming to mitigate fibrosis development.
4. Comparing clinical progression across groups over the 21-day study.
5. Assessing lung function differences *via* PFTs in all groups.
6. Establishing a link between lung pathology extent and functionality through histological and IHC analyses.
7. Demonstrating significant differences using statistical analyses between:
    - The control group with advanced fibrosis and healthy, untreated mice.
    - BLM-challenged groups receiving standard treatments and the control group.

B) Model of Ovalbumin-Induced Asthma

1. Developing a 24-day acute asthma mouse model, with the positive control group showing peak eosinophilic asthma lesions after four consecutive ovalbumin bronchial challenges on days 20-23.
2. Mitigating inflammation in test groups with oral dexamethasone or inhaled fluticasone propionate during the challenge phase on days 20-23.
3. Evaluating lung function differences through a bronchoprovocation test using escalating Mch doses 24 hours post-final OVA challenge.
4. Comparing pulmonary function across all groups before and after Mch exposure to highlight intergroup differences.
5. Analyzing BALF for variations in inflammatory cell types, IgE, and cytokines IL-4, IL-5, and IL-13.

6. Establishing a correlation between lung pathology severity and functional capacity.
7. Statistically validating significant distinctions between:
    - Healthy, untreated mice and the positive control group with acute eosinophilic asthma lesions.
    - The positive control group with advanced lesions and the test groups treated with dexamethasone and fluticasone propionate.

3.2 HYPOTHESIS

The assumption was that animal models' retrograde evaluation of available treatment, so-called "gold standards," would demonstrate similar effects as in humans. The hypothesis was evaluated using clinically relevant analyses such as PFTs in preclinical models. In mouse models of BLM-induced pulmonary fibrosis and OVA-induced asthma, standard treatment with pirfenidone and nintedanib in the former, and dexamethasone and fluticasone in the latter, will improve values of lung function parameters. This included reduction of AHR and increased lung functionality, correlating with a reduction in pathological changes in the lungs. Determining the efficacy range for these "gold standards" (or clinically approved) therapies in mouse models of lung fibrosis and allergic asthma will improve the translatability of these models by enabling better selection of new molecules and further clinical research in future studies.

4 MATERIAL AND METHODS

The survey incorporated two mouse models: BLM-induced pulmonary fibrosis and OVA-induced asthma. Each model underwent a separate experiment, conducted over two days, limited by the measurement capabilities of DSI's Buxco® PFT and RC systems.

4.1 ANIMALS

Two strains of SPF (specific pathogen-free) mice were utilized in the study: C57BL/6NCrl mice for the BLM-induced pulmonary fibrosis model with a total of 70 animals (n=70) and BALB/cAnNCrl mice for the OVA-induced asthma model, involving 48 animals (n=48). Both strains were acquired from Charles River Deutschland GmbH, Sulzfeld, Germany.

4.1.1 Animals Husbandry

All mice were housed in conventional polysulfone cages (TECNIPLAST S.p.A., Buguggiate VA, Italy, cages, type III) with a 3-4 cm thick ALPHA-dri® dust-free bedding (pure cellulose fiber, uniform particle size 5mm sq, highly absorbent, LBS Serving Biotechnology, London, UK). Each cage was enriched with cotton nestlets for nest-making and paper shelter (Lillico Serving Biotechnology, London, UK).

Cages were supplied with high-fat pelleted food for mice (SDS VRF 1 (P), LBS Serving Biotechnology, London, UK), and water coming from municipal water main (bottles TECNIPLAST S.p.A., Buguggiate VA Italy); ad libitum.

Room conditions were set to a temperature of 22°C ±2, relative humidity of 55% ±10, and a cycle of 15 - 20 air changes per hour. A light cycle of 12 hours of light/dark was maintained. The animals were tested during the light period.

4.1.2 Animal Welfare and Euthanasia Criteria

All experimental procedures were approved by the internal ethical committee CARE (Committee on Animal Research Ethics) of Fidelta d.o.o. (CAREZG_13-06-14_44, CAREZG_07-06-20_03, CAREZG_17-03-3066), the Ministry of Agriculture of the Republic of Croatia (UP/I-322-01/17-01/164 and UP/I-322-01/17-01/133) and Veterinary Faculty of Zagreb (640-01/19-17/63).

Animals that reached respiratory models' euthanasia criteria were excluded from the experiments according to the clinical score system described by HUET et al., 2013, and TALBOT et al., 2020.

Animals were examined twice a day clinically during the 21 days in the BLM-induced pulmonary fibrosis model and 24 days in the OVA-induced asthma model.

Body weight was measured using a precise analytical balance, and individual body weight was recorded daily: in the BLM-induced pulmonary fibrosis starting from the challenge day (D0) until the last day of the study (D21); in OVA-induced asthma from the day of the first challenge (D20) until the last day (D24). If an animal was found in a weak condition or with enduring signs of severe distress described in the scoring system (HUET et al., 2013, TALBOT et al., 2020), it was humanely killed.

4.2 ANIMAL MODELS

4.2.1 Model of Bleomycin-Induced Pulmonary Fibrosis

A BLM-induced pulmonary fibrosis model was obtained to investigate pulmonary function changes using an invasive test system in restrictive pulmonary disorder.

4.2.1.1 Experimental Groups

Male C57BL/6NCrl mice, nine weeks old, with an approx. bodyweight of 24 g were allocated into four groups: PBS challenged control group (PBS Ctrls, n=10), BLM challenged positive control group (BLM Ctrls, n=20), BLM challenged and nintedanib treated (BLM/Nintedanib, n=20) and BLM challenged group and pirfenidone treated group (BLM/Pirfenidone, n=20) (Table 3). In total, 70 mice were enrolled in this experiment.

Table 3 Bleomycin-induced pulmonary fibrosis experiment design
List of experimental groups, challenge, treatment regimen, and sampling of animals in the BLM-induced pulmonary fibrosis study

Groups		No of mice	Challenge on D0	Dose	Treatment regimen Days	Sampling on D21
1	**PBS Ctrl**	**10** (1-10)	**PBS *i.n.***	**NA**	**NA**	**PFT and lung tissue**
2	**BLM Ctrl**	**20** (11-30)	**Bleomycin 30 µg/50 µL/ mouse *i.n.***	**10 mL/kg**	**D7-D21 *bid p.o***	
3	**BLM/ Nintedanib**	**20** (31-50)		**60 mg/kg**	**D7-D21 *bid p.o.***	
4	**BLM/ Pirfenidone**	**20** (51-70)		**100 mg/kg**	**D7-D21 *bid p.o***	

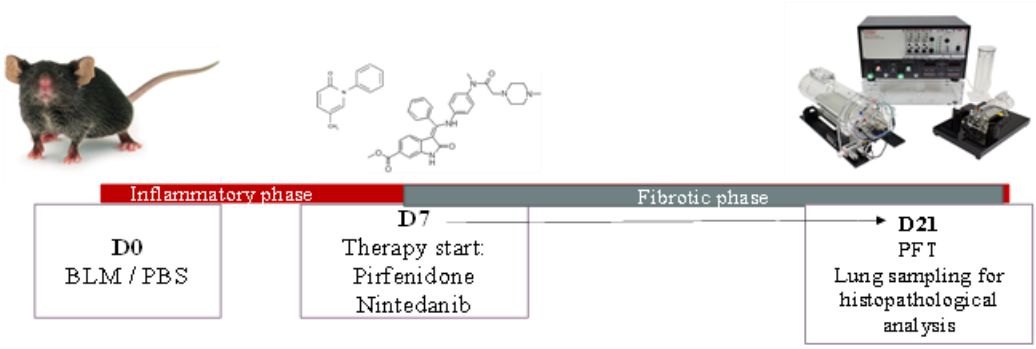

Figure 7 BLM-induced pulmonary fibrosis model scheme
C57Bl/6 mice were subjected to a challenge on day 0 of the study, with treatments starting on day 7. Pirfenidone and nintedanib were administered daily up to day 21. Pulmonary function tests were conducted on the final day, and lung samples were collected for subsequent analysis afterward.

Abbreviations in Table 3 and Figure 7: PBS-phosphate buffer saline, Ctrl-control, BLM-bleomycin, No.-number, *i.n.*-intranasally, NA- not applied, *bid*-twice a day, *p.o.*- perorally, D-day, PFT-pulmonary function tests

4.2.1.2 Bleomycin Preparation, Challenge, and Anesthesia

Pulmonary fibrosis in mice was developed by *i.n.* instillation of BLM sulfate (Enzo Life Sciences, Inc., New York, USA) on the first day of the experiment, marked as day zero (D0). Animals in the first control group received PBS (Merck KGaA, Darmstadt, Germany) *i.n.*, while animals in the positive control group and testing groups were challenged with BLM. An experiment lasted for 21 days. PFT measurements were performed on the last day of the experiment, and lungs were sampled for histopathological analysis (Table 3, Figure 7).

Prior to *i.n* administration, mice were anesthetized with a combination of ketamine hydrochloride (Bioveta, a.s. the Ivanovice na Hané, Czech Republic) and xylazine hydrochloride (Alfasan International B.V, Woerden, Netherlands). A working solution of 4 mg/ 10.2 mL xylazine and 100 mg/ 10.2 mL ketamine concentration was administered *i.p.* at a volume of 10 mL/kg.

A BLM sulfate was dissolved in PBS and applied to the mouse at an app. 30 µg/50 µL/ mouse concentration. The dose of BLM solution for the challenge was approximately 1 mg/kg body weight of the mouse. Installation to lungs was achieved by *i.n.* administration to a mildly anesthetized mouse. For *i.n.* instillation of BLM, mice were held in a tilted supine position with their heads elevated to between 60 and 75 degrees above their feet during and after (for approximately 0.5 minutes) administration.

4.2.1.3 Treatment Preparation and Administration Regimen

Referent substances or vehicle treatment started on day seven and lasted until day 21 of the experiment, each day at approximately the same time. Nintedanib and pirfenidone were administered orally (*p.o.*), with approx. 7.5 h interval between two daily administrations (Table 3, Figure 7).

The BLM-challenged positive control (BLM Ctrls) group was administered only with 0.5% carboxymethylcellulose (CMC) solution. Based on the 3R rule of reduction of animals, the group receiving 0.1% hydroxyethyl-cellulose solution as a vehicle was not included because results were known from previous experiments (HRVAČIĆ et al., 2018, ANZULOVIĆ ŠANTA et al., 2023).

Animals from the first testing group (BLM/Nintedanib) were administered with nintedanib (methyl 2-hydroxy- 3 -[N -[4 -[methyl -[2 - (4 – methylpiperazin –1 – yl) acetyl] amino] phenyl] -C-enylcarbonimidoyl] - 1H-indole-6-carboxylate, eNovation Chemicals LLC, New Jersey, USA) in a dose of 60 mg/kg twice daily (*bid*). Nintedanib formulation was prepared by dissolving the dry compound in a 0.1% hydroxyethyl-cellulose solution (Merck KGaA, Darmstadt, Germany) at 6 mg/mL concentration (Table 3).

The second testing group (BLM/Pirfenidone) was administered with pirfenidone (5-methyl-1-phenylpyridin-2(IH)-one; BePharm Ltd., Münster, Germany) in a dose of 100 mg/kg *bid*. The formulation was prepared by dissolving the dry compound in a 0.5% CMC (Sigma-Aldrich Chemie GmbH, Munich, Germany) in a concentration of 10 mg/mL (Table 3**)**.

4.2.1.4 Sampling Procedures

On the 21st day after challenge with BLM or PBS, lung function was assessed using the DSI's Buxco® PFT system. Following the PFT measurements, the mice were euthanized due to anesthesia overload, and lung samples were collected for histopathological analysis. Each sample was carefully labeled with details like the experimental code, tissue type, group, and animal numbers to maintain consistency across all analyses.

The recorded values for each parameter from surviving animals were statistically analyzed and compared with those from the BLM control group. This comparison extended to histomorphological evaluations, including the Ashcroft score and the levels of αSMA and COL1A1.

4.2.2 Model of Ovalbumin-Induced Asthma

In the OVA-induced asthma model, functional characteristic of obstructive pulmonary disorders were investigated using invasive PFT and assessments of AHR.

4.2.2.1 Experimental Groups

Male BALB/cAnNCrl mice, eight weeks old with approx. 23 g of body weight were allocated into four groups: PBS-sensitized and saline-challenged control group (PBS/Saline Ctrls, n=8), OVA sensitized and OVA-challenged positive control group treated with respective vehicle (OVA/OVA Ctrls, n=10), OVA sensitized and OVA-challenged group treated with dexamethasone (OVA/OVA Dexamethasone, n=10) and OVA sensitized and OVA challenged group treated with fluticasone propionate (OVA/OVA Fluticasone propionate, n=10) (Table 4). In total, 48 mice were enrolled in this experiment.

Table 4 Ovalbumin-induced asthma experiment design
List of experimental groups, sensitization, treatment regimen, challenge, and sampling of animals in the OVA-induced asthma study

Group no	No of mice	Treatment	Sensitization *i.p.* D0 and D14	Dose *qd*	Treatment regimen D20-23	Challenge *i.n.* D20-23	24 h post-challenge
							Procedures/ sampling D24
1	**8** (1-8)	**PBS/Saline Ctrls**	**PBS**	**0.2 mL**	**NA**	**saline *i.n.*/mouse**	**PFT** **AHR** **BALF cellular composition and cytokines analysis** **Lungs for histopathology**
2	**10** (9-18)	**OVA/OVA Ctrls**	**10 µg OVA / 2 mg Alu-Gel-S / 0.2 mL /mouse**	**Vehicle 0.5 % CMC *p.o.***	**60 minutes prior to the challenge**	**50 µg OVA / 50 µL saline/ animal *i.n.***	
3	**10** (19-28)	**OVA /Dexamethasone**		**3 mg/kg *p.o.***			
4	**10** (29-38)	**OVA/OVA Ctrls**		**Vehicle Tween/Saline vehicle (0.2/99.8) *i.n.***	**30 mins prior to the challenge**		
5	**10** (39-48)	**OVA/ Fluticasone propionate**		**2 mg/kg *i.n.***			

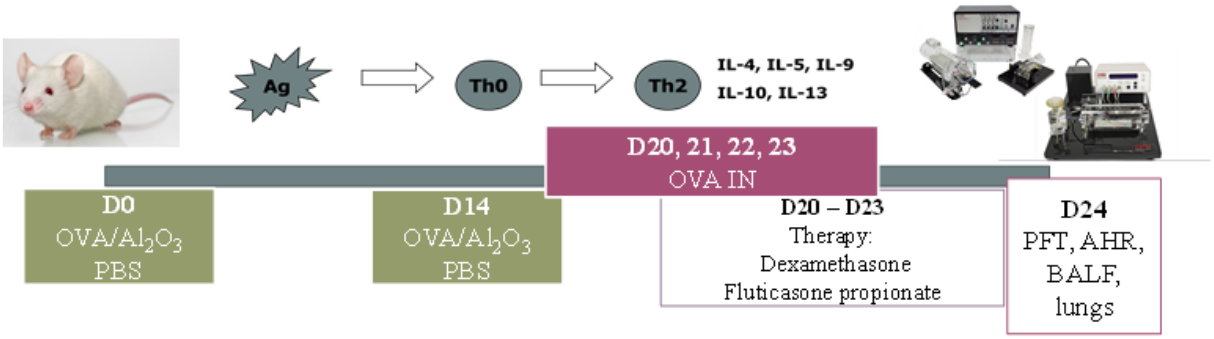

Figure 8 OVA-induced asthma model scheme
Balb/c mice were sensitized *i.p.* with the solution of OVA in aluminium hydroxide on days 0 and 14 of the experiment. Starting from day 20, mice were challenged *i.n.* daily until day 23, and treatment was applied each day before the challenge. On day 24, pulmonary function testing and airway hyperresponsiveness measurements were performed, followed by bronchoalveolar lavage and lung sampling.

Abbreviations in Table 4 and Figure 8: Ag-antigen, IL-interleukin, OVA-ovalbumin, PBS-phosphate buffer saline, Ctrls-controls, *i.p.*- intraperitoneally, No.-number, *i.n.*/IN-intranasally, *qd*-once daily, NA-not applied, *p.o.*-perorally, D-day, AHR-airway hyperresponsiveness, PFT-pulmonary function tests, BALF-bronchoalveolar lavage

4.2.2.2 Ovalbumin Preparation, Sensitization, Challenge, and Anesthesia

Acute asthma in mice was developed by systemic immunization with the antigen ovalbumin and subsequently challenged directly through the airways with the same antigen (Table 4, Figure 8).

Systemic immunization was conducted twice, on the first day of the experiment, marked as day zero (D0) and day 14 (D14). Ovalbumin (grade VI, Sigma-Aldrich Chemie GmbH, Munich, Germany) emulsified in aluminium hydroxide Al_2O_3 (Alu-Gel-S, SERVA Electrophoresis GmbH, Heidelberg, Germany) was injected *i.p.*

The direct challenge of airways was conducted four times by *i.n.* instillation of OVA solution on days 20, 21, 22, and 23 of the experiment. In the first control group, animals received PBS (Merck KGaA, Darmstadt, Germany) *i.p.* on D0 and D14, and saline (0.9%; Pliva, Zagreb, Croatia) *i.n.* on D20, 21, 22, and 23. Animals in the positive control groups (OVA/OVA Ctrls *p.o.* and *i.n.*) and testing groups (OVA/OVA Dexamethasone and OVA/OVA Fluticasone propionate) were sensitized and challenged with OVA as described. An experiment lasted for 24 days (Table 4, Figure 8).

The solution of OVA in aluminium hydroxide for the sensitization on D0 and D14 was prepared by dissolving OVA lyophilized powder in PBS (Merck KGaA, Darmstadt, Germany)

followed by emulsification of OVA solution in aluminium hydroxide. The final emulsion resulted in a 50 µg OVA/10 mg Al_2O_3/1 mL concentration.

The dose of OVA/Al_2O_3 solution for the sensitization was 10 µg OVA/2 mg Al_2O_3/0.2 mL per mouse.

The solution for the challenge was prepared fresh on the day of administration by dissolving OVA lyophilized powder in saline at 1 mg/mL concentration. Challenge installation to lungs was achieved by *i.n.* administration of 50 µL of OVA/saline solution to a mildly anesthetized mouse. For *i.n.* instillation of OVA/saline, mice were held in a tilted supine position with their heads elevated to between 60 and 75 degrees above their feet during and after (for approximately 0.5 minutes) administration.

Prior to *i.n* administration, mice were anesthetized with a combination of ketamine hydrochloride (Bioveta, a.s. the Ivanovice na Hané, Czech Republic) and xylazine hydrochloride (Alfasan International B.V, Woerden, Netherlands.). A working solution at a concentration of 4 mg/ 10.2 mL of xylazine and 100 mg/ 10.2 mL of ketamine was administered *i.p.* at a dosing volume of 10 mL/kg.

4.2.2.3 Treatment Preparation and Administration Regimen

Treatment with two referent substances or respective vehicles started on D20 and lasted until D23 of the experiment, each day at approximately the same time. Both substances were administered once daily, *i.n.* or *p.o.*, 30 or 60 minutes prior to the OVA *i.n.* challenge (Table 4, Figure 8).

OVA-challenged positive control groups were administered with vehicles respective to the tested substances, dexamethasone or fluticasone propionate, in the same treatment regimen.

The respective vehicle administered positive control group (OVA/OVA Ctrls *p.o.*) was administered with 0.5% CMC solution at the same treatment regimen as the group treated with dexamethasone (OVA/OVA Dexamethasone).

The second respective vehicle administered positive control group (OVA/OVA Ctrls *i.n.*) was administered with Tween™ 80/saline (v/v, 0.2/99.8) solution at the same treatment regimen as OVA/OVA Fluticasone propionate group.

Animals from the first testing group (OVA/OVA Dexamethasone) were treated with dexamethasone ((11β,16α)- 9 -Fluoro - 11,17,21 – trihydroxy – 16 – methylpregna - 1,4 – diene - 3,20 - dione, Sigma-Aldrich Chemie GmbH, Munich, Germany). The administration was given *p.o.* in a dose of 3 mg/kg once daily (*qd*), 60 minutes prior to the OVA *i.n.* administration on all four challenge days (Table 4). Dexamethasone formulation was prepared by dissolving the dry compound in a 0.5% CMC solution (Sigma-Aldrich Chemie GmbH, Munich, Germany) at 0.3 mg/mL concentration.

The second testing group was treated with fluticasone propionate ((6α,11β,16α,17α)- 6,9- Difluoro- 11- hydroxy- 16- methyl- 3- oxo- 17- (1-oxopropoxy) androsta- 1,4-diene- 17- carbothioic acid S-(fluoromethyl) ester, Sigma-Aldrich Chemie GmbH, Munich, Germany). The administration was *i.n.*, in a dose of 2 mg/kg *qd*, 30 minutes prior to the OVA *i.n.* administration on all four challenge days (Table 4).

The formulation was prepared by dissolving the dry compound in a solution of Tween™ 80 (Sigma-Aldrich Chemie GmbH, Munich, Germany) and saline (v/v, 0.2/99.8) in a final concentration of 0.8 mg/mL.

4.2.2.4 Sampling Procedures

On D24, approximately 24 hours following the last *i.n.* instillation of OVA solution or saline, AHR, and lung function measurements were performed using DSI's Buxco® PFT system (Figure 9) and Buxco® RC (Figure 10). Post AHR and PFT measurements, mice were euthanized with anesthesia overload, BAL was performed, and samples of lungs were taken (Table 4, Figure 8). All collected samples were labeled with experimental code, tissue type, group no., and animal no. Through all analyses, the values conducted had the same labels.

PFT and AHR parameter values of individual animals that survived until the end of the experiment were recorded and statistically compared to respective vehicles. The following analyses were compared to obtain results: cellular composition, ILs and IgE levels in the BALF, and histomorphological values of general inflammation, epithelial damage, and goblet cell metaplasia score (Table 4, Figure 8).

4.3 PULMONARY FUNCTION TESTING

4.3.1 Buxco® Pulmonary Function Test

Buxco® PFT (DSI™, New Brighton, USA) is a system for the animal in vivo invasive lung function measurement, similar to spirometry in cooperative humans (Figure 9).

This type of measurement requires the animal to be anesthetized and instrumented before airway functions can be measured. Animals were intubated extra-oral by tracheostomy procedure, inserting a tracheal tube into the trachea directly to the lung and avoiding interference of upper airways. Measurements were performed on the experiment's last day, regardless of the employed model, due to the invasiveness of the tracheostomy surgical procedure.

4.3.1.1 Anesthesia and Tracheostomy Procedures

Mice were anesthetized with a combination of ketamine hydrochloride and xylazine hydrochloride for surgery at 100 mg/kg and 10 mg/kg concentration and applied to an animal in 10 mL/kg volume.

The procedure for tracheostomy in an unconscious animal, typically performed in a supine position, involves testing the depth of anesthesia by pinching the hind paw or ear to ensure no reflex response. Once confirmed, a median cervical incision is made to access the trachea. Surrounding tissues, including the thyroid gland and muscles, are carefully moved aside to reveal the larynx and trachea. A precise cut between tracheal rings allows for the insertion and secure placement of a tracheal catheter, typically an 18 Gauge Stainless Tube shortened to around 25 mm, which is then fixed with one or two ligatures using MERKSILK Sole 4-0 (Ethicon, New Jersey, USA).

4.3.1.2 System Set-up

Invasive techniques were employed to measure parameters such as airway pressure, lung volumes and capacities, pulmonary Ri, and Cdyn. To ensure accuracy, animals were kept unconscious to eliminate spontaneous breathing, with ventilation controlled by a computer-operated system. This setup maintained constant TV and respiratory rate, with the ventilator programmed to deliver 120 breaths per minute, a maximum mouth pressure of 8-10 mmH2O, and a deep breath peak of 40 mmH2O.

Prior to conducting measurements, the system underwent calibration in line with the Fine Pointe™ PFT manual's guidelines. For the actual PFTs, a new study was set up in the Buxco® FinePointe™ software, categorizing animals into groups as delineated in Table 3 and Table 4.

4.3.1.3 Test Sequences

The animals were loaded into a plethysmograph, and the tracheal catheter was connected to the system. Measurement was initiated by manually starting the task sequence in the FinePointe™ program. Four test sequences were applied to every animal. During the first three measuring sequences, the animal was breathing spontaneously. After it was completed, mechanical ventilation was used for the RC measurements.

Three semiautomatic maneuvers were performed with the Buxco system: Boyle's law FRC, quasistatic P-V, and fast flow volume maneuver.

The FRC was determined with Boyle's law FRC. The R2 measurement indicates success in this task and should be closer to 1.

A second test sequence in a row, the quasistatic P-V maneuver, was performed to measure TLC, RV, IC, VC, Te, and Cchord. Lungs were inflated to a standard pressure of +30 mmH_2O and then slowly exhaled to a negative pressure of -30 mmH_2O.

With the fast flow volume maneuver, third test sequence, forced expiratory flows (FEFs) as PEF and FEF, Te, Ti, and FEVs, such as FVC, FEV100, and FEV200, were recorded. In this test, the lungs are first inflated to 3 cm H_20 and then quickly exhaled.

After these three task sequences were performed, the automated maneuver RC sequence was started with obliquity automatic ventilation of the animal.

The PFT sequence fast flow volume maneuver was repeated post-AHR test in the OVA-induced asthma model.

Each maneuver was repeated in each animal until three acceptable measurements were recorded, of which the average was then calculated. Data were calculated using an automated data acquisition software Fine pointe™ (Buxco®).

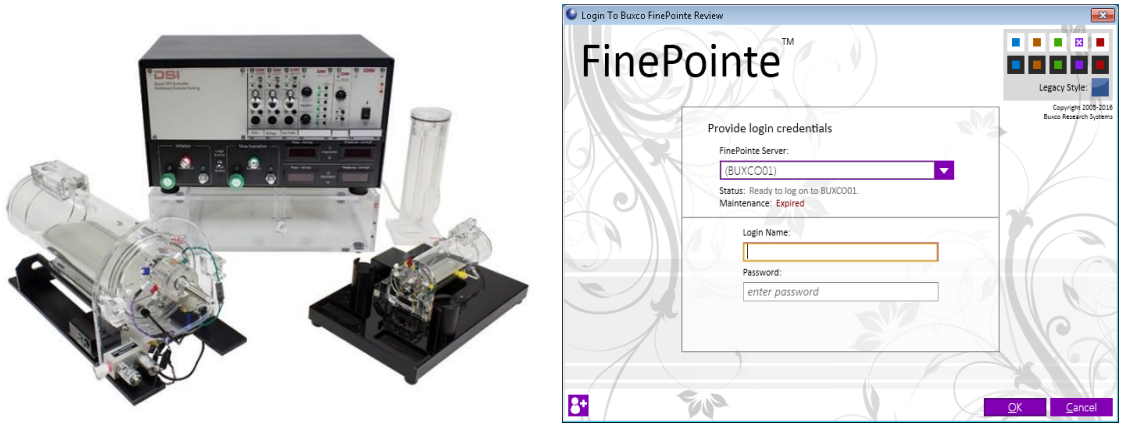

Figure 9 Buxco© Pulmonary Function Test
PFT controller, plethysmograph, and calibration tower are on the left, and Fine Pointe™ software is on the right (www.datasci.com).

4.3.2 Buxco® FinePointe Resistance and Compliance

DSI's Buxco® FinePointe Series RC (DSI™, New Brighton, USA) sites provide the hardware necessary to collect invasive Ri and Cdyn in anesthetized animals.

The RC system is a FOT similar to the PFT system. This system enables the nebulization of liquids. A nebulizator is a part of the hardware that converts liquids into an aerosol using ultrasound technology, enabling in-line aerosol delivery to the lungs (Figure 10). RC system measurements were only conducted in the OVA asthma model, evaluating AHR as a bronchoconstriction reaction provoked by aerosolized Mch (2-acetyloxypropyl(trimethyl)azanium;chloride, Sigma-Aldrich Chemie GmbH, Munich, Germany).

4.3.2.1 Animal Preparation and Methacholine Delivery

The animal preparation and connection for the Buxco® PFT involve several steps. Initially, mice undergo anesthesia followed by tracheostomy surgery, during which a tracheal tube is inserted. After the surgery, the mice are positioned supine within a plethysmograph, and a tube filled with a water/ethanol mixture is inserted two-thirds down the esophagus to ensure proper esophageal pressure measurement.

Once the mice are secured in place, the tracheal tube connects them to a mechanical ventilation system, allowing for direct measurement of respiratory flow and lung pressure. To ensure muscle relaxation and prevent reflexive movements during testing, each mouse receives an *i.p.* injection of diluted ketamine (1 ml ketamine mixed with 9 ml saline), administered at a

dosage of 0.1 mL/10 g body weight. This comprehensive preparation ensures accurate and reliable pulmonary function measurements.

4.3.2.2 System Set-up

For artificial ventilation during the experiment, a pump was adjusted to a stroke volume proportional to body weight (BW/100) with a set breathing rate of 120 breaths per minute. Measurements of AHR were assessed by initially exposing the mice to aerosolized PBS to establish baseline measurements. Subsequent exposure involved nebulized Mch at escalating concentrations to evaluate AHR. The specific concentrations used were 0.625, 2.5, 5.0, and 12.5 mg/mL, each nebulized for 3 minutes in a 5 µL volume, during which lung functions were meticulously recorded.

The FinePointe™ software facilitated continuous recording of various fundamental parameters throughout the procedure. It automatically calculated Ri and Cdyn values and conducted statistical analyses in real-time. The data collected at each concentration level allowed for the plotting of Ri and Cdyn as curves, visually representing the response of each group to the Mch challenge.

Figure 10 Buxco® FinePointe Resistance and Compliance system
RC controller units (x4), and a computer with Fine Pointe™ software. (www.datasci.com)

4.4 BRONCHOALVEOLAR LAVAGE SAMPLING

Collection of BALF was carried out solely for the subjects in the OVA-induced asthma model. After completing the PFTs, the animals were euthanized using an overdose of anesthesia, specifically a combination of ketamine hydrochloride and xylazine hydrochloride at a dosage of 200/16 mg/kg.

4.4.1 Euthanasia and BAL Procedure

The trachea was cannulated using plastic tubes (Instech Laboratories, Inc., Gravers, USA) to collect BALF from mice in the OVA asthma model. Cold PBS was used as the lavage fluid. Three volumes (0.4 + 0.3 + 0.3 ml, a total of 1 ml) were gently instilled and withdrawn on three consecutive occasions using a 1 ml plastic syringe and then placed in an Eppendorf tube. Batches of these were next centrifuged in a desktop Eppendorf® centrifuge 5430 (5 min/ 3500 rpm/4˚C). Supernatants were removed, and cell pellets were re-suspended in 600 µl of PBS by shaking closed tube content on IKA® Vortex mixer.

4.4.2 Cells Count Analysis

The absolute and relative cell counts in the re-suspended BALF samples were quantified using the Sysmex XT-2000iV™ hematological analyser. The outcomes were showcased as the total counts of cells in BALF, including lymphocytes, monocytes, neutrophils, and eosinophils, with the results expressed in units of 10^9 cells per litre (10^9/L).

4.4.3 Measurement of IL-4, IL-5 and IL-13 in the BALF Supernatant

Mouse IL-4, IL-5, and IL-13 DuoSet ELISA (enzyme-linked immunosorbent assay) kits (R&D Systems, Minneapolis, USA) were used to measure concentrations of IL-4, IL-5, and IL-13, respectively, in BALF supernatants *per* the manufacturer's protocols.

Reagent preparation was performed through the following steps. Recombinant mouse IL-4 standard was reconstituted with 0.5 mL 1% bovine serum albumin (BSA) (Sigma-Aldrich Chemie GmbH, Munich, Germany) in PBS (Sigma-Aldrich Chemie GmbH, Munich, Germany) and diluted 150-fold to 1000 pg/mL, followed by six consecutive 2-fold dilutions.

Recombinant mouse IL-5 standard was reconstituted with 0.5 mL 1% BSA in PBS and diluted 30-fold to 2000 pg/mL, followed by six consecutive 2-fold dilutions.

Recombinant mouse IL-13 standard was reconstituted with 0.5 mL 1% BSA in PBS and diluted 72.5-fold to 4000 pg/mL, followed by six consecutive 2-fold dilutions.

For each assay, 1% BSA in PBS was used as the blank.

Biotinylated detection antibodies to mouse IL-4, IL-5, and IL-13 (goat anti-mouse IL-4, rat anti-mouse IL-5, and goat anti-mouse IL-13) were each reconstituted in 1 mL of 1% BSA in PBS. Vials were diluted 60-fold (final concentrations of 200, 50, and 200 ng/mL, respectively) in 1% BSA in PBS.

Streptavidin-HRP (horseradish peroxidase) was diluted 40-fold in 1% BSA in PBS.

Rat anti-mouse IL-4, IL-5, and IL-13 capture antibodies were each reconstituted in 0.5 mL of PBS and diluted 120-fold (final concentrations of 4, 1, and 4 µg/mL, respectively) in PBS.

The day before the analysis, 96-well microplates were coated with 100 µL/well of diluted IL-4, IL-5, or IL-13 capture antibody in PBS and stored overnight at room temperature (RT). The next day, plates were washed three times with 0.05% Tween™ 20 (Sigma-Aldrich Chemie GmbH, Munich, Germany) in PBS (400 µL/well) and dry-blotted against paper towels. Blocking buffer (1% BSA in PBS) was added to each well (300 µL) and incubated for 1 hour at RT. Plates were washed, and 100 µL/well of undiluted BALF supernatant samples or IL-4, IL-5, and IL-13 standards were added and incubated for 2 hours at RT. Plates were washed, detection antibody was added (100 µL/well), and plates were incubated for 2 hours at RT. Plates were washed, streptavidin-HRP was added (100 µL/well), and plates were incubated for 20 minutes at RT. Plates were washed, a substrate solution (Substrate reagent pack, 1:1 mixture, R&D Systems, Minneapolis, USA) was added (100 µL/well), and plates were incubated for 20 minutes at RT. Reactions were stopped with 50 µL/well of 2 sulfuric acid c (Merck KGaA, Darmstadt, Germany). Absorbance at 450 nm was measured using the INFINITE® F500 plate reader (TECAN, San Jose, CA, USA). Concentrations of IL-4, IL-5, and IL-13 in samples were determined by interpolation from a 4-parameter logistic curve fit.

4.4.4 Measurement of IgE in the BALF Supernatant

A mouse IgE uncoated ELISA kit (R&D Systems, Minneapolis, USA) was used to measure concentrations of total IgE in BALF supernatants per the manufacturer's protocols.

As the blank, PBS with 1% Tween™-20 and 10% BSA was used.

Reagent preparation was performed through the following steps. Mouse IgE standard was reconstituted with distilled water and diluted in PBS with 1% Tween™-20 and 10% BSA 150-fold to 500 ng/mL, followed by five consecutive 2-fold dilutions.

Biotinylated detection anti-mouse IgE monoclonal antibody vials were diluted 250-fold in PBS with 1% Tween™-20 and 10% BSA.

Streptavidin-HRP was diluted 400-fold in 1% BSA with 1% Tween™-20 and 10% BSA.

Pre-titrated, purified anti-mouse IgE monoclonal capture antibody was diluted 250-fold in 1:10 dilution of PBS in deionized water.

The day before the analysis, the Corning™ Costar™ 9018 ELISA plate was coated with 100 µL/well of diluted IgE capture antibody in 1:10 dilution of PBS (10X) in deionized water and stored overnight at RT. The next day, plates were washed twice with 0.05% Tween™-20 in PBS (400 µL/well) and dry-blotted against paper towels. Blocking buffer (1:10 dilution of PBS with 1% Tween™-20 and 10% BSA mixture in deionized water) was added to each well (250 µL) and incubated for 2 hours at RT. To make a standard curve, 2-fold serial dilutions of the standards with PBS with 1% Tween™-20 and 10% BSA were performed. Plates were prefilled with 50 µL/well of PBS with 1% Tween™-20 and 10% BSA and 50 µL/well of undiluted BALF supernatant samples and incubated for 2 hours at RT. Plates were washed four times, detection antibody was added (100 µL/well), and plates were incubated for 1 hour at RT. Plates were washed four times, streptavidin-HRP was added (100 µL/well), and plates were incubated for 30 minutes at RT. Plates were washed four times, a substrate solution (Tetramethylbenzidine (TMB) Substrate Solution, R&D Systems, Minneapolis, USA) was added (100 µL/well), and plates were incubated for 15 minutes at RT. Reactions were stopped with 100 µL/well of 2 sulfuric acid c (Merck KGaA, Darmstadt, Germany). Absorbance at 450 nm was measured using the INFINITE® F500 plate reader (TECAN, San Jose, CA, USA). IgE concentration in samples was determined by interpolation from a 4-parameter logistic curve fit.

4.5 HISTOLOGY

4.5.1 Lung Tissue Fixation and Paraffin Blocks Preparation

Immediately after excision, the lungs were immersed in marked containers filled with 10% buffered formalin (Shandon™ Formal-Fixx™ Neutral Buffered Formalin, Thermo Fisher Scientific, Rockford, IL, USA) for histopathological examination, with each sample meticulously logged in the sample book. Following a 24-hour formalin fixation period, the lungs were dissected into left and right lobes. The left lobe was sectioned transversally before placement in embedding cassettes, while the right lobes were placed whole. Each cassette was marked with the respective animal numbers (Thermo Fisher Scientific, Rockford, IL, USA).

The tissues in cassettes underwent a 24-hour fixation in 10% neutral formalin, followed by a dehydration sequence in an automatic tissue processor, Shandon Excelsior ES® (Thermo Fisher Scientific, Rockford, IL, USA), using a 16-hour "Routine Overnight" program. This program involved a 12-step process utilizing ethanol at concentrations of 70% and 96%, xylene p.a. (Merck KGaA, Darmstadt, Germany), and paraffin (Histoplast™, Thermo Fisher Scientific, Rockford, IL, USA). Post-dehydration, the cassettes were transferred to a Leica EG1160 auto tissue embedder (Leica Biosystems, Deer Park, IL, USA) for embedding into paraffin blocks, preparing them for subsequent sectioning and analysis.

4.5.2 Histology Slides Preparation

Paraffin block with embedded lung tissue was cooled and processed using Thermo Scientific™ HM 450 Sliding Microtome. Blocks were trimmed to even out the composition to the desired cutting surface. A 1 μm thick-sliced paraffin tissue sections were floated in distilled water into a water bath and transferred to the glass slide (Menzel Gläser, SuperFrost®, Thermo Fisher Scientific, Rockford, IL, USA).

Histological slides were dried by placing them into a Thermo Scientific Heraeus® incubator (Thermo Fisher Scientific, Rockford, IL, USA) at 60ºC for 15 minutes. Histological slides underwent deparaffinization and hydration procedures and were subsequently stained according to model protocol. Deparaffinization using xylene (Merck KGaA, Darmstadt, Germany) baths was performed to remove the paraffin that penetrated the tissue. After deparaffinization, the remaining xylene on the slides was removed with 100% ethanol (Merck KGaA, Darmstadt, Germany). Then, slides were hydrated in a series of graded alcohols (95% and 70%) and finally rinsed with distilled water.

4.5.3 Histology Procedures and Assessments in a Model of Bleomycin-Induced Pulmonary Fibrosis

4.5.3.1 Crossman's Trichrome for Muscle and Collagen Staining

Lung tissue sections were prepared and stained manually according to Crossman's Trichrome for muscle and collagen staining protocol. Prepared histological slides were placed into Tissue-Tek® DRS™ 2000 (Sakura Finetek Europe, the Netherlands) for deparaffinization. Slides were stained in Mayer's hemalaum solution for three minutes, rinsed, and placed for three minutes in the solution of acid fuchsin (Sigma-Aldrich Chemie GmbH, Munich, Germany), orange G, ACROS organics™ (Thermo Fisher Scientific, Rockford, IL, USA), acetic acid glacial (Merck KGaA, Darmstadt, Germany) and distilled water; samples were rinsed in distilled water and immersed in the solution of dodeca molybdophsphoric acid (Kemika, Zagreb, Croatia) and distilled water for five minutes; and in the final solution of Light green SF yellowish (Merck KGaA, Darmstadt, Germany), acetic acid glacial and distilled water for five minutes. Slides were dehydrated in 96% (2x for two minutes) and 100% ethanol (2 x for three minutes) and xylene accordingly, and finally mounted with Shandon™ Consul-Mount™ (Thermo Fisher Scientific, Rockford, IL, USA) in a ClearVue™ Coverslipper (Thermo Fisher Scientific, Rockford, IL, USA).

4.5.3.2 Matsuse Modification of the Ashcroft Score

Slides were examined under a light microscope Axio Imager.A1 (Carl Zeiss, Jena, Germany).

Matsuse's modification of the Ashcroft score (ASHCROFT et al., 1988 and MATSUSE et al., 1999) was used to evaluate fibrosis in lung specimens. Samples were examined under magnification 50x, and ten fields were scored according to Table 5. When microscopic lesions present lower and higher score criteria, a half score was added. Screening fields covered the left and right pulmonary lobes. The left pulmonary lobe contained four low-power fields (LPFs), and the right lobe had six LPFs (lobus cranialis 2xLPF, lobus caudalis 2xLPF, lobus medius 1xLPF, and lobus accessorius 1xLPF). Each animal's final score was calculated as a mean from 10 LPFs. The group score was presented as the median score of all animals in the experimental group.

Table 5 Matsuse modification of Ashcroft score
Five score system criteria were described in the table following Matsuse's modification of the Ashcroft score (ASHCROFT et al., 1988 and MATSUSE et al., 1999)

Matsuse modified Ashcroft score	
1	Normal lung (no fibrosis)
2	Minimal fibrotic thickening of alveolar or bronchial walls (network of fine collagen fibrils)
3	Moderate fibrotic thickening of walls without obvious damage to lung architecture
4	Fibrosis with damage of pulmonary structure (coarse fibrous bands or small fibrous masses, intra-alveolar collagen fibrils
5	Large fibrous areas with severe distortion of lung structure

4.5.4 Histology Procedures and Assessments in a Model of Ovalbumin-Induced Asthma

4.5.4.1 The Periodic Acid-Schiff Staining Method

Lung tissue sections were deparaffinized to prepare samples for manual staining according to the periodic acid-Schiff (PAS) staining protocol. Prepared histological slides were placed into Tissue-Tek® DRS™ 2000 (Sakura Finetek Europe, Alphen aan den Rijn, Netherlands). Slides were treated with periodic acid (Merck KGaA, Darmstadt, Germany) solution for 7 minutes and subsequently rinsed for five minutes with distilled water; further, slides were treated with Shiff's reagents (Merck KGaA, Darmstadt, Germany) for 15-30 minutes. Slides were immersed into three 0.5% potassium metabisulfite solution baths (Merck KGaA, Darmstadt, Germany) for two minutes each and then rinsed for five minutes with distilled water. Afterward, slides were immersed in Mayer's hemalaum solution for three minutes and rinsed with tap water for 10 minutes. Post-staining slides were dehydrated by immersing into baths of a series of graded alcohols (95% and 100%), baths of xylene, and finally mounted with the Richard-Allan Scientific™ Cytoseal™ XYL (Thermo Fisher Scientific, Rockford, IL, USA).

4.5.4.2 Histological Assessment of General Pulmonary Inflammation, Epithelial Damage, and Goblet Cell Metaplasia

Slides were examined under a light microscope Axio Imager.A1 (Carl Zeiss, Jena, Germany).

General pulmonary inflammation and epithelial damage protocol was used to score named changes in lung specimens. Samples were examined as the total lung surface under magnification 50x. For each animal, the severity and distribution of inflammation and/ or

epithelial changes of bronchi and alveoli were scored as described in Table 6. In addition, goblet cell metaplasia was evaluated separately at a level of large airways and terminal airways (Table 7). The group score was presented as the median score of all animals in the experimental group.

Table 6 General pulmonary inflammation and/or epithelial damage scoring criteria
Criteria for each score are noted in the table below.

General pulmonary inflammation and/or epithelial damage score	
0	None
1	Minimal focal
2	Minimal multifocal
3	Minimal diffuse
4	Moderate focal
5	Moderate focal and minimal diffuse
6	Moderate multifocal
7	Moderate diffuse
8	Marked focal
9	Marked focal and moderate multifocal
10	Marked multifocal
11	Marked focal and moderate diffuse
12	Marked diffuse

Table 7 Goblet cell metaplasia scoring criteria
Criteria for each score are noted in the table below.

Goblet cell metaplasia score	
0	No mucus-containing cells along the basement membrane
1	Few positive cells along the basement membrane with less than 75% of the cytoplasm stained
2	Few positive cells along the basement membrane with more than 75% of the cytoplasm stained
3	Numerous positive cells along the basement membrane with less than 75% of the cytoplasm stained
4	Numerous positive cells along the basement membrane with more than 75% of the cytoplasm stained

4.6 IMMUNOHISTOCHEMISTRY

Additional histology slides from the BLM fibrosis model were prepared for immunostaining as described previously. Slides were prepared from lung tissue paraffin blocks sampled in the BLM-induced pulmonary fibrosis model.

4.6.1 Collagen Type 1 Presence in the Lungs

The IHC staining for COL1A1 was performed using the PT Link model and the Autostainer Link48 systems from DAKO Agilent, Santa Clara, CA, USA. The procedure followed the manufacturer's protocols closely to ensure precise and dependable staining outcomes.

Deparaffinization and rehydration were performed in the Tissue-Tek® DRS™ 2000 (Sakura Finetek Europe, the Netherlands) and target retrieval in PT Link using Target Retrieval Solution (DAKO Agilent, Santa Clara, CA, USA) pH 6. Slides were then processed on the Autostainer Link 48 (Dako AS480) using an automated staining protocol following Vector anti-rabbit protocol Vector Laboratories ImmPRESS™ Polymer Kit. The COL1A1 IHC staining protocol included the sequential application of a blocking reagent BLOXALL™, Endogenous Peroxidase and Alkaline Phosphatase Blocking Solution (Vector Laboratories, Inc., Burlingame, CA, USA), 2.5% normal horse serum and a 1:2000 diluted COL1A1 / Rabbit anti-Mouse Polyclonal (aa1192-1207) Antibody (LifeSpan BioSciences, Inc., Washington, USA). Afterward, slides were treated with rabbit IgG control antibody, visualization kit ImmPRESS® HRP Horse Anti-Rabbit IgG Polymer Detection Kit, Peroxidase (Vector Laboratories, Inc., Burlingame, CA, USA) consisting of a micropolymer of highly active HRP attached to the affinity purified secondary antibodies in addition with 2.5% normal horse serum. Control samples were included in the staining process by order: negative control reagent without primary antibody and isotype control, treated with PBS instead; Positive control samples treated with COL1A1 / Rabbit anti-Mouse Polyclonal (aa1192-1207) Antibody prepared as described before; and isotope control treated with rabbit IgG control antibody. After all kit steps were performed, slides were treated with 3,3′-diaminobenzidine tetrahydrochloride (DAB+) chromogen reagent with hydrogen peroxide substrate and a DAB enhancer, which modifies the color of the precipitated chromogen (DAKO Agilent, Santa Clara, CA, USA). As a final step, slides were stained in Mayer's hemalaum solution for one minute, dehydrated in 100% ethanol, and mounted with Shandon™ Consul-Mount™ (Thermo Fisher Scientific, Rockford, IL, USA).

4.6.2 Myofibroblast Presence in the Lungs

Myofibroblast presence in the lungs was evaluated by quantifying αSMA using IHC staining.

A protocol for the αSMA IHC staining is the same as described previously in the COL1A1 staining procedure. In this protocol, staining was performed using a human rabbit anti-mouse αSMA antibody, 1:1000 dilution (Abcam, Cambridge, UK).

4.6.3 Digital Quantification of Immunohistochemically Stained Slides

Myofibroblast (αSMA, IHC) accumulation and *de novo* collagen (COL1A1, IHC) deposition in the lungs was assessed by digital image analysis CaloPix software (TRIBVN, Châtillon, France) using manufacturer immunosurface protocol. IHC stained slides were scanned using the Axio Scan.Z1 scanner (Carl Zeiss, Jena, Germany). The tissue was manually marked, and the immunosurface protocol was adjusted to distinguish the background from the stained tissue. Blue staining represents collagen-negative tissue, while the colour ranges from yellow to red, representing collagen-positive tissue. Results were given as tissue area in mm^2.

The procedure for the αSMA digital quantification was the same with the same colour tissue marks, and results were given as tissue area in mm^2.

4.7 STATISTICAL ANALYSIS

Statistical analysis and graphical representation were conducted using Graph Pad Prism software (version 9). For both the BLM-induced pulmonary fibrosis and OVA-induced asthma models, body weight data were analyzed using a two-way ANOVA multiple comparisons test, with results presented as mean values for each group on specific experimental days.

In the BLM-induced pulmonary fibrosis model, analyses covered body weight, PFTs, and Ashcroft, αSMA, and COL1A1 scores. The mean rank of each experimental group was compared with the control group's mean rank (BLM Ctrls group). Non-parametric statistics, including the Wilcoxon Signed Rank Test and Kruskal-Wallis test with Dunn's multiple comparison test, were applied to Ashcroft score results, using group medians for evaluation. For COL1A1/αSMA deposition data, one-way ANOVA with Dunnett's multiple comparison test or Kruskal-Wallis test with Dunn's multiple comparison test was selected based on the D'Agostino & Pearson normality test results. Additionally, Spearman's correlation was used to compare histological data with PFT outcomes.

The OVA-induced asthma model followed a similar data processing approach for body weight, PFTs, BALF cell counts, BALF supernatant IgE, ILs analyses, and histomorphology scoring. Comparisons were made between OVA/OVA Ctrls groups and PBS/Saline Ctrls, and treatment effects were assessed by comparing treatment groups with the corresponding OVA/OVA Ctrls group. Data distribution for BALF cell count, IgE, and ILs was determined using the D'Agostino & Pearson test, and analysis was conducted using either parametric one-way ANOVA with Dunnett's multiple comparisons post hoc test or non-parametric Kruskal-Wallis with Dunn's multiple comparison test, depending on the data distribution.

Inflammation, epithelial damage, and goblet cell metaplasia scores were analysed using non-parametric statistics, with group medians serving as the basis for evaluation. Both models PFTs' values were analysed as group means, using unpaired t-tests and presented graphically.

Statistically significant differences were recognized at $p < 0.05$.

5 RESULTS

In this study, results are shown as average or median values with standard error of the mean (sem) on the final experimental day, analyzed using suitable statistical tests. For data over time or depicted as curves, values are presented as means without sem.

5.1 RESPIRATORY MODELS' EUTHANASIA CRITERIA OUTCOMES

5.1.1 Model of Bleomycin-Induced Pulmonary Fibrosis

During the 21-day BLM-induced pulmonary fibrosis study, eight animals were euthanized due to not meeting the physical condition criteria:

- In the BLM Ctrls group of 20 mice, euthanasia was necessary for mouse no. 15 on day 14, mouse no. 19 on day 17, mouse no. 27 on day 11, and mouse no. 29 on day 18.
- The BLM/Nintedanib 60 mg/kg *p.o. bid* group also started with 20 mice, with mouse no. 33 euthanized on day 13 and mouse no. 47 on day 19.
- In the BLM/Pirfenidone 100 mg/kg *p.o. bid* group of 20 mice, mouse no. 60 was euthanized on day 14 and mouse no. 66 on day 15.
- All mice in the PBS Ctrls group, totalling 10 animals, met the criteria for sampling on the last day of the experiment.

After these considerations, 62 mice continued to the next phase of the experiment on day 21, with detailed raw data available in Table 8 and Appendix 1.

Table 8 Euthanasia list and number of mice that survived *per* group

Group	No. of mice at the beginning of the experiment	Mouse no./euthanasia day				No. of mice survived
PBS Ctrls	10	/	/	/	/	10
BLM Ctrls	20	No. 15 D14	No. 19 D17	No.27 D11	No. 29 D18	16
BLM/Nintedanib 60 mg/kg *p.o. bid*	20	No. 33 D13	No. 47 D19	/	/	18
BLM/Pirfenidone 100 mg/kg *p.o. bid*	20	No. 60 D14	No. 66 D15	/	/	18

Abbreviations: No-number, PBS-phosphate buffered saline, BLM-bleomycin, Ctrls-controls, *p.o.*-perorally, *bid*-twice a day, D-day of the experiment

5.1.2 Model of Ovalbumin-Induced Asthma

No severe signs of distress were observed in the OVA-induced asthma experiments, and all animals were sampled on the last day of the study (experiment raw data are presented in Appendix 2).

5.2 BODY WEIGHT RESULTS

5.2.1 Model of Bleomycin-Induced Pulmonary Fibrosis

Body weight measurements throughout the experiment are detailed as daily individual weights in grams in Appendix 1. A graphical summary of daily average weights per group and statistical findings are displayed in Figure 11.

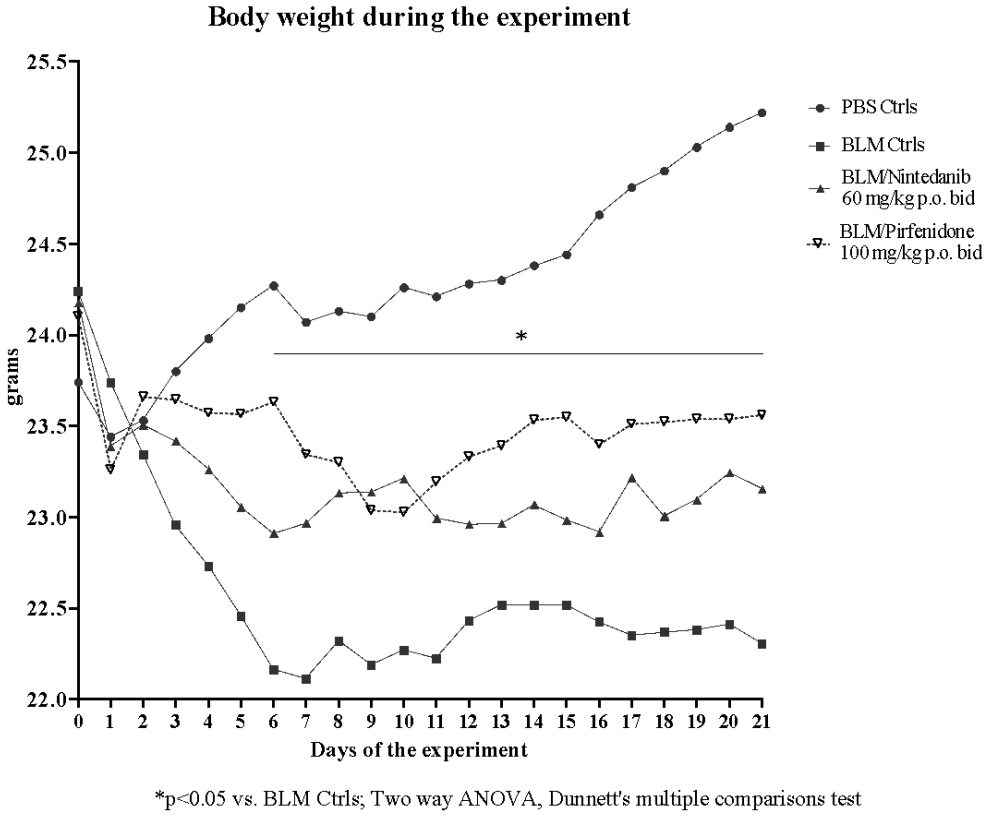

Figure 11 Body weight values over days in the BLM-induced pulmonary fibrosis model
The body weight group's mean on each day of the experiment are presented in the graph. Each group's mean value on the indicated day was compared to the BLM Ctrls group.

Abbreviations: PBS-phosphate buffered saline, BLM-bleomycin, Ctrls-controls, *p.o.*-perorally, *bid*-twice a day, vs.-*versus*, ANOVA-analysis of variances

On the initial challenge day (D0), the average weights were as follows: PBS Ctrls (10 animals) at 23.7 g, BLM Ctrls (16 animals) at 24.2 g, BLM/Nintedanib group (18 animals) at 24.2 g, and BLM/Pirfenidone group (18 animals) at 24.1 g (Figure 11).

In the first six days, the BLM group's weights dropped, while the PBS Ctrl group saw continuous weight gains. A significant weight difference emerged from day 6, with PBS Ctrls averaging 24.3 g and BLM Ctrls 22.2 g. This gap persisted, ending with PBS Ctrls at 25.2 g and BLM Ctrls at 22.3 g. The BLM/Nintedanib and BLM/Pirfenidone groups maintained stable

weights from days 6-21, showing no significant difference from the BLM Ctrls. Final weights were 23.2 g for BLM/Nintedanib and 23.6 g for BLM/Pirfenidone. Graphical data in Figure 11 illustrate the impact of fibrosis on weight in BLM mice and how standard treatments mitigated weight loss.

5.2.2 Model of Ovalbumin-Induced Asthma

Body weights were monitored from the first OVA or saline *i.n.* challenge, recorded daily until the experiment's conclusion. Figure 12 displays the body weight trajectory, showing average values for each group during the challenge phase and on the study's final day, along with statistical analyses.

On the challenge day, average body weights were as follows: PBS/Saline Ctrls (8 animals) averaged 23.4 g; OVA/OVA Ctrls *p.o.* (10 animals) averaged 23.9 g; OVA/Dexamethasone (10 animals) averaged 22.7 g; OVA/OVA Ctrls *i.n.* (10 animals) averaged 23.8 g; OVA/Fluticasone propionate (10 animals) averaged 23.5 g. These findings, including raw body weight data, are detailed in Appendix 2 and summarized in Figure 12.

From day 20 to day 24, the PBS/Saline Ctrls group and both OVA/OVA Ctrls groups maintained stable body weights, whereas the treatment groups experienced a continuous decrease. Specifically, dexamethasone treatment led to a notable decline in body weight from day 21 to day 24, with weights dropping from 21.6 g to 21 g, in contrast to the OVA/OVA Ctrls *p.o.* group, which saw weights increase from 23.5 g to 24.2 g. Similarly, the fluticasone propionate-treated group showed weight decreases in the experiment's final two days (22.2 g to 21.8 g), as opposed to the OVA/OVA Ctrls *i.n.* group, which had weights from 23.7 g to 24 g.

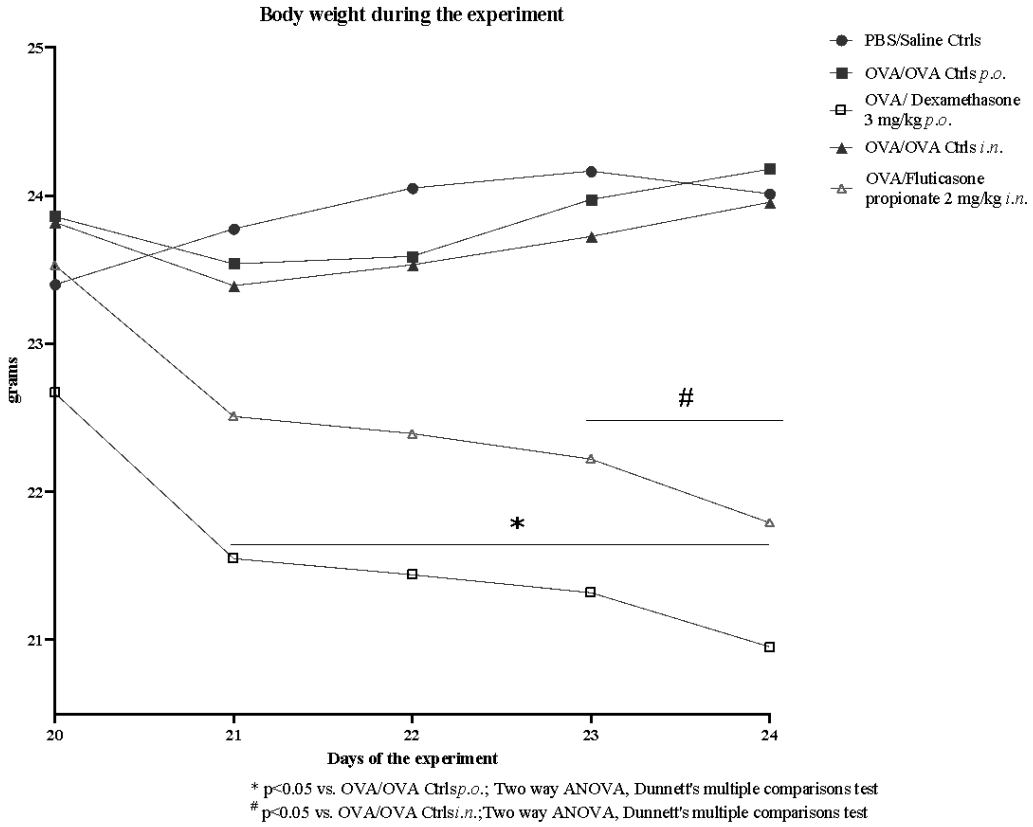

Figure 12 Body weight values over days in the OVA-induced asthma model
Body weights group mean values records each day starting from the day of the first *i.n.* challenge and recorded daily until the end of the experiment. Statistical analysis compared group values on an indicated day to corresponding OVA/OVA Ctrls.

Abbreviations: PBS-phosphate buffered saline, Ctrls-controls, OVA-ovalbumin, *p.o.*-perorally, *i.n.*-intranasally, vs.-*versus*, ANOVA-analysis of variances

5.3 PULMONARY FUNCTION TESTING RESULTS

5.3.1 Model of Bleomycin-Induced Pulmonary Fibrosis

On day 21 of the BLM-induced pulmonary fibrosis experiment, PFTs were conducted on 62 animals, with the raw data available in Appendix 3. The PFTs encompassed four distinct sequences:

- Boyle's law functional residual capacity test
- Quasistatic pressure volume test
- Fast flow volume maneuver test
- Resistance and compliance test

The results from these PFT sequences were statistically analysed using an unpaired t-test (significance level set at p=0.05) to compare the mean values across groups. The outcomes of these analyses are visually detailed in Figures 13-19. Overview of lung function parameters values measured in the BLM-induced pulmonary fibrosis model using the DSI's Buxco® PFT system is presented in Table 9.

5.3.1.1 Sequence 1. Boyle's Law Functional Residual Capacity Test

The FRC parameter was measured and reported in the first PFT of Boyle's law functions residual capacity test (Figure 13, Appendix 3).

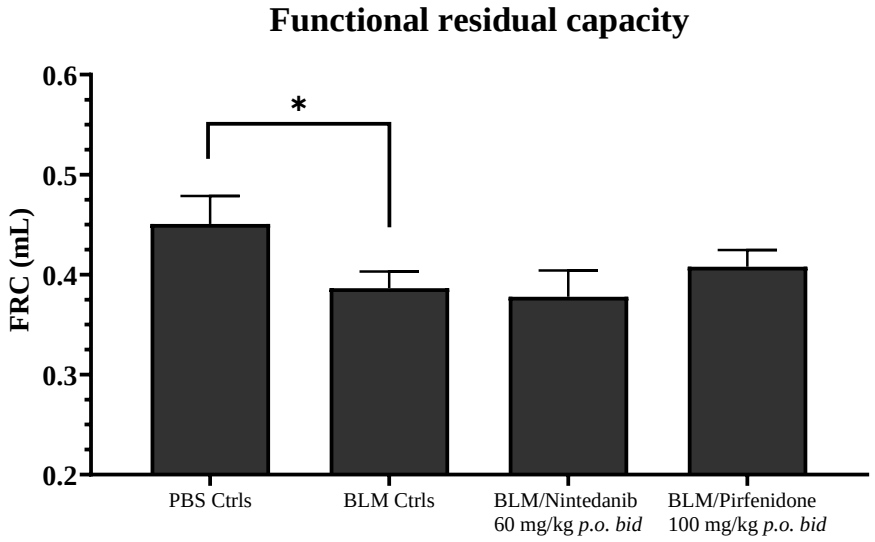

* p<0.05 vs. BLM Ctrls; Unpaired t test

Figure 13 PFT sequence 1. Functional residual capacity parameter
An FRC value of each observed group measured in the Boyle's law functional residual capacity at day 21 in the BLM-induced pulmonary fibrosis model was presented as a group mean + sem.

Abbreviations: PBS-phosphate buffered saline, FRC-functional residual capacity, BLM-bleomycin, Ctrls-controls, *p.o.*-perorally, *bid*-twice a day, vs.-*versus,* sem-standard error of the mean

In the PBS Ctrls group of 10 animals, the FRC mean value was 0.451 mL, significantly higher (p=0.0226) than the BLM Ctrls group's mean of 0.386 mL, which comprised 16 animals, as shown in Figure 13 and detailed in Appendix 3. For the nintedanib-treated group, the mean FRC from 17 valid measurements was 0.378 mL (one measurement was excluded due to invalidity), whereas the pirfenidone-treated group had a mean FRC of 0.408 mL from 18 animals.

The treatment with reference standards nintedanib and pirfenidone did not significantly alter the FRC values when compared to the BLM Ctrls group, with p-values of 0.3947 and 0.1843, respectively, as illustrated in Figure 13.

5.3.1.2 Sequence 2. Quasistatic Pressure Volume Test

In a quasistatic pressure volume test, TLC, RV, IC, VC, Te, and Cchord values were measured in the second PFT, forming a P-V curve (Figure 14 and Figure 15). Individual raw data values are listed in Appendix 3 and Appendix 4.

In the PBS Ctrls group, all ten animals had valid measures in all parameters reported in the sequence 2 test, presenting mean physiological values of TLC, RV, IC, VC, Te, and Cchord (1.114, 0.338, 0.663, 0.777 mL, 1.16 sec, and 0.039 mL/cm H2O, respectively) (Appendix 3, Figure 14).

BLM challenged Ctrls group consisted of 16 animals. The mean values of sequence two measured parameters were as follows: 0.832, 0.303, 0.446, 0.529 mL, 0.682 sec, and 0.026 mL/cm H2O, respectively (Appendix 3, Figure 14).

Nintedanib treatment mean group values (n=18) of IC, VC, Te, and Cchord were 0.564, 0.678 mL, 0.892 sec, and 0.034 mL/cm H2O, respectively. In the TLC and RV parameters, one animal value was not valid. Therefore, these two measurements consisted of n=17 animal measurements per parameter, resulting in 0.943 and 0.266 mL mean group values, respectively (Appendix 3, Figure 14).

Pifrenidone treated group included 18 animals, and each animal value per parameter was valid, resulting in 0.886, 0.294, 0.478, 0.591 mL, 0.807 sec, and 0.028 mL/cm H2O, respectively (Appendix 3, Figure 14).

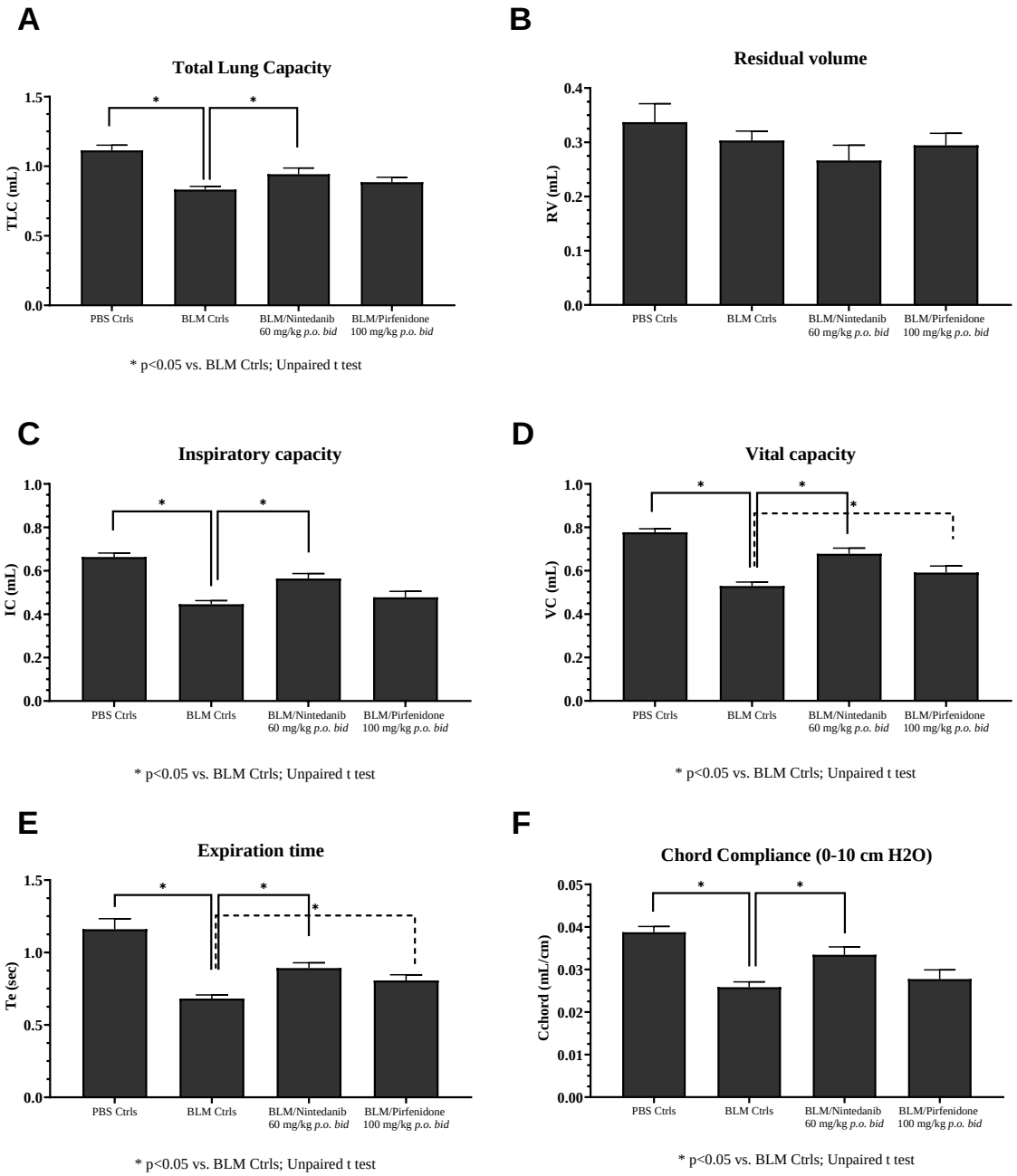

Figure 14 PFT sequence 2: TLC, RV, IC, VC, Te, and Cchord parameters

Parameters of A) total lung capacity, B) residual volume, C) inspiratory capacity, D) vital capacity, E) expiration time, and F) compliance of the cord generated in the quasistatic pressure volume test on day 21 in the BLM-induced pulmonary fibrosis model, presented as group mean+sem.

Abbreviations: PBS-phosphate buffered saline, BLM-bleomycin, Ctrls-controls, *p.o.*-perorally, *bid*-twice a day, TLC-total lung capacity, RV-residual volume, Cchord – chord compliance, IC-inspiratory capacity, VC-vital capacity, Te-expiration time, vs.-*versus,* sem-standard error of the mean

The BLM challenge induced a significant decrease in TLC, IC, VC, Te, and Cchord compared to the unchallenged PBS Ctrls group ($p<0.0001$), as depicted in Figure 14.

Nintedanib treatment notably improved all affected parameters (TLC, IC, VC, Te, and Cchord) compared to BLM Ctrls ($p=0.018$, $p=0.0001$, $p<0.0001$, $p<0.0001$, and $p=0.0011$, respectively), while pirfenidone treatment only significantly improved VC and Te ($p=0.0473$ and $p=0.0065$, respectively). TLC, IC, and Cchord remained unaffected ($p=0.1083$, $p=0.1720$, and $p=0.2323$, respectively) (Figure 14).

The RV parameter was not significantly affected by the BLM challenge ($p=0.168$) nor by nintedanib and pirfenidone treatments ($p=0.14$ and $p=0.3785$, respectively) (Figure 14).

In the quasistatic pressure volume test, P-V curves were generated for each group (Figure 15, Appendix 4), with Cchord, a value between 0 and +10 cm H2O, defining the slope.

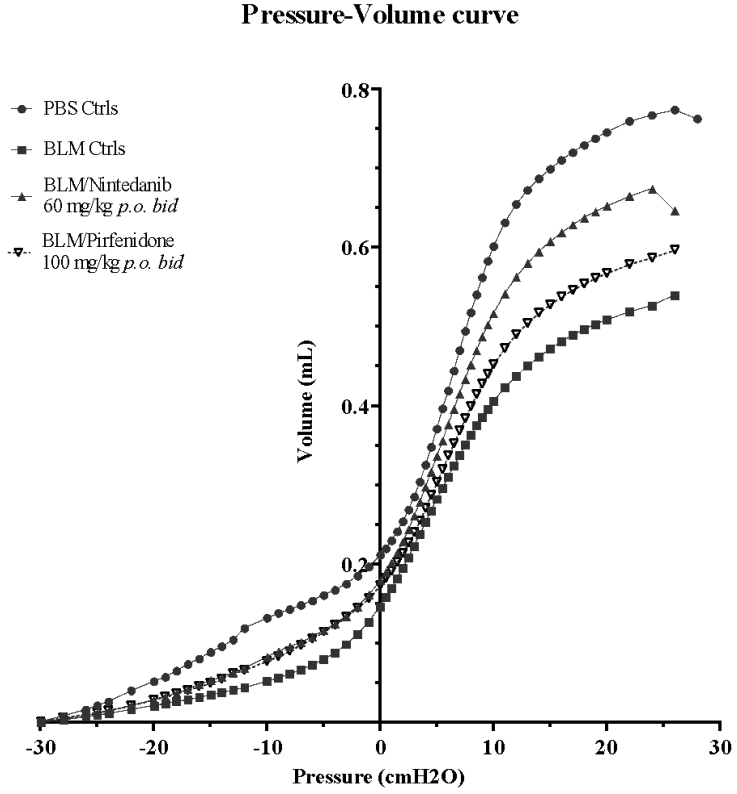

Figure 15 PFT sequence 2: A pressure-volume curve
The P-V curve was generated in the quasistatic pressure volume test on day 21 in the BLM-induced pulmonary fibrosis model, presenting the mean values of volume measured under different airway pressures.

Abbreviations: PBS-phosphate buffered saline, BLM-bleomycin, Ctrls-controls, *p.o.*-perorally, *bid*-twice a day

A significantly decreased Cchord parameter of BLM-challenged mice resulted in a right and downward slope shift compared to the unchallenged PBS Ctrls group (Figure 15).

Treatment with nintedanib and pirfenidone affected the curve shift toward the unchallenged group, placing the nintedanib group curve closer to the PBS Ctrls curve as the Cchord mean value was significantly improved over the BLM Ctrls group (Figure 15).

5.3.1.3 Sequence 3. Fast Flow Volume Maneuver Test

A following test sequence, a fast flow volume maneuver test, generated the F-V curve by plotting the flow against the lung volume between RV and TLC. The F-V curve is presented in Figure 16 (raw data are presented in Appendix 5).

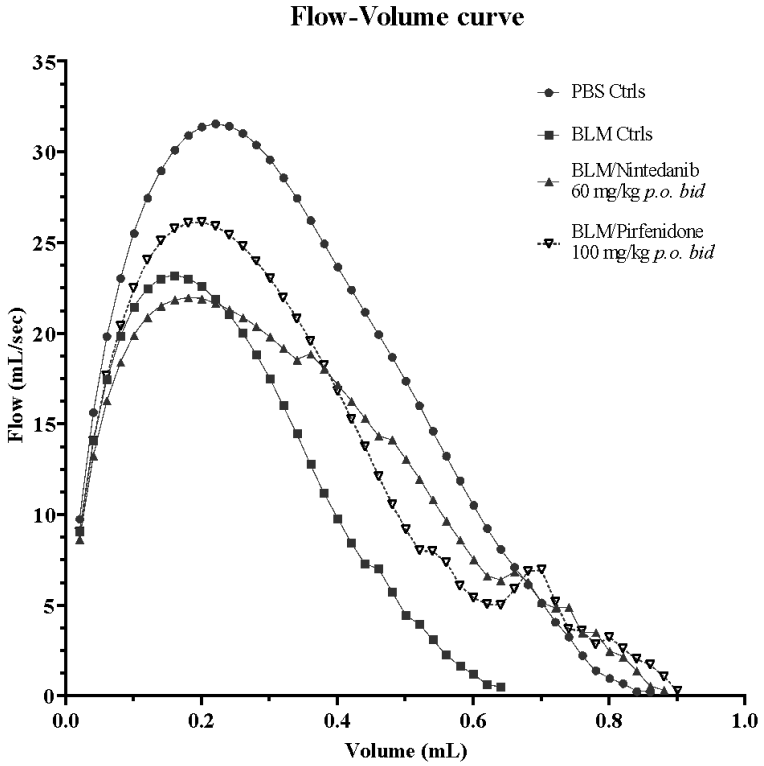

Figure 16 PFT sequence 3: A pressure-volume curve
The F-V curve was generated in the fast flow volume maneuver test on day 21 in the BLM-induced pulmonary fibrosis model, presenting mean group values of flow measured in different airway volumes.

Abbreviations: F-V-flow volume, PBS-phosphate buffered saline, BLM-bleomycin, Ctrls-controls, *p.o.*-perorally, *bid*-twice a day

A curve shape and slope are characterized by the following parameters measured in this test sequence: FVC, FEV100, PEF, and MMEF. Their values and statistical correspondence between observed groups are shown in Figure 17 and Appendix 3.

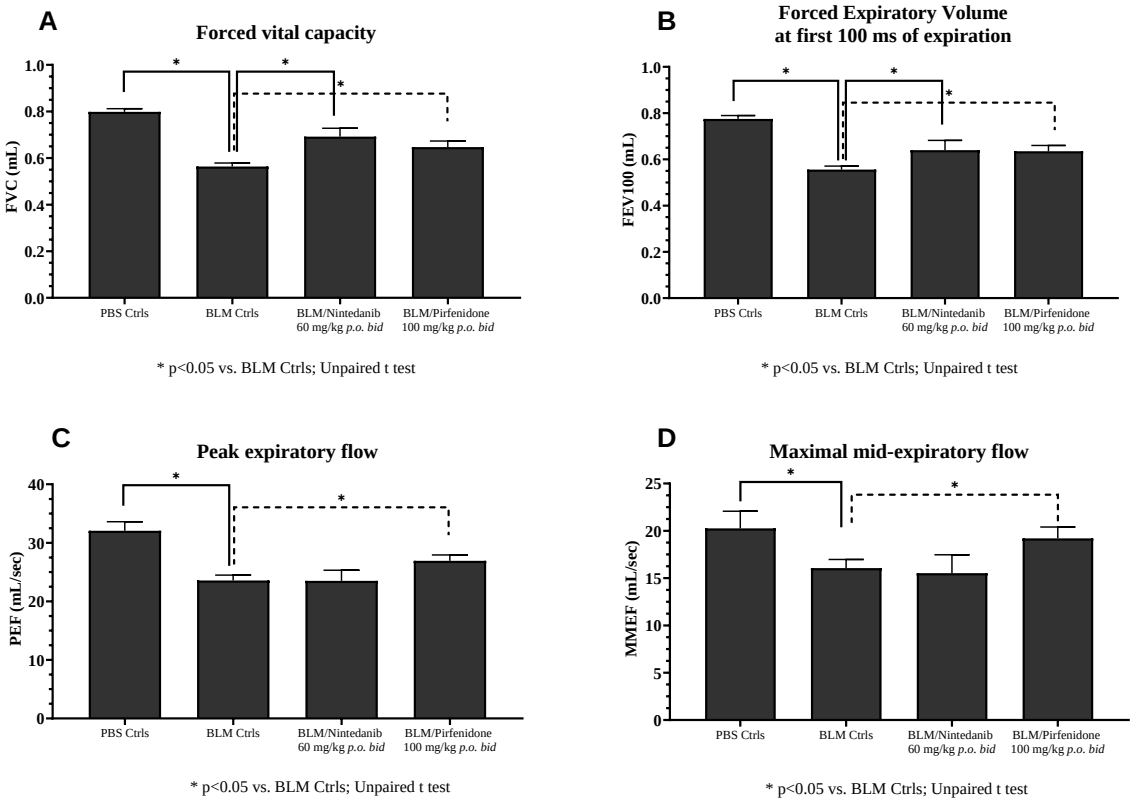

Figure 17 PFT sequence 3: FVC, FEV100, PEF and MMEF parameters
Parameters of A) forced vital capacity, B) forced expiratory volume at 100 ms, C) peak expiratory flow, and D) maximal mid-expiratory flow, generated in the fast flow volume maneuver test on day 21 in the BLM-induced pulmonary fibrosis model, presented as group mean+sem.

Abbreviations: PBS-phosphate buffered saline, BLM-bleomycin, Ctrls-controls, *p.o.*-perorally, *bid*-twice a day, FVC-forced expiratory volume, FEV100-forced expiratory volume at 100 ms, PEF-peak expiratory flow, MMEF-maximal mid-expiratory flow, vs.-*versus,* sem-standard error of the mean

A PBS Ctrls F-V curve presents a characteristic forced exhalation shape of a healthy individual. The curve shows a rapid ascent to PEF (32.06 mL/sec), with a FEV100 of 0.775 mL, and subsequently a slow linear descent (MMEF=20.27 mL/sec) proportional to the FVC (0.798 mL) (Figure 16 and Figure 17).

BLM challenge significantly reduced the curve area on the graph, affecting the decrease of PEF, FEV100, MMEF, and FVC values (23.56 mL/sec, 0.556 mL, 16.07 mL/sec, and 0.563

mL, respectively) ($p<0.0001$ for PEF, FEV100, and FVC, while MMEF value $p=0.0153$) (Figure 16 and Figure 17).

Nintedanib treatment significantly improved both FVC (0.692 mL) and FEV100 (0.640 mL/sec) parameters ($p=0.0018$ and $p=0.0418$, respectively) but did not affect PEF (23.5 mL/sec) and MMEF (15.52 mL/sec) parameters ($p=0.4882$ and $p=0.405$, respectively). These values resulted in a curve with the highest peak similar to the BLM Ctrls group but with a slower descent, resulting in the FVC similar to the unchallenged animals (Figure 16 and Figure 17).

Pirfenidone treatment significantly improved all observed parameters, resulting in the curve with a higher PEF of 26.92 mL/sec, FEV100 of 0.635 mL, MMEF of 19.2 mL/sec, and FVC of 0.647 mL ($p=0.0104$, $p=0.068$, $p=0.0246$, and $p=0.0054$, respectively) (Figure 16 and Figure 17).

The Tiffeneau index, calculated from the fast flow volume maneuver test parameters, was presented as a ratio between FEV100 and FVC values, with mean values of the evaluated groups shown in Figure 18. Individual raw data are listed in Appendix 3.

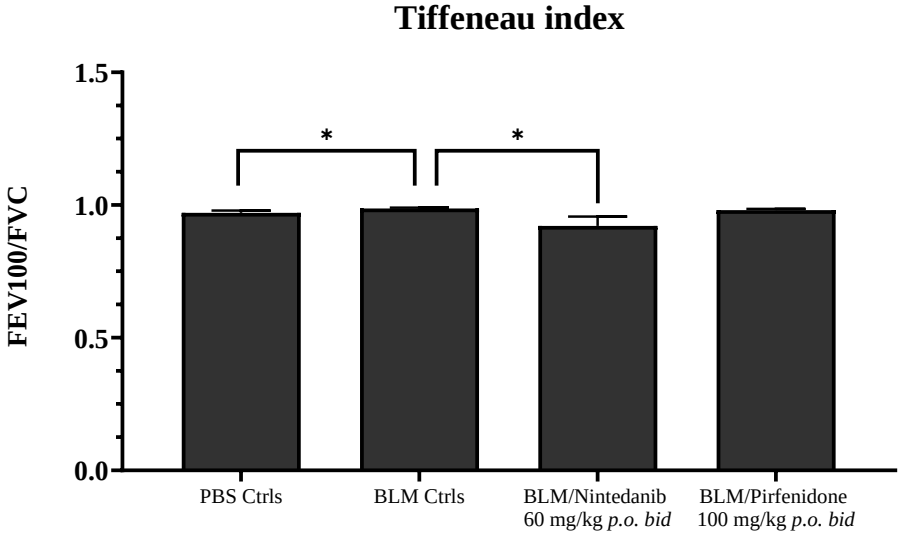

* $p<0.05$ vs. BLM Ctrls; Unpaired t test

Figure 18 Tiffeneau index

A Tiffeneau index was obtained by calculating a ratio of FEV100 and FVC measured in a fast flow volume maneuver test on day 21 in the BLM-induced pulmonary fibrosis model. Values are presented as group mean + sem.

Abbreviations: PBS-phosphate buffered saline, BLM-bleomycin, Ctrls-controls, *p.o.*-perorally, *bid*-twice a day, FVC-forced expiratory volume, FEV100-forced expiratory volume at 100 ms, vs.-*versus*, sem-standard error of the mean

A Tiffeneau index resulted in a significantly increased value (p=0.0248) in the BLM Ctrls groups (0.987) over PBS Ctrls (0.971).

Nintedanib treatment significantly decreased (0.921), while pirfenidone did not affect the FEV100/FVC ratio (0.981) (p=0.0451 and p=0.1376, respectively) (Figure 18).

5.3.1.4 Sequence 4. Resistance And Compliance Test

The last sequence, an automated RC maneuver, tested Ri and Cdyn parameters presented in Figure 19. Individual raw data values are listed in Appendix 3.

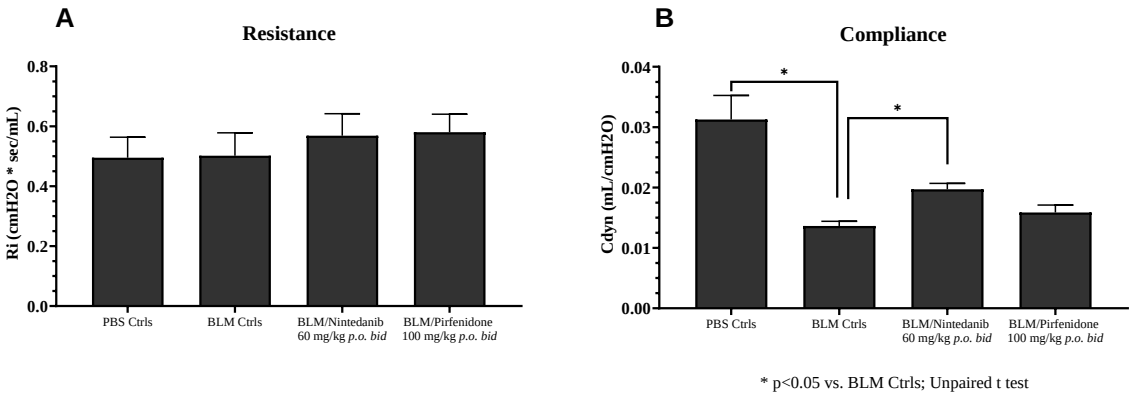

Figure 19 PFT sequence 4: Resistance and compliance parameters
The value of A) resistance and B) compliance parameters measured in the RC test on day 21 in the BLM-induced pulmonary fibrosis model were presented as a group mean + sem.

Abbreviations: PBS-phosphate buffered saline, BLM-bleomycin, Ctrls-controls, *p.o.*-perorally, *bid*-twice a day, Ri- resistance, Cdyn-dynamic compliance

A significant decline (p<0.0001) in the Cdyn parameter values was observed in the group challenged with BLM (0.014 mL/cm H2O) compared to PBS Ctrls (0.031 mL/cm H2O) (Figure 19).

Nintedanib treatment significantly improved (p<0.0001) values (0.020 mL/cm H2O), while pirfenidone reached no significance (0.016 mL/cm H2O) (p=0.0743) (Figure 19).

The difference between the observed groups was not recorded in the Ri parameter analysis (0.495, 0.502, 0.569, and 0.58 cm H2O*sec/mL, respectively) compared to the BLM Ctrls group (p=0.4773 vs. PBS Ctrls, p=0.2726 vs. nintedanib treated group, and p=0.2097 vs. pirfenidone treated group) (Figure 19).

Table 9 Overview of lung function parameters values measured in the BLM-induced pulmonary fibrosis model using the DSI's Buxco® Pulmonary function testing system

Reported parameters across test sequences are expressed as groups mean ± sem values

Buxco® Pulmonary Function Test	Parameter	PBS Ctrls	BLM Ctrls	BLM/ Nintedanib 60 mg/kg *p.o. bid*	BLM/ Pirfenidone 100 mg/kg *p.o. bid*
Sequence 1. Boyle's law functional residual capacity test	**Functional residual capacity (FRC) (mL)**	0.451 ± 0.028	0.386 ± 0.017	0.378 ± 0.026	0.408 ± 0.017
Sequence 2. Quasistatic pressure volume test	**Total lung capacity (TLC) (mL)**	1.114 ± 0.037	0.832 ± 0.023	0.943 ± 0.044	0.886 ± 0.035
	Residual volume (RV) (mL)	0.338 ± 0.034	0.303 ± 0.017	0.266 ± 0.028	0.294 ± 0.022
	Inspiratory capacity (IC) (mL)	0.663 ± 0.018	0.446 ± 0.017	0.564 ± 0.023	0.478 ± 0.028
	Vital capacity (VC) (mL)	0.777 ± 0.016	0.529 ± 0.018	0.678 ± 0.026	0.591 ± 0.03
	Expiration time (Te) (sec)	1.16 ± 0.073	0.682 ± 0.025	0.892 ± 0.037	0.807 ± 0.039
	Chord compliance (Cchord) (mL/cm H2O)	0.039 ± 0.001	0.026 ± 0.001	0.034 ± 0.002	0.028 ± 0.002
Sequence 3. Fast flow volume manuever test	**Forced vital capacity (FVC) (mL)**	0.798 ± 0.014	0.563 ± 0.015	0.692 ± 0.036	0.647 ± 0.026
	Forced expiratory volume at 100 ms (FEV100) (mL)	0.775 ± 0.015	0.556 ± 0.015	0.640 ± 0.042	0.635 ± 0.025
	Peak expiratory flow (PEF) (mL/sec)	32.06 ± 1.552	23.56 ± 0.931	23.5 ± 1.825	26.92 ± 1.005
	Maximal mid-expiratory flow (MMEF) (mL/sec)	20.27 ± 1.807	16.07 ± 0.913	15.52 ± 1.951	19.2 ± 1.197
	Tiffneau index (FEV100/FVC)	0.971 ± 0.008	0.987 ± 0.003	0.921 ± 0.035	0.981 ± 0.004
Sequence 4. Resistance and compliance test	**Resistance (Ri) (cm H2O*sec/mL)**	0.495 ± 0.068	0.502 ± 0.0767	0.569 ± 0.073	0.580 ± 0.06
	Compliance (Cdyn) (mL/cm H2O)	0.032 ± 0.004	0.014 ± 0.001	0.02 ± 0.001	0.016 ± 0.001

Abbreviations: PBS-phosphate buffered saline, BLM-bleomycin, Ctrls-controls.

5.3.2 Model of Ovalbumin-Induced Asthma

In the OVA-induced asthma experiment, sampling was conducted on day 24, approximately 24 hours after the last challenge. Initially, PFTs assessment was performed (Figure 20-27), presenting an overview of lung function parameters values in the Table 10, followed by AHR (Figure 28, Tables 11 and 12), and another PFT evaluation focusing on obstruction *via* the fast flow volume manuever (Figure 29 and 30, Table 13).

On the final day of the experiment, 48 animals underwent PFT measurements (raw data in Appendix 6) across four sequences. Each experimental group contributed valid measurements as follows:

- PBS/Saline Ctrls: eight valid measurements in all parameters;
- OVA/OVA Ctrls *p.o.*: ten valid measurements in all parameters;
- OVA/Dexamethasone 3 mg/kg *p.o.*: ten valid measurements in all parameters;
- OVA/OVA Ctrls *i.n.*: ten valid measurements in all parameters;
- OVA/Fluticasone propionate 2 mg/kg *i.n.*: ten valid measurements in all PFT parameters.

5.3.2.1 Sequence 1. Boyle's Law Functional Residual Capacity Test

The FRC parameter was measured and reported during the first PFT, specifically in the Boyle's law functional residual capacity test (Figure 20, Appendix 6).

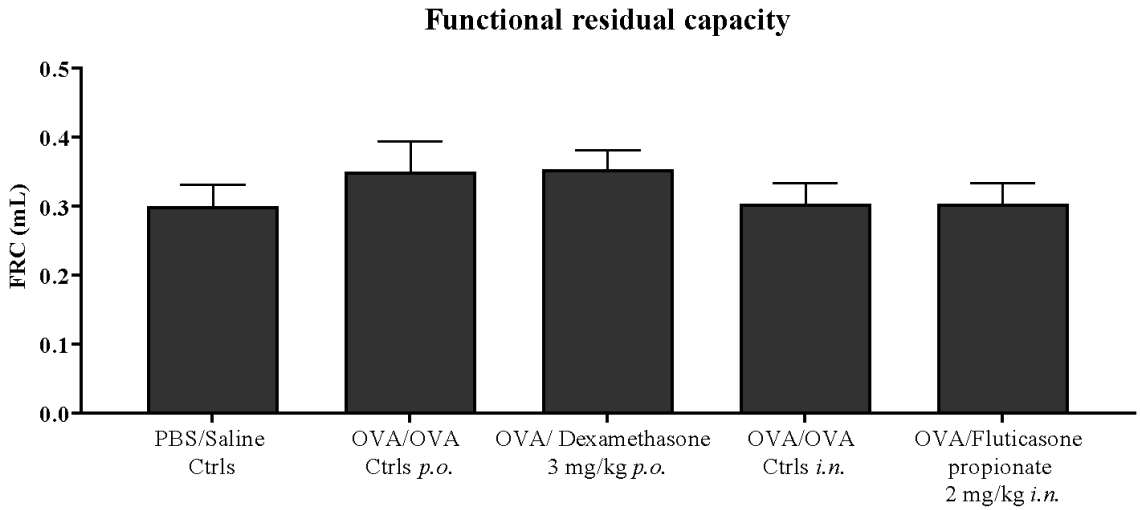

Figure 20 PFT sequence 1. Functional residual capacity parameter
An FRC value of each evaluated group measured in the Boyle's law functional residual capacity at day 24 in the OVA-induced asthma model was presented as a group mean + sem.

Abbreviations: FRC-functional residual capacity, PBS-phosphate buffered saline, OVA-ovalbumin, Ctrls-controls, *p.o.*-perorally, *i.n.*-intranasally

In the PBS Ctrls group, the mean FRC parameter was 0.3 mL, similar to OVA/OVA Ctrls *p.o.* (0.35 mL) and OVA/OVA Ctrls *i.n.* (0.303 mL) groups (p=0.1994 and p=0.476, respectively) (Figure 20, Appendix 6).

The dexamethasone-treated group had a mean FRC of 0.354 mL, comparable to the OVA/OVA Ctrls *p.o.* group (p=0.4698) (Figure 20, Appendix 6).

Fluticasone propionate *i.n.* treatment resulted in a mean FRC of 0.303 mL, similar to the corresponding vehicle control (p=0.5) (Figure 20, Appendix 6).

5.3.2.2 Sequence 2. Quasistatic Pressure Volume Test

In the second PFT, a quasistatic pressure-volume test measured TLC, RV, IC, VC, Cchord, and Te values, forming a P-V curve (Figure 21 - 23, Appendix 6 and 7).

The curve slope showed a right and downward shift in OVA/OVA Ctrls groups, while unchallenged animals displayed a curve slope characteristic of healthy animals. Both dexamethasone and fluticasone propionate improved the curve slope toward the PBS/Saline Ctrls curve (Figure 21, Appendix 7).

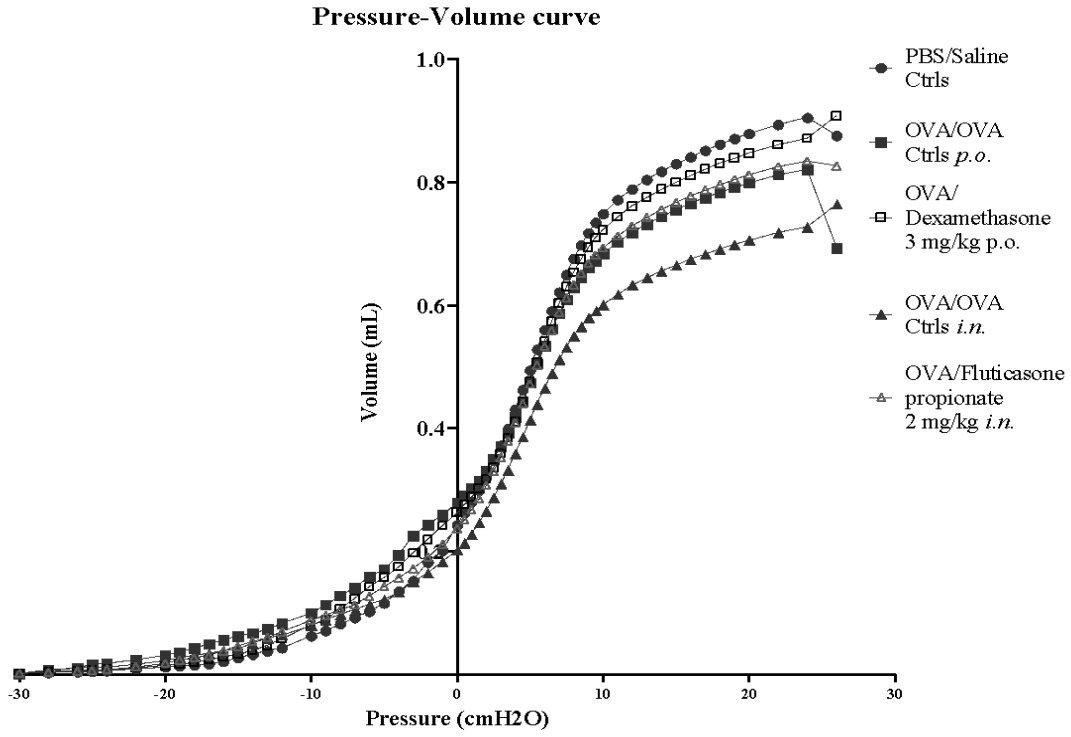

Figure 21 PFT sequence 2. A pressure-volume curve
The P-V curve was generated in the quasistatic pressure volume test on day 24 in the OVA-induced asthma model, presenting the mean values of volume measured under different airway pressures.

Abbreviations: PBS-phosphate buffered saline, OVA-ovalbumin, Ctrls-controls, *p.o.*-perorally, *i.n.*-intranasally

The Cchord parameter, representing the slope of the P-V curve between 0 and +10 cm H2O, was significantly decreased in OVA/OVA Ctrls *p.o.* (0.04 mL/cm H20) and OVA/OVA Ctrls *i.n.* (0.04 mL/cm H20) compared to PBS/Saline Ctrls (0.05 mL/cm H20) (p=0.0053 and p=0.0045, respectively) (Figure 21 and 22, Appendix 6).

Dexamethasone treatment significantly improved the Cchord parameter (0.046 mL/cm H20) compared to OVA/OVA Ctrls *p.o.* (p=0.0257) (Figure 21 and 22, Appendix 6).

Fluticasone propionate treatment did not reach significance (p=0.1477) as the Cchord value was 0.045 mL/cm H20 and was not significantly improved compared to OVA/OVA Ctrls *i.n.* (Figure 21 and 22, Appendix 6).

Parameter Te values were similar across experimental groups (1.017, 0.996, 0.962, 0.832, and 0.9 sec, respectively). However, the OVA/OVA Ctrls *i.n.* group showed significantly aggravated expiration time compared to PBS/Saline Ctrls (p=0.01) (Figure 21 and 22, Appendix 6).

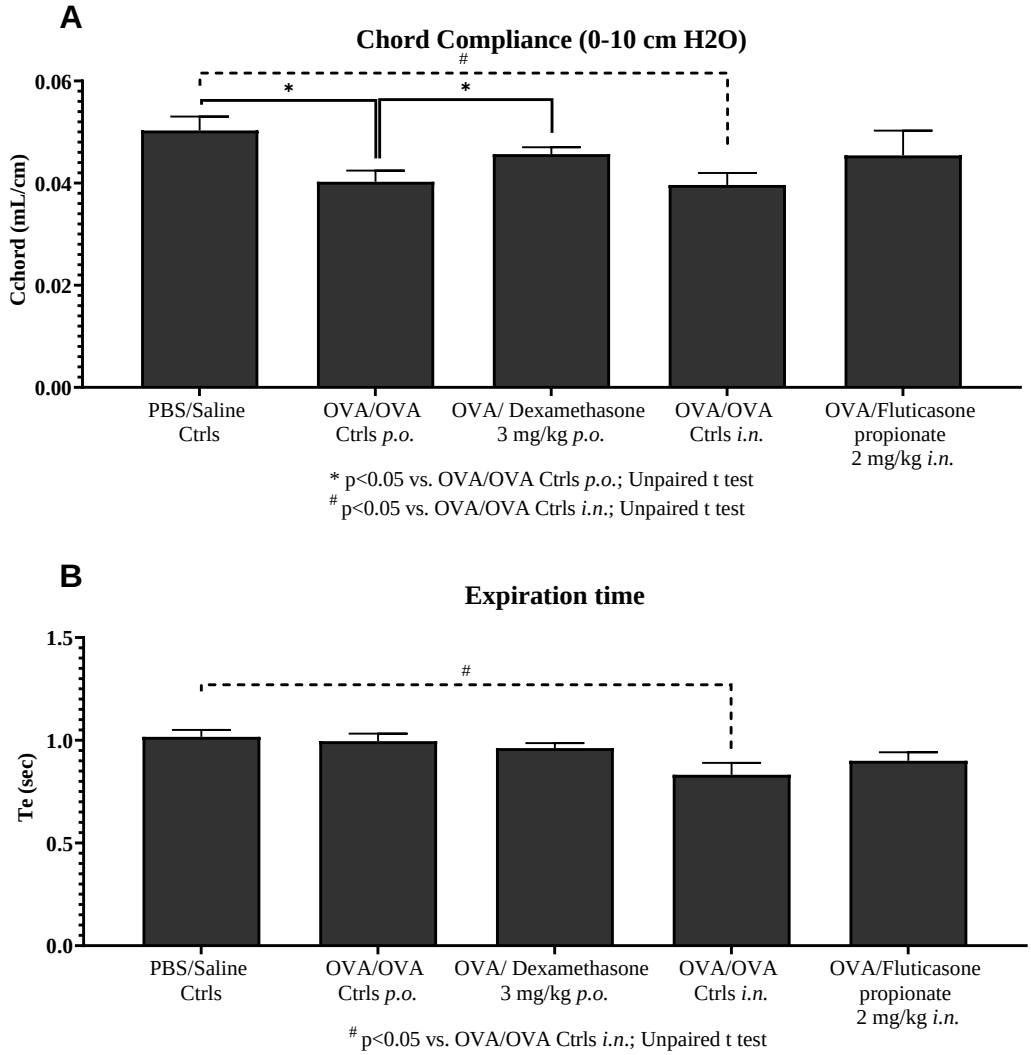

Figure 22 PFT sequence 2: Cchord and Te parameters
Parameters of A) compliance of the cord and B) expiration time generated in the quasistatic pressure volume test on day 24 in the OVA-induced asthma model, presented as group mean+sem.

Abbreviations: PBS-phosphate buffered saline, OVA-ovalbumin, Ctrls-controls, *p.o.*-perorally, *i.n.*-intranasally, Te-expiration time, Cchord – chord compliance, vs.-*versus*, sem-standard error of the mean

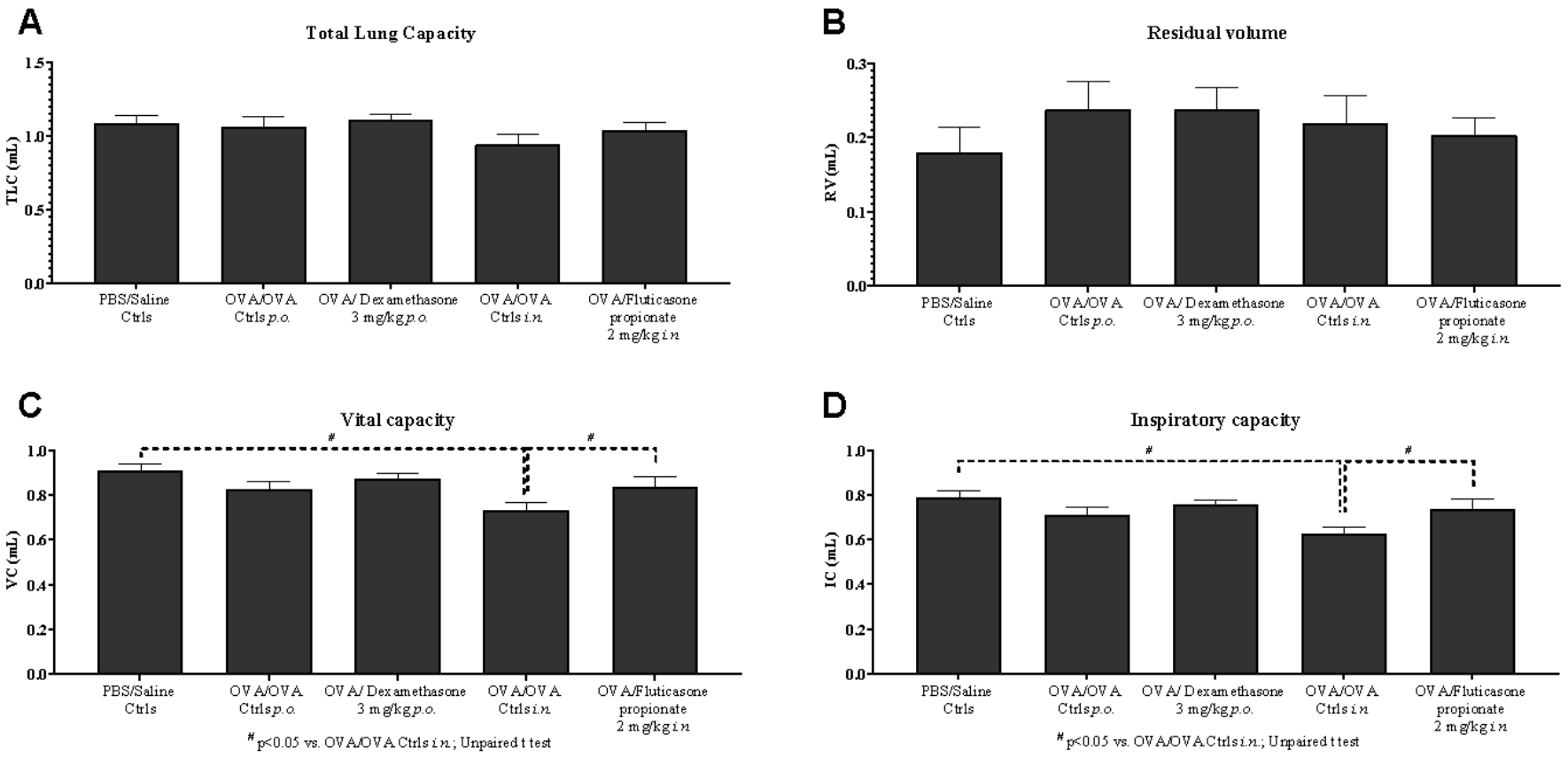

Figure 23 PFT sequence 2: TLC, RV, VC, and IC parameters

Parameters of A) total lung capacity, B) residual volume, C) vital capacity, and D) inspiratory capacity generated in the quasistatic pressure volume test on day 24 in the OVA-induced asthma model, presented as group mean+sem.

Abbreviations: PBS-phosphate buffered saline, OVA-ovalbumin, Ctrls-controls, *p.o.*-perorally, *i.n.*-intranasally, TLC-total lung capacity, RV-residual volume, IC-inspiratory capacity, VC-vital capacity, vs.-*versus,* sem-standard error of the mean

Analyses of TLC, RV, VC, and IC parameters, calculated from the P-V curve, did not affect OVA/OVA Ctrls *p.o.* (1.06, 0.237, 0.823, and 0.71 mL, respectively), compared to PBS/Saline Ctrls (1.088, 0.1789, 0.909, and 0.788, respectively) (p=0.3849, p=0.1498, p=0.0543, and p=0.0657, respectively) (Figure 23, Appendix 6).

Dexamethasone treatment showed no effect on observed parameters (1.133, 0.239, 0.874, and 0.759 mL, respectively) compared to the corresponding control group administered *p.o.* (p=0.2612, p=0.4908, p=0.1317, and p=0.1235, respectively) (Figure 23, Appendix 6).

In the group sensitized and challenged with OVA, administered with vehicle-corresponding fluticasone propionate treatment (OVA/OVA Ctrls *i.n.*), a significant decrease of VC and IC parameters (0.73 and 0.625 mL, respectively) was observed as compared to PBS/Saline Ctrls healthy group (p=0.0016 and 0.0022, respectively). However, the effect was not observed at the TLC and RV parameters (0.948 and 0.218 mL, respectively) (p=0.076 and p=0.2373, respectively) (Figure 23, Appendix 6).

The fluticasone propionate treatment significantly improved VC and IC values (0.837 and 0.737 mL, respectively) compared to the corresponding vehicle control group (p=0.0494 and p=0.0362, respectively). The effect on the TLC and RV parameters (1.04 and 0.203 mL) was not observed (p= 0.1651 and p=0.3661, respectively) (Figure 23, Appendix 6).

5.3.2.3 Sequence 3. Fast Flow Volume Maneuver Test

The subsequent test sequence, the fast flow volume maneuver test, produced an F-V curve (Figure 24), and parameter data including FVC, FEV100, PEF, and MMEF are depicted in Figure 25. The Tiffeneau index is presented in Figure 26. Individual value data are provided in Appendix 6 and Appendix 8.

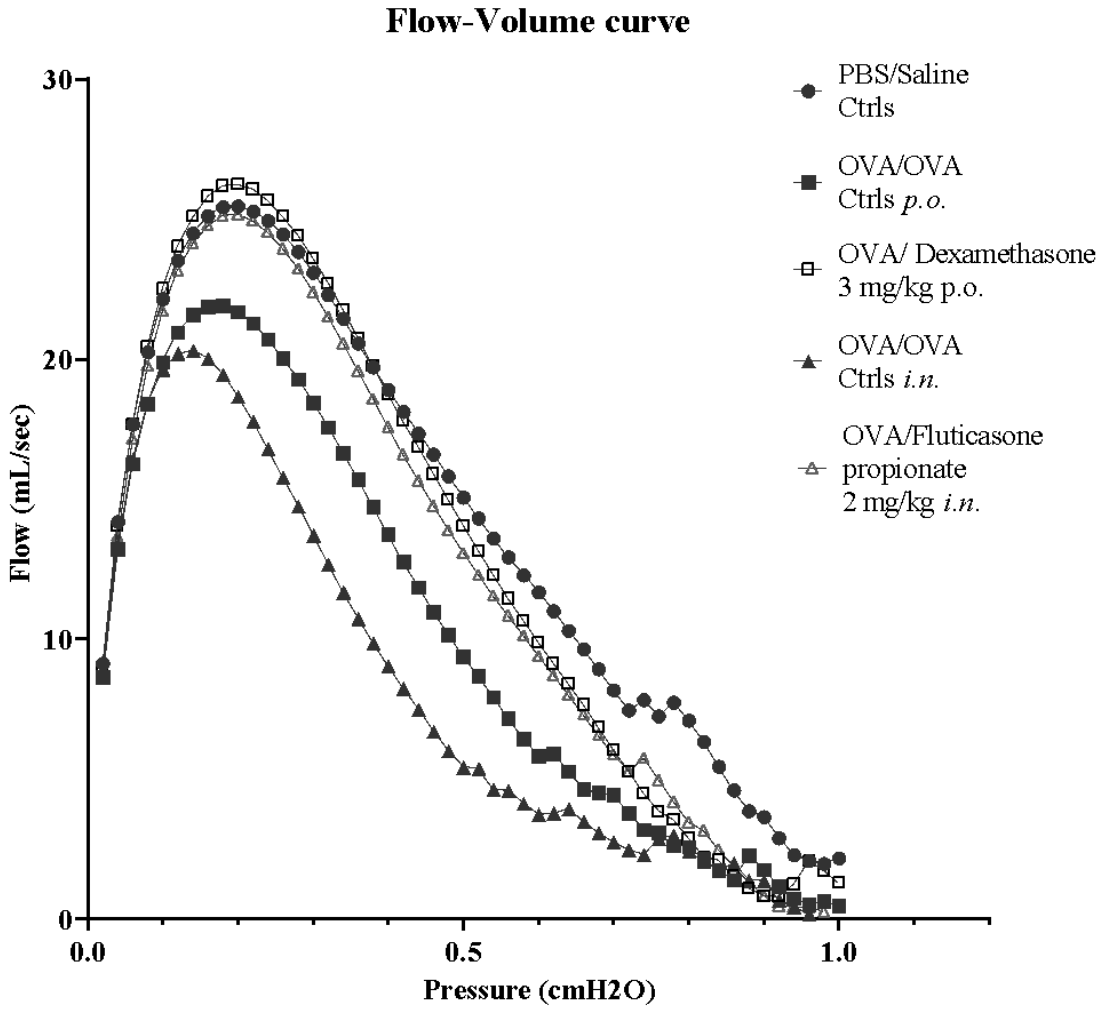

Figure 24 PFT sequence 3: A pressure-volume curve
The F-V curve was generated in the fast flow volume maneuver test on day 24 in the OVA-induced asthma model, presenting mean group values of flow measured in different airway volumes.

Abbreviations: F-V-flow volume, PBS-phosphate buffered saline, OVA-ovalbumin, Ctrls-controls, *p.o.*-perorally, *i.n.*-intranasally

The PBS/Saline Ctrls group's F-V curve displays the typical forced exhalation pattern of healthy BALB/c male mice. It exhibits a swift rise to PEF (14.75 mL/sec), followed by a FEV100 of 0.885 mL, and then a gradual linear decline (MMEF=26.06 mL/sec), in line with the FVC (0.918 mL) (Figure 24 and Figure 25).

OVA-induced sensitization and *i.n.* challenge significantly diminished the curve area for both control groups, leading to reduced PEF, FEV100, MMEF, and FVC values (Figure 24 and Figure 25).

The OVA/OVA Ctrls *p.o.* group depicted a concave F-V curve with PEF at 11.37 mL/sec and FEV100 at 0.706 mL. Describing the curve's descent, the MMEF value was 22.7 mL/sec, with an FVC of 0.804 mL (Figure 24 and Figure 25).

Treatment with dexamethasone aligned the F-V curve closer to that of the PBS/Saline Ctrls group, with PEF at 14.26 mL/sec, FEV100 at 0.812 mL, MMEF at 26.78 mL/sec, and FVC at 0.891 mL (Figure 24 and Figure 25).

Similarly, the OVA/OVA Ctrls *i.n.* group exhibited a concave F-V curve, with PEF at 9.501 mL/sec, FEV100 at 0.636 mL, MMEF at 20.74 mL/sec, and FVC at 0.714 mL (Figure 24 and Figure 25).

Fluticasone treatment improved PEF, FEV100, MMEF, and FVC values (14.35 mL/sec, 0.813 mL, 25.72 mL/sec, and 0.872 mL, respectively), positioning the F-V curve closer to that of the healthy controls (Figure 24 and Figure 25).

When compared to healthy animals, both OVA control groups exhibited significantly decreased FVC, FEV100, and PEF values ($p=0.0454$, $p=0.0077$, and $p=0.0435$, respectively in OVA/OVA Ctrls *p.o.* group; $p=0.0034$, $p=0.0002$, and $p=0.0015$, respectively in OVA/OVA Ctrls *i.n.* group). Additionally, the MMEF value was significantly decreased in the OVA/OVA Ctrls *i.n.* group ($p=0.0093$), while in the OVA/OVA Ctrls *p.o.* group, the significance was not reached ($p=0.1326$) (Figure 25).

In comparison to the corresponding OVA/OVA Ctrls *p.o.* group, dexamethasone treatment significantly improved the FEV100 value ($p=0.0345$), while FVC and MMEF values reached borderline significance ($p=0.0532$ and $p=0.0523$, respectively). No significant effect on the PEF value was observed ($p=0.0869$) (Figure 25).

Fluticasone propionate treatment, in comparison to the corresponding OVA/OVA Ctrls *i.n.* group, significantly improved all reported values in this test (FVC $p=0.0054$, FEV100 $p=0.0005$, PEF $p=0.0080$, and MMEF $p=0.0093$) (Figure 25).

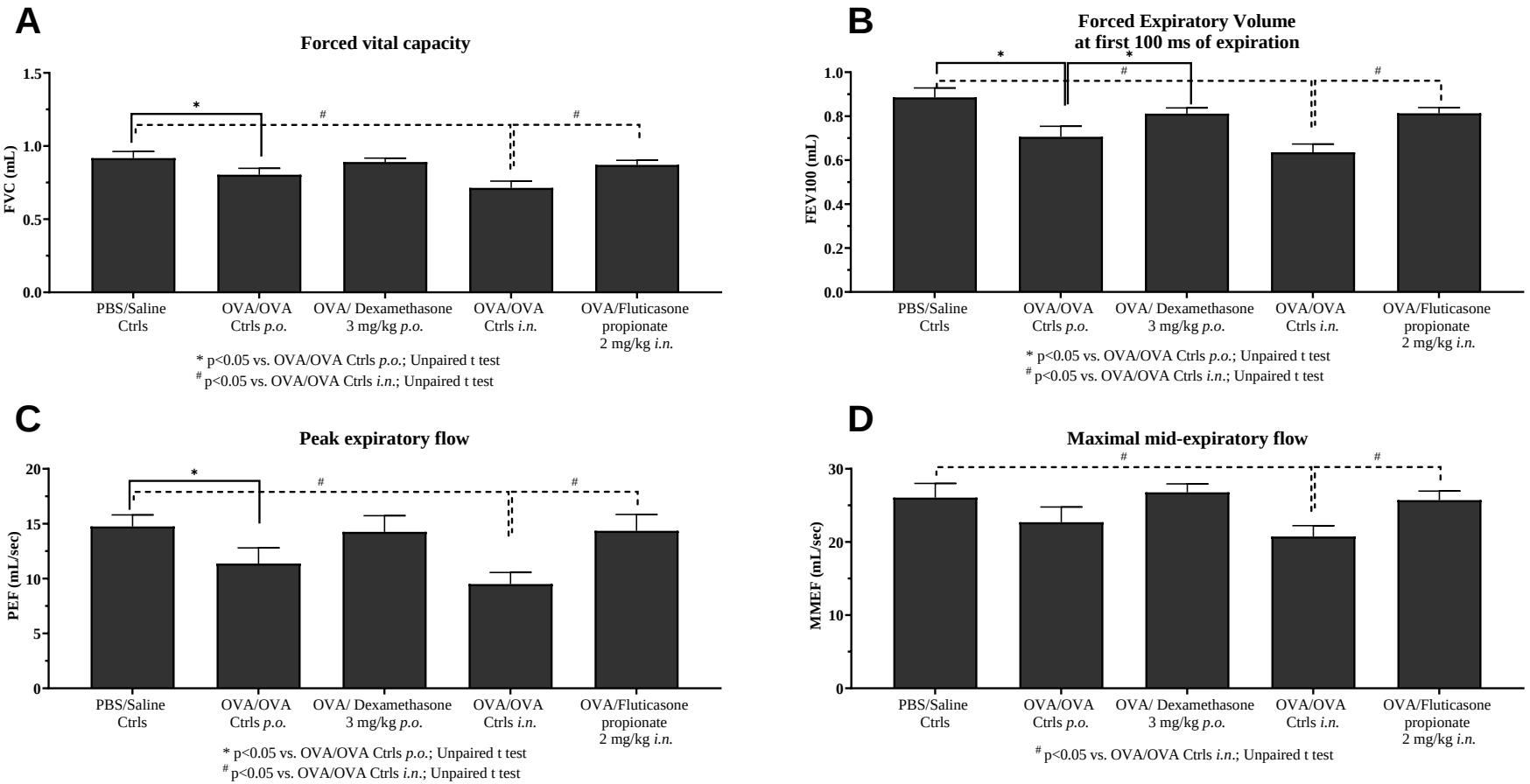

Figure 25 PFT sequence 3: FVC, FEV100, PEF and MMEF parameters

Parameters of A) forced vital capacity, B) forced expiratory volume at 100 ms, C) peak expiratory flow, and D) maximal mid-expiratory flow, generated in the fast flow volume maneuver test on day 24 in the OVA-induced asthma model, presented as group mean+sem.

Abbreviations: PBS-phosphate buffered saline, OVA-ovalbumin, Ctrls-controls, *p.o.*-perorally, *i.n.*-intranasally, FVC-forced expiratory volume, FEV100-forced expiratory volume at 100 ms, PEF-peak expiratory flow, MMEF- maximal mid-expiratory flow, vs.-*versus,* sem-standard error of the

A Tiffeneau index value was calculated in the OVA-induced asthma model from the FEV100 and FVC, representing their ratio. The mean groups' values and the results of statistical analysis are presented in Figure 26. Individual raw data are listed in Appendix 6.

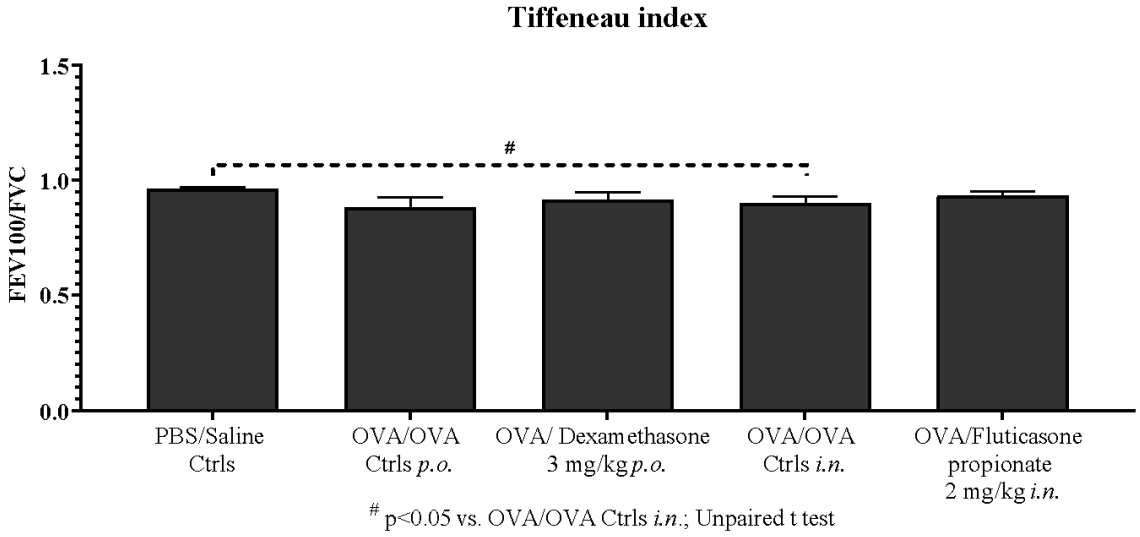

Figure 26 Tiffeneau index
A Tiffeneau index was obtained by calculating the ratio of FEV100 and FVC measured in the fast flow volume maneuver test on day 24 in the OVA-induced asthma model. Values are presented as group mean + sem.

Abbreviations: PBS-phosphate buffered saline, OVA-ovalbumin, Ctrls-controls, *p.o.*-perorally, *i.n.*-intranasally, FVC-forced expiratory volume, FEV100-forced expiratory volume at 100 ms, vs.-*versus*, sem-standard error of the mean

A Tiffeneau index resulted in a significantly decreased (p=0.0405) value in the OVA/OVA Ctrls *i.n.* group (0.9) over PBS/Saline Ctrls groups (0.965). However, when compared to fluticasone propionate treatment group (0.936), the difference was not observed (p=0.1605) (Figure 26).

An OVA/OVA Ctrls *p.o.* group (0.883), when compared to the healthy control group (0.965), reached borderline significance (p=0.0586), which was not affected by dexamethasone treatment (0.917) (p=0.2694) (Figure 26).

5.3.2.4 Sequence 4. Resistance and Compliance Test

The last sequence, an automated RC maneuver, tested Ri and Cdyn parameters presented in Figure 27. Individual raw data values are listed in Appendix 6.

A value of smooth muscle contraction, Ri, and lung elasticity Cdyn were recorded for each experimental group as follows:

- PBS/Saline Ctrls: 0.933 H2O*sec/mL (Ri) and 0.034 mL/cm H2O (Cdyn);
- OVA/OVA Ctrls *p.o*: 1.796 cm H2O*sec/mL (Ri) and 0.029 mL/cm H2O (Cdyn);
- OVA/OVA Dexamethasone 3 mg/kg *p.o.*:0.715 cm H2O*sec/mL (Ri) and 0.033 mL/cm H2O (Cdyn);
- OVA/OVA Ctrls *i.n.*: 1.33 cm H2O*sec/mL (Ri) and 0.027 mL/cm H2O (Cdyn);
- OVA/OVA Fluticasone propionate 2 mg/kg *i.n.*: 0.921 cm H2O*sec/mL (Ri) and 0.029 mL/cm H2O (Cdyn) (Figure 27, Appendix 6).

Statistical analysis, applying an unpaired t-test, showed only the effect of OVA immunization and challenge (OVA/OVA Ctrls *i.n.* group) on the decrease of Cdyn compared to the non-treated control group (p=0.0145). The Ri value was not significantly different between the two compared groups (p=0.1177) (Figure 27).

OVA/OVA Ctrls *p.o.* group when compared to non-treated control group PBS/Saline Ctrls) reached no significance in the Ri (p=0.1292) or Cdyn (p=0.086) parameters (Figure 27).

Dexamethasone treatment showed no effect on the Ri and Cdyn parameters, compared to corresponding vehicle control (OVA/OVA Ctrls *p.o.*) (p=0.2464 and p=0.158, respectively) (Figure 27).

Fluticasone propionate treatment did not affect the Ri parameter compared to corresponding vehicle control (OVA/OVA Ctrls *i.n.*) (p=0.0988). A significant difference was observed in neither Cdyn parameter measured in this test sequence (p=0.2508) (Figure 27).

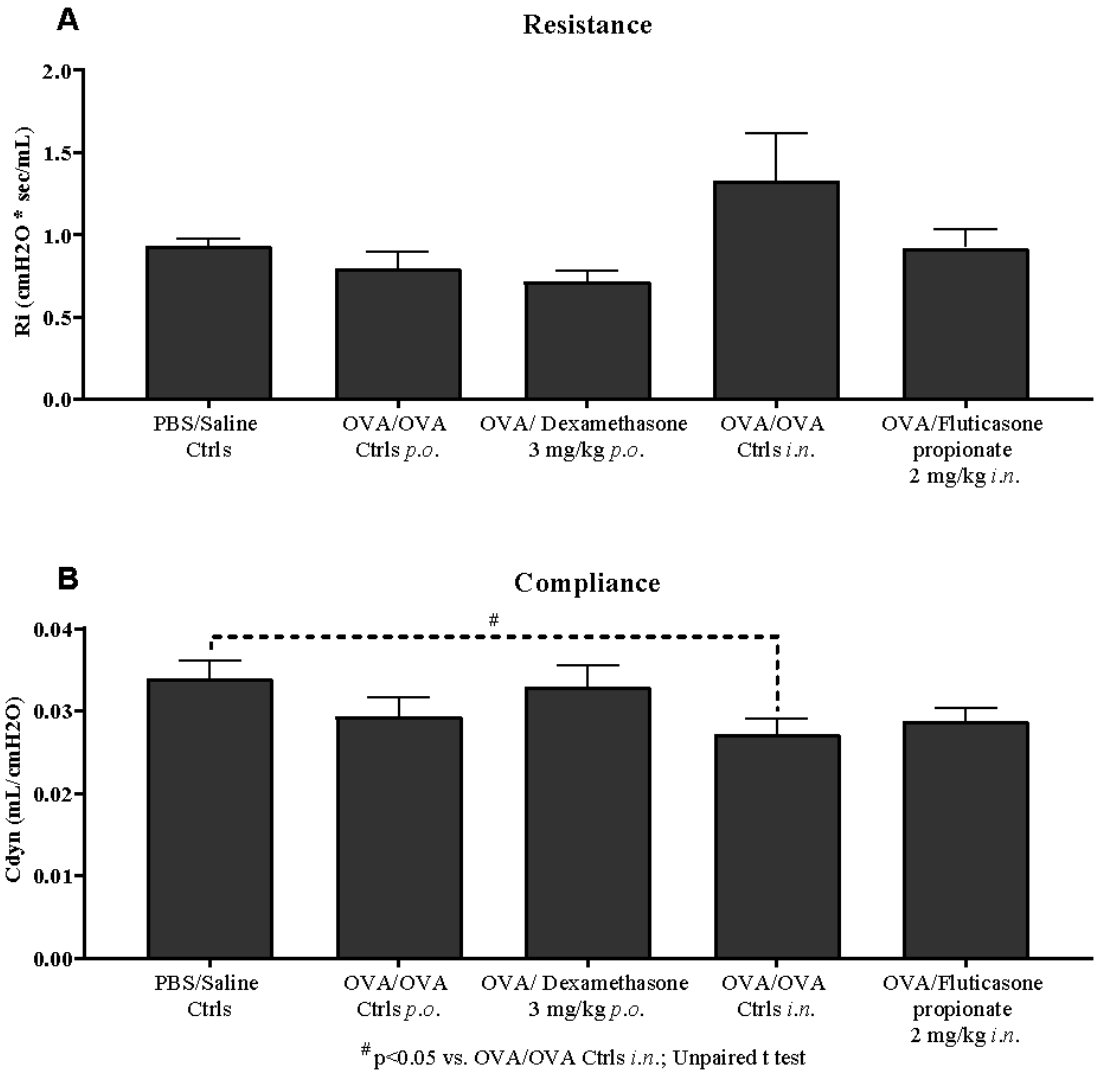

Figure 27 PFT sequence 4: Resistance and compliance parameters
The values of A) resistance and B) compliance parameters measured in the RC test on day 24 in the OVA-induced asthma model are presented as group mean+sem.

Abbreviations: PBS-phosphate buffered saline, OVA-ovalbumin, Ctrls-controls, *p.o.*-perorally, *i.n.*-intranasally, Ri-resistance, Cdyn-dynamic compliance vs.-*versus*, sem-standard error of the mean

Table 10 Overview of lung function parameters values measured in the OVA-induced asthma model using the DSI's Buxco® Pulmonary function testing system

Buxco® Pulmonary Function Test	Parameter	PBS/ Saline Ctrls	OVA/OVA Ctrls *p.o.*	OVA/ Dexamethasone 3 mg/kg *p.o.*	OVA/OVA Ctrls *i.n.*	OVA/Fluticasone propionate 2 mg/kg *i.n.*
Sequence 1. Boyle's law functional residual capacity test	**Functional residual capacity (FRC) (mL)**	0.300 ± 0.031	0.350 ± 0.045	0.354 ± 0.028	0.303 ± 0.03	0.303 ± 0.03
Sequence 2. Quasistatic pressure volume test	**Total lung capacity (TLC) (mL)**	1.088 ± 0.053	1.06 ± 0.072	1.113 ± 0.036	0.948 ± 0.071	1.04 ± 0.057
	Residual volume (RV) (mL)	0.179 ± 0.035	0.237 ± 0.039	0.239 ± 0.03	0.218 ± 0.038	0.203 ± 0.024
	Inspiratory capacity (IC) (mL)	0.788 ± 0.033	0.71 ± 0.035	0.759 ± 0.021	0.625 ± 0.035	0.737 ± 0.047
	Vital capacity (VC) (mL)	0.909 ± 0.029	0.823 ± 0.039	0.874 ± 0.022	0.73 ± 0.04	0.837 ± 0.047
	Expiration time (Te) (sec)	1.017 ± 0.034	0.996 ± 0.037	0.962 ± 0.024	0.832 ± 0.058	0.9 ± 0.042
	Chord compliance (Cchord) (mL/cm H2O)	0.05 ± 0.003	0.04 ± 0.002	0.046 ± 0.001	0.04 ± 0.002	0.045 ± 0.005
Sequence 3. Fast flow volume manuever test	**Forced vital capacity (FVC) (mL)**	0.918 ± 0.045	0.804 ± 0.043	0.891 ± 0.027	0.714 ± 0.046	0.872 ± 0.031
	Forced expiratory volume at 100 ms (FEV100) (mL)	0.885 ± 0.043	0.706 ± 0.048	0.812 ± 0.026	0.636 ± 0.038	0.813 ± 0.026
	Peak expiratory flow (PEF) (mL/sec)	14.75 ± 1.05	11.37 ± 1.43	14.26 ± 1.46	9.501 ± 1.05	14.35 ± 1.49
	Maximal mid-expiratory flow (MMEF) (mL/sec)	26.06 ± 1.95	22.7 ± 2.08	26.78 ± 1.16	20.74 ± 1.49	25.72 ± 1.23
	Tiffneau index (FEV100/FVC)	0.965 ± 0.007	0.883 ± 0.044	0.917 ± 0.032	0.9 ± 0.031	0.936 ± 0.017
Sequence 4. Resistance and compliance test	**Resistance (Ri) (cm H2O*sec/mL)**	0.933 ± 0.044	0.796 ± 0.098	0.715 ± 0.064	1.33 ± 0.283	0.921 ± 0.111
	Compliance (Cdyn) (mL/cm H2O)	0.034 ± 0.002	0.029 ± 0.002	0.033 ± 0.003	0.027 ± 0.002	0.029 ± 0.002

Reported parameters across test sequences are expressed as groups mean ± sem values
Abbreviations: PBS-phosphate buffered saline, OVA-ovalbumin, Ctrls-controls.

5.4 AIRWAY HYPERRESPONSIVENESS TEST

5.4.1 Model of Ovalbumin-Induced Asthma

An AHR test was conducted only in the OVA-induced asthma model by exposing animals to increasing concentrations of nebulized Mch solution. First, animals were exposed to PBS to measure baseline values and, subsequently, to 0.625, 2.5, 5, and 12.5 mg/mL Mch. Results are presented in Figure 28, where each group's Ri and Cdyn were plotted against Mch concentrations. Each concentration P value were compared to the corresponding control group and presented in Tables 11 and 12. Raw data are listed in Appendix 9.

The PBS/Saline Ctrls group consisted of eight valid measurements, Ri mean group values of PBS exposure, and Mch in the increasing doses of 0.625, 2.5, 5, and 12.5 mg/mL were as follows: 1.6603, 1.7273, 2.2544, 2.8268 and 3.667 cmH2O*sec/mL, respectively. Values of Cdyn in the aforementioned PBS and Mch doses were 0.0292, 0.0269, 0.0232, 0.0199, and 0.0159 mL/cmH2O, respectively (Figure 28).

In the OVA/OVA Ctrls *p.o.* group, one animal died post-PFT test, and nine valid measurements were recorded. Mean group Ri values were 1.8994, 2.4653, 3.4717, 5.3391, and 9.4386 cmH2O*sec/mL, respectively. Values of Cdyn were 0.0238, 0.02, 0.015, 0.01, and 0.0063 mL/cmH2O, respectively (Figure 28).

The corresponding reference standard treated group was OVA/Dexamethasone 3 mg/kg *p.o.* Ri values were 1.7276, 1.8047, 2.2211, 3.8344, and 5.667 cmH2O*sec/mL, respectively. Values of Cdyn in this group were 0.0247, 0.0219, 0.0197, 0.0134, and 0.0106 mL/cmH2O, respectively (Figure 28). Mean group values included ten valid measurements throughout all PBS and Mch exposures.

The second control group OVA/OVA Ctrls *i.n.* mean Ri values of 10 valid measurements were 2.4324, 3.0286, 4.0034, 5.7308, and 7.7374 cmH2O*sec/mL, respectively. Values of Cdyn were 0.0235, 0.0188, 0.0159, 0.0126, and 0.0092 mL/cmH2O, respectively (Figure 28).

Fluticasone propionate treated group Ri values (10 valid measurements mean value) were 1.7516, 1.8636, 2.0219, 2.6332, and 4.5322 cmH2O*sec/mL, respectively. Values of Cdyn were 0.0317, 0.0282, 0.0253, 0.0224, and 0.0146, respectively (Figure 28).

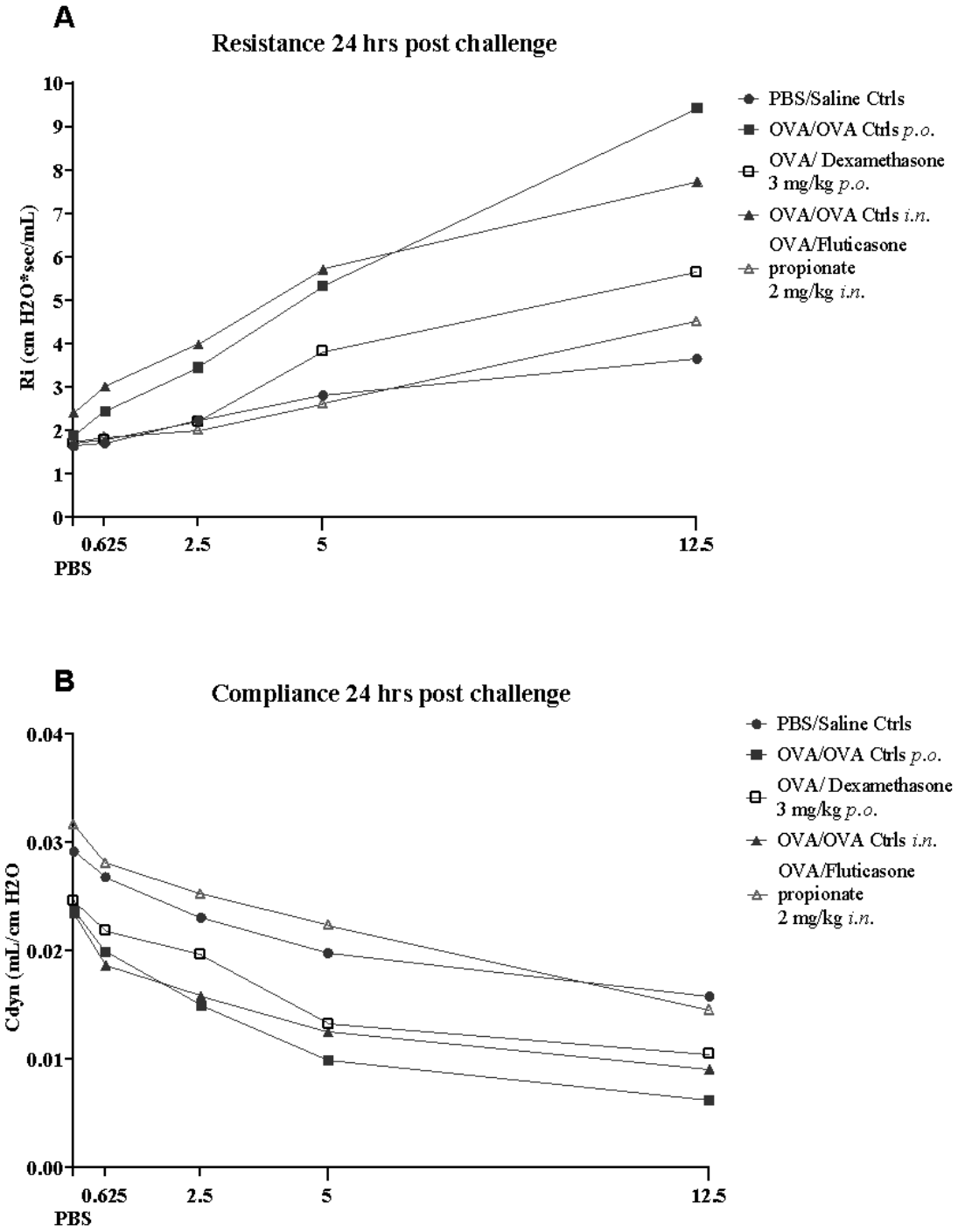

Figure 28 AHR test resistance and compliance curves

A change to the PBS and methacholine aerosolized concentration levels of 0.625, 2.5, 5, and 12.5 mg/mL affecting A) resistance and B) compliance parameters measured 24 h post last OVA challenge in the OVA-induced asthma model. Values of measured parameters plotted against PBS or Mch concentration are presented as group means.

Abbreviations: PBS-phosphate buffered saline, OVA-ovalbumin, Ctrls-controls, *p.o.*-perorally, *i.n.*-intranasally, Ri-resistance, Cdyn-dynamic compliance, Mch-methacholine, AHR-airway hyperresponsiveness

Table 11 Resistance changes to increasing methacholine levels and statistical analysis results

Resistance AHR parameter group values measured following exposure to increasing concentrations of PBS or Mch were compared to corresponding control groups' mean value at the observed challenge point. Groups were compared to related vehicle controls: OVA/OVA Ctrls *p.o.* or OVA/OVA Ctrls *i.n.* Unpaired t-test analysis p values are reported in the table. Statistically significant p values ($p<0.05$) are highlighted in grey.

*p<0.05 vs. OVA/OVA Ctrls *p.o.*	Resistance, Unpaired t test				
	PBS	0.625 mg/mL	2.5 mg/mL	5 mg/mL	12.5 mg/mL
PBS/Saline	0.3397	0.0223	0.0056	0.0004	0.0003
OVA/ Dexamethasone 3 mg/kg *p.o.*	0.4906	0.0630	0.0010	0.0494	0.0061
*p<0.05 vs. OVA/OVA Ctrls *i.n.*	Resistance, Unpaired t test				
	PBS	0.625 mg/mL	2.5 mg/mL	5 mg/mL	12.5 mg/mL
PBS/Saline	0.1464	0.0849	0.0753	0.0306	0.0067
OVA/ Fluticasone propionate 2 mg/kg *i.n.*	0.1620	0.0984	0.0272	0.0127	0.0332

Table 12 Dynamic compliance changes to increasing methacholine levels and statistical analysis results

Dynamic compliance AHR parameter group values measured following exposure to increasing concentrations of PBS or Mch were compared to corresponding control groups' mean value at the observed challenge point. Statistically significant p values ($p<0.05$) are highlighted in grey. Groups were compared to corresponding vehicle controls: OVA/OVA Ctrls *p.o.* or OVA/OVA Ctrls *i.n*

*p<0.05 vs. OVA/OVA Ctrls *p.o.*	Compliance, Unpaired t test				
	PBS	0.625 mg/mL	2.5 mg/mL	5 mg/mL	12.5 mg/mL
PBS/Saline	0.0313	0.0053	0.0015	0.0000	0.0000
OVA/ Dexamethasone 3 mg/kg *p.o.*	0.7297	0.3944	0.0186	0.0204	0.0186
*p<0.05 vs. OVA/OVA Ctrls *i.n.*	Compliance, Unpaired t test				
	PBS	0.625 mg/mL	2.5 mg/mL	5 mg/mL	12.5 mg/mL
PBS/Saline	0.1170	0.0465	0.0461	0.0402	0.0371
OVA/ Fluticasone propionate 2 mg/kg *i.n.*	0.0421	0.0297	0.0162	0.0206	0.1775

Abbreviations in Table 11 and Table 12: PBS-phosphate buffered saline, OVA-ovalbumin, Ctrls-controls, *p.o.*-perorally, *i.n.*-intranasally, *vs.*-*versus*.

OVA challenge in the OVA/OVA Ctrls *p.o.* significantly increased Ri starting from the lowest Mch concentration (0.625 mg/mL), while Cdyn values decreased significantly starting from baseline, compared to the PBS/Saline Ctrls group (Figure 28, Table 11 and 12).

The dexamethasone treatment significantly reduced both Ri and Cdyn, starting from 2.5 mg/mL Mch concentration (Figure 28, Table 11 and 12).

OVA challenge in the OVA/OVA Ctrls *i.n.* significantly increased Ri starting from 5 mg/mL Mch, while Cdyn values decreased significantly starting from the lowest concentration, compared to the PBS/Saline Ctrls group (Figure 28, Table 11 and 12).

The fluticasone propionate treatment significantly reduced Ri starting from 2.5 mg/mL Mch concentration. Furthermore, Cdyn reduction was significant starting from the baseline value (Figure 28, Table 11 and 12).

5.5 PULMONARY FUNCTION TESTING POST MCH CHALLENGE

After AHR measurements under maximal Mch concentration (12.5 mg/mL), animals were transferred back to the Buxco© PFT system to perform the fast flow volume maneuver test. Values of observed parameters pre-Mch and post-Mch exposure, measured in this test sequence, are listed in Table 13. An F-V curve graph is presented in Figure 29. Raw individual data are presented in Appendix 10. Due to system limitations in the capacity of tested subjects, the particular animal no per group was tested:

- from the PBS/Saline Ctrls group of four mice;
- OVA/OVA Ctrls *p.o.* seven mice;
- OVA/ Dexamethasone 3 mg/kg *p.o.* seven mice;
- OVA/OVA Ctrls *i.n.* seven mice;
- OVA/Fluticasone propionate 2 mg/kg *i.n.* seven mice were measured post-AHR.

A PBS/Saline Ctrls group F-V curve after the Mch challenge had a significantly lower AUC than the curve measured before the challenge (Figure 29). The curve shows a lower ascent to PEF (6.324 mL/sec), with a FEV100 of 0.618 mL, subsequently a slow linear descent (MMEF=12.29 mL/sec) and FVC value of 0.894 mL (Figure 29 and Figure 30, Table 13).

OVA/OVA Ctrls *p.o.* group data formed a concave F-V curve with a smaller AUC than the pre-challenge curve (Figure 29). The parameter values calculated from the curve were PEF of 4.192 mL/sec and FEV100 of 0.479 mL. The MMEF value describing curve descent was 11.24 mL/sec, while the FVC value was 0.673 mL (Figure 30, Table 13). Compared to the PBS/Saline Ctrls group, only the FVC parameter significantly decreased (p=0.0116). At the same time, FEV100 and PEF values, which were significant prior to the Mch challenge, showed no significance (p=0.0885 and p=0.1161, respectively) (Table 13).

OVA/OVA Ctrls *i.n.* group data also formed a concave F-V curve with a smaller AUC than before the Mch challenge (Figure 29). A PEF value of 6.931 mL/sec, FEV100 of 0.547 mL, and MMEF of 14.82 mL/sec showed no significance (p=0.3799, p=0.2199, and p=0.1573, respectively) as compared to non-OVA sensitized and challenged group. Although, prior to the Mch challenge, all parameters were significant compared to non-OVA exposed animals, post-challenge, only an FVC value of 0.64 mL reached a significant decrease over the control group (p=0.0117) (Figure 30 and Table 13).

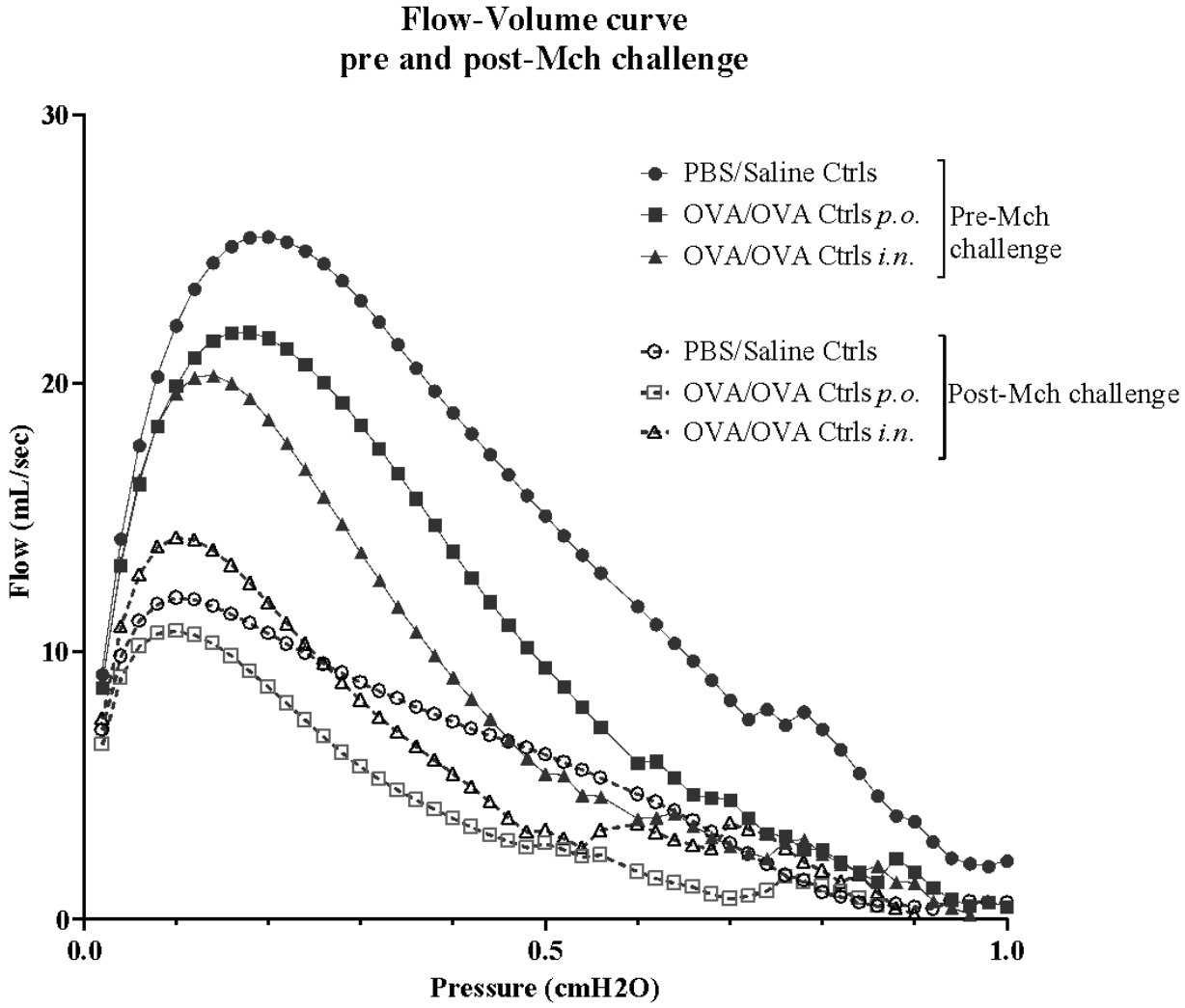

Figure 29 A pre and post-Mch exposure flow-volume curve of Ctrl groups
Values of flow measured in different airway volumes are presented as group mean.

Abbreviations: F-V-flow volume, PBS-phosphate buffered saline, OVA-ovalbumin, Ctrls-controls, *p.o.*-perorally, *i.n.*-intranasally

Dexamethasone treatment improved F-V curve AUC as compared to the corresponding OVA/OVA Ctrls *p.o.* group as described with the following: significant increase of PEF (8.018 mL/sec, p=0.0151) and MMEF (15.76 mL/sec, p=0.0165) values which were not significant prior to Mch challenge, and FEV100 (0.651 mL, p=0.0216). A FVC showed no significance at 0.768 mL (p=0.0951) (Figure 30, Table 13).

Fluticasone treatment group after the Mch challenge formed a concave curve with the following values of PEF, FEV100, MMEF, and FVC: 7.843 mL/sec, 0.696 mL, 17.24 mL/sec,

and 0.86 mL, respectively. Although prior to the Mch challenge, the significance was reached in all described parameters, in this test, the FVC parameter only reached the significance when compared to the corresponding OVA/OVA Ctrls *i.n.* group parameter value (p=0.0233) (Figure 30, Table 13).

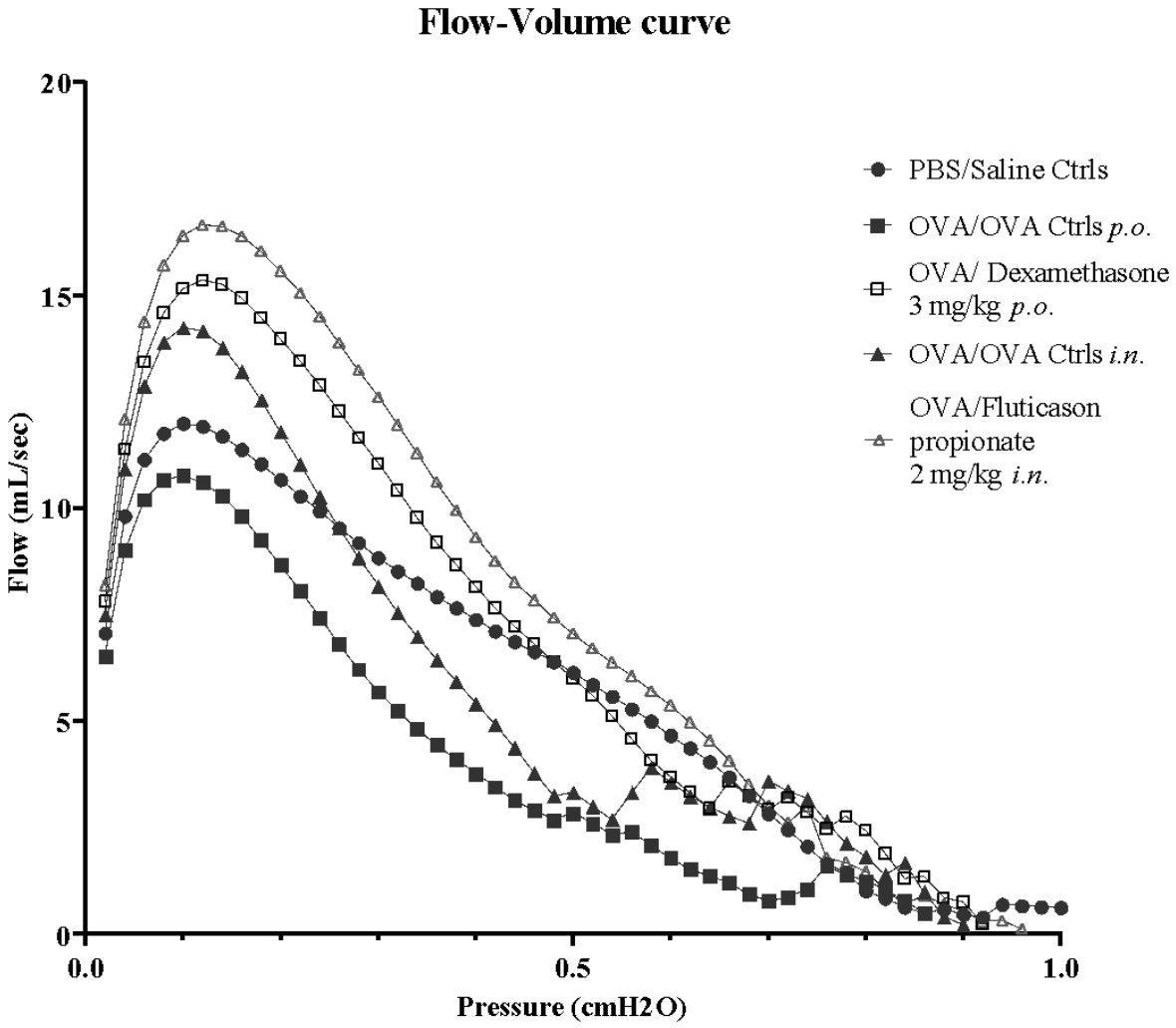

Figure 30 PFT sequence 3: A flow-volume curve measured post-Mch exposure

The F-V curve was generated in the fast flow volume maneuver test repeated on day 24 post-Mch exposure in the AHR test. Values of flow measured in different airway volumes are presented as group mean.

Abbreviations: F-V-flow volume, PBS-phosphate buffered saline, OVA-ovalbumin, Ctrls-controls, *p.o.*-perorally, *i.n.*-intranasally

Table 13 Statistical analysis of fast flow volume maneuver parameter values before and after methacholine challenge

PFT sequence three parameters measured prior to an AHR test and repeated post-Mch exposure on several animals *per* group are reported in the table. Values were compared to the corresponding control groups' mean values within the exact measurement. Groups were compared to the corresponding vehicle controls: *p<0.05 vs. OVA/OVA Ctrls *p.o.*; #p<0.05 vs. OVA/OVA Ctrls *i.n.*, Unpaired t-test. The underlined values of the statistical analysis outcome differ from pre-Mch measured values. The parameter values in bold text significantly differed from those measured before Mch exposure. An unpaired t-test was employed.

Parameter	PBS/Saline Ctrls		OVA/OVA Ctrls *p.o.*		OVA/ Dexamethasone 3 mg/kg *p.o.*		OVA/OVA Ctrls *i.n.*		OVA/Fluticasone propionate 2 mg/kg *i.n.*	
	Prior Mch n=8	**Post Mch n=4**	**Prior Mch n=10**	**Post Mch n=7**	**Prior Mch n=10**	**Post Mch n=7**	**Prior Mch n=10**	**Post Mch n=7**	**Prior Mch n=10**	**Post Mch n=7**
FVC	0.918 * #	0.894 * #	0.804	**0.673**	0.891	**0.768**	0.714	0.64	0.872 #	0.86 #
FEV100	0.885 * #	**0.618**	0.706	**0.479**	0.812 *	**0.651 ***	0.636	0.547	0.813 #	0.696
PEF	14.75 * #	**6.324**	11.37	**4.192**	14.26	**8.018 ***	9.50	6.931	14.35 #	**7.843**
MMEF	26.06 #	**12.29**	22.70	**11.24**	26.78	**15.76 ***	20.74	**14.82**	25.72 #	**17.24**
FEV100/ FVC	0.965 #	**0.714**	0.883	**0.706**	0.917	0.851 *	0.9	0.866	0.936	**0.807**

Abbreviations: PBS-phosphate buffered saline, OVA-ovalbumin, Ctrls-controls, *p.o.*-perorally, *i.n.*-intranasally, FVC- forced vital capacity, FEV100-forced expiratory volume at 100 ms, PEF- peak expiratory flow, MMEF-maximal mid-expiratory flow

The parameter values measured in the fast flow volume maneuver test post-Mch challenges were compared to the same parameters obtained prior to the challenge. An unpaired t-test was employed, and significantly different values were marked in bold text in Table 13.

In a PBS/Saline Ctrls group, FEV100, PEF, and MMEF values were significantly decreased post-Mch challenge (p=0.0065, p=0.0007, and p=0.0007, respectively), while FVC value was not significantly different (p=0.378) (Table 13).

In both the OVA/OVA Ctrls *p.o.* group and the dexamethasone-treated group, all parameters were significantly decreased as compared to corresponding values prior to the Mch challenge (FVC p=0.0354 and p=0.0114; FEV100 p=0.0029 and p=0.068; PEF p=0.0007 and 0.0046; and MMEF p=0.0003 and p<0.0001; respectively) (Table 13).

OVA/OVA Ctrls *i.n.* group MMEF value was significantly decreased over pre Mch value (p=0.0067), while FVC, FEV100, and PEF values showed no significance (p=0.1732, p=0.0678, and p=0.0576, respectively) (Table 13).

OVA/Fluticasone propionate group reached a significance over pre-challenge values in PEF and MMEF parameters (p=0.0036 and p=0.0006, respectively), while FVC and FEV100 values showed no significance (p=0.4399 and p=0.0574, respectively) (Table 13).

A Tiffeneau index measured post-Mch challenge significantly increased the dexamethasone-treated group (0.851, p=0.0408). At the same time, the difference was not observed in the non-OVA-exposed group (0.714, p=0.4732), as compared to the OVA/OVA Ctrls *p.o.* group (0.706) (Table 13).

OVA/OVA Ctrls *i.n.* group (0.866) over PBS/Saline Ctrls groups, nor when compared to fluticasone treated group (0.807) reached no significance for Tiffeneau index (p=0.0802 and p=0.1439, respectively) (Table 13).

Compared to values measured prior to Mch challenge, a Tiffeneau index showed a significant change over PBS/Saline Ctrl group (p=0.0083), OVA/OVA Ctrls *p.o.* group (p=0.0072), and fluticasone treated group (p=0.005), while dexamethasone-treated group and OVA/OVA Ctrls *i.n.* group showed no significance (p=0.1660 and p=0.2189, respectively) (Table 13).

5.6 BRONCHOALVEOLAR LAVAGE CELL COUNT

In the OVA-induced asthma model, BALF sampling was performed post-AHR or PFT measurements from all animals. The total and differential cell count in the BALF was evaluated to describe lung inflammation, and the results are presented in Figure 31. Raw data, including individual animal values of total cell count, macrophages, eosinophils, lymphocytes, and neutrophils count, are listed in Appendix 11.

The PBS/Saline Ctrls group consisted of eight valid measurements, total cell count, macrophage, eosinophil, lymphocytes, and neutrophil cell count mean group values were as follows: 0.3, 0.278, 0, 0.0188, and 0.004 x 10^9/L, respectively (Figure 31).

In the OVA/OVA Ctrls *p.o.* group, one animal died post-PFT test, and two samples contained blood, recording seven valid measurements. Analyses of the aforementioned cell groups' mean values in noted order were the following: 1.676, 0.549, 1.761, 0.037, and 0.041 10^9/L, respectively (Figure 31).

Corresponding reference standard treated group, OVA/Dexamethasone 3 mg/kg *p.o.*, mean group values included ten valid measurements. Total cell count, macrophage, eosinophil, lymphocytes, and neutrophil cell count mean group values were as follows: 0.274, 0.205, 0.008, 0.014, and 0.045 x 10^9/L, respectively (Figure 31).

In the second OVA control group (OVA Ctrls *i.n.*), two animal samples contained blood and were excluded. Therefore, eight valid measurements were included in group mean values of total cell count, macrophage, eosinophil, lymphocytes, and neutrophil cell count (0.913, 0.391, 1.403, 0.03, and 0.055 x 10^9/L, respectively) (Figure 31).

The fluticasone propionate-treated group included nine valid measurements (trachea of one animal was raptured during the withdrawal, and a sample could not be obtained). Mean values of total cell count, macrophage, eosinophil, lymphocytes, and neutrophil cell count measured in this group were the following: 0.358, 0.288, 0.017, 0.019, and 0.032 x 10^9/L, respectively) (Figure 31).

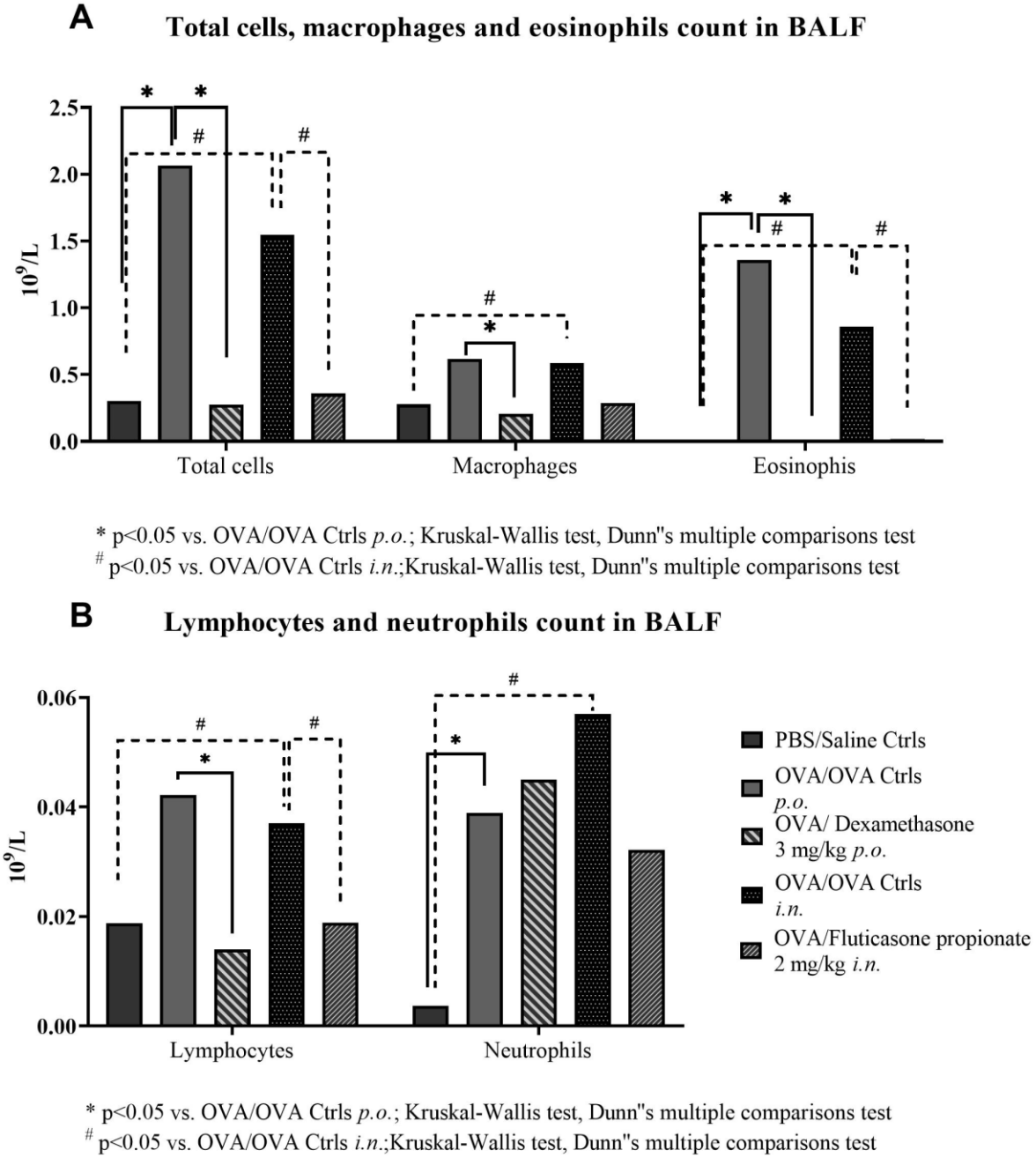

Figure 31 Graphical presentation of bronchoalveolar lavage fluid cell count analysis in the OVA-induced asthma model

A group mean value of A) total cell count, macrophages, and eosinophils and B) lymphocyte and neutrophils count in the bronchoalveolar lavage count sampled 24 h hours post last challenge in the OVA-induced asthma model.

Abbreviations: BALF- bronchoalveolar lavage fluid, PBS-phosphate buffered saline, OVA-ovalbumin, Ctrls-controls, *p.o.*-perorally, *i.n.*-intranasally, vs.-*versus*

Analyzes employing the Kruskal-Wallis test, with Dunn's multiple comparison tests, confirmed the increase of observed BALF cell populations in the animals sensitized and challenged with OVA, as well as the effect of tested treatment (Figure 31).

The OVA exposure increased all observed cell populations. Compared to PBS/Saline Ctrls group, OVA exposure significantly affected the BALF influx of total cell count ($p=0.022$ vs. OVA/OVA Ctrls *p.o.*, and $p=0.0006$ vs. OVA/OVA Ctrls *i.n.*), macrophages ($p=0.0452$ vs. OVA/OVA Ctrls *i.n.*), eosinophils ($p<0.0001$ vs. OVA/OVA Ctrls *p.o.*, and OVA/OVA Ctrls *i.n.*), lymphocytes ($p=0.0319$ vs. OVA/OVA Ctrls *i.n.*), and neutrophils ($p=0.0034$ vs. OVA/OVA Ctrls *p.o.*, and $p=0.0006$ OVA/OVA Ctrls *p.o.*,). The significance was not reached in OVA/OVA Ctrls *p.o.* group for macrophages and lymphocytes influx count ($p=0.149$ and $p=0.0912$, respectively) (Figure 31).

The predominant cell population in the BALF collected from OVA-exposed animals are the eosinophils, which were significantly decreased in the dexamethasone-treated group ($p=0.0016$) and the fluticasone propionate-treated group ($p=0.0219$), as compared to corresponding vehicle Ctrl group (Figure 31).

The macrophage count was affected only by dexamethasone treatment ($p=0.0206$) compared to the corresponding vehicle control, while fluticasone propionate treatment reached no significance ($p=0.1507$, as compared to OVA/OVA Ctrls *i.n.*) (Figure 31).

Lymphocyte and neutrophil cell count, although present in small amounts, was also influenced by OVA exposure. Thus, the effect of both standards treatments was observed only on lymphocyte count analysis ($p=0.0121$ dexamethasone-treated vs. OVA/OVA Ctrls *p.o.*, and $p=0.0428$ fluticasone propionate treated group vs. OVA/OVA Ctrls *i.n.*), while the neutrophils count was decreased with the fluticasone propionate treatment, but a significance was not reached ($p=0.6229$). Dexamethasone treatment showed no effect on the BALF neutrophil count as compared to the corresponding vehicle control ($p>0.9999$) (Figure 31).

5.7 IMMUNOGLOBULIN E AND CYTOKINE ANALYSES IN THE BALF

Levels of IgE and cytokines IL-4, IL-5 and IL-13 measured in BAL supernatant fluid sampled 24 hours post-last challenge are presented in Figure 32. Individual raw data are listed in Appendix 12.

Analyses of IL-4 and IL-5 consisted of the same valid measurements *per* group as BALF cell count analyses, while IL-13 measurements consisted of seven valid measurements in the PBS Ctrls group and nine in the dexamethasone treated group due to technical errors. IgE analysis included also seven valid measurements in the PBS Ctrl group, ten in the OVA/OVA Ctrls *p.o.*, eight in the dexamethasone treated group, nine in the OVA/OVA Ctrls *i.n.*, and eight in the fluticasone propionate treatment, also due to results interpretation technical error in several samples (Figure 32, Appendix 12).

OVA immunization and direct airway challenge induced a significant increase of IL-4 ($p=0.0076$) and IgE levels ($p=0.0017$) in BALF of the OVA/OVA Ctrls *p.o*. group (8.791 and 44.25 pg/mL, respectively) as compared to PBS/Saline Ctrls (2.731 and 11.48 pg/mL, respectively) (Figure 32).

Induction of IL-4 and IgE section was detected also in OVA/OVA Ctrls *i.n.* group (13.04 and 26.02 pg/mL, respectively), but the effect was not significant due to high individual variability ($p=0.1275$ and $p=0.1472$, respectively). The IL-5 and IL-13 cytokine levels (1.59 and 11.91 pg/mL, respectively) were not significantly affected in the observed group as compared to PBS/Saline Ctrls ($p=0.8599$ and $p=0.6457$, respectively) (Figure 32).

The effect of dexamethasone treatment was observed in IL-4 ($p=0.0002$) and IL-13 ($p=0.0106$) cytokines analysis (0.403 and 7.779 pg/mL, respectively) and the IgE analysis (13.14 pg/mL) in BALF ($p=0.0017$), compared to corresponding vehicle control group (8.791, 32.30, and 44.25 pg/mL, respectively). Although the treatment decreased the IL-5 cytokines concentration in BALF, it reached no significance ($p=0.1091$) (Figure 32).

The fluticasone propionate effect could not be reached as compared to OVA/OVA Ctrls *i.n.* high variable values group. The values and significance of observed parameters in this group were the following: IL-4 BALF levels (1.717 pg/mL, $p=0.078$), IL-5 (4.157 pg/mL, $p=0.4924$), and IL-13 (15.16 pg/mL, $p=0.8929$) cytokines analysis and the IgE analysis (21.05 pg7mL, $p=0.7528$) (Figure 32).

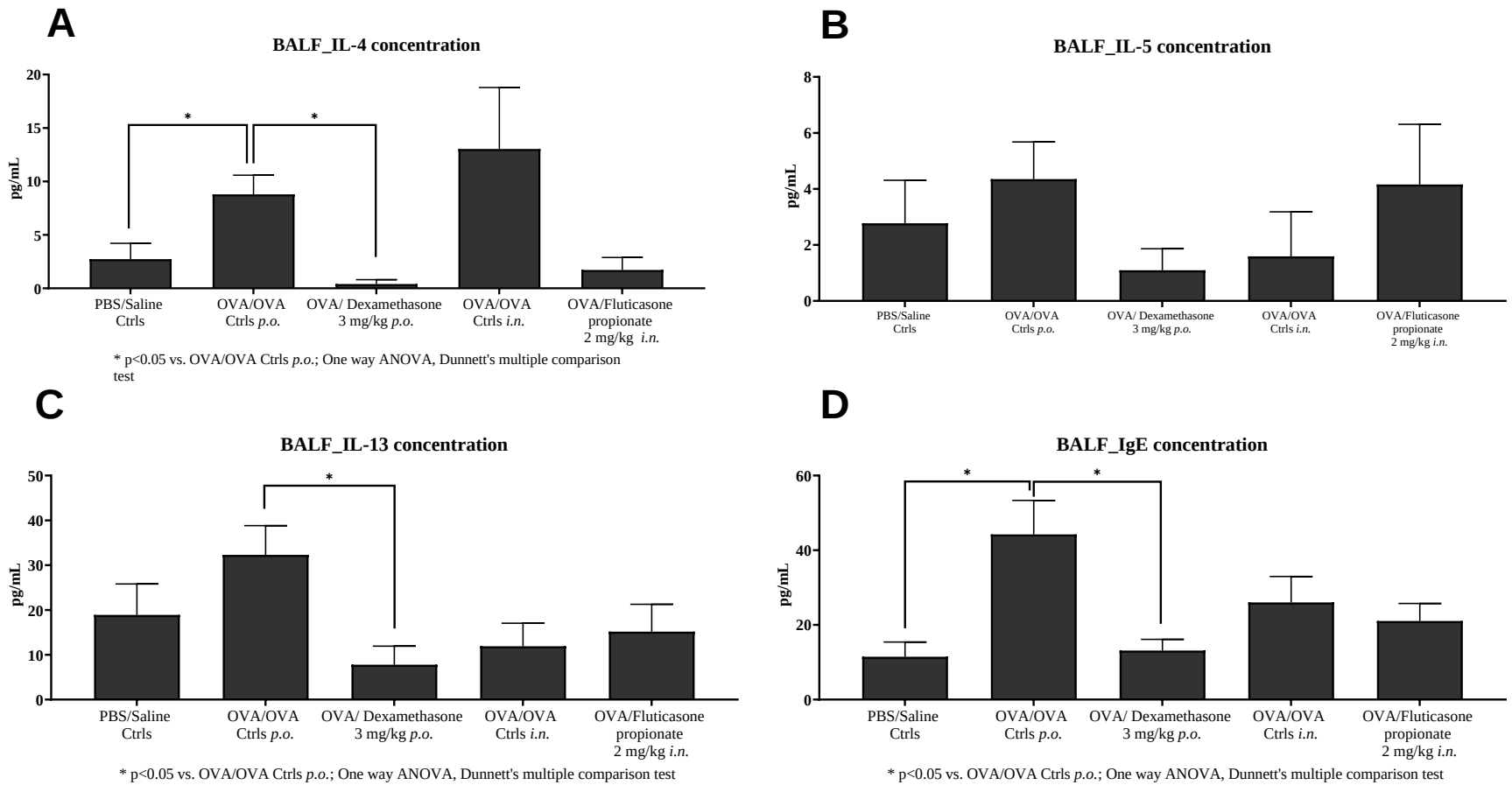

Figure 32 Graphical presentation and statistical analyses of IgE and cytokines concentrations measured in the BALF of animals in the OVA-induced asthma model

Concentration levels of IL-4 A), IL-5 B), IL-13 C), and IgE D) in the BALF of animals in the OVA-induced asthma model, sampled 24 h post last challenge and presented as group mean + sem.

Abbreviations: BALF- bronchoalveolar lavage fluid, IL-interleukin, IgE- immunoglobulin E, PBS-phosphate buffered saline, OVA-ovalbumin, Ctrls-controls, *p.o.*-perorally, *i.n.*-intranasally, vs.-*versus*, sem-standard error of the mean.

5.8 HISTOLOGY RESULTS

5.8.1 Model of Bleomycin-Induced Pulmonary Fibrosis

An Ashcroft score modification according to Matsuse, was employed to evaluate fibrotic changes, their localization, and the degree of lung structure distortion. Results were presented as groups median and statistically analysed, as shown in Figure 33, with raw data in Appendix 13.

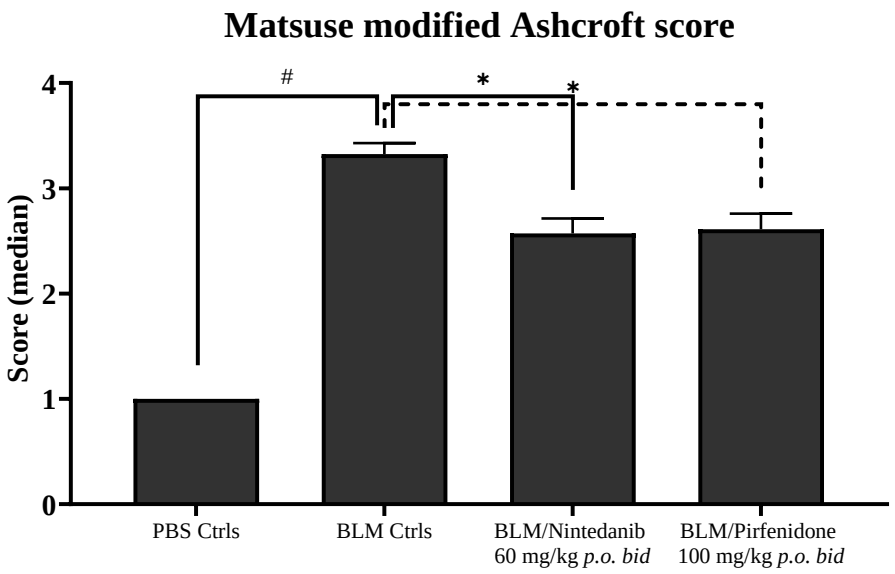

#p<0.05 vs. BLM Ctrls; Wilcoxon Signed Rank Test
*p<0.05 *vs* BLM Ctrls; Kruskal-Wallis test, Dunn's multiple comparisons test

Figure 33 Graphical presentation of the fibrotic score and statistical analyses results
Pulmonary fibrosis changes scored in all four examined groups from day 21 in the BLM-induced pulmonary fibrosis model defined by modified Ashcroft score and presented as a group median + sem.

Abbreviations: PBS-phosphate buffered saline, BLM-bleomycin, Ctrls-controls, *p.o.*-perorally, *bid*-twice a day, vs.-*versus*, sem-standard error of the mean

Statistical analysis employing the Wilcoxon Signed Rank test confirmed a statistically significant increase of modified Ashcroft score in the BLM-challenged control group (BLM Ctrls) compared to the non-challenged control group (PBS Ctrls) (<0.0001) (Figure 33).

Analyzes employing the Kruskal-Wallis test, with Dunn's multiple comparison tests, confirmed significant improvement of both nintedanib and pirfenidone treatment compared to the control BLM-challenged group (p=0.0008 and p=0.0017, respectively) (Figure 33).

Microscopic analyses revealed different stages of pulmonary fibrosis scored according to Matsuse modified Ashcroft criteria as follows:

No fibrotic changes were observed in the PBS Ctrls group, resulting in a score of 1 group median value in all ten examined lung tissue samples (Figure 34, Appendix 13).

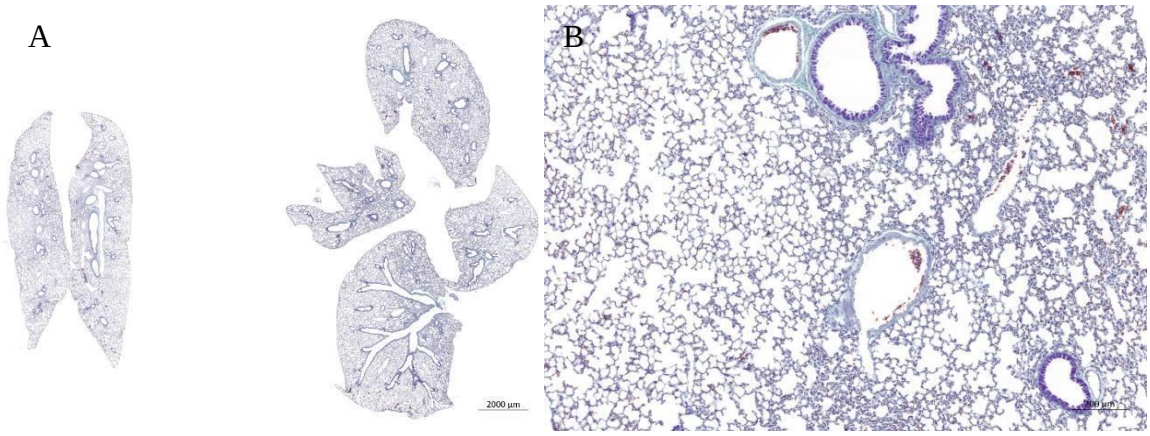

Figure 34 PBS Ctrls group fibrotic changes in lungs stained by Crossman's Trichrome
Normal lung tissue samples presented at the high magnification (2000 µm, Figure A) and low magnification (200 µm, Figure B)

BLM Ctrls group had a median score of 3.3 estimated in 16 lung samples analyzed, with a score of 2.6 presenting minimal fibrotic thickening of alveolar walls to score four demonstrating loss of pulmonary architecture due to coarse fibrous bands and/or small fibrous masses and intra-alveolar fibrils depositions (Figure 35, Appendix 13).

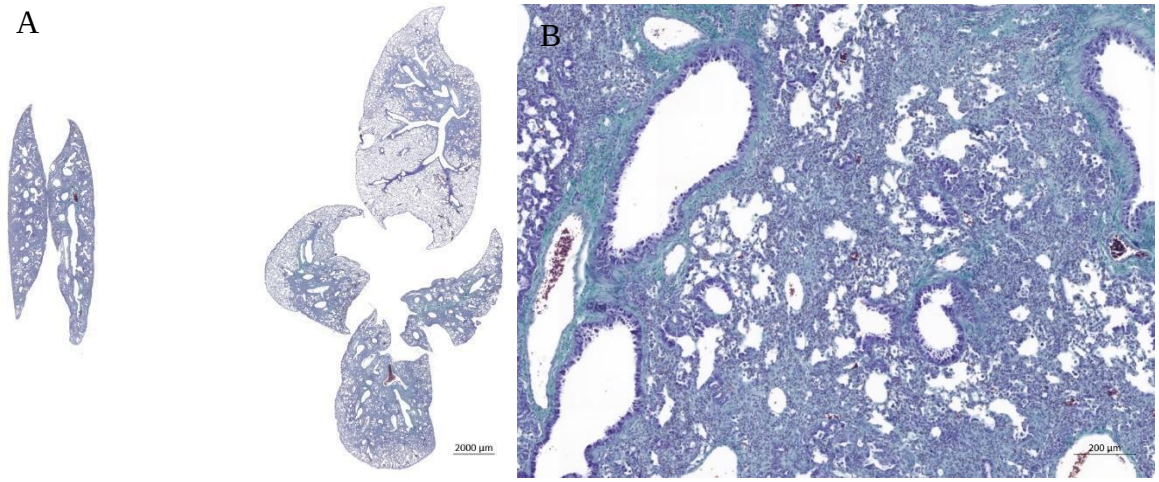

Figure 35 BLM Ctrls group fibrotic changes in lungs stained by Crossman's Trichrome staining
Marked multifocal deposition of *de novo* synthesized collagen within the alveolar septa and alveoli with severe distortion of lung structure presented at the high magnification (2000 µm, Figure A) and low magnification (200 µm, Figure B)

Nintedanib treated median group score of 2.5 in 18 lung samples analyzed and scored in a range of normal lungs (score 1.3) to loss of pulmonary architecture due to coarse fibrous bands and/or small fibrous masses and intra-alveolar fibrils depositions (score 4) (Figure 36, Appendix 13).

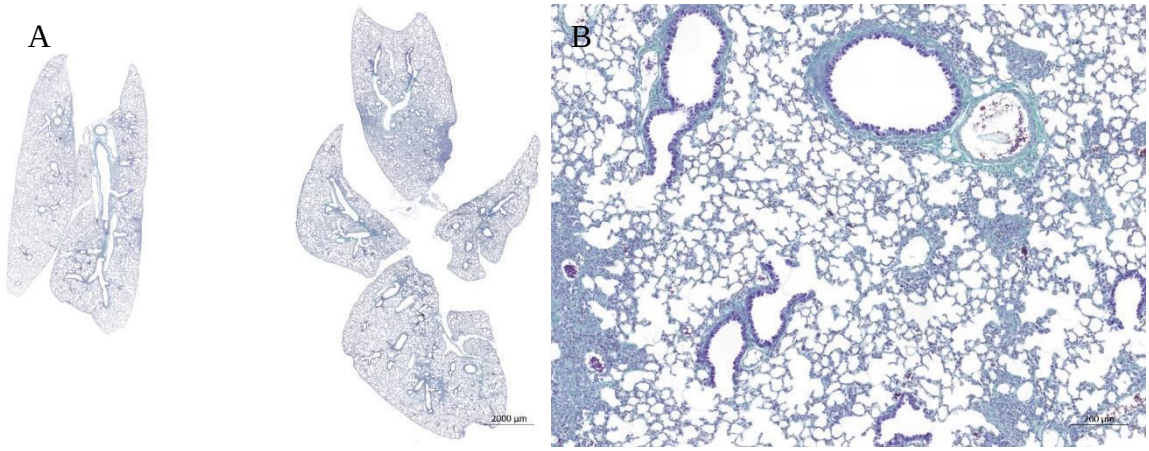

Figure 36 BLM/Nintedanib 60 mg/kg *p.o. bid* group fibrotic changes in lungs stained by Crossman's Trichrome staining
Moderate multifocal deposition of *de novo* synthesized collagen within the alveolar septa presented at the high magnification (2000 µm, Figure A) and low magnification (200 µm, Figure B)

Pirfenidone treatment resulted in a group median of 2.6 of 18 lung samples analyzed and scored in a range of normal lungs (score 1.3) to loss of pulmonary architecture due to coarse fibrous bands and/or small fibrous masses and intra-alveolar fibrils depositions (score 3.5) (Figure 37, Appendix 13).

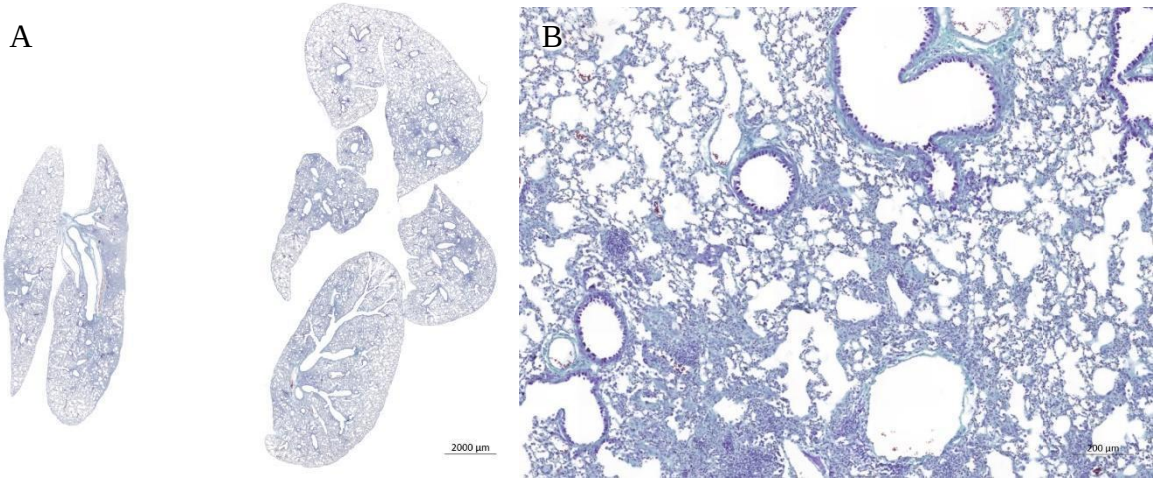

Figure 37 BLM/Pirfenidone 100 mg/kg *p.o. bid* group fibrotic changes in lungs stained by Crossman's Trichrome staining
Moderate multifocal deposition of *de novo* synthesized collagen within the alveolar septa presented at the high magnification (2000 µm, Figure A) and low magnification (200 µm, Figure B)

5.8.2 Model of Ovalbumin-Induced Asthma

Lungs for histopathological analyses in the OVA-induced asthma experiment were sampled on day 24 of the study, 24 hours post-last challenge. Lung tissue PAS-stained slides were examined for the histology score of general pulmonary inflammation and epithelial damage of bronchi and alveoli. The histology score was expressed as a sum of all three scores. The scores' graph results are presented in Figure 38, and the raw data is in Appendix 14.

Inflammation in the OVA-exposed control groups was evaluated from moderate focal and minimal diffuse to marked focal and moderate diffuse inflammation (median score of 7.5 in the *p.o.* vehicle administered and 8.25 in the *i.n.* vehicle administered group), none to moderate focal bronchial (median score of 1.5 in both groups), and minimal multifocal to marked focal alveolar epithelial damage (median score of 5 and 4.75, respectively) in the observed lung tissue. A median group value of 13.5 in the OVA/OVA Ctrls *p.o.* estimated in ten lung samples shows moderate diffuse to marked focal inflammation, minimal focal to multifocal bronchial epithelial damage, and moderate focal and minimal diffuse alveolar epithelial damage (Figure 38, Appendix 14).

OVA/OVA Ctrls *i.n.* median group value of 14.5 estimated in 10 lung samples represents a marked focal inflammation, minimal focal to multifocal bronchial, and moderate focal and minimal diffuse alveolar epithelial damage (Figure 38, Appendix 14).

A general histology score of both OVA-exposed control groups ($p=0.002$ for both Ctrl groups) was significantly increased over the PBS/Saline Ctrls group, where no inflammatory nor epithelial damage was observed (median group's score 0 in all evaluated scores) (Figure 38, Appendix 14).

A dexamethasone treatment decreased the inflammation score to the lowest of minimal diffuse bronchial epithelial damage score in one animal, resulting in median score of 2.75. Yet, minimal focal to moderate focal bronchial epithelial damage was present in four animals, while in the rest of the animals there were no damage observed, resulting in median score of 0. On the other hand, alveolar epithelial damage scores ranged from minimal focal to moderate focal and minimal diffuse (median score of 1.75 estimated in 10 lung samples). Statistical analyses revealed a dexamethasone treatment effect on significantly decreasing inflammation score ($p=0.0001$), epithelial damage in bronchi ($p=0.0039$) and in alveoli ($p=0.0005$), resulting in

significant general histology score (median score of 4.5) compared to the corresponding OVA-exposed control group ($p=0.0001$) (Figure 38, Appendix 14).

The fluticasone propionate treatment decreased the inflammation score from none to minimal diffuse (median score of 1.5), as bronchial epithelial damage was absent in this group (median score of 0). Yet, alveolar damage was present in only five animals, ranging from minimal focal to minimal diffuse damage score (median score of 0.5). A general histology score median of 2 estimated in 10 lung samples was significantly decreased ($p<0.0001$) compared to the corresponding OVA-exposed control group. The general score outcome was expected as the inflammation, bronchial, and alveolar scores were significant as well ($p<0.0001$, $p=0.0004$, and $p<0.0001$, respectively) (Figure 38).

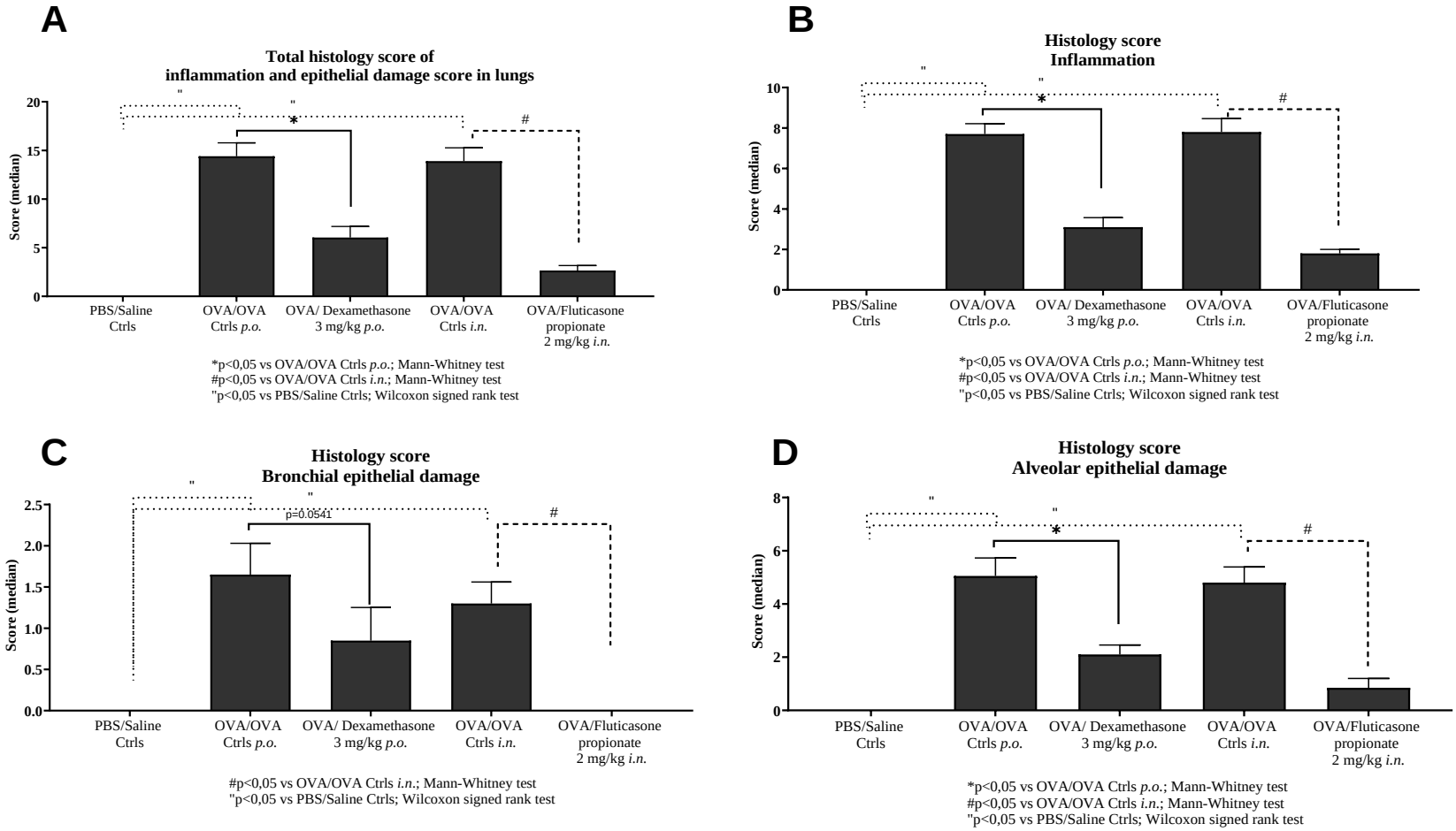

Figure 38 Graphical presentation and statistical analyses of general pulmonary inflammation and/or epithelial damage score results in the OVA-induced asthma model

Pulmonary inflammation and epithelial changes score sum A), and a separate score of inflammation B), bronchial epithelial damage C), and alveolar epithelial damage score D) in all five examined groups from day 24 in the OVA-induced asthma model presented as a group median + sem

Abbreviations: PBS-phosphate buffered saline, OVA-ovalbumin, Ctrls-controls, *p.o.*-perorally, *i.n.*-intranasally, vs.-*versus*

5.8.3 Goblet Cell Metaplasia in Large and Terminal Airways

The goblet cell metaplasia score results in large and terminal airways are presented in Figure 39, with representative histology photos in Figure 40. The exact number of lung samples *per* group, as in the histopathological assessment, was employed in this analysis.

A significant increase in the goblet cell metaplasia score was observed in both OVA-exposed Ctrls *p.o.* (median score of 3) and *i.n.* (median score of 3.5) groups ($p<0.0001$ for both Ctrl groups) compared to PBS/Saline Ctrls (median score of 0.5). Treatment with the referent substance dexamethasone decreased the group's median score of 2. However, the significance was not reached ($p=0.2227$). On the other hand, fluticasone propionate (median score of 1) significantly decreased the score compared to the corresponding vehicle ($p<0.0001$).

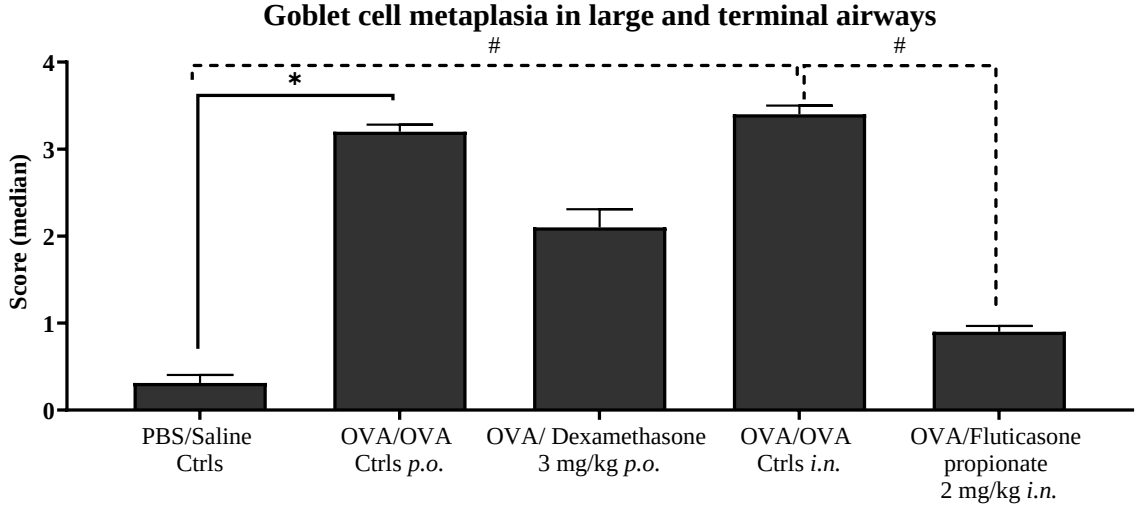

*p<0.05 *vs.* OVA/OVA Ctrls *p.o.*; Kruskal-Wallis test, Dunn's multiple comparison test
#p<0.05 *vs.* OVA/OVA Ctrls *i.n.*; Kruskal-Wallis test, Dunn's multiple comparison test

Figure 39 Graphical presentation and statistical analysis of goblet cell metaplasia in large and terminal airways score results in the OVA-induced asthma model
Terminal and large airways goblet cell metaplasia score results evaluated in lungs from all five examined groups sampled on day 24 in the OVA-induced asthma model. Values are presented as a group median + sem.

Abbreviations: PBS-phosphate buffered saline, OVA-ovalbumin, Ctrls-controls, *p.o.*-perorally, *i.n.*-intranasally, vs.-*versus*

Microscopic analyses revealed different stages of goblet cell metaplasia scored according to employed criteria as follows:

No mucus-containing cells to few positive cells along the basement membrane with less than 75% of the cytoplasm stained were observed in the PBS Ctrls group, resulting in a score of 0.5 in all ten examined lung tissue samples (Figure 39, Figure 40 A, Appendix 14).

OVA/OVA Ctrls *p.o.* group had a median score of three, representing a finding of numerous positive cells along the basement membrane with less than 75% of the cytoplasm stained. OVA/OVA Ctrls *i.n.* group had a median score of 3.5 because some animals' findings included numerous positive cells along the basement membrane with more than 75% of the cytoplasm stained. (Figure 39, Figure 40 B, Appendix 14).

The dexamethasone-treated group median score was 2, including the animals with few positive cells to numerous positive cells with less than 75% of the cytoplasm stained (Figure 39, Figure 40 C, Appendix 14).

The fluticasone propionate-treated group had a median of one, including animals with findings of no mucus-containing cells and findings of few positive cells along the basement membrane with less than 75% of the cytoplasm stained (Figure 39, Figure 40 D, Appendix 14).

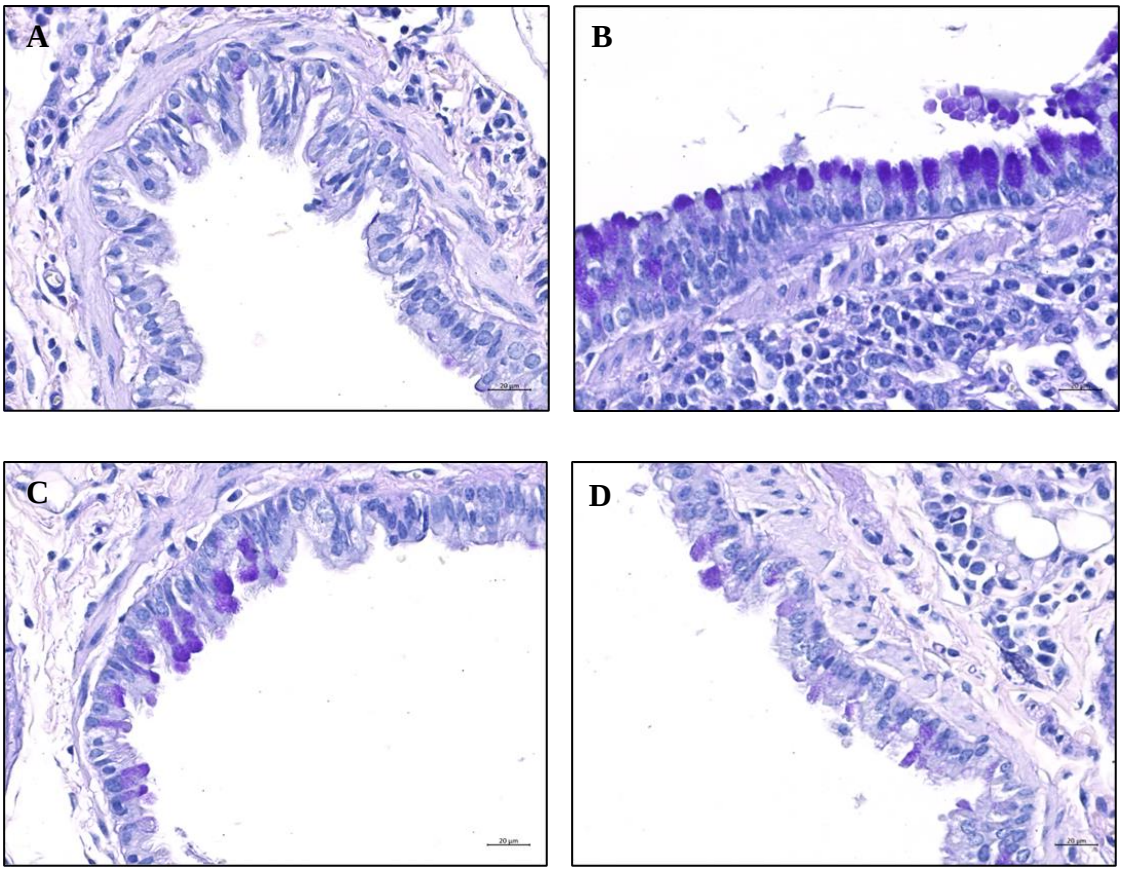

Figure 40 Goblet cell metaplasia in large airways (PAS staining 20x).
Pictures present a non-exposed animal with non-mucus-containing cells along the basement membrane of large airways (A); OVA exposed animal with numerous positive cells with more than 75% of the cytoplasm stained (B); dexamethasone-treated animal with few positive cells with more than 75% (C); and less than 75% stained along the basement membrane in the fluticasone propionate treated animal (D).

Abbreviations: PBS-phosphate buffered saline, OVA-ovalbumin, Ctrls-controls, *p.o.*-perorally, *i.n.*-intranasally

5.9 IMMUNOHISTOCHEMISTRY RESULTS

Immunohistochemistry analyses were performed on the lung tissue slides from the BLM-induced pulmonary fibrosis model sampled on day 21 of the experiment. The exact number of samples per group was analyzed as in the histological assessments of fibrotic score. Tissue *de novo* COL1A1 deposition and αSMA pulmonary content as a reflection of myofibroblast accumulation are analyzed by CaloPix software as a tissue surface stained from yellow to red and expressed as tissue area in mm^2. An example of a *de novo* COL1A1 scanned slide and digital image process by CaloPix software are presented in Figure 41.

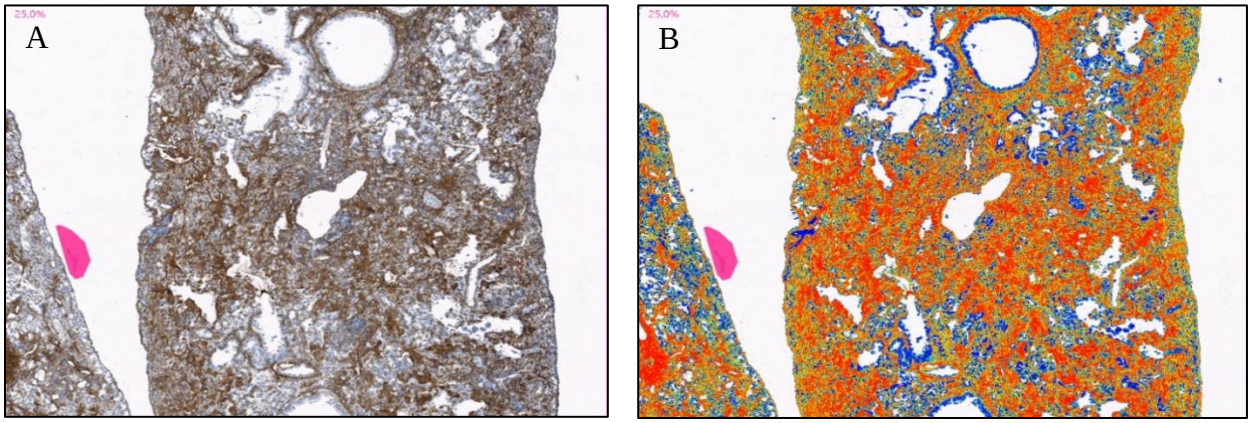

Figure 41 *De novo* collagen type I deposition in the lungs of BLM Ctrls animal

Slide scans of the lungs at 25% magnification are presented as A) stained and scanned slide and B) digital image analysis CaloPix software processed slide.

5.9.1 Results of Collagen Type 1 Presence in the Lungs

The collagen type 1 immunological staining and digital quantification were employed to evaluate the presence of COL1A1 tissue in the lungs and its localization. Results were presented as group mean and statistically analysed, as shown in Figure 42, and raw data is presented in Appendix 13.

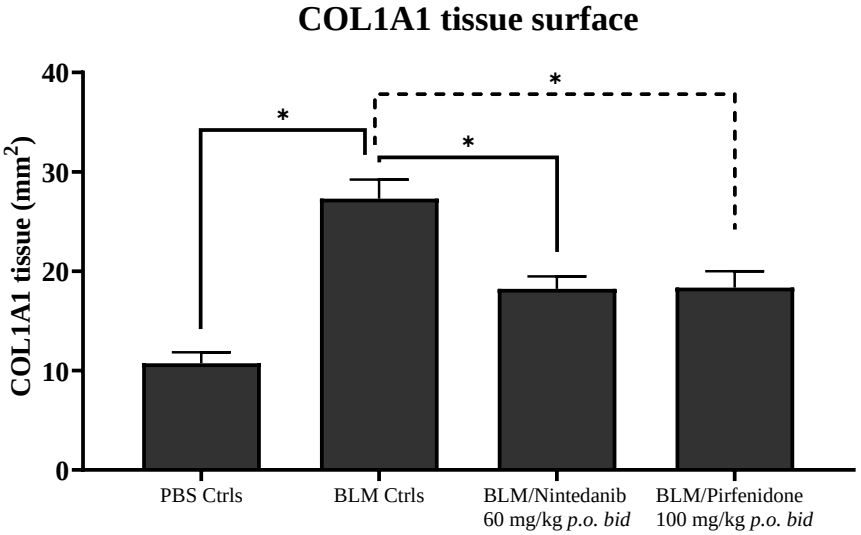

*p<0.05 *vs* BLM Ctrls; One-way ANOVA, Dunnett's multiple comparisons test

Figure 42 Graphical quantification of immunohistochemically stained collagen type 1 in the lungs

Histological slides of the lung tissue sampled on day 21 in the BLM-induced pulmonary fibrosis model were stained for collagen type 1. Automated quantification was performed, and the presence of the IHC stained area was expressed in mm^2 of group mean + sem.

Abbreviations: PBS-phosphate buffered saline, BLM-bleomycin, Ctrls-controls, *p.o.*-perorally, *bid*-twice a day, vs.-*versus*, IHC- İmmunohistochemistry, COL1A1-collagen type 1, ANOVA-analysis of variance, sem-standard error of the mean

One-way ANOVA test evaluating all groups, followed by Dunnett's multiple comparison test statistical analysis, tested mean differences within groups compared to the BLM Ctrls group.

A BLM challenge induced a significant increase of *de novo* COL1A1 deposition in the BLM Ctrls group compared to the non-challenged PBS Ctrls group ($p<0.0001$) (Figure 42).

Treatment with both referent substances, nintedanib, and pirfenidone, significantly reduced collagen deposition over the non-treated BLM-challenged group (BLM Ctrls) ($p=0.0003$ for both analyses) (Figure 42).

Digital quantification of IHC stained slides measures the scanned slides' COL1A1 positive signal stained (yellow to red) area. The PBS Ctrls group's IHC signal of COL1A1 presence was detected around the bronchi and blood vessels, as well as into the alveolar wall. The measured mean value was 10.73 mm^2. COL1A1 tissue area within a physiological location ranged in a minimal value from 5.06 mm^2 to a max value of 15.93 mm^2 of total scanned tissue surface (Figure 43, Appendix 13).

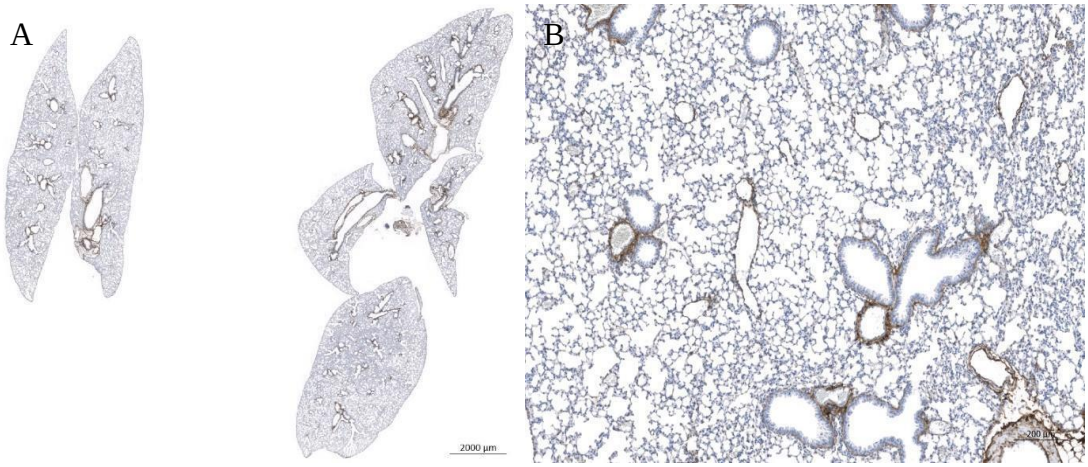

Figure 43 PBS Ctrls group COL1A1 IHC stained lung sample
Normal lung tissue samples presented at the high magnification (2000 µm, figure A) and low magnification (200 µm, figure B)

A characteristic deposition of *de novo* COL1A1 in fibrotic lungs is placed into alveolar walls and space, with expressed collagen deposition around bronchi and blood vessels. BLM Ctrls group had a mean positive tissue area of 27.31 mm^2, with a minimal measured area of 14.19 mm^2 and a maximal area of 42.45 mm^2 (Figure 44, Appendix 13).

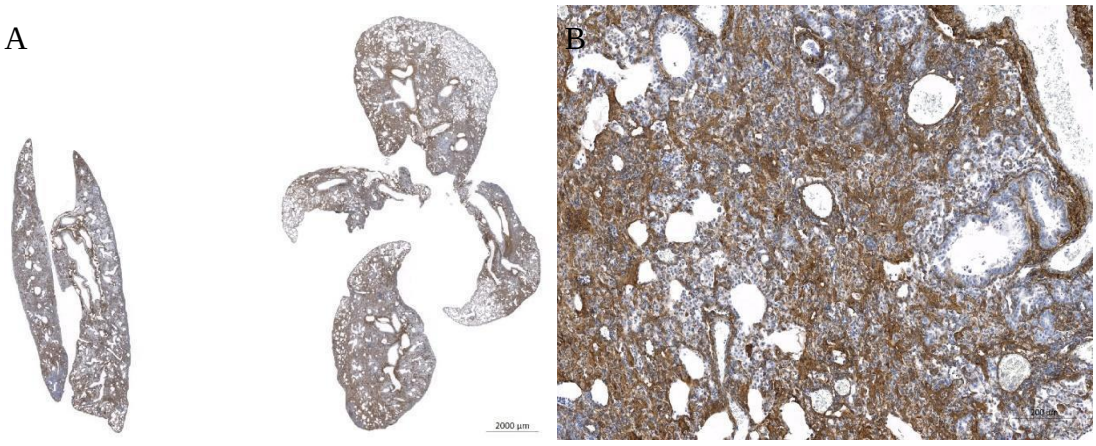

Figure 44 BLM Ctrls group COL1A1 IHC stained lung sample
Marked multifocal deposition of *de novo* synthesized collagen within the alveolar septa and alveoli presented at the high magnification (2000 µm, figure A) and low magnification (200 µm, figure B)

Nintedanib treated mean group had COL1A1 positive stained tissue area of 18.23 mm^2. This group's measured positive tissue areas range from 9.04 mm^2 to 28.06 mm^2 (Figure 45, Appendix 13).

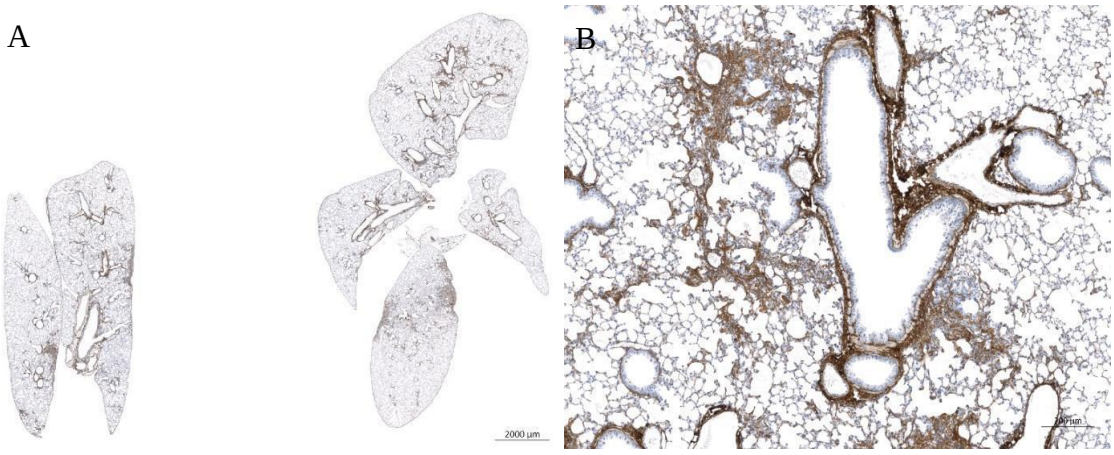

Figure 45 BLM/Nintedanib 60 mg/kg *p.o. bid* group COL1A1 IHC stained lung sample
Moderate multifocal deposition of *de novo* synthesized collagen within the alveolar septa presented at the high magnification (2000 µm, figure A) and low magnification (200 µm, figure B)

The pirfenidone-treated mean group had a COL1A1-positive stained tissue area of 18.35 mm^2. This group's measured positive tissue areas range from 7.63 mm^2 to 30.04 mm^2 (Figure 46, Appendix 13).

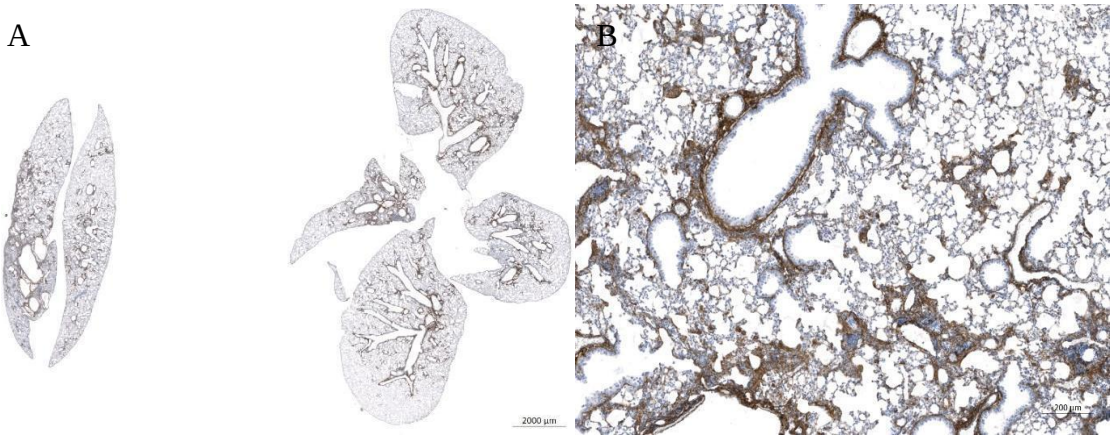

Figure 46 BLM/Pirfenidone 100 mg/kg *p.o. bid* group COL1A1 IHC stained lung sample
Moderate multifocal deposition of synthesized collagen within the alveolar septa presented at the high magnification (2000 µm, figure A) and low magnification (200 µm, figure B)

5.9.2 Results of Myofibroblast Presence in the Lungs

The αSMA immunological staining and digital quantification were employed to evaluate myofibroblasts' presence in the lungs and their localization. Results were presented as groups' mean and statistically analysed, as shown in Figure 47, with raw data in Appendix 13.

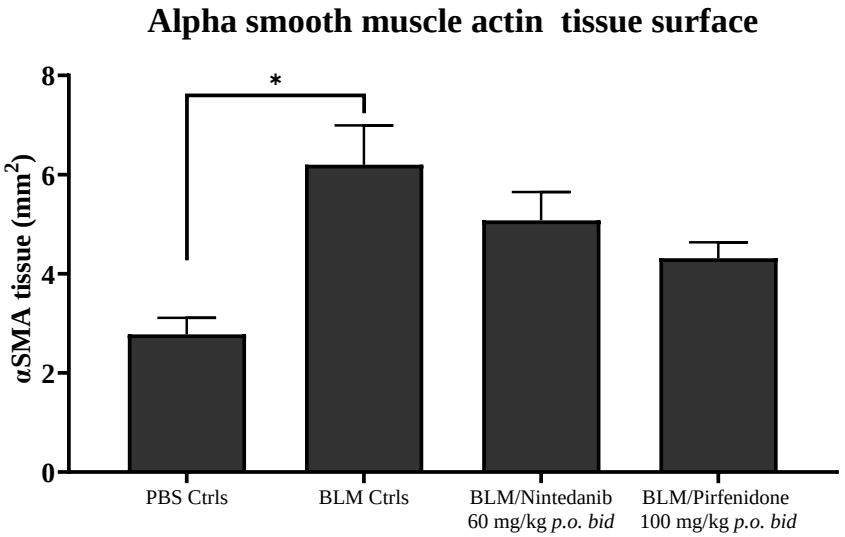

*p<0.05 *vs* BLM Ctrls; Kruskal-Wallis test, Dunn's multiple comparisons test

Figure 47 Graphical quantification of immunohistochemically stained myofibroblasts in the lungs

Histological slides of the lung tissue sampled on day 21 in the BLM-induced pulmonary fibrosis model were stained for alpha-smooth muscle actin for myofibroblasts' presence. Automated quantification was performed, and the presence of the IHC stained area was expressed in mm^2 of group mean + sem.

Abbreviations: PBS-phosphate buffered saline, BLM-bleomycin, Ctrls-controls, *p.o.*-perorally, *bid*-twice a day, vs.-*versus*, IHC- immunohistochemistry, αSMA-alpha-smooth muscle actin, ANOVA-analysis of variance, sem-standard error of the mean

The difference between examined groups in the αSMA IHC analysis was tested employing the non-parametric Kruskal-Wallis test (Figure 47). Dunn's multiple comparison tests compared each group with the BLM Ctrls group, and the following results were obtained.

BLM challenge resulted in a significantly higher myofibroblast accumulation revealed by αSMA positive tissue area compared to the non-challenged PBS Ctrls group ($p<0.0001$) (Figure 47).

Treatment with nintedanib resulted in a lower myofibroblast accumulation. However, the significance was not reached ($p= 0.6306$) (Figure 47).

Pirfenidone treatment also did not reach significance, reducing myofibroblasts accumulation analyzed as αSMA positive tissue area ($p=0.1496$) (Figure 47).

The PBS Ctrls group's IHC signal of αSMA presence was detected only around the bronchi and blood vessels. The measured mean value of the negative control group was 2.78 mm^2. Myofibroblasts within a physiological location ranged in a minimal value from 1.55 mm2 to a max value of 3.6 mm2 of the total scanned tissue surface (Figure 48, Appendix 13).

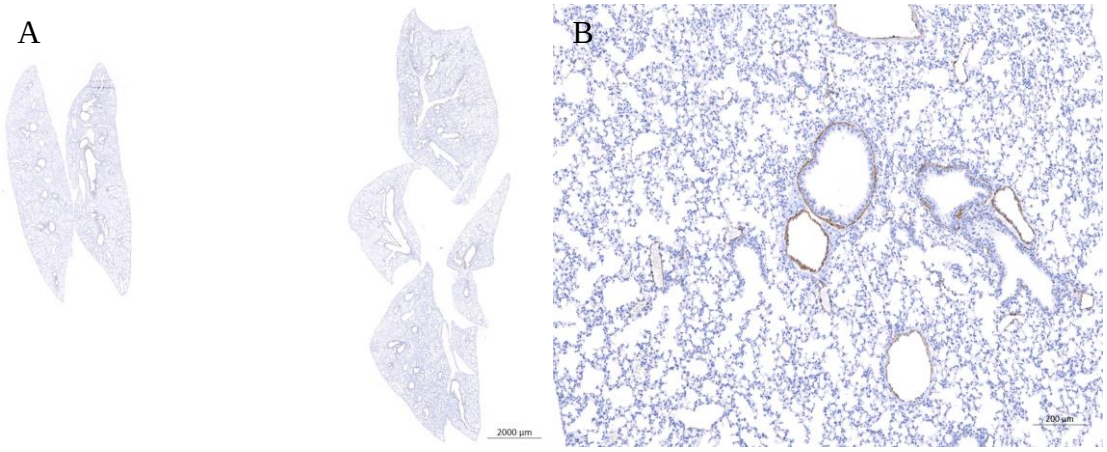

Figure 48 PBS Ctrls group αSMA IHC stained lung sample
Normal lung tissue samples presented at the high magnification (2000 µm, figure A) and low magnification (200 µm, figure B)

The BLM Ctrls group's IHC signal of αSMA presence was detected around the bronchi and blood vessels and stained accumulated myofibroblasts in the lung tissue. A mean positive tissue area of 6.02 mm^2 was observed, with a minimal measured area of 3.32 mm^2 and a maximal area of 15.34 mm^2 (Figure 49, Appendix 13).

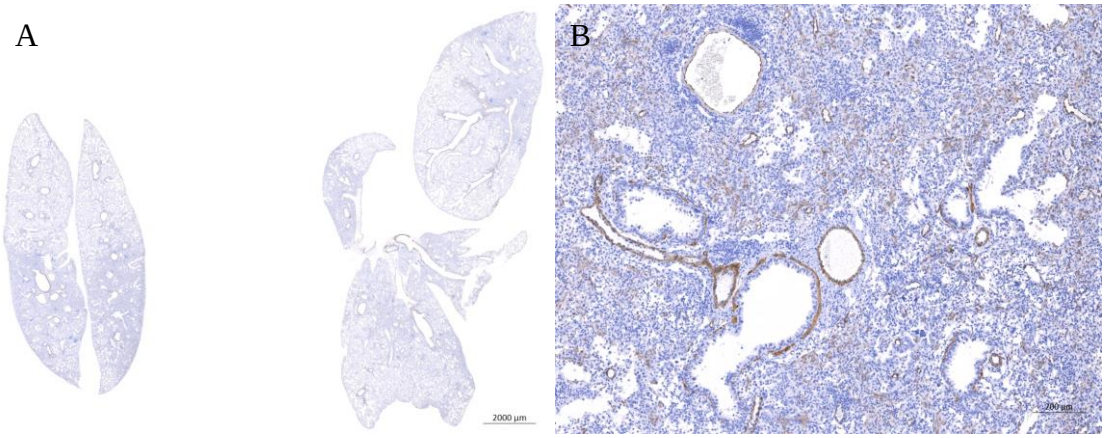

Figure 49 BLM Ctrls group αSMA IHC stained lung sample
Myofibroblast accumulation visualized as αSMA protein expression in lung tissue of BLM-challenged animal, presented at the high magnification (2000 µm, figure A) and low magnification (200 µm, figure B)

Nintedanib treated mean group had αSMA positive stained tissue area of 5.08 mm^2. This group's measured positive tissue areas range from 2.7 mm^2 to 12.14 mm^2 (Figure 50, Appendix 13).

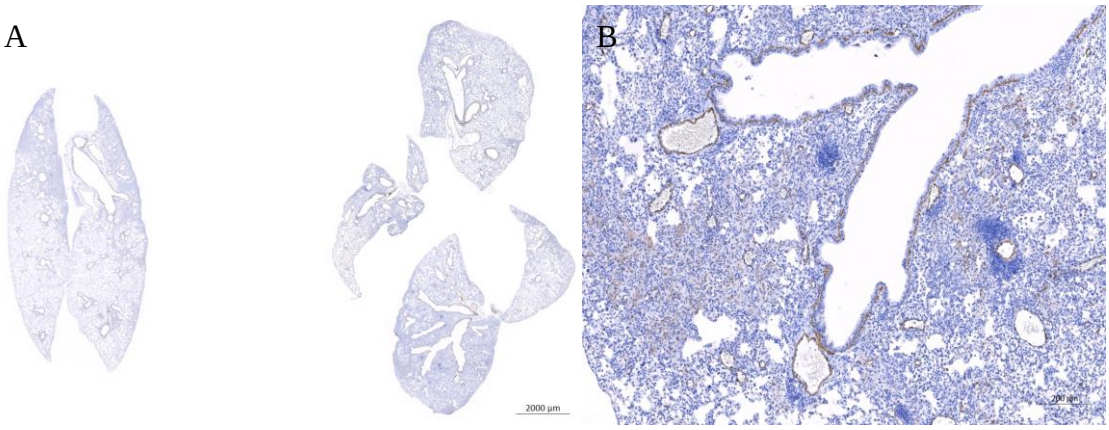

Figure 50 BLM/Nintedanib 60 mg/kg *p.o. bid* group αSMA IHC stained lung sample
Myofibroblast accumulation visualized as αSMA protein expression in lung tissue of nintedanib treated animal, presented at the high magnification (2000 µm, figure A) and low magnification (200 µm, figure B)

Pirfenidone treated mean group had αSMA positive stained tissue area of 4.31 mm^2. This group's measured positive tissue areas range from 2.49 mm^2 to 7.64 mm^2 (Figure 51, Appendix 13).

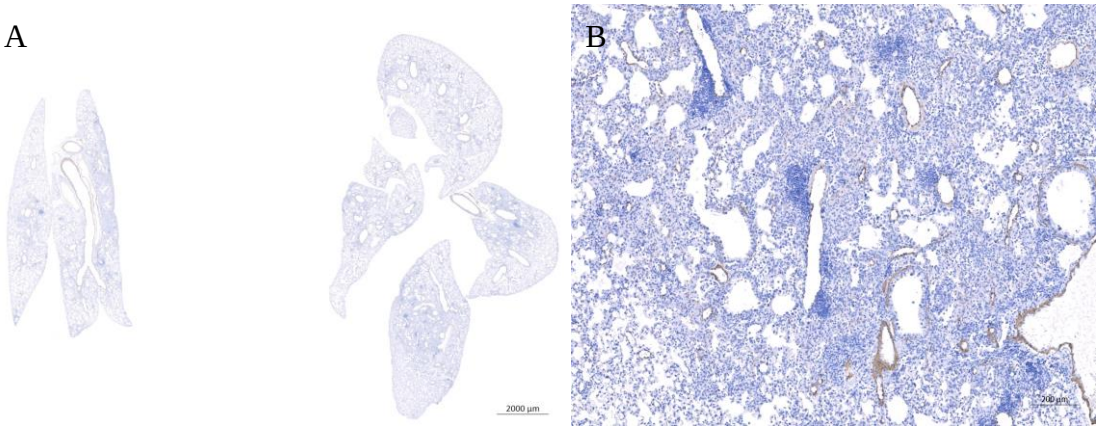

Figure 51 BLM/Pirfenidone 100 mg/kg *p.o. bid* group αSMA IHC stained lung sample
Myofibroblast accumulation visualized as αSMA protein expression in lung tissue of pirfenidone treated animal, presented at the high magnification (2000 µm, figure A) and low magnification (200 µm, figure B)

5.10 CORRELATION ANALYSES

A correlation between the histological scores and critical PFT parameters in the restrictive disorder in the BLM-induced pulmonary fibrosis model and for the obstructive disease in the OVA-induced asthma model was performed in this survey (Figure 52 and Figure 53). Both PBS Ctrls and PBS/Saline Ctrls groups were not included in the correlation calculations as the score for all animals in the group was the same (1 and 0.5, respectively).

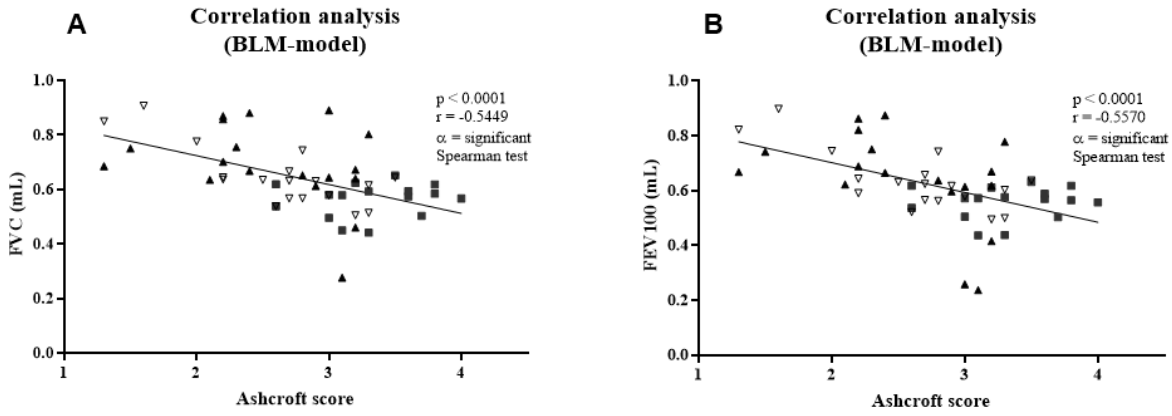

Figure 52 Spearman correlation between the modified Ashcroft score and PFT parameters evaluated in the model of bleomycin-induced pulmonary fibrosis

The correlation between the Ashcroft score and forced vital capacity (**A**) and Ashcroft score and FEV100 (**B**) pulmonary function test measurement parameters, respectively, was tested employing the Spearman test. ■ BLM Ctrls ▲ BLM/Nintedanib 60 mg/kg *p.o. bid* ▽ BLM/Pirfenidone 100 mg/kg *p.o. bid*

Abbreviations: BLM-bleomycin, FVC-forced vital capacity, FEV100-forced expiratory volume at 100 ms, Ctrls-controls, *p.o.*-perorally, *bid*-twice a day

Correlations between the PFT parameters FVC and FEV100 and the Ashcroft score in the model of BLM-induced pulmonary fibrosis were evaluated using simple linear regression and Spearman correlation. As observed in both estimated parameters, Ashcroft score mean values demonstrated a significant correlation to lung function (FVC: $r = -0.5449$ $p < 0.0001$; FEV100: $r = -0.5570$ $p < 0.001$) (Figure 52).

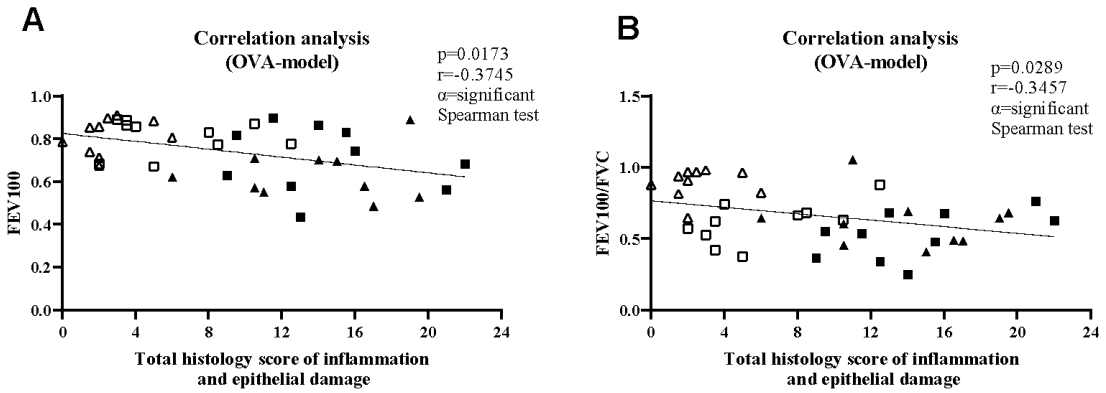

Figure 53 Spearman correlation between the total histology score of general pulmonary inflammation and epithelial damage of bronchi and alveoli and PFT parameters evaluated in the model of ovalbumin-induced asthma

Correlation between the total histology score of general pulmonary inflammation and epithelial damage of bronchi and alveoli and forced expiratory volume at 100 ms (**A**) and total histology score and Tiffeneau index (**B**) pulmonary function test measurement parameters, respectively, was tested employing the Spearman test. ■ OVA/OVA Ctrls *p.o.* □ OVA/ Dexamethasone 3 mg/kg *p.o.* ▲ OVA/OVA Ctrls *i.n.* ▽ OVA/Fluticasone propionate 2 mg/kg *i.n.*

Abbreviations: OVA-ovalbumin, FEV100-forced expiratory volume at 100 ms, FVC-forced vital capacity, Ctrls-controls, *p.o.*-perorally, *i.n.*-intranasally;

Correlations between the PFT parameters FEV100 and Tiffeneau index and the total histology score of inflammation and epithelial damage score in the model of OVA-induced asthma were evaluated using simple linear regression and Spearman correlation. As observed in both estimated parameters, histological score mean values significantly correlated to lung function (FEV100: r= -0.3745 p=0.0173; Tiffeneau index: r =-0.3457 p=0.0289) (Figure 53).

6 DISCUSSION

This research provides valuable insights into the applicability of PFTs in preclinical respiratory models, their correlation with other measures, and their relevance to clinical outcomes. Specifically, these results reveal that PFT assessment in preclinical models of BLM-induced pulmonary fibrosis and OVA-induced allergic asthma demonstrates restrictive and obstructive trends, respectively. Furthermore, treatment with established "gold standard" therapies improves lung function impaired by these challenge agents, mirroring improvements observed in patients. Therefore, these results indicate that achieving the specific aims of this research has led to the determination of "gold standard" PFT range values in restrictive and obstructive respiratory preclinical models, which could improve the translatability of these models by enabling the better selection of new molecules and their further clinical research in future studies. These correlations underscore the utility of PFTs in preclinical research for predicting and evaluating therapeutic interventions for respiratory conditions.

The results of this thesis showing a typical restrictive type of PFT trend in BLM-induced pulmonary fibrosis and a typical obstructive pattern of OVA-induced asthma model, respectively, are in accordance with well-known findings observed in positive control. These results obtained in the pulmonary fibrosis model are corroborated with data published by VANOIRBEEK et al. in 2010 and ANZULOVIĆ ŠANTA et al. in 2023. However, the employed model of allergic asthma exhibited more pronounced and convincing PFT results compared to those reported by VANOIRBEEK et al. in 2010. The results of the retrospective analysis of "gold standards" and the significance of the findings compared to other readouts were discussed across different pulmonary disorders:

6.1 A RESTRICTIVE PULMONARY DISORDER

VANOIRBEEK and his colleagues (2010) were the first to report that mice with pathologically proven fibrosis have a restrictive pulmonary function pattern of breathing. Nevertheless, according to MANALI et al., 2011, the amount of collagen may not directly correlate to lung mechanics, as the spatial organization of collagen fibers and the connection to other matrix components may be crucial. Therefore, in this research, PFT measurements were employed in BLM-control animals and compared to non-challenged animals to evaluate the extent of functional disagreement.

Consistent with known data (VANOIRBEEK et al., 2010), mice challenged with BLM at a dose of approximately 1 mg/kg *i.n.*, on day 21 post-challenge demonstrated a restrictive pulmonary function pattern characterized by reduced values of key pulmonary function

parameters such as FVC, FEV100, TLC, PEF, MMEF, and alterations in F-V and P-V curve shape. An F-V loop showed a smaller AUC in the BLM-challenged animals, affecting the significantly lower values of forced expiration flow parameters. Parameters such as FVC and FEV100, as parameters of interest in the BLM-induced pulmonary fibrosis models, are approx. 30% decreased as compared to healthy, non-challenged control mice. A P-V curve shows a typical left and downward shift of fibrotic lungs with increased recoil affecting the significant decrease in TLC, IC, VC, and Te, but the RV parameter was not affected (ALHAMAD et al., 2001, PELLEGRINO et al., 2005, GILDEA and MCCARTHY, 2010, VANOIRBEEK et al., 2010).

Both Cchord and Cdyn were significantly decreased in the challenged animals as the lungs were less elastic. As Cdyn greatly determines breathing work (DESAI and MOUSTARAH, 2022), it is reasonable that other parameters such as FRC, IC, VC, Te, and TLC are significantly decreased in the control animals.

However, parameters related to obstruction, such as RV and Ri, showed no significant effect, indicating that inflammation was not predominant in this model. The absence of the obstruction in this model is also confirmed by a significant increase in the Tiffeneau index in animals with developed fibrotic changes (VANOIRBEEK et al., 2010).

In accordance with the thesis objectives, these findings indicate that the BLM-induced pulmonary fibrosis model, utilized for assessing potential IPF treatments, displayed pathological alterations to the desired degree by day 21 of the study, revealing a restrictive pattern of pulmonary function. As emphasized in the studies by DENAYER et al. (2014) and EPSTEIN et al. (2017), the objective of novel therapies is to surpass or match established benchmarks' effects. Given that the impact of therapies on functional parameters is scrutinized in clinical respiratory conditions, it is reasonable to evaluate approved treatments in preclinical investigations of PFT parameters retrospectively. Consequently, the impact on pulmonary function was assessed in animals treated with the "gold standard" medications, nintedanib and pirfenidone.

Nintedanib and pirfenidone were administered in a therapeutic treatment regimen to resemble the treatment induction in patients, as recommended in the animal models guidelines (DENAYER et al., 2014, JENKINS et al., 2017, KOLB et al., 2020). Both treatments were initiated on day seven of the study when pathological changes were reported (IZBICKI et al.,

2002, MOORE and HOGABOAM, 2008), given daily at indicated doses *p.o.*, and lasted until the day of PFTs and lung sampling.

The treatment with nintedanib significantly improved FVC, FEV100, and TLC, directly contributing to a significant enhancement of the Tiffeneau index, characteristic parameters of restrictive pulmonary disorders (ALHAMAD et al., 2001, PELLEGRINO et al., 2005, GILDEA and MCCARTHY, 2010). However, the PEF and MMEF parameters did not show improvement, as the highest peak of the F-V curve resembled that of the BLM-challenged group, with a slow descent to reach a given FVC value.

On the other hand, pirfenidone treatment resulted in improvements in FVC and FEV100 parameters. Additionally, it significantly enhanced PEF and MMEF, as evidenced by an increased highest point on the F-V curve and a faster descent to an FVC value similar to that of the nintedanib-treated group.

Analyzing the P-V curve, the slope of the nintedanib treatment group was positioned more upward and to the right compared to the healthy, non-challenged PBS Ctrls group. In contrast, the slope curve of the pirfenidone treatment group tended more toward the challenged diseased BLM Ctrls group. This difference affected a significant improvement observed only in VC and Te parameters measured in this test sequence. As anticipated from the curve slope, nintedanib demonstrated significance in TLC, IC, VC, Te, and Cchord parameters compared to the challenged diseased group. Furthermore, nintedanib significantly improved parameters such as the Tiffeneau index and Cdyn, whereas pirfenidone treatment did not lead to advancements in these parameters, nor did it affect Cchord, TLC, and IC.

An FRC parameter was significantly increased in the healthy, non-challenged group compared to challenged diseased animals. Nevertheless, as mice have a very compliant chest wall, affecting the measurement of this parameter, these values are not discussed as relevant (VANOIRBEEK et al., 2010).

Both nintedanib and pirfenidone were primarily evaluated in clinical trials based on the improvement of FVC over time (KING JR. et al., 2014, RICHELDI et al., 2014, FLAHERTY et al., 2018, FAINBERG et al., 2022). In this study, on the final day of the investigation, nintedanib demonstrated a significant improvement in the FVC parameter by 23% compared to the diseased BLM Ctrl group. Pirfenidone also showed improvement, albeit minor, with a 15% increase over the BLM Ctrl group. This discrepancy may be correlated with clinical outcomes,

as indicated by a meta-analysis of these two treatments in IPF patients, revealing a superior nintedanib effect on FVC outcomes (LOVEMAN et al., 2015).

In line with the specific objectives defined in this thesis, the conducted experiment of the BLM-induced pulmonary fibrosis model has recapitulated the hallmarks of a successful lung fibrosis model for the preclinical investigation of IPF (MOELLER et al., 2008, DEGRYSE and LAWSON, 2011, MOORE et al., 2013). This is corroborated by the severity of the model, evidenced by increased mortality, alterations in pulmonary functionality parameters, and the presence of pathological changes such as an elevated Ashcroft score, deposition of new collagen, and accumulation of myofibroblasts. The BLM model employed in this study adhered to the guidelines outlined by the ATS regarding animal species, strain, sex, age, challenge dose, treatment choice, and regimen (JENKINS et al., 2017).

The evaluation of the clinical condition of the mice allocated in this BLM-model survey resulted in a significant decrease in body weight in the BLM Ctrls group. Animals that reached the criteria for euthanasia (four animals in this group) had increased body weight loss and signs of distress such as decreased general activity, piloerection, hunched posture, dyspnea, and closed eyes (HUET et al., 2013, TALBOT et al., 2020). The body weight readout and the distress signs observations confirmed the severity of the BLM model.

Nintedanib and pirfenidone treatments, referent substances for IPF disease, showed an improvement in the observed readouts, as evidenced by a decrease in the total number of euthanized animals (two in both groups). The body weight observation during the twenty-one-day study course was stable, *i.e.*, decreased compared to the non-challenged PBS Ctrls group, but improved over the challenged diseased group BLM Ctrls. The effect of the treatment on body weight loss is expected, as we know from the literature that their impact on the digestive tract is reported in clinical trials (KING JR. et al., 2014, RICHELDI et al., 2014, LOVEMAN et al., 2015).

On the final day of the study, on day 21, terminal histopathological and IHC evaluation analyses confirmed the development of characteristic fibrotic lesions as expected in the model of BLM-induced pulmonary fibrosis.

The histological assessment of lung tissue confirmed the anticipated changes in the control group, including diffuse intra-alveolar fibrosis, focal dense fibrosis, often subpleural, and epithelial hyperplasia in alveolar ducts. These findings align with previous studies by

MOELLER et al. (2008), DEGRYSE and LAWSON (2011), and MOORE et al. (2013), which concluded that the BLM-induced model is a suitable animal model for mimicking pulmonary fibrosis. The presence of the desired extent of pulmonary fibrosis on the 21st day after a single administration of BLM was confirmed by a significant increase in the Matsuse modified Ashcroft score and IHC analyses of *de novo* COL1A1 deposition and myofibroblast accumulation in the BLM-challenged control group compared to healthy, non-challenged animals. As the destruction of lung architecture is evident, functional aberrations are a logical consequence.

Most lung tissue samples from nintedanib and pirfenidone-treated animals showed minimal fibrotic thickening of alveolar or bronchial walls, characterized by a network of fine collagen fibrils. This resulted in a significantly lower median score than the diseased-challenged BLM control group.

Originally, the Ashcroft score included a scoring range of up to 8 (ASHCROFT et al., 1988). However, MATSUSE and colleagues (1999) modified this score to a maximum of 5 due to differences in fibrotic changes in mouse lungs, as epithelial damage in mice occurs at different time points. Additionally, a limitation of this score is its focus solely on fibrotic changes in lung tissue. To evaluate the extent of the inflammatory component, myofibroblast accumulation, and resolution processes, additional IHC analyses should be conducted.

As known from the literature, myofibroblasts play a key role in the pathogenesis of IPF by synthesizing and depositing ECM, overexpressing αSMA and COL1A1, and contributing to excessive accumulation of fibrillar collagens (KLINGBERG et al., 2013). Therefore, IHC analyses of αSMA and COL1A1 expression were performed in this study to evaluate myofibroblast accumulation and deposition of *de novo* collagen, respectively. Automated image analysis was conducted to ensure unbiased evaluation and adhere to the highest standards of IHC evaluation in preclinical studies (GILHODES et al., 2017).

The evaluation of COL1A1 expression revealed increased deposition of synthesized collagen in peribronchial and perivascular areas, alveolar septa, and alveoli in the lung tissue of diseased animals in the BLM control group. However, in groups treated with nintedanib and pirfenidone, collagen deposition was significantly reduced, with moderate deposition observed within the alveolar wall and inside alveoli.

The analysis of αSMA expression, indicative of myofibroblast presence in the lungs, showed a positive signal around major blood vessels, bronchi, fibrotic tissue, and accumulated myofibroblasts in animals challenged with BLM. This resulted in a significantly higher signal-positive lung tissue area in the diseased BLM control group compared to healthy animals in the PBS control group. In groups treated with nintedanib and pirfenidone, the αSMA-positive tissue surface area was lower; however, statistical significance was not reached.

The data presented in this study contribute to a clearer understanding of PFT applicability in the context of pulmonary fibrosis modeling. To underscore its significance, this thesis conducted a correlation analysis between FVC and FEV100, key parameters in restrictive disease, and the Ashcroft score, a commonly used histological assessment, in animals challenged with BLM. The Spearman test confirmed a significant correlation between the histological score of fibrotic changes and the impairments observed in functional parameters, thereby highlighting their causal relationship and the possibility of predicting the type of lung lesions present based on the values of functional parameters.

6.2 AN OBSTRUCTIVE PULMONARY DISORDER

Similar to restrictive diseases, VANOIRBEEK and his colleagues in 2010 were the first to describe the utility of PFT in the obstructive pulmonary disease model. However, as corroborated in their report, employing a different OVA-asthma model did not yield the expected changes in PFTs using the same equipment as used in this thesis methodology. Therefore, they have repeated measurements post-Mch exposure to magnify the functional changes caused by the airway obstruction.

On the final day of the study reported in this thesis, 24 hours after the last OVA challenge, terminal analyses of PFT, AHR, total and differential cell count, IgE, and Th2 cytokine analyses in BALF, along with histopathological evaluation, confirmed the development of characteristic hallmarks of human allergic asthma in the OVA-induced asthma model.

The pharmacological standards utilized in this model research were administered *via* different routes, necessitating the inclusion of two control groups in the asthma model survey: OVA/OVA Ctrls *p.o*. and OVA/OVA Ctrls *i.n*.

In line with the hypothesis and as stated in the literature (VANOIRBEEK et al., 2010), the techniques employed in this survey could distinguish between various pathologies, as they are based on similar lung functional variables routinely used in humans. However, the results obtained in this survey of the OVA-induced allergic asthma model contradict their findings, as they demonstrate expected changes 24 hours post-fourth *i.n.* challenge with OVA, assessed using the Buxco® PFT, an invasive measurement technique.

The systematic sensitization to OVA and direct *i.n.* challenge resulted in a reduction of the AUC in the F-V loop in both OVA/OVA control groups, indicative of a typical concave airflow limitation pattern characteristic of obstructive respiratory disorders. This was accompanied by a significant decrease in FVC, FEV100, PEF, and MMEF, along with a reduction of the Tiffeneau index compared to non-challenged animals in the PBS/Saline controls, confirming the presence of bronchial obstructions typically observed in asthma patients (WALKER et al., 2013).

The changes were also observed in the P-V curve, leading to a significant decrease in the Cchord parameter in both OVA control groups, likely due to fibrotic changes in the subepithelial area. Despite the observed curve shape in both OVA/OVA control groups, a more pronounced effect on parameters measured in this test sequence was confirmed in the OVA/OVA controls *i.n.* group, with significantly decreased IC, VC, and Te values compared to the non-sensitized and challenged control group. These parameters in the OVA/OVA control *p.o.* group were reduced but did not reach significance compared to the PBS/Saline control group. Values of the TLC parameter in the OVA/OVA control groups did not differ from those in the non-sensitized and challenged group, which aligns with the expected findings in asthma patients (GILDEA and MCCARTHY, 2010). However, the values of the RV parameter in the control groups were increased compared to healthy controls, as anticipated in obstructive disorders. Nevertheless, this impairment did not reach statistical significance (GILDEA and MCCARTHY, 2010, PELLEGRINO et al., 2005, REDDEL et al., 2009, GINA, 2023).

FRC findings, similar to those in the BLM-induced lung fibrosis model, did not differ among the observed groups.

Nevertheless, the results for Ri and Cdyn, parameters measured in the last PFT sequence, showed similar findings as reported by VANOIRBEEK and colleagues (2010), as no

difference was observed between the OVA/OVA controls and PBS/Saline controls, except for the Cdyn value in the OVA/OVA controls *i.n.* group.

The most important symptom and objective confirmation of asthma, AHR, was assessed in this model by measuring Ri and Cdyn values in response to increasing doses of Mch. To evaluate the presence of inflammation, AHR is performed, as normal spirometry findings can be observed in asthma patients (MCCRACKEN et al., 2017). This study utilized an invasive DSI's Buxco® FinePointe RC, an FOT tool recommended as the technique of choice (LUNDBLAD, 2012, KIM et al., 2019). As KIM et al. in 2019 explained, increases in airway smooth muscle mass, mucus secretion, and inflammatory exudates induce AHR. Since most of these factors were confirmed with other measurements, such as histopathological scoring of inflammation and epithelial damage, goblet cell metaplasia, and BALF analyses, the presence of AHR was expected in this model.

In the results, baseline Ri was unchanged in the OVA/OVA control groups compared to non-OVA sensitized and challenged control animals. However, there was an alteration in the slope of both OVA-sensitized and challenged groups: a significant increase in the Mch response was observed in the *p.o.* administered OVA/OVA control group, starting from the lowest dose, while significance in the *i.n.* administered OVA/OVA control group was observed at the two highest Mch doses. According to WALKER and his colleagues (2013), changes in slope define a reactivity linked to airway narrowing in response to a contractile stimulus. Additionally, the aforementioned article stated that bronchoconstrictor concentrations could be considered relevant if the curve midpoint dose causes a 50% increase in the baseline value, a criterion achieved in the OVA control groups in this study. Therefore, the applied Mch doses in this study can be considered relevant for the OVA-induced asthma model utilized. As expected, a gradual increase in respiratory Ri after the Mch challenge was accompanied by a significant drop in Cdyn. A more prominent decline was observed in the *p.o.* administered OVA/OVA control group, showing a significant change starting at the baseline level compared to the PBS/Saline control group. Conversely, significance was not observed in the *i.n.* administered OVA/OVA control group's baseline; instead, it started at the lowest Mch dose.

In accordance with VANOIRBEEK's report (2010), the fast flow volume maneuver test was repeated in several animals per group in the asthma model after performing AHR measurements under the maximal Mch concentration (12.5 mg/mL). Despite confirming apparent obstruction in the employed model through PFT measurements prior to Mch exposure,

the test sequence was still conducted. Results of the fast flow volume maneuver test conducted post maximal Mch dose exposure revealed a significant decrease in flow variables, reducing the AUC of PBS/Saline and both OVA/OVA control groups. Consequently, differences between those control groups challenged with OVA and the non-OVA-challenged group changed. The FVC parameter value was significantly reduced in the OVA/OVA control groups compared to the PBS/Saline control group, consistent with observations in the pre-Mch measurements. However, the FEV100 and Tiffeneau index spirometry parameters of airway obstructions (WALKER et al., 2013, MCCRACKEN et al., 2017) differed from the pre-Mch results. While FEV100 values were significantly decreased in the OVA/OVA control groups post-Mch exposure, no differences were observed compared to the PBS/Saline control group. Tiffeneau index results from post-Mch exposure revealed a similar trend, with no difference between control groups obtained. Although VANOIRBEEK's report suggests a more prominent obstructive hallmark parameter observed post-Mch exposure, these results indicate that the obtained OVA-model, including four local challenges, induced functional changes in the lungs, revealing obstructive disease in pre- and, although less prominent, in post-Mch PFT measurements.

In a manner akin to the mice model of the restrictive pulmonary disorder, the impact on pulmonary function was evaluated in the model of OVA-induced asthma, which represents an obstructive condition, through the administration of the "gold standard" medications, dexamethasone and fluticasone propionate, to the animals. In the report on utilizing the mouse asthma model in drug discovery and development (2017), EPSTEIN and colleagues emphasized the significance of comparing new drug candidates against inhaled and oral reference standards. To adhere to this recommendation, systemic corticosteroid dexamethasone was administered orally to the animals in this study, while fluticasone propionate was administered locally *via* the *i.n.* route.

Treatment with dexamethasone and fluticasone propionate positively influenced PFTs by improving key obstructive parameters, namely FEV100 and the Tiffeneau index. The FEV100 parameter showed significant enhancement in both groups treated with the reference standards compared to their respective vehicle groups (OVA/OVA Ctrls *p.o.* for dexamethasone and OVA/OVA Ctrls *i.n.* for fluticasone propionate). While the FVC parameter was notably improved in the fluticasone propionate-treated group compared to its corresponding vehicle group, FVC in the dexamethasone-treated group and Tiffeneau index values in both groups treated with the standards showed improvement but did not reach statistical significance.

Other parameters of the fast flow volume maneuver test demonstrated improvements in PEF and MMEF parameters, with fluticasone treatment reaching statistical significance, while dexamethasone treatment showed improvement in these parameters but did not reach statistical significance. These improvements influenced the shape of the F-V curve, which resembled that of the PBS/Saline control group.

Several significant differences were observed in the quasistatic pressure-volume test maneuver parameters, as anticipated, given that this maneuver is not specific to obstructive disorders (VANOIRBEEK et al., 2010). Specifically, dexamethasone treatment improved Cchord, while fluticasone propionate enhanced IC and VC parameter values compared to the corresponding vehicle-treated control groups. However, TLC, RV, and Te parameters showed no variation, as no impairments were noted in the OVA/OVA control groups. Additionally, when examining the P-V curve graph, the slopes of both standards' curves inclined upwards, closer to the curve of the PBS/Saline control group.

The Ri and Cdyn test maneuver parameters showed no impairments, similar to the results obtained in the control groups.

However, during the Mch bronchial challenge of the AHR test, Ri and Cdyn values indicated the presence of inflammation in control OVA groups, the absence of inflammation in the PBS/Saline control group, and improvement of these changes in the groups treated with reference substances, dexamethasone and fluticasone propionate, respectively. The Ri curve slope for both treatment groups showed a downward trend toward the curve of non-OVA-challenged animals, resulting in a significant decrease at the mid-Mch dose and the two highest doses compared to corresponding OVA controls. Consequently, the Cdyn results exhibited a significant decline in the dexamethasone-treated animals from the mid-dose to the highest dose compared to the corresponding vehicle control. Fluticasone propionate treatment also showed a significant difference compared to the related vehicle, starting at the baseline value and continuing for the following three Mch doses, although significance was not reached at the highest Mch dose (12.5 mg/mL).

Since the differences in the baseline Ri and Cdyn values measured in the AHR and PFT test sequences do not correlate, it can be concluded that this PFT sequence is not optimal for evaluating inflammation in obstructive disorder models, which is consistent with clinical findings (MCCRACKEN et al., 2017).

Subsequently, seven mice from each of the reference standards treatment groups underwent a repeated fast flow volume maneuver test following exposure to the maximal Mch dose. Similar to the control groups, these measurements revealed a significantly lower AUC, resulting in significantly decreased flow variables compared to the pre-Mch measurements of F-V curve parameters. Specifically, in the dexamethasone-treated group, there were significant decreases in PEF, MMEF, and Tiffeneau index values compared to the same parameters measured before the AHR test. Similarly, the fluticasone propionate-treated group exhibited significant decreases in FEV100, PEF, and MMEF values. The dexamethasone-treated group demonstrated the presence of an obstruction in the post-Mch fast flow volume maneuver test by significantly improving FEV100, PEF, MMEF, and Tiffeneau index values compared to the corresponding vehicle control group. However, obstruction was not confirmed in the fluticasone treatment group, as a significant difference compared to the related vehicle control group was only achieved in the FVC parameter value. Given that the AHR evaluation with fluticasone propionate demonstrated increased sensitivity and decreased reactivity, i.e., significance at baseline but not at the highest Mch dose, exploring the correlation with post-Mch F-V parameters would be an intriguing subject for further study.

The BALF collected immediately after performing PFT/AHR measurements provided crucial insights into inflammatory cell infiltration and the levels of IgE/cytokines in the lungs. These findings align closely with previous research reported by TRIFILIEFF et al. in 2000, READER et al. in 2003 and KIM et al. in 2019, bolstering the consistency and reliability of obtained results within the existing literature. Specifically, in the OVA/OVA control groups, there was a significant increase in total cell count compared to the PBS/Saline control group. Eosinophils were the predominant cell type in the inflammatory infiltrate observed in this study. Additionally, there was a notable rise in macrophages, lymphocytes, and neutrophils compared to the PBS/Saline group, particularly in the OVA/OVA *i.n.* control group. While there was a trend towards increased levels of these cell types in the OVA/OVA *i.n.* control group, the difference did not reach statistical significance (except in the neutrophil count).

Dexamethasone demonstrated the effect of significantly reducing eosinophils, macrophages, and lymphocytes, leading to a substantial decrease in total cell count compared to the corresponding vehicle group. Fluticasone propionate treatment significantly decreased eosinophils, lymphocytes, and total cell count.

Additional analyses conducted on BALF samples included ELISA quantification of IgE, IL-4, IL-5, and IL-13 levels in the supernatants. As highlighted in the literature, Th2 cytokines, such as IL-4, IL-5, and IL-13, play crucial roles in the development and maintenance of asthma (KUMAR et al., 2008, KIM et al., 2019). IL-4, known for promoting mucus hypersecretion, IgE synthesis, and Th2 cell differentiation, exhibited a significant increase in the OVA/OVA control group administered *p.o*. compared to the PBS/Saline group. However, in the other OVA control group (OVA/OVA control group administered *i.n.*), IL-4 values showed an increase, but the high variability within the animals affected the statistical outcome. Conversely, the IL-5 cytokine, which promotes eosinophilic inflammation and airway infiltration, did not show a significant increase in the BALF supernatant of the OVA-sensitized and challenged groups compared to the PBS/Saline controls. As for the IL-13 cytokine, which is reported to have a significant impact on AHR (KIM et al., 2019), although BALF supernatants were increased in the OVA/OVA control group administered *p.o.,* they did not reach statistical significance compared to the PBS/Saline control animals in my study. Moreover, the values in the other control group did not differ from those in the healthy control group. These findings align with reported patient findings in acute allergic asthma (NIALS and UDDIN, 2008, FINKELMAN et al., 2010, AUN et al., 2017).

Additionally, IgE, a significant contributor to AHR, is known to be overproduced in allergic asthma models in response to OVA sensitization and allergic reactions (TRIFILIEFF et al., 2000, KUMAR et al., 2008, KIM et al., 2019). Consistent with expectations, IgE levels were significantly elevated in the OVA/OVA control group administered *p.o.* compared to the PBS/Saline control group. Although the IgE levels in the other OVA control group (*i.n.* administration) showed an increase, statistical significance was not reached.

Analysis of IgE and cytokines in the BALF supernatants revealed a significant decrease in IgE, IL-4, and IL-13 levels in the dexamethasone-treated group compared to the corresponding vehicle control group. However, fluticasone propionate treatment did not significantly affect these parameters compared to the related vehicle control group despite the confirmed improvement in inflammation and obstruction with other measurements in this study. Further investigation is needed to understand the underlying reasons for these results. Additionally, considering the timing of peak IgE and cytokine levels in this model and determining the optimal sample type for evaluating these parameters would be beneficial, as previous studies have used serum or lung tissue samples (TRIFILIEFF et al., 2000, KIM et al., 2019).

In accordance with the specific objectives outlined in this thesis, the experiment employing the OVA-induced asthma model has effectively reproduced the essential features necessary for preclinical investigations of allergic asthma (TRIFILIEFF et al., 2000, LUNDBLAD, 2012, WALKER et al., 2013, EPSTEIN et al., 2017, FAHRENBACH et al., 2017). This is evidenced by the severity of the PFT parameters, indicating obstruction and confirming inflammation through AHR, eosinophilic predominance, and the presence of cytokines in BALF. However, it's important to note that mice do not display typical clinical signs such as coughing and wheezing. Therefore, monitoring body weight was the sole clinical parameter observed.

Animals' body weight was measured daily, starting from the first challenge day, to monitor their general health status during the experimental phase. In the quadruple *i.n.* OVA challenge model at a dose of 50 µg, neither mortality nor severe clinical signs are expected. Body weights in the PBS/Saline and OVA/OVA control groups remained stable, while a significant decrease in body weight was observed in the groups treated with steroids. It's worth noting that a reduction of body weight due to oral steroid treatment is a well-documented finding in OVA asthma models (RAM et al., 2006). Therefore, these observations in my study did not raise concerns regarding the progression of the research.

Further on, histological assessments were conducted to confirm the suspected lung lesions identified through the findings of PFTs and BALF analyses to evaluate inflammation, epithelial damage, and goblet cell metaplasia, ultimately determining the presence of airway remodeling in this model. The key histopathological features of asthma expected in this model, as reported by TRIFILIEFF et al. in 2000, were observed, including marked to moderate focal and multifocal inflammation with inflammatory cell infiltration, increased airway smooth muscle mass, epithelial shedding in the bronchial and alveolar areas, goblet cell hyperplasia, mucus hypersecretion, and a significantly elevated total histology score for inflammation and epithelial damage.

As hypothesized and supported by data published by TRIFILIEFF and colleagues in 2000, histological assessment of inflammation and epithelial damage scores revealed a significant reduction in values with the administration of the reference substances. Both treatment groups exhibited a notable decrease in histological scores. Dexamethasone treatment led to moderate focal to minimal diffuse pulmonary inflammation and epithelial damage, as indicated by the general score. Conversely, fluticasone treatment resulted in minimal multifocal

inflammation and minimal focal alveolar epithelial damage. Goblet cell metaplasia assessment showed a decrease in both treatment scores compared to the corresponding vehicle control groups, with significance reached only in the evaluation of fluticasone propionate treatment.

Similar to the findings obtained in the previously presented model, these data offer valuable insights into the utility of PFTs in the context of modeling acute allergic asthma. To underscore their significance, this thesis conducted a correlation analysis between key parameters in obstructive disorders, specifically FEV100 and the Tiffeneau index, and the overall histological score assessing pulmonary inflammation and epithelial shedding. The Spearman test confirmed a significant correlation between the histological score and the impairments observed in functional parameters, thereby highlighting their causal relationship and their importance in the preclinical asthma model.

The findings presented in this thesis hold significant implications for the application and interpretation of PFTs in both preclinical research and clinical practice, particularly within the realms of pulmonary fibrosis and allergic asthma models.

Integrating PFTs with histological evaluations enhances the comprehensiveness of preclinical studies. By combining functional and morphological assessments, researchers can achieve a more holistic understanding of disease progression and treatment effects, thus facilitating the translation of preclinical findings into clinical applications. To substantiate this hypothesis, this research aimed to utilize the most widely acknowledged PFT systems and tailor the mouse models in accordance with established guidelines. As indicated in the literature, it is crucial to incorporate clinically relevant endpoints to bridge the translational gap between preclinical observations and clinical outcomes (MOELLER et al., 2008, DEGRYSE and LAWSON, 2011, DENAYER et al., 2014, MCGRONIGLE and RUGGERI, 2014, SAGAR et al., 2015, JENKINS et al., 2017). Studies by MANALI et al. in 2011, LUNDBLAD in 2012, and WALKER et al. in 2013 have supported the use of specific test types in preclinical models of pulmonary fibrosis and asthma, providing detailed explanations and recommendations for their application. In line with these guidelines, the measurements in this thesis utilizing the Buxco® systems are primarily based on techniques such as PEEP, FOT, and quasistatic P-V curves, which have been identified as the most sensitive and accurate according to these reports. Moreover, to ensure the accuracy and quality of PFT values, these models were planned taking into account available guidelines for successful animal models and objective proofs for the validity of indicated models described in the literature (KUMAR et al., 2008, SCOTTON and

CHAMBERS, 2010, DENAYER et al., 2014, EPSTEIN et al., 2017, FAHRENBACHER et al., 2017, JENKINS et al., 2017).

Moreover, VANOIRBEEK's findings (2010) support the need to tailor the model, wherein the asthma model utilized in that study did not recapitulate clear evidence of obstructive disorder. In contrast, the results presented in this thesis demonstrate clear evidence of the disorder type.

This thesis studies provide insights into the characteristic PFT trends associated with different pulmonary pathologies, specifically restrictive patterns in BLM-induced pulmonary fibrosis and obstructive patterns in OVA-induced allergic asthma. By elucidating these distinct functional profiles, our findings contribute to a deeper understanding of the underlying pathophysiological mechanisms and highlight the importance of tailored PFT assessments in disease characterization.

While previous studies were focused on reporting key parameters in the models' control groups, as corroborated by VANOIRBEEK et al. in 2010, WALKER et al. in 2013, FERNANDEZ et al. in 2016, GILHODES et al. in 2017 and ANZULOVIĆ ŠANTA et al. in 2023, this study aimed to evaluate all available parameters of the specific utilized tests.

Moreover, the retrospective evaluation of known clinical PFT parameters of patients treated with nintedanib and pirfenidone, and dexamethasone and fluticasone propionate, respectively (TRIFILIEFF et al., 2000, LOVEMAN et al., 2015), in preclinical models lends higher translational value to the findings of this thesis.

The correlation between PFT results and histological findings in preclinical models enhances the translational relevance of preclinical research to clinical practice. This alignment, coupled with the correspondence between preclinical and clinical assessments, facilitates the translation of experimental findings into meaningful therapeutic interventions for patients.

Limitations in this study stem from the nature of PFTs as terminal measurements, as tracheostomy is required and can only be performed on the last day of the study. Consequently, tracking treatment improvements at different time points during therapy is not feasible. Additionally, the lack of normalization of parameter values to body weight necessitates a sufficiently large sample size to ensure the median value's representativeness. To address this, including animals of the same age in the study helps minimize variations in body weight.

Furthermore, stratifying animals based on body weight on the day therapy is initiated can further reduce variability.

Another limitation is the relatively short-term nature of the models, characterized by a brief therapeutic window. This limitation raises the possibility that some therapies may not achieve their maximum effect within the available timeframe.

Despite these constraints, the results offer valuable insights into the effects of various therapeutic interventions on pulmonary fibrosis and allergic asthma. They contribute to understanding disease mechanisms and treatment responses in preclinical models, guiding future research directions, and potentially informing clinical practice.

Moving forward, it will be essential to further refine and validate preclinical models of pulmonary fibrosis to better recapitulate the complexity of human disease. Additionally, exploring novel outcome measures and biomarkers that capture disease heterogeneity and treatment response will improve the translational relevance of preclinical studies and accelerate the development of effective therapies for pulmonary diseases.

As a recommendation, standardizing PFT measurements in other animal models of respiratory diseases, including different species such as rats, and incorporating chronic models into future research would be beneficial. Furthermore, improving the application of PFTs across various time points in preclinical settings could involve repeated measurements by implementing and refining oropharyngeal intubation techniques in mice, as detailed in the study by DE VLEESCHAUWER et al. in 2011.

Moreover, it is crucial to further refine and standardize PFT protocols for preclinical studies to ensure consistency and reproducibility across different experimental models. Additionally, integrating advanced imaging techniques, such as HRCT and MRI, with PFTs may provide complementary information on lung structure and function, enabling a more comprehensive assessment of disease severity and treatment response.

.

7 CONCLUSIONS

- The retrospective analysis of approved human therapies' effects on mouse lung function underscores the critical importance of integrating pulmonary function assessments into preclinical respiratory disease models.
- Adopting expert guidelines and recommendations, including using relevant mouse models, appropriate strains, age, sex, and clinically meaningful diagnostic tools such as PFTs, is essential for conducting robust preclinical studies in respiratory drug development.
- The robust correlation between histological fibrotic changes and functional parameter impairments provides compelling evidence for validating PFTs as surrogate endpoints in preclinical investigations of pulmonary fibrosis. This direct association between structural modifications and functional limitations underscores the sensitivity of PFTs in capturing disease advancement and therapeutic efficacy.
- Integrating PFTs as routine assessments in preclinical respiratory disease models not only enhances the predictive value of these models but also facilitates the identification of potential therapeutic candidates with greater efficacy and translational potential.
- The successful attainment of therapeutic goals in both BLM-induced pulmonary fibrosis and OVA-induced asthma models, as evidenced by improvements in lung function parameters following treatment with standard medications, underscores the validity of employing these models for drug development research.
- The retrospective demonstration of comparable effects of approved human therapies on mouse lung function underscores the significance of incorporating lung function assessments in both BLM-induced lung fibrosis and OVA-induced asthma mouse models.
- The consistent correlation between changes in mouse lung function and the effects of established human therapies underscores the ability of PFTs to accurately assess disease progression and treatment response in preclinical models of respiratory diseases.
- Values of "gold standards" PFT parameters measured by Buxco© PFT and FinePointe RC systems in BLM-induced lung fibrosis and OVA-induced asthma models are a goal to be reached or exceeded with novel tested treatments in the drug development processes. This approach could increase the probability of finding a more effective drug in the shortest possible time, which is extremely important in fatal human diseases such as IPF and asthma.

8 REFERENCES

1. ALHAMAD, E. H., J. P. LYNCH, F. J. MARTINEZ (2001): Pulmonary function tests in interstitial lung disease: what role do they have? Clin. Chest. Med. 22, 715-750. DOI: 10.1016/s0272-5231(05)70062-9
2. ALVARADO-VAZQUEZ, P. A., E. MENDEZ-ENRIQUEZ, J. HALLGREN (2020): Use of spirometry-like measurements to monitor house dust mite-induced experimental asthma in mice. Allergy. 76, 2204 DOI: 10.1111/all.14681
3. ANZULOVIĆ ŠANTA, Ž., A. OGNJENOVIĆ, M. ANTOLIĆ, S. ČUŽIĆ, I. GLOJNARIĆ, B. HRVAČIĆ, F. BOŽIĆ (2023): Retrospective assessment of nintedanib in the mice model of pulmonary fibrosis: alignment with patient outcomes in idiopathic pulmonary fibrosis. Vet. Stan. 54, 395-406. DOI: 10.46419/vs.54.4.4
4. ASHCROFT T., J. M. SIMPSON, V. TIMBRELL (1988): Simple method of estimating severity of pulmonary fibrosis on a numerical scale. J. Clin. Pathol. 41, 467–470. DOI: 10.1136/jcp.41.4.467
5. AUN, M. V., R. BONAMICHI-SANTOS, F. M. ARANTES-COSTA, J. KALIL, P. GIAVINA-BIANCHI (2017): Animal models of asthma: utility and limitations. J. Asthma Allergy 10, 293-301. DOI: 10.2147/JAA.S121092
6. BARRATT, S. L., A. CREAMER, C. HAYTON, N. CHAUDHURI (2018): Idiopathic pulmonary fibrosis (IPF): an overview. J. Clin. Med. 7, 201-221. DOI: 10.3390/jcm7080201
7. BARRIOS R. (2008): Animal Models of Lung Disease. In: Molecular Pathology of Lung Diseases. (ZANDER D. S., H. H. POPPER, J. JAGIRDAR, A. K. HAQUE, P. T. CAGLE, R. BARRIOS) Molecular Pathology Library, vol 1. Springer, New York, NY, pp. 144-149. DOI: 10.1007/978-0-387-72430-0_14
8. BATES, J. H., C. G. IRVIN (2003): Measuring lung function in mice: the phenotyping uncertainty principle. J. Appl. Physiol. 94, 1297-1306. DOI: 10.1152/japplphysiol.00706.2002.
9. BONNARDEL, E., R. PREVEL, M. CAMPAGNAC, M. DUBREUIL, R. MARTHAN, P. BERGER, I. DUPIN (2019): Determination of reliable lung function parameters in intubated mice. Resp. Res. 20, 1-14. DOI: 10.1186/s12931-019-1177-9
10. BONNIAUD, P., A. FABRE, N. FROSSARD, C. GUIGNABERT, M. INMAN, W. M. KUEBLER, M. KOLB (2018): Optimising experimental research in respiratory diseases: an ERS statement. Eur. Respir. J. 51, 1702133. DOI: 10.1183/13993003.02133-2017

11. BOONPIYATHAD, T., Z. C. SÖZENER, P. SATITSUKSANOA, C. A. AKDIS (2019): Immunologic mechanisms in asthma. Semin. Immun. 46. DOI: 10.1016/j.smim.2019.101333
12. CHUNG, M. P., M. M. MONICK, N. Y. HAMZEH, N. S. BUTLER, L. S. POWERS, G. W. HUNNINGHAKE (2003): Role of repeated lung injury and genetic background in bleomycin-induced fibrosis. Am. J. Resp. Cell. Mol. 29, 375-380. DOI: 10.1165/rcmb.2003-0029OC
13. COCKCROFT, D. W., B. E. DAVIS (2006): Mechanisms of airway hyperresponsiveness. J. Allergy. Clin. Immun. 118, 551-559. DOI:10.1016/j.jaci.2006.07.012
14. COSTA, D. L. (1985): Interpretation of new techniques used in the determination of pulmonary function in rodents. Fund. Appl. Toxicol. 5, 423-434. DOI:10.1016/0272-0590(85)90090-9
15. DAUBEUF, F., N. FROSSARD (2013): Acute asthma models to ovalbumin in the mouse. Curr. Protoc. Mouse Biol. 3, 31-37. DOI: 10.1002/9780470942390.mo120202
16. DE ANDRADE CASTRO, J. M., M. RUSSO (2019): Use and limitations of noninvasive and invasive methods for studying pulmonary function. Drug Discov. Today: Disease Models 29, 3-9. DOI:10.1016/j.ddmod.2019.07.001
17. DE VLEESCHAUWER, S. I., M. RINALDI, V. DE VOOGHT, J. A. VANOIRBEEK, B. M. VANAUDENAERDE, E. K. VERBEKEN, M. DECRAMER, G. N. GAYAN-RAMIREZ, G. M. VERLEDEN, W. JANSSENS (2011): Repeated invasive lung function measurements in intubated mice: an approach for longitudinal lung research. Lab. Anim. 45,81-9. DOI: 10.1258/la.2010.010111
18. DEGRYSE, A. L., W. E. LAWSON (2011): Progress toward improving animal models for idiopathic pulmonary fibrosis. Am. J. Med. Sci. 341, 444-449. DOI:10.1097/MAJ.0b013e31821aa000.
19. DENAYER, T., T. STÖHR, M. VAN ROY (2014): Animal models in translational medicine: Validation and prediction. New. Horiz. Transl. Med 2, 5-11. DOI:10.1016/j.nhtm.2014.08.001
20. DESAI, J. P., F. MOUSTARAH (2022): Pulmonary compliance. StatPearls Publishing. Available from: https://www.ncbi.nlm.nih.gov/books/NBK538324/
21. EPSTEIN, M. M. (2004). Do mouse models of allergic asthma mimic clinical disease? Int. Arch. Allergy Imm. 133, 84-100. DOI: 10.1159/000076131

22. EPSTEIN M., C. TILP, K. J. ERB (2017): The Use of Mouse Asthma Models to Successfully Discover and Develop Novel Drugs. Int. Arch. Allergy Immunol. 173, 61-70. DOI: 10.1159/000473699
23. FAINBERG, H. P., J. M. OLDHAM, P. L. MOLYNEAU, R. J. ALLEN, L. M. KRAVEN, W. A. FAHY, R. G. JENKINS (2022): Forced vital capacity trajectories in patients with idiopathic pulmonary fibrosis: a secondary analysis of a multicentre, prospective, observational cohort. Lancet Digit. Health 4, 862-872. DOI: 10.1016/S2589-7500(22)00173-X
24. FEHRENBACH, H., C. WAGNER, M. WEGMANN (2017): Airway remodeling in asthma: what really matters. Cell Tissue Res. 367, 551-569. DOI: 10.1007/s00441-016-2566-8
25. FERGESON, J. E., S. S. PATEL, R. F. LOCKEY (2017): Acute asthma, prognosis, and treatment. J. Allergy. Clin. Immunol. 139, 438-47. DOI: 10.1016/j.jaci.2016.06.054
26. FERNANDEZ I. E., O. V. AMARIE, K. MUTZE, M. KÖNIGSHOFF, A. Ö. YILDIRIM, O. EICKELBERG (2016): Systematic phenotyping and correlation of biomarkers with lung function and histology in lung fibrosis. Am J Physiol Lung Cell Mol Physiol. 310, 919-927. DOI: 10.1152/ajplung.00183.2015.
27. FINKELMAN F. D., S. P. HOGAN, G. K. KHURANA HERSHEY, M. E. ROTHENBERG, M. WILLS-KARP (2010): Importance of Cytokines in Murine Allergic Airway Disease and Human Asthma. J. Immunol. 184, 1663–1674. DOI:10.4049/jimmunol.0902185.
28. FLAHERTY, K. R., M. KOLB, C. VANCHERI, W. TANG, C. S. CONOSCENTI, L. RICHELDI (2018): Stability or improvement in forced vital capacity with nintedanib in patients with idiopathic pulmonary fibrosis. Eur. Respir. J. 52, 1702593. DOI:10.1183/13993003.02593-2017
29. FORUM OF INTERNATIONAL RESPIRATORY SOCIETIES (FIRS) (2017): The Global Impact of Respiratory Disease – Second Edition. Proceedings of World Health Assembly., 25 May Switzerland, Geneva Available from: https://www.firsnet.org/images/publications/The_Global_Impact_of_Respiratory_Disease.pdf
30. GILDEA, T. R., K. MCCARTHY (2010): Pulmonary function testing. In: Current Clinical Medicine. (Cleveland Clinic), Saunders Elsevier, St. Louis, pp. 1084-1095. DOI:10.1016/B978-1-4160-6643-9.00169-7

31. GILHODES J. C., Y. JULE, S. KREUZ, B. STIERSTORFER, D. STILLER, L. WOLLIN (2017): Quantification of pulmonary fibrosis in a bleomycin mouse model using automated histological image analysis. PloS ONE 12, e0170561 DOI: 10.1371/journal.pone.0170561
32. GLOBAL ASTHMA REPORT. Auckland, Global Asthma Network (GAN), 2022. Available from: http://www.globalasthmareport.org/resources/Global_Asthma_Report_2022.pdf
33. GLOBAL INITIATIVE FOR ASTHMA (GINA), 2023. Global Strategy for Asthma Management and Prevention (updated 2023). Available from: https://ginasthma.org/wp-content/uploads/2023/07/GINA-2023-report_23_07_06-1-wms.pdf.
34. GOMES, R. F. M., X. SHEN, R. RAMCHANDANI, R. S. TEPPER, J. H. T. BATES (2000): Comparative respiratory system mechanics in rodents. J. Appl. Physiol. 89, 908-916. DOI: 10.1152/jappl.2000.89.3.908
35. GRAHAM, B. L., I. STEENBRUGGEN, M. R. MILLER, I. Z. BARJAKTAREVIC, B. G. COOPER, G. L. HALL, T. S. HALLSTRAND, D. A. KAMINSKY, K. MCCARTHY, M. C. MCCORMACK, C. E. OROPEZ, M. ROSENFELD, S. STANOJEVIC, M. P. SWANNEY, B. R. THOMPSON, (2019): Standardization of spirometry 2019 update. An official American thoracic Society and European respiratory Society technical statement. Am. J. Resp. Crit. Care 200, 70-88. DOI: 10.1164/rccm.201908-1590ST
36. HOYMANN, H. G. (2012): Lung function measurements in rodents in safety pharmacology studies. Front. Pharmacol. 3, 156. DOI: 10.3389/fphar.2012.00156
37. HOYT JR, R. E., J. V. HAWKINS, M. B. ST CLAIR, M. J. KENNETT (2007): Mouse physiology. In: The mouse in biomedical research. (FOX, J., S. BARTHOLD, M. DAVISSON, C. NEWCOMER, F. QUIMBY, A. SMITH, Eds.) Academic Press, Massachusetts pp. 23-90 DOI: 10.1016/B978-012369454-6/50056-X
38. HRVAČIĆ, B., I. GLOJNARIĆ, M. ANTOLIĆ KLASNIĆ, D. PEŠIĆ, S. KOŠTRUN, M. BOSNAR, S. ČUŽIĆ (2018): A novel macrocyclic compound reduces fully developed pulmonary fibrosis in the mouse bleomycin model. Proceedings of the 2nd International Conference in “Tissue Repair, Regeneration and Fibrosis” 13.-18- June, Chaia, Greece, poster
39. HUET, O., D. RAMSEY, S. MILJAVEC, A. JENNEY, C. AUBRON, A. APRICO, N. STEFANOVIC, B. BALKAU, G. A. HEAD, J. B. DE HAAN, J P. E. CHIN-DUSTING (2013): Ensuring Animal Welfare While Meeting Scientific Aims Using a Murine Pneumonia Model of Septic Shock. Shock 39, 488-494.
DOI: 10.1097/SHK.0b013e3182939831

40. IVETIĆ TKALČEVIĆ V., B. HRVAČIĆ, M. DOMINIS KRAMARIĆ., D. ŠEVELJEVIĆ-JARAN, S. ČUŽIĆ, K. BRAJŠA (2014): Laboratory mice and rat sin biomedical research, rationale and principles of use. Medicinska naklada, Croatia, Zagreb.
41. IZBICKI, G., M. J. SEGEL, T. G. CHRISTENSEN, M. W. CONNER, R. BREUER (2002): Time course of bleomycin-induced lung fibrosis. Int. J. Exp. Path. 83, 111-119. DOI: 10.1046/j.1365-2613.2002.00220.x
42. JENKINS, R. G., B. B. MOORE, R. C. CHAMBERS, O. EICKELBERG, M. KÖNIGSHOFF, M. KOLB, G. J. LAURENT, C. B. NANTHAKUMAR, M. A. OLMAN, A. PARDO, M. SELMAN, D. SHEPPARD, P. J. SIM, A. M. TAGER, A. L. TATLER, V. J. THANNICKAL, E. S. WHITE (2017): An official American Thoracic Society workshop report: use of animal models for the preclinical assessment of potential therapies for pulmonary fibrosis. Am. J. Respir. Cell. Mol. Biol. 56, 667-679. DOI: 10.1165/rcmb.2017-0096ST
43. KIM, D. I., M. K. SONG, K. LEE (2019): Comparison of asthma phenotypes in OVA-induced mice challenged *via* inhaled and intranasal routes. BMC Pulm. Med., 19, 1-11. DOI: 10.1186/s12890-019-1001-9
44. KING JR, T. E., A. PARDO, M. SELMAN (2011): Idiopathic pulmonary fibrosis. The Lancet 378, 1949-1961. DOI: 10.1016/S0140-6736(11)60052-4
45. KING JR, T. E., W. Z. BRADFORD, S. CASTRO-BERNARDINI, E. A. FAGAN, I. GLASPOLE, M.K. GLASSBERG, P. W. NOBLE (2014): A phase 3 trial of pirfenidone in patients with idiopathic pulmonary fibrosis. N. Eng. J. Med. 370, 2083-2092. DOI: 10.1056/NEJMoa1402582
46. KLINGBERG F, B. HINZ, E. S. WHITE (2013): The myofibroblast matrix: implications for tissue repair and fibrosis. J Pathol. 229, 298-309. DOI: 10.1002/path.4104.
47. KOLB P, C. UPAGUPTA, M. VIERHOUT, E. AYAUB, P. S. BELLAYE, J. GAULDIE, C. SHIMBORI, M. INMAN, K. ASK, M. R. J. KOLB (2020): The importance of interventional timing in the bleomycin model of pulmonary fibrosis. Eur. Respir. J. 55. DOI: 10.1183/13993003.01105-2019
48. KUMAR, R. K., C. HERBERT, P. S. FOSTER, P. S (2008): The “classical” ovalbumin challenge model of asthma in mice. Curr. Drug Targets 9, 485-494. DOI:10.2174/138945008784533561
49. LOVEMAN, E., V. R. COPLEY, D. A. SCOTT, J. L. COLQUITT, A. J. CLEGG, K. M. O’REILLY (2015): Comparing new treatments for idiopathic pulmonary fibrosis–a network meta-analysis. BMC Pulm. Med. 15, 37-43. DOI: 10.1186/s12890-015-0034-y

50. LUNDBLAD, L. K. (2012): Issues determining direct airways hyperresponsiveness in mice. Front. Psychol., 3, 408. DOI: 10.3389/fphys.2012.00408
51. MANALI, E. D., C. MOSCHOS, C. TRIANTAFILLIDOU, A. KOTANIDOU, I. PSALLIDAS, S. P. KARABELA, H. ROUSSOS, S. PAPIRIS, A. ARMAGANIDIS, G. T. STATHOPOULOS, N. A. MANIATIS (2011): Static and dynamic mechanics of the murine lung after intratracheal bleomycin. BMC Pulm. Med. 11, 1-13. DOI: 10.1186/1471-2466-11-33
52. MATSUSE, T., S. TERAMOTO, H. KATAYAMA, E. SUDO, H. EKIMOTO, MITSUHASHI, Y. UEJIMA, Y. FUKUCHI and Y. OUCHI (1999): ICAM-1 mediates lung leukocyte recruitment but not pulmonary fibrosis in a murine model of bleomycin-induced lung injury. Eur. Respir. J. 13, 71-77. DOI: 10.1183/09031936.99.13107199
53. MCCRACKEN, J. L., S. P. VEERANKI, B. T. AMEREDES, W. J. CALHOUN (2017). Diagnosis and management of asthma in adults: a review. Jama 318, 279-290. DOI:10.1001/jama.2017.8372
54. MCFADDEN JR, E. R. (2004): A century of asthma. Am. J. Resp. Crit. Care Med. 170, 215-221. DOI: 10.1164/rccm.200402-185OE
55. MCGONIGLE, P., B. RUGGERI (2014): Animal models of human disease: challenges in enabling translation. Biochem. Pharm. 87, 162-171. DOI: 10.1016/j.bcp.2013.08.006
56. MELTZER, E. B., P. W. NOBLE (2008): Idiopathic pulmonary disease. Orphanet. J. Rare. Dis. 3, 1-15. DOI: 10.1186/1750-1172-3-8
57. MOELLER, A., K. ASK, D. WARBURTON, J. GAULDIE, M. KOLB (2008): The bleomycin animal model: a useful tool to investigate treatment options for idiopathic pulmonary fibrosis? Int. J. Biochem. Cell. Biol. 40, 362-382. DOI: 10.1016/j.biocel.2007.08.011
58. MOHS, R. C., N. H. GREIG (2017): Drug discovery and development: Role of basic biological research. Alzheimers Dement. 3, 651-657. DOI: 10.1016/j.trci.2017.10.005
59. MOORE, B. B., C. M. HOGABOAM (2008). Murine models of pulmonary fibrosis. Am. J. Physiol. Lung. Cell. Mol. Physiol. 294, 152-160. DOI:10.1152/ajplung.00313.2007
60. MOORE, B. B., W. E. LAWSON, T. D. OURY, T. H. SISSON, K. RAGHAVENDRAN, C. M. HOGABOAM (2013): Animal models of fibrotic lung disease. Am. J. Respir. Cell. Mol. Biol. 49, 167–179. DOI: 10.1165/rcmb.2013-0094TR
61. MOURATIS, M. A., V. AIDINIS (2011): Modeling pulmonary fibrosis with bleomycin. Curr. Opin. Pulm. Med. 17, 355-361. DOI: 10.1097/MCP.0b013e328349ac2b

62. NIALS, A. T., S. UDDIN (2008): Mouse models of allergic asthma: acute and chronic allergen challenge. Dis. Model. Mech. 1, 213-220. DOI: 10.1242/dmm.000323
63. O'BYRNE, P. M., M. D. INMAN (2003): Airway hyperresponsiveness. Chest 123, 411-416. DOI: 10.1378/chest.123.3_suppl.411S
64. PELLEGRINO R., G. VIEGI, V. BRUSASCO, R. O. CRAPO, F. BURGOS, R. CASABURI, A. COATES, C. P. M. VAN DER GRINTEN, P. GUSTAFSSON, J. HANKINSON, R. JENSEN, D. C. JOHNSON, N. MACINTYRE, R. MCKAY, M. R. MILLER, D. NAVAJAS, O. F. PEDERSEN, J. WANGER (2005): Interpretative strategies for lung function tests. Eur. Respir. J. 26, 948-968. DOI: 10.1183/09031936.05.00035205
65. PENG R., S. SRIDHAR, G. TYAGI, J. E. PHILLIPS, R. GARRIDO, P. HARRIS, L. BURNS, L. RENTERIA, J. WOODS, L. CHEN, J. ALLARD, P. RAVINDRAN, H. BITTER, Z. LIANG, C. M. HOGABOAM, C. KITSON, D. C. BUDD, J. S. FINE, C. M. T. BAUER, C. S. STEVENSON (2013): Bleomycin induces molecular changes directly relevant to idiopathic pulmonary fibrosis: a model for “active” disease. PloS one 8. DOI: 10.1371/journal.pone.0059348
66. QUANJER, P. H., G. J. TAMMELING, J. E. COTES, O. F. PEDERSEN, R. PESLIN, J. C. YERNAULT (1993): Lung volumes and forced ventilatory flows. Eur. Respir. J. 6, 5-40. DOI: 10.1183/09041950.005s1693
67. RAGHU, G., H. R. COLLARD, J. J. EGAN, F. J. MARTINEZ, J. BEHR, K. K. BROWN, D. A. LYNCH (2011): An official ATS/ERS/JRS/ALAT statement: idiopathic pulmonary fibrosis: evidence-based guidelines for diagnosis and management. Am. J. Resp. Crit. Care 183, 788-824. DOI: 10.1164/rccm.2009-040GL
68. RAGHU, G., M. REMY-JARDIN, J. L. MYERS, L. RICHELDI, C. J. RYERSON, D. J. LEDERER, K. C. WILSON (2018): Diagnosis of idiopathic pulmonary fibrosis. An official ATS/ERS/JRS/ALAT clinical practice guideline. Am. J. Resp. Crit. Care 198, 44-68. DOI: 10.1164/rccm.201807-1255ST
69. RAGHU, G., M. REMY-JARDIN, L. RICHELDI, C. C. THOMSON, Y. INOUE, T. JOHKOH, K. C. WILSON (2022): Idiopathic pulmonary fibrosis (an update) and progressive pulmonary fibrosis in adults: an official ATS/ERS/JRS/ALAT clinical practice guideline. Am. J. Resp. Crit. Care 205, 18-47. DOI: 10.1164/rccm.202202-0399ST
70. RAGHU, G., B. ROCHWERG, Y. ZHANG, C. A. C. GARCIA, A. AZUMA, J. BEHR, H. J. SCHÜNEMANN (2015): An official ATS/ERS/JRS/ALAT clinical practice guideline: treatment of idiopathic pulmonary fibrosis. An update of the 2011 clinical practice guideline. Am. J. Resp. Crit. Care 192, 3-19. DOI: 10.1164/rccm.201506-1063ST

71. RAM, A., U. MABALIRAJAN, M. DAS, I. BHATTACHARYA, A. K. DINDA, S. V. GANGAL, B. GHOSH (2006): Glycyrrhizin alleviates experimental allergic asthma in mice. In. Immunopharmacol. 6, 1468-1477. DOI:10.1016/j.intimp.2006.04.020
72. RAMSAHAI, J. M., P. M. HANSBRO, P. A. WARK (2019): Mechanisms and management of asthma exacerbations. Am. J. Resp. Crit. Care Med. 199, 423-432. DOI: 10.1164/rccm.201810-1931CI
73. RANU, H., M. WILDE, B. MADDEN (2011): Pulmonary Function Tests. Ulster Med. J. 80, 84-90.
74. READER, J. R., J. S. TEPPER, E. S. SCHELEGLE, M. C. ALDRICH, L. F. PUTNEY, J. W. PFEIFFER, D. M HYDE (2003): Pathogenesis of mucous cell metaplasia in a murine asthma model. Am. J. Pathol 162, 2069-2078. DOI: 10.1016/S0002-9440(10)64338-6
75. REDDEL, H. K., D. R. TAYLOR, E. D. BATEMAN, L. P. BOULET, H. A. BOUSHEY, W. W. BUSSE, T. B. CASALE, P. CHANEZ, P. L. ENRIGHT, P. G. GIBSON, J. C. DE JONGSTE, H. A. M. KERSTJENS, S. C. LAZARUS, M. L. LEVY, P. M. O'BYRNE, M. R. PARTRIDGE, I. D. PAVORD, M. R. SEARS, P. J. STERK, S. W. STOLOFF, S. D. SULLIVAN, S. J. SZEFLER, M. D. THOMAS, S. E. WENZEL (2009): An official American Thoracic Society/European Respiratory Society statement: asthma control and exacerbations: standardizing endpoints for clinical asthma trials and clinical practice. Am. J. Resp. Crit. Care Med. 180, 59-99. DOI: 10.1164/rccm.200801-060ST
76. REINERT T., C. S. D. R. BALDOTTO, F. A. P. NUNES, A. A. D. S. SCHELIGA (2013): Bleomycin-induced lung injury. J. Canc. Res. 2013. DOI: 10.1155/2013/480608
77. RICHELDI, L., R. M. DU BOIS, G. RAGHU, A. AZUMA, K. K. BROWN, U. COSTABEL, H. R. COLLARD (2014): Efficacy and safety of nintedanib in idiopathic pulmonary fibrosis. N. Eng. J. Med. 370, 2071-2082. DOI: 10.1056/NEJMoa1402584
78. ROBINSON, N.B., K. KRIEGER, F. M. KHAN, W. HUFFMAN, M. CHANG, A. NAIK, R. YONGLE, I. HAMEED, K. KRIEGER, L. N. GIRARDI, M. GAUDINO (2019): The current state of animal models in research: A review. Int. J. Surg. 72, 9-13. DOI: 10.1016/j.ijsu.2019.10.015
79. ROWE, B. H., M. L. EDMONDS, C. H. SPOONER, B. DINER, C. A. CAMARGO (2004): Corticosteroid therapy for acute asthma. Resp. Med. 98, 275-284. DOI:10.1016/j.rmed.2003.11.016
80. SAGAR, S., H. AKBARSHAHI, L. ULLER (2015): Translational value of animal models of asthma: challenges and promises. Eur. J. Pharm. 759, 272-277. DOI: 10.1016/j.ejphar.2015.03.037

81. SCOTTON, C. J., R. C. CHAMBERS (2010): Bleomycin revisited: towards a more representative model of IPF? Am. J. Physiol. Lung. Cell. Mol. Physiol. 299, 439-441. DOI: 10.1152/ajplung.00258.2010
82. SGALLA, G., B. IOVENE, M. CALVELLO, M. ORI, F. VARONE, L. RICHELDI (2018): Idiopathic pulmonary fibrosis: pathogenesis and management. Respir. Res. 19, 32. DOI: 10.1186/s12931-018-0730-2
83. SOMOGYI, V. N. CHAUDHURI, S. E. TORRISI, N. KAHN, V. MÜLLER, M. KREUTER (2019): The therapy of idiopathic pulmonary fibrosis: what is next? Eur. Respir. Rev. 28. DOI: 10.1183/16000617.0021-2019
84. TALBOT, S. R., S. BIERNOT, A. BLEICH, R.M. VAN DIJK, L. ERNST, C. HÄGER, S. O. A. HELGERS, B. KOEGEL, I. KOSKA, A. KUHLA, N. MILJANOVIC, F. T. MULLER-GRAFF, K. ACHWABE, R. TOLBA, B. VOLLMAR, N. WEEGH, T. WOLK, F. WOLF, A. WREE, L. ZIEGLOWSKI, H. POTSCHKA, D. ZECHNER (2020): Defining body-weight reduction as a humane endpoint: a critical appraisal. Lab. Anim. 54, 99-110. DOI: 10.1177/0023677219883319
85. TRIFILIEFF, A., A. EL-HASHIM, C. BERTRAND (2000): Time course of inflammatory and remodeling events in a murine model of asthma: effect of steroid treatment. Am. J. Physiol. Lung Cell Mol. Physiol. 279, 1120–1128. DOI: 10.1152/ajplung.2000.279.6.l1120
86. VANOIRBEEK, J. A., M. RINALDI, V. DE VOOGHT, S. HAENEN, S. BOBIC, G. GAYAN-RAMIREZ, P. H. M. HOET, E. VERBEKEN, M. DECRAMER, B. NEMERY, W. JANSSENS (2010): Noninvasive and invasive pulmonary function in mouse models of obstructive and restrictive respiratory diseases. Am. J. Resp. Cell. Mol. 42, 96-104. DOI: 10.1165/rcmb.2008-0487OC
87. WALKER, J. K. L., M. KRAFT, J. T. FISHER (2013): Assessment of murine lung mechanics outcome measures: alignment with those made in asthmatics. Front. Psychol. 3, 491. DOI: 10.3389/fphys.2012.00491
88. WANGER, J., J.L. CLAUSEN, A. COATES, O. F. PEDERSEN, V. BRUSASCO, F. BURGOS, R. CASABURI, R. CRAPO, P. ENRIGHT, C. P. M. VAN DER GRINTEN, P. GUSTAFSSON, J. HANKINSON, R. JENSEN, D. JOHNSON, N. MACINTYRE, R. MCKAY, M. R. MILLER, D. NAVAJAS, R. PELLEGRINO G. VIEGI (2005): Standardisation of the measurement of lung volumes. Eur. Respir. J. 26, 511-522. DOI: 10.1183/09031936.05.00035005
89. WILSON, M. S., T. A WYNN (2009): Pulmonary fibrosis: pathogenesis, etiology and regulation. Mucosal Immunol. 2, 103-121. DOI: 10.1038/mi.2008.85

90. WOLLIN, L., E. WEX, A. PAUTSCH, G. SCHNAPP, K. E HOSTETTLER, S. STOWASSER, M. KOLB (2015): Mode of action of nintedanib in the treatment of idiopathic pulmonary fibrosis. Eur. Respir. J. 45, 1434-1445. DOI: 10.1183/09031936.00174914
91. YANAGIHARA, T., S. G. CHONG, M. VIERHOUT, J. A. HIROTA, K. ASK, M. KOLB (2020): Current models of pulmonary fibrosis for future drug discovery efforts. Expert. Opin. Drug. Discov.15, 931-341. DOI: 10.1080/17460441.2020.1755252

9 APPENDICES

Appendix 1 Body weight (g) raw data in the BLM-induced lung fibrosis model

Group	Animal no	D0	D1	D2	D3	D4	D5	D6	D7	D8	D9	D10	D11	D12	D13	D14	D15	D16	D17	D18	D19	D20	D21
1 PBS Ctrls	1	23.4	22.0	21.2	21.7	21.8	21.8	22.7	21.7	22.9	21.8	21.6	21.4	22.0	22.0	21.9	22.5	22.6	22.9	23.0	23.2	23.1	23.3
	2	22.1	21.9	22.5	23.8	22.6	22.0	22.1	21.5	21.8	22.0	22.1	23.0	23.1	22.8	22.3	22.8	23.0	23.2	23.5	24.1	24.2	24.6
	3	24.8	24.8	24.9	25.0	24.9	25.0	25.4	25.4	25.3	25.4	25.5	25.1	25.6	25.5	25.7	25.4	25.9	26.0	26.1	26.3	26.5	26.7
	4	23.2	23.0	23.3	23.3	23.6	24.4	23.9	23.9	23.7	23.6	23.9	24.0	24.0	24.1	24.2	24.4	24.5	24.7	24.9	25.0	25.3	25.5
	5	23.0	23.1	22.9	22.9	23.5	23.8	23.7	23.9	23.9	23.6	23.7	23.3	22.4	23.2	23.4	23.4	23.7	23.8	24.0	24.1	24.4	24.5
	6	26.0	25.8	26.4	26.5	26.7	26.9	27.0	27.4	26.5	26.6	26.9	26.6	26.9	26.6	26.8	26.6	26.6	27.1	26.9	27.0	27.4	27.2
	7	25.5	25.1	25.0	25.2	26.3	26.5	26.4	26.1	25.7	26.1	26.3	26.4	26.3	26.3	26.5	26.4	26.3	26.2	26.4	26.4	26.6	26.6
	8	22.3	22.0	21.7	21.9	22.1	22.4	22.6	22.5	22.5	23.0	23.4	23.3	23.7	23.5	23.7	23.8	24.2	24.3	24.2	24.3	24.0	23.9
	9	25.0	24.8	25.3	25.4	25.6	25.8	25.9	25.6	25.5	25.6	25.6	25.7	25.6	25.7	25.9	25.7	26.0	26.0	26.0	26.0	26.0	26.0
	10	22.1	21.9	22.1	22.3	22.7	22.9	23.0	22.7	23.5	23.3	23.6	23.3	23.2	23.3	23.4	23.4	23.8	23.9	24.0	23.9	23.9	23.9
2 BLM Ctrls	11	25.5	24.8	24.4	24.1	23.7	23.4	23.0	22.3	22.4	22.2	21.4	20.8	21.0	21.5	21.2	21.4	21.2	21.2	21.2	21.3	21.4	22.4
	12	22.7	22.1	21.7	21.6	21.6	21.0	20.7	20.3	20.7	20.8	20.4	20.4	20.3	20.4	20.3	20.0	19.8	19.8	20.0	20.0	20.3	20.2
	13	27.3	26.9	26.3	26.0	25.8	25.4	25.1	24.6	24.3	23.8	24.0	24.0	24.4	24.5	24.6	25.0	25.2	25.2	25.3	25.4	26.0	26.4
	14	24.6	24.0	23.2	22.9	22.4	22.3	22.1	22.0	22.2	21.6	21.5	20.9	20.7	21.1	20.5	19.9	19.2	18.3	17.8	17.7	17.3	17.0
	16	23.6	23.1	22.8	22.6	22.5	22.4	22.0	21.4	22.1	21.4	21.1	20.5	20.7	20.6	21.0	20.9	20.3	19.4	18.8	18.8	19.0	18.9
	17	23.1	22.4	21.6	21.4	21.0	20.7	20.4	20.8	21.6	21.9	22.3	22.6	22.6	23.2	23.3	23.5	23.7	23.4	23.4	23.5	24.0	23.9
	18	24.3	24.1	23.8	23.5	23.4	23.1	23.0	24.0	24.4	24.3	24.3	24.1	24.5	23.7	23.3	23.2	22.5	22.3	22.0	22.2	22.0	21.3
	20	22.3	21.8	21.0	20.7	21.0	21.3	21.5	21.8	22.2	22.1	22.4	22.6	22.5	22.7	22.9	22.6	22.7	22.7	22.8	22.7	22.8	22.7
	21	23.8	23.5	23.8	23.6	23.1	22.6	21.9	21.5	21.3	20.9	21.3	21.5	21.6	22.2	22.2	22.2	22.2	22.3	22.5	22.5	22.4	23.2
	22	25.4	25.0	24.7	24.3	24.3	24.1	23.7	23.9	24.4	24.5	24.8	24.7	24.9	25.0	25.3	25.2	25.4	25.4	25.4	25.6	24.7	24.4
	23	23.1	22.4	21.8	20.6	20.5	20.7	20.0	20.1	20.2	20.5	20.8	20.6	20.7	20.6	20.4	20.5	20.6	20.7	20.8	21.0	21.4	21.0
	24	24.2	23.9	23.7	23.3	23.5	23.5	23.3	23.1	23.4	23.2	23.2	23.6	23.9	24.0	24.1	24.0	23.8	24.1	24.5	24.1	23.7	23.1
	25	23.4	23.0	22.8	22.0	22.3	22.2	21.5	21.7	21.8	21.5	21.7	21.4	22.1	21.5	21.9	22.1	22.0	22.3	22.5	22.7	22.8	22.5
	26	26.1	25.8	25.5	25.0	24.1	23.3	23.2	23.6	23.3	23.6	24.0	24.0	24.2	24.3	24.4	24.7	24.7	24.9	25.0	25.1	25.3	25.2
	28	25.6	25.0	25.0	24.9	24.0	23.1	23.0	22.7	22.9	22.7	22.9	23.4	23.9	24.0	24.2	24.4	24.7	24.6	24.8	24.6	24.4	24.0
	30	22.8	22.0	21.4	20.8	20.5	20.2	20.2	20.0	19.9	20.0	20.2	20.5	20.9	21.0	20.7	20.7	20.8	21.0	21.1	20.9	21.1	20.7
3 BLM/ Nintedanib 60 mg/kg *p.o. bid*	31	24.0	23.2	22.1	22.3	22.9	23.0	23.4	23.9	23.7	23.8	24.3	24.1	24.3	24.9	24.6	24.5	24.4	24.2	24.4	24.4	24.7	24.4
	32	25.1	24.0	24.3	24.0	23.6	23.2	22.9	22.7	22.4	22.4	22.6	22.5	22.5	22.6	22.6	22.4	23.0	23.0	23.1	23.3	23.5	23.2
	34	22.6	21.4	21.7	21.0	20.6	19.3	19.0	18.8	18.6	18.3	18.0	17.9	17.4	17.2	17.1	17.0	16.8	16.7	16.5	16.8	17.3	18.0
	35	25.3	24.6	24.0	23.7	23.5	23.9	24.3	25.2	25.2	25.5	25.5	25.2	25.1	25.6	25.4	25.3	25.2	25.4	25.3	25.3	25.4	25.5
	36	22.0	21.1	21.0	21.5	21.3	21.0	20.9	21.4	21.4	21.6	21.9	21.7	21.4	21.3	21.2	21.4	21.5	21.5	21.7	21.8	21.9	22.0
	37	23.6	22.9	22.7	22.1	22.0	21.6	21.4	21.7	21.9	21.5	21.1	21.0	20.8	20.7	20.8	20.6	20.5	20.3	19.7	19.4	19.4	19.3
	38	23.5	22.9	23.2	23.1	22.8	22.3	21.5	21.5	21.4	21.3	21.3	21.1	21.0	20.9	21.0	21.1	21.4	21.3	21.3	21.5	21.8	21.9
	39	24.5	24.1	23.9	23.7	24.0	24.1	24.7	24.4	24.7	24.7	24.4	24.3	24.4	24.4	24.5	24.4	24.1	24.4	25.1	25.0	26.1	24.7
	40	24.0	23.2	23.0	23.6	23.1	23.0	22.7	22.5	23.8	23.5	23.8	23.6	23.6	23.5	23.7	23.6	23.5	26.4	23.1	23.3	23.4	23.5
	41	22.1	21.8	21.4	21.5	20.8	20.2	20.2	20.4	20.5	20.9	21.5	21.4	21.5	21.7	21.6	21.6	21.8	21.7	21.9	22.0	22.1	22.2
	42	23.8	23.0	23.4	23.6	23.8	23.6	23.8	23.9	23.8	24.8	24.5	24.5	24.5	24.4	24.2	24.2	24.1	24.4	24.3	24.0	24.0	23.8
	43	21.0	20.3	20.6	20.8	19.9	19.3	19.1	19.6	20.3	20.1	20.2	20.0	20.1	20.5	20.9	21.0	20.8	20.7	21.0	21.2	21.1	21.3
	44	24.5	23.4	23.7	23.5	23.3	22.9	22.3	22.5	22.6	22.4	22.0	21.2	21.1	21.1	20.9	20.8	20.5	20.6	20.4	20.5	20.4	20.4
	45	24.7	23.4	23.2	23.0	23.1	23.1	23.0	22.7	22.8	23.3	23.5	23.4	24.1	23.8	24.0	24.1	24.1	24.3	24.0	24.5	24.3	24.4
	46	25.0	24.1	24.7	24.2	23.6	23.0	22.5	22.5	22.4	21.6	21.1	20.3	20.7	20.3	21.8	21.6	21.8	23.0	22.7	23.1	23.3	23.2
	48	25.2	24.8	25.2	24.9	25.0	25.1	25.0	24.8	25.3	25.2	25.9	26.0	25.5	25.6	25.6	24.9	24.8	25.3	25.2	25.1	24.1	24.2
	49	24.3	23.7	24.3	24.1	24.0	24.2	23.5	23.5	24.4	23.8	24.2	23.9	23.3	23.1	23.6	23.6	23.1	23.4	23.3	23.2	23.9	23.4
	50	30.0	29.1	30.7	30.9	31.4	32.2	32.2	31.4	31.2	31.8	32.0	31.8	32.0	31.8	31.7	31.6	31.1	31.3	31.1	31.3	31.7	31.4
4 BLM/ Pirfenidone 100 mg/kg *p.o. bid*	51	25.9	25.1	26.2	25.7	24.9	23.7	24.0	23.1	24.1	23.5	23.1	23.8	24.0	22.9	23.1	23.3	23.6	24.2	24.2	24.5	24.4	24.5
	52	19.0	18.7	19.3	19.5	19.8	20.2	19.9	19.2	19.0	19.2	19.5	19.5	19.9	20.0	20.4	20.1	20.2	20.0	20.2	19.5	20.0	20.0
	53	21.0	20.5	21.4	21.1	21.0	20.8	21.8	21.9	22.2	22.0	21.8	22.2	22.4	21.9	22.0	21.8	21.5	22.0	22.0	22.0	22.2	22.5
	54	24.5	23.9	24.0	24.2	24.5	24.5	24.3	23.3	23.7	23.4	23.1	22.7	23.4	23.6	23.9	24.1	24.3	23.7	23.3	24.3	23.2	24.0
	55	22.9	22.0	22.8	22.9	23.1	23.4	23.0	23.0	23.0	22.9	22.7	23.0	23.1	23.3	23.3	23.1	23.0	23.0	23.1	22.9	23.3	23.4
	56	22.5	21.9	22.2	22.5	22.1	21.7	21.0	20.6	20.9	20.8	20.9	21.6	21.1	21.1	21.3	21.6	21.0	21.4	21.6	21.9	22.2	21.5
	57	23.9	23.0	24.2	23.9	23.2	22.6	22.0	22.0	21.7	21.0	20.8	20.6	20.3	20.2	20.1	19.8	19.2	19.2	19.0	18.3	18.3	18.2
	58	23.7	22.6	22.5	22.4	22.0	21.9	21.7	22.4	22.2	21.7	21.8	21.6	21.3	21.3	20.7	20.3	20.3	20.3	19.9	20.1	20.2	20.4
	59	25.2	24.2	24.4	24.3	24.0	23.9	23.8	23.5	22.0	22.7	23.6	24.3	24.3	24.7	24.6	24.7	24.8	24.8	25.0	24.7	24.8	24.3
	61	31.4	30.4	31.2	31.6	32.2	33.0	33.6	33.0	33.1	32.9	32.2	32.8	32.9	33.0	33.5	33.7	33.3	34.0	33.5	34.1	33.9	34.1
	62	23.8	22.9	23.7	23.5	23.4	23.1	22.7	22.9	23.0	23.1	22.3	22.8	22.8	22.7	23.0	22.6	22.6	22.5	22.2	22.3	22.5	22.4
	63	24.8	24.0	23.7	23.5	23.3	23.1	23.5	23.2	23.4	23.3	23.9	23.6	23.8	24.3	24.7	24.7	24.5	24.4	24.8	25.2	24.9	24.9
	64	25.6	24.9	25.2	25.0	24.9	25.3	25.7	25.3	25.1	24.8	24.6	25.0	25.2	25.2	25.2	25.9	25.7	25.9	25.9	25.7	25.8	26.2
	65	24.0	23.1	23.3	23.5	23.4	23.1	23.0	22.5	22.4	21.7	22.3	22.6	22.8	23.4	23.8	23.9	23.8	23.7	23.9	24.0	23.7	24.1
	67	24.1	23.0	23.2	23.3	23.6	23.9	24.2	24.1	23.7	22.8	23.1	22.7	23.0	23.5	23.5	23.5	23.6	23.4	23.8	23.6	23.9	23.7
	68	23.3	22.1	21.8	22.0	22.3	22.7	23.0	21.7	21.0	20.0	20.3	20.3	20.9	21.1	21.3	21.8	21.9	22.2	22.4	22.2	22.2	21.9
	69	24.1	23.0	24.2	23.9	23.6	23.8	24.5	25.0	25.0	25.2	25.3	25.2	25.5	25.4	25.4	25.4	25.0	25.0	25.2	25.0	25.2	25.2
	70	24.1	23.4	22.6	22.8	23.0	23.5	23.7	23.5	23.9	23.7	23.2	23.2	23.3	23.5	23.8	23.6	22.9	23.5	23.4	23.4	23.0	22.8

Appendix 2 Raw data body weight (g) in the OVA-induced asthma model

Group	Animal no	D20	D21	D22	D23	D24
1 PBS/Saline Ctrls	1	24.1	26.2	26.0	26.3	26.2
	2	24.0	24.1	24.3	24.2	24.2
	3	21.9	22.1	22.4	22.7	22.4
	4	20.5	19.8	20.7	20.4	19.7
	5	24.2	24.5	24.8	24.9	24.8
	6	25.5	25.8	25.9	26.0	25.9
	7	24.6	24.8	25.2	25.5	25.4
	8	22.4	22.9	23.1	23.3	23.5
2 OVA/OVA Ctrls *p.o.*	9	22.6	22.8	22.9	23.5	23.6
	10	24.8	23.3	23.8	24.0	24.4
	11	26.0	25.0	24.8	25.5	25.5
	12	23.2	23.0	23.2	23.3	23.4
	13	26.1	26.1	25.6	26.0	26.0
	14	23.6	23.5	24.0	24.2	24.5
	15	24.0	23.8	24.3	24.3	24.9
	16	21.8	21.5	21.4	21.8	22.0
	17	21.9	21.3	20.9	21.5	21.6
	18	24.6	25.1	25.0	25.6	25.9
3 OVA/ Dexamethasone 3 mg/kg *p.o.*	19	23.1	22.2	22.1	22.1	21.7
	20	23.1	21.8	21.5	21.4	21.0
	21	21.9	21.2	21.5	21.4	21.1
	22	23.0	21.7	22.3	21.5	21.4
	23	25.1	24.1	23.5	23.5	23.5
	24	19.4	18.5	18.0	18.2	17.7
	25	21.5	19.8	19.5	19.5	19.2
	26	22.5	21.0	20.8	20.6	20.4
	27	24.5	23.1	23.4	23.0	22.1
	28	22.6	22.1	21.8	22.0	21.4
4 OVA/OVA Ctrls *i.n.*	29	26.6	25.5	25.0	25.0	25.0
	30	24.4	24.1	24.5	24.6	24.6
	31	23.0	22.7	22.4	22.6	22.5
	32	23.7	23.7	24.0	24.4	24.6
	33	24.4	24.4	24.4	24.7	24.8
	34	20.3	19.8	20.2	20.5	21.1
	35	23.5	23.0	23.3	23.1	23.8
	36	25.2	24.9	24.8	25.0	24.9
	37	22.7	22.4	22.6	23.0	23.2
	38	24.4	23.4	24.1	24.3	25.0
4 OVA/ Fluticasone propionate 2 mg/kg *i.n.*	39	25.7	24.7	24.4	24.1	23.7
	40	22.6	21.0	21.2	21.5	20.6
	41	23.1	22.5	22.2	21.6	21.0
	42	23.6	22.6	22.5	22.4	22.3
	43	25.9	24.5	24.9	24.6	24.3
	44	23.5	22.5	22.6	22.2	22.0
	45	22.8	21.6	21.1	21.1	20.7
	46	23.1	22.1	21.9	21.9	21.6
	47	21.7	20.9	20.8	20.7	20.4
	48	23.3	22.7	22.3	22.1	21.3

Appendix 3 PFTs parameters in the BLM-induced lung fibrosis model

Group	Animal no	FRC (mL)	TLC (mL)	RV (mL)	Te (sec)	Cchord (mL/cm H2O)	IC (mL)	VC (mL)	FVC (mL)	FEV100 (mL)	PEF (mL/sec)	MMEF (mL/sec)	Ri (cm H2O sec/mL)	Cdyn (ml/cm H2O)	FEV1/ FVC
1 PBS Ctrls	1	0.518	1.152	0.377	1.350	0.038	0.633	0.774	0.795	0.787	37.936	16.413	0.726	0.035	0.990
	2	0.520	1.134	0.413	1.111	0.040	0.614	0.722	0.767	0.762	36.623	29.528	0.522	0.034	0.993
	3	0.455	1.174	0.412	1.572	0.031	0.719	0.762	0.784	0.764	25.496	14.918	0.698	0.062	0.974
	4	0.580	1.297	0.498	1.323	0.037	0.718	0.799	0.857	0.800	35.603	22.236	0.459	0.032	0.934
	5	0.540	1.249	0.455	1.365	0.038	0.709	0.794	0.776	0.712	34.151	20.787	0.840	0.033	0.918
	6	0.456	1.108	0.297	1.071	0.038	0.652	0.812	0.803	0.797	28.436	17.452	0.188	0.021	0.994
	7	0.395	1.101	0.272	0.940	0.046	0.705	0.828	0.853	0.831	23.205	14.075	0.491	0.023	0.974
	8	0.375	0.984	0.213	1.043	0.038	0.609	0.771	0.814	0.809	35.181	29.835	0.461	0.021	0.994
	9	0.342	0.902	0.234	0.843	0.036	0.561	0.669	0.708	0.685	32.085	21.686	0.188	0.019	0.967
	10	0.326	1.039	0.200	0.986	0.045	0.713	0.839	0.827	0.804	31.842	15.727	0.379	0.032	0.973
2 BLM Ctrls	11	0.392	0.839	0.284	0.685	0.026	0.446	0.554	0.585	0.565	23.432	17.542	0.330	0.014	0.966
	12	0.389	0.776	0.314	0.582	0.022	0.387	0.462	0.503	0.503	24.876	15.731	0.226	0.012	0.999
	13	0.416	0.848	0.348	0.622	0.024	0.432	0.500	0.575	0.569	26.056	18.366	0.279	0.013	0.990
	14	0.313	0.832	0.192	0.795	0.035	0.520	0.641	0.619	0.617	26.427	18.956	0.340	0.022	0.998
	16	0.406	0.772	0.343	0.543	0.017	0.366	0.429	0.567	0.557	19.025	12.593	1.116	0.009	0.982
	17	0.492	0.816	0.325	0.657	0.019	0.324	0.491	0.538	0.536	27.465	21.829	0.332	0.013	0.996
	18	0.288	0.779	0.215	0.665	0.027	0.491	0.564	0.579	0.572	24.235	17.383	0.662	0.014	0.988
	20	0.421	0.897	0.343	0.695	0.030	0.476	0.555	0.619	0.618	23.176	14.078	0.417	0.011	0.998
	21	0.416	0.806	0.361	0.548	0.023	0.390	0.445	0.496	0.505	30.275	23.649	0.141	0.011	1.018
	22	0.313	0.688	0.269	0.580	0.022	0.375	0.419	0.450	0.436	20.974	13.237	0.288	0.009	0.969
	23	0.311	0.797	0.224	0.775	0.028	0.485	0.573	0.580	0.572	18.396	14.756	0.615	0.015	0.986
	24	0.272	0.663	0.193	0.615	0.022	0.391	0.470	0.442	0.438	19.068	16.574	1.187	0.016	0.991
	25	0.415	0.938	0.308	0.885	0.030	0.523	0.630	0.651	0.632	19.869	11.781	0.444	0.014	0.970
	26	0.453	0.957	0.395	0.726	0.031	0.505	0.562	0.624	0.611	21.399	9.468	0.459	0.015	0.980
	28	0.469	0.946	0.423	0.715	0.027	0.477	0.523	0.594	0.588	29.690	14.311	0.361	0.017	0.991
	30	0.415	0.962	0.316	0.823	0.031	0.547	0.646	0.593	0.576	22.590	16.803	0.830	0.014	0.971
3 BLM/ Nintedanib 60 mg/kg *p.o. bid*	31	0.401	1.030	0.333	0.838	0.038	0.630	0.697	0.750	0.741	23.953	18.152	0.283	0.019	0.988
	32	0.361	0.848	0.263	0.705	0.031	0.488	0.586	0.613	0.597	22.453	14.831	0.528	0.016	0.975
	34	0.511	1.246	0.411	1.082	0.045	0.734	0.834	0.857	0.821	22.913	14.689	0.535	0.026	0.958
	35	0.366	0.883	0.308	0.728	0.029	0.517	0.575	0.668	0.664	22.390	13.956	0.205	0.015	0.994
	36	0.393	1.048	0.255	1.036	0.044	0.655	0.792	0.802	0.778	21.630	12.698	0.785	0.023	0.969
	37	0.408	0.897	0.295	0.718	0.027	0.489	0.602	0.461	0.416	12.171	5.706	0.623	0.015	0.902
	38	0.363	0.820	0.266	0.772	0.027	0.457	0.553	0.635	0.622	26.348	17.649	0.796	0.017	0.980
	39	0.406	0.975	0.249	0.930	0.037	0.569	0.726	0.755	0.750	27.307	20.259	0.355	0.020	0.993
	40	0.390	1.085	0.263	1.095	0.044	0.695	0.823	0.870	0.862	35.331	31.076	0.655	0.027	0.991
	41	0.342	0.870	0.238	0.910	0.017	0.527	0.632	0.652	0.637	28.222	21.750	0.240	0.019	0.976
	42	0.396	1.109	0.218	1.161	0.041	0.713	0.891	0.880	0.875	36.751	28.736	0.925	0.027	0.993
	43	technical error			0.880	0.036	0.554	0.700	0.672	0.669	28.600	18.684	0.891	0.020	0.995
	44	0.427	0.886	0.357	0.627	0.026	0.459	0.529	0.277	0.237	8.359	3.582	1.879	0.015	0.856
	45	0.387	0.909	0.307	0.863	0.031	0.522	0.602	0.644	0.258	7.700	1.249	1.153	0.018	0.401
	46	-0.010	0.385	-0.144	0.785	0.024	0.395	0.529	0.890	0.614	24.784	1.803	1.137	0.015	0.689
	48	0.437	1.010	0.292	0.897	0.035	0.573	0.718	0.702	0.689	27.696	17.126	technical error		0.981
	49	0.465	0.980	0.330	0.923	0.029	0.515	0.650	0.640	0.618	23.073	19.219	1.064	0.019	0.966
	50	0.383	1.046	0.285	1.111	0.041	0.662	0.760	0.685	0.668	23.250	18.237	1.013	0.023	0.975
4 BLM/ Pirfenidone 100 mg/kg *p.o. bid*	51	0.361	0.799	0.226	0.830	0.026	0.438	0.573	0.632	0.624	25.837	19.300	0.605	0.021	0.987
	52	0.427	0.905	0.292	0.913	0.030	0.478	0.613	0.743	0.742	21.817	11.460	0.775	0.018	0.998
	53	0.290	0.791	0.126	0.813	0.033	0.501	0.665	0.644	0.643	27.430	19.350	0.914	0.020	0.999
	54	0.303	0.694	0.156	0.665	0.026	0.391	0.538	0.514	0.500	24.992	18.376	0.554	0.013	0.972
	55	0.458	1.076	0.312	1.157	0.043	0.618	0.764	0.776	0.745	23.077	12.946	1.091	0.027	0.960
	56	0.349	0.869	0.271	0.751	0.030	0.521	0.598	0.667	0.657	28.873	20.451	0.972	0.014	0.985
	57	0.282	0.666	0.181	0.683	0.023	0.384	0.485	0.506	0.495	25.784	16.640	0.579	0.013	0.978
	58	0.463	0.918	0.363	0.734	0.029	0.455	0.556	0.644	0.637	29.453	18.945	0.339	0.015	0.989
	59	0.425	0.754	0.176	0.827	0.014	0.329	0.578	0.635	0.631	31.857	27.250	0.542	0.015	0.994
	61	0.471	1.195	0.371	1.165	0.041	0.724	0.824	0.850	0.822	27.491	23.620	0.342	0.021	0.967
	62	0.390	0.814	0.378	0.612	0.019	0.423	0.436	0.616	0.603	28.765	21.001	0.668	0.011	0.978
	63	0.492	0.951	0.489	0.621	0.023	0.459	0.462	0.630	0.617	31.836	22.521	0.644	0.012	0.979
	64	0.394	0.966	0.304	0.878	0.038	0.572	0.662	0.637	0.590	17.520	7.207	0.279	0.018	0.927
	65	0.409	0.817	0.381	0.728	0.020	0.408	0.437	0.539	0.522	27.063	19.729	0.462	0.011	0.968
	67	0.402	0.850	0.349	0.705	0.022	0.448	0.501	0.578	0.578	27.065	20.222	0.293	0.010	0.999
	68	0.536	0.836	0.281	0.855	0.015	0.300	0.555	0.568	0.562	27.304	23.003	0.786	0.010	0.990
	69	0.462	1.180	0.301	0.971	0.044	0.719	0.879	0.907	0.898	36.289	27.237	0.198	0.025	0.990
	70	0.429	0.861	0.343	0.623	0.023	0.432	0.518	0.567	0.565	22.120	16.411	0.404	0.011	0.997

Appendix 4 P-V curve values in the BLM-induced lung fibrosis model

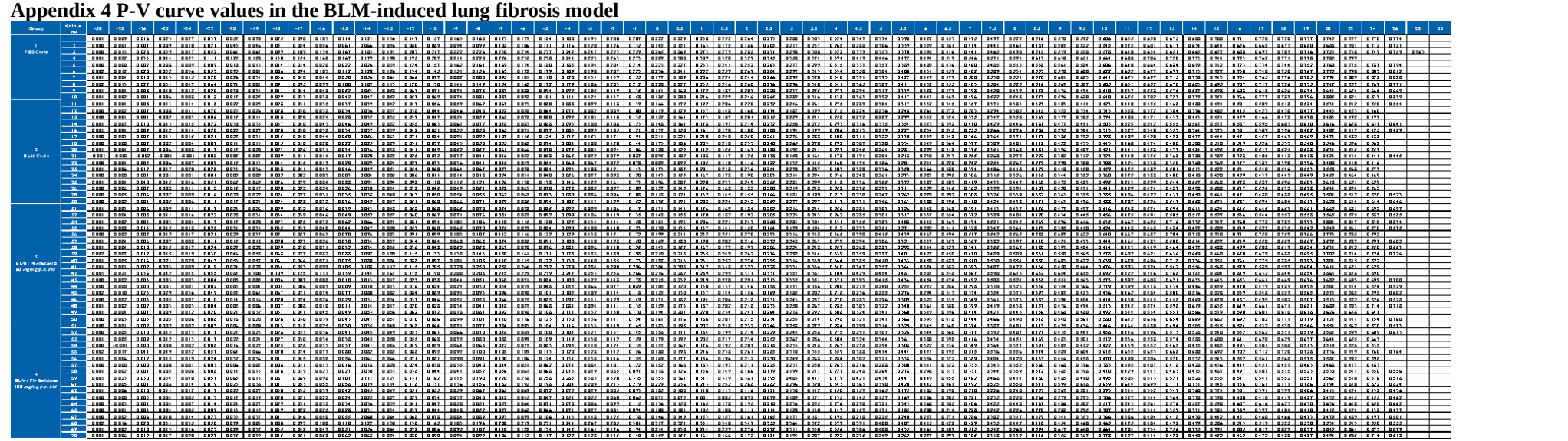

Appendix 5 F-V curve values in the BLM-induced lung fibrosis model

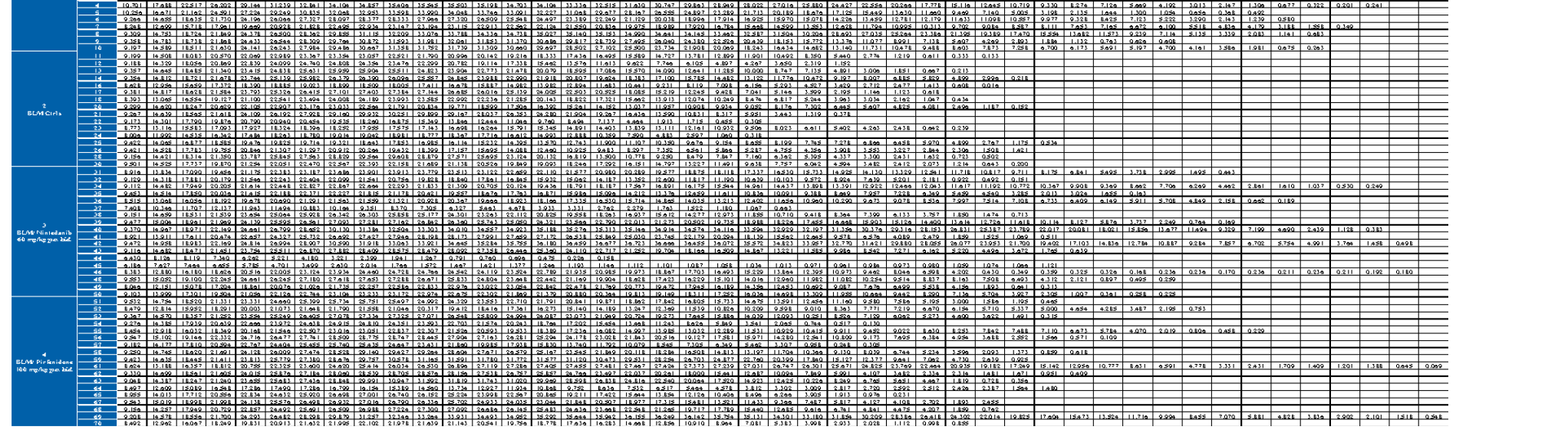

Appendix 6 PFTs parameters in the OVA-induced asthma model

Group	Animal no	FRC (mL)	TLC (mL)	RV (mL)	Te (sec)	Cchord (mL/cm H2O)	IC (mL)	VC (mL)	FVC (mL)	FEV100 (mL)	PEF (mL/ sec)	MMEF (mL/ sec)	Ri (cm H2O sec/mL)	Cdyn (ml/cm H2O)	FEV100 /FVC
1 PBS/Saline Ctrls	1	0.397	1.307	0.304	1.140	0.052	0.910	1.003	1.061	1.039	20.980	35.529	0.667	0.041	0.979
	2	0.318	1.077	0.202	0.925	0.045	0.759	0.875	0.890	0.863	14.692	28.342	0.934	0.030	0.969
	3	0.385	1.210	0.273	1.086	0.049	0.825	0.937	0.982	0.929	12.402	27.537	0.918	0.035	0.945
	4	0.198	0.802	0.051	0.898	0.037	0.604	0.750	0.690	0.670	12.198	29.033	0.904	0.022	0.970
	5	0.368	1.162	0.256	0.992	0.051	0.794	0.906	0.959	0.892	11.793	17.528	1.085	0.041	0.930
	6	0.207	0.992	0.090	1.010	0.050	0.786	0.903	0.939	0.921	15.680	25.345	0.940	0.035	0.981
	7	0.335	1.081	0.200	0.943	0.054	0.746	0.880	0.778	0.765	14.415	20.473	1.022	0.033	0.983
	8	0.195	1.075	0.058	1.140	0.064	0.880	1.017	1.041	1.005	15.826	24.707	0.991	0.035	0.965
2 OVA/OVA Ctrls *p.o.*	9	0.409	1.133	0.262	1.048	0.040	0.724	0.871	0.877	0.437	2.475	9.835	1.143	0.033	0.498
	10	0.301	0.860	0.177	0.875	0.029	0.559	0.684	0.646	0.563	6.879	19.392	0.558	0.017	0.871
	11	0.486	1.215	0.370	1.015	0.044	0.729	0.845	0.792	0.745	16.854	26.597	0.687	0.033	0.941
	12	0.241	0.822	0.129	0.895	0.033	0.581	0.693	0.601	0.579	11.339	20.122	1.296	0.017	0.965
	13	0.623	1.527	0.486	1.100	0.054	0.904	1.041	1.020	0.899	13.626	23.500	0.991	0.036	0.881
	14	0.410	1.245	0.264	1.236	0.044	0.835	0.981	0.966	0.867	11.347	28.841	0.486	0.034	0.897
	15	0.188	0.840	0.093	0.923	0.035	0.652	0.747	0.736	0.685	9.181	20.809	0.534	0.023	0.930
	16	0.289	0.909	0.213	0.850	0.044	0.620	0.696	0.690	0.630	10.624	17.467	1.092	0.032	0.913
	17	0.167	0.927	0.102	0.995	0.042	0.760	0.825	0.856	0.833	17.404	32.499	0.438	0.032	0.974
	18	0.385	1.123	0.278	1.021	0.038	0.738	0.845	0.859	0.820	13.941	27.923	0.738	0.036	0.955
3 OVA/ Dexamethasone 3 mg/kg *p.o.*	19	0.459	1.256	0.341	0.941	0.049	0.797	0.915	0.939	0.891	16.404	23.853	0.802	0.037	0.949
	20	0.263	0.909	0.110	0.960	0.039	0.646	0.798	0.760	0.685	8.412	22.730	0.953	0.029	0.901
	21	0.468	1.236	0.386	0.850	0.049	0.768	0.850	0.911	0.859	15.586	25.843	0.792	0.036	0.942
	22	0.429	1.171	0.297	0.923	0.042	0.742	0.873	0.916	0.872	14.558	31.724	0.807	0.031	0.952
	23	0.412	1.145	0.299	0.995	0.040	0.733	0.847	0.812	0.777	13.707	20.866	0.466	0.021	0.958
	24	0.345	1.026	0.233	0.943	0.048	0.680	0.793	0.812	0.775	14.912	31.485	0.935	0.030	0.954
	25	0.217	0.992	0.121	1.047	0.044	0.775	0.871	0.875	0.830	18.011	28.009	0.626	0.048	0.949
	26	0.296	1.189	0.144	1.056	0.053	0.892	1.044	1.066	0.672	4.148	25.846	0.605	0.026	0.630
	27	0.363	1.143	0.265	1.055	0.047	0.780	0.878	0.897	0.866	18.848	27.195	0.823	0.043	0.965
	28	0.285	1.060	0.189	0.850	0.045	0.775	0.871	0.918	0.889	18.008	30.233	0.337	0.028	0.969
4 OVA/OVA Ctrls *i.n.*	29	0.201	0.778	0.161	0.713	0.034	0.577	0.617	0.613	0.582	9.850	19.762	3.571	0.021	0.949
	30	0.467	1.122	0.377	0.781	0.042	0.655	0.745	0.728	0.703	15.382	27.611	0.786	0.033	0.967
	31	0.166	0.600	0.073	0.623	0.029	0.434	0.527	0.502	0.488	10.638	20.960	0.896	0.021	0.971
	32	0.495	1.187	0.353	0.923	0.038	0.692	0.834	0.874	0.712	6.509	23.193	0.728	0.021	0.815
	33	0.292	0.990	0.145	1.026	0.040	0.698	0.844	0.838	0.624	6.400	11.016	0.879	0.019	0.744
	34	0.440	1.281	0.333	1.141	0.056	0.841	0.949	0.945	0.892	11.883	25.714	0.989	0.034	0.944
	35	0.166	0.682	0.067	0.610	0.035	0.515	0.614	0.595	0.575	9.555	18.449	2.238	0.027	0.966
	36	0.418	1.014	0.303	0.896	0.035	0.596	0.711	0.758	0.554	4.309	19.312	1.099	0.032	0.731
	37	0.201	0.789	0.103	0.660	0.041	0.587	0.685	0.552	0.530	7.943	17.735	1.051	0.032	0.961
	38	0.385	1.037	0.268	0.948	0.045	0.652	0.769	0.732	0.698	12.537	23.692	1.049	0.030	0.953
4 OVA/ Fluticasone propionate 2 mg/kg *i.n.*	39	0.364	1.068	0.286	0.823	0.044	0.704	0.782	0.803	0.740	11.473	23.572	1.128	0.031	0.922
	40	0.235	0.822	0.132	0.813	0.038	0.586	0.690	0.717	0.713	21.528	28.376	0.979	0.031	0.995
	41	0.352	1.089	0.238	0.881	0.050	0.737	0.851	0.909	0.854	11.392	26.647	0.926	0.031	0.940
	42	0.244	0.685	0.162	0.695	0.009	0.442	0.524	0.698	0.676	13.507	20.889	1.460	0.020	0.968
	43	0.447	1.181	0.285	0.956	0.048	0.735	0.896	0.917	0.886	18.104	21.514	1.198	0.030	0.967
	44	0.272	1.283	0.195	1.003	0.071	1.010	1.088	0.979	0.807	8.045	26.379	1.194	0.032	0.825
	45	0.369	1.164	0.273	1.055	0.053	0.795	0.891	0.929	0.900	17.654	33.399	0.888	0.035	0.968
	46	0.175	0.957	0.080	0.833	0.048	0.783	0.877	0.896	0.786	9.548	24.489	0.470	0.022	0.878
	47	0.398	1.162	0.260	1.125	0.047	0.764	0.902	0.942	0.858	11.788	22.798	0.636	0.030	0.911
	48	0.175	0.985	0.115	0.820	0.047	0.810	0.869	0.926	0.911	20.450	29.184	0.335	0.026	0.984

Appendix 7 P-V curve valued in the model of OVA-induced asthma model

Group	Animal no	-30	-28	-26	-25	-24	-22	-20	-19	-18	-17	-16	-15	-14	-13	-12	-10	-9	-8	-7	-6	-5	-4	-3	-2	-1	0	0.5	1	1.5	2
1 PBS/Saline Ctrls	1	0.001	0.003	0.005	0.006	0.006	0.008	0.010	0.011	0.013	0.017	0.022	0.047	0.052	0.060	0.066	0.080	0.087	0.093	0.100	0.109	0.117	0.127	0.137	0.150	0.168	0.311	0.328	0.346	0.361	0.386
	2	0.001	0.002	0.004	0.005	0.006	0.009	0.015	0.018	0.021	0.024	0.029	0.032	0.036	0.040	0.044	0.095	0.100	0.106	0.112	0.117	0.121	0.127	0.160	0.222	0.238	0.257	0.304	0.317	0.331	0.343
	3	0.000	0.002	0.003	0.003	0.004	0.012	0.015	0.017	0.018	0.020	0.023	0.026	0.029	0.039	0.045	0.057	0.066	0.082	0.094	0.101	0.135	0.201	0.215	0.258	0.276	0.295	0.308	0.323	0.344	0.366
	4	0.001	0.004	0.007	0.009	0.010	0.022	0.030	0.032	0.034	0.036	0.046	0.050	0.054	0.057	0.060	0.080	0.094	0.099	0.102	0.105	0.107	0.128	0.146	0.183	0.194	0.239	0.255	0.266	0.280	0.294
	5	0.001	0.002	0.003	0.004	0.004	0.005	0.007	0.008	0.009	0.011	0.015	0.022	0.027	0.032	0.040	0.053	0.064	0.091	0.106	0.133	0.153	0.166	0.183	0.199	0.215	0.235	0.246	0.257	0.274	0.292
	6	0.001	0.002	0.004	0.004	0.005	0.006	0.007	0.008	0.009	0.010	0.012	0.017	0.032	0.041	0.050	0.065	0.074	0.087	0.101	0.115	0.134	0.152	0.169	0.187	0.206	0.227	0.239	0.251	0.267	0.287
	7	0.000	0.001	0.002	0.002	0.003	0.004	0.005	0.006	0.006	0.007	0.009	0.010	0.012	0.015	0.018	0.028	0.034	0.041	0.049	0.057	0.067	0.078	0.091	0.116	0.144	0.180	0.203	0.231	0.255	0.283
	8	0.000	0.001	0.002	0.002	0.003	0.003	0.004	0.005	0.006	0.006	0.008	0.009	0.011	0.014	0.019	0.034	0.044	0.054	0.066	0.074	0.089	0.098	0.113	0.139	0.165	0.196	0.218	0.250	0.275	0.309
2 OVA/OVA Ctrls *p.o.*	9	0.000	0.016	0.020	0.030	0.031	0.036	0.049	0.051	0.069	0.077	0.090	0.096	0.100	0.120	0.138	0.144	0.151	0.153	0.166	0.176	0.198	0.242	0.285	0.301	0.318	0.333	0.339	0.355	0.371	0.397
	10	0.001	0.005	0.008	0.009	0.011	0.015	0.019	0.023	0.029	0.044	0.050	0.056	0.061	0.069	0.079	0.098	0.109	0.116	0.122	0.131	0.161	0.196	0.217	0.237	0.256	0.274	0.285	0.300	0.311	0.324
	11	0.002	0.007	0.011	0.013	0.015	0.022	0.031	0.036	0.048	0.053	0.059	0.078	0.083	0.088	0.095	0.159	0.166	0.173	0.182	0.193	0.201	0.210	0.223	0.237	0.252	0.276	0.290	0.300	0.319	0.344
	12	0.001	0.003	0.005	0.040	0.043	0.050	0.061	0.064	0.068	0.070	0.071	0.073	0.074	0.075	0.108	0.114	0.136	0.144	0.151	0.167	0.178	0.188	0.198	0.209	0.220	0.231	0.239	0.247	0.257	0.270
	13	0.002	0.006	0.010	0.013	0.015	0.021	0.029	0.034	0.040	0.047	0.059	0.065	0.074	0.082	0.089	0.107	0.116	0.142	0.163	0.171	0.180	0.211	0.230	0.266	0.296	0.324	0.345	0.364	0.377	0.397
	14	0.002	0.014	0.026	0.032	0.034	0.040	0.044	0.050	0.052	0.053	0.070	0.073	0.077	0.080	0.082	0.105	0.107	0.163	0.172	0.181	0.190	0.193	0.312	0.325	0.352	0.377	0.394	0.403	0.418	0.429
	15	0.001	0.003	0.005	0.006	0.008	0.018	0.030	0.038	0.049	0.052	0.055	0.057	0.061	0.066	0.070	0.078	0.082	0.087	0.130	0.167	0.173	0.207	0.215	0.229	0.242	0.263	0.270	0.281	0.291	0.300
	16	0.001	0.002	0.003	0.004	0.006	0.010	0.015	0.019	0.022	0.025	0.028	0.031	0.043	0.048	0.055	0.069	0.074	0.079	0.087	0.094	0.099	0.104	0.113	0.123	0.135	0.150	0.165	0.183	0.201	0.224
	17	0.000	0.001	0.001	0.002	0.002	0.008	0.011	0.014	0.016	0.037	0.041	0.045	0.048	0.050	0.052	0.057	0.059	0.088	0.091	0.096	0.100	0.138	0.192	0.214	0.228	0.243	0.254	0.259	0.264	0.273
	18	0.001	0.005	0.007	0.008	0.010	0.017	0.022	0.025	0.027	0.030	0.033	0.038	0.047	0.051	0.054	0.062	0.125	0.131	0.137	0.211	0.227	0.249	0.262	0.283	0.295	0.308	0.323	0.330	0.337	0.347
3 OVA/ Dexamethasone 3 mg/kg *p.o.*	19	0.001	0.002	0.003	0.004	0.005	0.007	0.012	0.019	0.024	0.029	0.034	0.041	0.053	0.058	0.063	0.085	0.103	0.130	0.148	0.158	0.172	0.189	0.212	0.232	0.247	0.273	0.287	0.303	0.318	0.339
	20	0.001	0.002	0.005	0.007	0.009	0.013	0.017	0.020	0.023	0.027	0.036	0.042	0.047	0.055	0.062	0.089	0.102	0.111	0.119	0.125	0.129	0.132	0.193	0.204	0.237	0.260	0.268	0.280	0.294	0.306
	21	0.001	0.004	0.006	0.006	0.007	0.007	0.008	0.009	0.009	0.010	0.010	0.011	0.013	0.014	0.017	0.030	0.041	0.051	0.063	0.086	0.113	0.141	0.167	0.183	0.199	0.219	0.232	0.250	0.265	0.284
	22	0.002	0.004	0.006	0.007	0.008	0.010	0.013	0.015	0.021	0.029	0.036	0.042	0.047	0.051	0.077	0.104	0.111	0.117	0.153	0.198	0.223	0.242	0.259	0.272	0.291	0.309	0.318	0.327	0.340	0.357
	23	0.001	0.003	0.005	0.009	0.009	0.012	0.020	0.022	0.024	0.029	0.033	0.037	0.042	0.048	0.052	0.085	0.091	0.108	0.121	0.165	0.183	0.202	0.212	0.232	0.244	0.273	0.299	0.307	0.316	0.329
	24	0.001	0.003	0.004	0.005	0.006	0.007	0.010	0.011	0.012	0.014	0.017	0.020	0.024	0.034	0.043	0.058	0.065	0.072	0.082	0.090	0.101	0.115	0.126	0.139	0.157	0.179	0.193	0.210	0.230	0.252
	25	0.001	0.003	0.005	0.006	0.007	0.010	0.018	0.021	0.025	0.030	0.035	0.042	0.046	0.054	0.067	0.086	0.098	0.138	0.158	0.188	0.200	0.217	0.233	0.247	0.261	0.276	0.283	0.293	0.302	0.315
	26	0.001	0.002	0.003	0.004	0.005	0.006	0.009	0.012	0.015	0.020	0.025	0.030	0.034	0.039	0.063	0.076	0.082	0.088	0.094	0.100	0.119	0.130	0.162	0.243	0.309	0.340	0.353	0.367	0.384	0.400
	27	0.001	0.008	0.010	0.011	0.011	0.014	0.017	0.018	0.020	0.022	0.023	0.026	0.028	0.058	0.064	0.081	0.084	0.126	0.146	0.155	0.167	0.197	0.210	0.224	0.242	0.254	0.264	0.274	0.286	0.301
	28	0.001	0.003	0.005	0.006	0.007	0.009	0.013	0.017	0.020	0.026	0.031	0.036	0.044	0.055	0.063	0.100	0.109	0.123	0.137	0.152	0.167	0.182	0.198	0.212	0.229	0.248	0.259	0.271	0.281	0.290
4 OVA/OVA Ctrls *i.n.*	29	0.000	0.001	0.002	0.003	0.004	0.005	0.006	0.008	0.009	0.011	0.014	0.017	0.021	0.025	0.029	0.045	0.052	0.059	0.065	0.073	0.080	0.089	0.100	0.111	0.123	0.140	0.149	0.162	0.177	0.195
	30	0.001	0.002	0.003	0.004	0.004	0.007	0.011	0.013	0.015	0.019	0.022	0.028	0.039	0.047	0.064	0.082	0.090	0.100	0.109	0.120	0.130	0.140	0.152	0.166	0.184	0.206	0.223	0.241	0.269	0.291
	31	0.001	0.002	0.003	0.004	0.005	0.007	0.011	0.015	0.018	0.020	0.023	0.027	0.031	0.035	0.038	0.048	0.053	0.058	0.064	0.070	0.077	0.086	0.097	0.108	0.122	0.151	0.164	0.182	0.199	0.217
	32	0.002	0.017	0.026	0.028	0.030	0.041	0.051	0.078	0.086	0.088	0.091	0.103	0.105	0.108	0.113	0.118	0.141	0.144	0.146	0.165	0.169	0.202	0.246	0.283	0.292	0.304	0.310	0.328	0.339	0.351
	33	0.002	0.013	0.030	0.032	0.034	0.047	0.054	0.056	0.064	0.066	0.066	0.067	0.104	0.108	0.111	0.139	0.155	0.178	0.180	0.182	0.183	0.185	0.206	0.210	0.260	0.269	0.272	0.277	0.299	0.319
	34	0.001	0.004	0.008	0.009	0.010	0.013	0.016	0.018	0.021	0.024	0.026	0.029	0.034	0.039	0.047	0.060	0.066	0.083	0.103	0.113	0.130	0.149	0.163	0.179	0.197	0.218	0.230	0.243	0.261	0.283
	35	0.001	0.002	0.003	0.003	0.004	0.007	0.009	0.011	0.014	0.017	0.019	0.023	0.026	0.030	0.034	0.043	0.050	0.056	0.062	0.069	0.077	0.088	0.104	0.119	0.138	0.158	0.170	0.186	0.203	0.220
	36	0.001	0.004	0.007	0.009	0.011	0.016	0.023	0.027	0.041	0.047	0.057	0.062	0.066	0.099	0.105	0.125	0.135	0.144	0.151	0.159	0.170	0.179	0.188	0.200	0.214	0.226	0.232	0.239	0.252	0.263
	37	0.001	0.002	0.003	0.004	0.005	0.007	0.010	0.012	0.013	0.015	0.017	0.019	0.022	0.025	0.028	0.038	0.044	0.050	0.056	0.064	0.073	0.084	0.096	0.113	0.132	0.159	0.177	0.195	0.216	0.240
	38	0.001	0.003	0.008	0.011	0.012	0.017	0.022	0.025	0.028	0.032	0.035	0.042	0.047	0.064	0.070	0.088	0.094	0.102	0.112	0.121	0.129	0.137	0.144	0.156	0.169	0.191	0.205	0.225	0.248	0.274
4 OVA/ Fluticasone propionate 2 mg/kg *i.n.*	39	0.001	0.002	0.004	0.005	0.007	0.012	0.018	0.022	0.027	0.032	0.038	0.053	0.060	0.065	0.071	0.086	0.093	0.101	0.109	0.117	0.129	0.142	0.156	0.173	0.195	0.216	0.229	0.249	0.267	0.285
	40	0.001	0.002	0.004	0.005	0.006	0.012	0.024	0.028	0.036	0.043	0.048	0.053	0.059	0.063	0.070	0.084	0.090	0.094	0.100	0.108	0.117	0.127	0.139	0.148	0.161	0.179	0.191	0.201	0.219	0.235
	41	0.001	0.002	0.003	0.004	0.005	0.007	0.011	0.014	0.018	0.021	0.025	0.030	0.039	0.053	0.061	0.079	0.087	0.096	0.104	0.113	0.127	0.138	0.152	0.167	0.185	0.217	0.235	0.260	0.282	0.312
	42	0.001	0.002	0.004	0.007	0.008	0.014	0.015	0.042	0.045	0.048	0.077	0.095	0.099	0.101	0.128	0.173	0.177	0.181	0.184	0.210	0.259	0.269	0.277	0.313	0.321	0.348	0.352	0.356	0.360	0.364
	43	0.001	0.004	0.007	0.009	0.013	0.025	0.034	0.037	0.041	0.046	0.052	0.057	0.071	0.080	0.086	0.106	0.118	0.125	0.131	0.152	0.165	0.177	0.186	0.203	0.244	0.271	0.298	0.318	0.343	0.382
	44	0.000	0.001	0.001	0.001	0.002	0.002	0.003	0.004	0.004	0.005	0.005	0.006	0.007	0.009	0.011	0.018	0.023	0.030	0.036	0.045	0.054	0.063	0.076	0.097	0.124	0.157	0.177	0.200	0.226	0.261
	45	0.001	0.003	0.005	0.006	0.007	0.009	0.013	0.015	0.017	0.020	0.022	0.026	0.031	0.035	0.041	0.054	0.062	0.070	0.084	0.097	0.107	0.119	0.141	0.163	0.184	0.213	0.228	0.248	0.271	0.297
	46	0.001	0.002	0.003	0.004	0.005	0.007	0.009	0.012	0.015	0.019	0.028	0.035	0.042	0.053	0.061	0.082	0.093	0.106	0.114	0.124	0.133	0.154	0.170	0.188	0.210	0.238	0.253	0.267	0.284	0.303
	47	0.001	0.005	0.011	0.014	0.017	0.024	0.035	0.043	0.046	0.049	0.053	0.058	0.063	0.067	0.083	0.103	0.111	0.129	0.136	0.162	0.186	0.209	0.233	0.249	0.267	0.287	0.301	0.313	0.326	0.344
	48	0.001	0.001	0.002	0.003	0.003	0.006	0.009	0.012	0.015	0.020	0.026	0.035	0.064	0.069	0.073	0.088	0.102	0.117	0.126	0.136	0.149	0.165	0.179	0.202	0.222	0.239	0.249	0.261	0.271	0.285

Group	Animal no	2.5	3	3.5	4	4.5	5	5.5	6	6.5	7	7.5	8	8.5	9	9.5	10	11	12	13	14	15	16	17	18	19	20	22	24	26	28	30
1 PBS/Saline Ctrls	1	0.407	0.425	0.450	0.491	0.512	0.551	0.589	0.624	0.660	0.691	0.731	0.759	0.776	0.798	0.815	0.833	0.857	0.876	0.891	0.906	0.919	0.931	0.942	0.952	0.962	0.970	0.985	0.998	1.003		
	2	0.406	0.415	0.425	0.437	0.457	0.481	0.504	0.528	0.555	0.581	0.604	0.633	0.656	0.678	0.696	0.712	0.736	0.755	0.772	0.786	0.799	0.811	0.820	0.829	0.838	0.845	0.858	0.870	0.875		
	3	0.389	0.405	0.433	0.466	0.508	0.543	0.582	0.623	0.651	0.683	0.707	0.730	0.749	0.764	0.777	0.787	0.807	0.822	0.835	0.848	0.860	0.870	0.881	0.891	0.900	0.908	0.923	0.934			
	4	0.306	0.334	0.358	0.378	0.401	0.424	0.441	0.458	0.479	0.505	0.527	0.546	0.566	0.584	0.600	0.612	0.632	0.647	0.660	0.672	0.681	0.690	0.698	0.706	0.714	0.720	0.732	0.742	0.749		
	5	0.311	0.344	0.377	0.410	0.445	0.484	0.528	0.556	0.589	0.625	0.651	0.677	0.701	0.720	0.736	0.747	0.768	0.786	0.801	0.813	0.826	0.838	0.848	0.859	0.869	0.878	0.894	0.905			
	6	0.307	0.327	0.357	0.388	0.428	0.457	0.487	0.524	0.558	0.587	0.618	0.644	0.672	0.695	0.713	0.730	0.755	0.773	0.790	0.804	0.818	0.829	0.841	0.852	0.861	0.870	0.887	0.899			
	7	0.311	0.344	0.372	0.404	0.438	0.472	0.511	0.542	0.572	0.602	0.630	0.658	0.682	0.699	0.714	0.728	0.750	0.766	0.782	0.795	0.807	0.818	0.828	0.838	0.848	0.856	0.871	0.880			
	8	0.344	0.380	0.419	0.471	0.511	0.540	0.584	0.623	0.661	0.697	0.730	0.757	0.781	0.804	0.826	0.841	0.869	0.888	0.902	0.917	0.930	0.942	0.955	0.966	0.976	0.985	1.001	1.013			
2 OVA/OVA Ctrls *p.o.*	9	0.418	0.445	0.470	0.493	0.519	0.555	0.587	0.617	0.640	0.662	0.680	0.696	0.710	0.722	0.732	0.742	0.758	0.772	0.785	0.797	0.808	0.818	0.828	0.837	0.846	0.854	0.867	0.871			
	10	0.336	0.349	0.363	0.378	0.394	0.414	0.432	0.452	0.471	0.490	0.509	0.523	0.536	0.549	0.559	0.569	0.583	0.596	0.608	0.617	0.626	0.635	0.642	0.650	0.656	0.662	0.673	0.682			
	11	0.371	0.403	0.437	0.469	0.498	0.531	0.561	0.587	0.615	0.638	0.655	0.670	0.684	0.696	0.707	0.717	0.733	0.748	0.761	0.773	0.783	0.793	0.802	0.811	0.818	0.826	0.839	0.845			
	12	0.289	0.307	0.325	0.352	0.377	0.397	0.420	0.441	0.466	0.485	0.504	0.520	0.535	0.547	0.554	0.562	0.580	0.595	0.606	0.618	0.627	0.636	0.645	0.652	0.659	0.666	0.678	0.687	0.693		
	13	0.430	0.456	0.494	0.540	0.573	0.610	0.649	0.685	0.720	0.754	0.782	0.800	0.821	0.840	0.854	0.868	0.889	0.909	0.925	0.941	0.955	0.968	0.980	0.991	1.002	1.011	1.028	1.041			
	14	0.445	0.460	0.477	0.496	0.523	0.561	0.597	0.635	0.670	0.701	0.725	0.750	0.774	0.794	0.805	0.816	0.838	0.857	0.875	0.889	0.902	0.914	0.924	0.935	0.943	0.952	0.969	0.980			
	15	0.314	0.327	0.345	0.369	0.390	0.420	0.459	0.488	0.509	0.535	0.556	0.573	0.587	0.599	0.609	0.618	0.635	0.649	0.662	0.672	0.682	0.691	0.699	0.707	0.715	0.722	0.734	0.744			
	16	0.254	0.280	0.313	0.346	0.382	0.424	0.450	0.469	0.492	0.520	0.536	0.550	0.561	0.572	0.581	0.588	0.602	0.614	0.625	0.634	0.644	0.653	0.660	0.668	0.675	0.681	0.693	0.696			
	17	0.286	0.300	0.319	0.340	0.364	0.397	0.431	0.468	0.501	0.524	0.556	0.588	0.610	0.630	0.649	0.664	0.689	0.707	0.724	0.738	0.751	0.762	0.773	0.782	0.791	0.798	0.811	0.821			
	18	0.357	0.373	0.383	0.396	0.411	0.430	0.461	0.496	0.528	0.560	0.588	0.614	0.638	0.660	0.677	0.692	0.716	0.734	0.749	0.762	0.773	0.784	0.794	0.802	0.811	0.819	0.833	0.844			
3 OVA/ Dexamethasone 3 mg/kg *p.o.*	19	0.364	0.396	0.423	0.456	0.496	0.529	0.564	0.595	0.625	0.657	0.684	0.705	0.723	0.741	0.756	0.767	0.787	0.804	0.819	0.832	0.844	0.855	0.865	0.873	0.882	0.890	0.904	0.914			
	20	0.322	0.344	0.359	0.379	0.405	0.427	0.448	0.479	0.518	0.541	0.561	0.579	0.605	0.628	0.642	0.655	0.677	0.694	0.708	0.721	0.732	0.742	0.752	0.760	0.768	0.776	0.789	0.798			
	21	0.304	0.335	0.370	0.390	0.425	0.461	0.496	0.531	0.568	0.594	0.616	0.641	0.663	0.680	0.695	0.706	0.724	0.740	0.754	0.767	0.778	0.789	0.800	0.809	0.818	0.826	0.841	0.850			
	22	0.378	0.395	0.414	0.443	0.479	0.510	0.538	0.567	0.597	0.627	0.649	0.666	0.686	0.702	0.717	0.730	0.749	0.766	0.779	0.792	0.803	0.813	0.823	0.832	0.841	0.849	0.863	0.873			
	23	0.341	0.353	0.370	0.389	0.413	0.439	0.464	0.495	0.520	0.553	0.577	0.602	0.626	0.648	0.664	0.679	0.705	0.725	0.741	0.755	0.767	0.779	0.789	0.798	0.807	0.816	0.830	0.842	0.846		
	24	0.279	0.311	0.347	0.374	0.408	0.439	0.468	0.499	0.528	0.556	0.581	0.604	0.623	0.638	0.651	0.662	0.681	0.696	0.709	0.720	0.730	0.739	0.748	0.756	0.764	0.771	0.783	0.793			
	25	0.328	0.352	0.380	0.408	0.446	0.481	0.513	0.551	0.575	0.608	0.639	0.658	0.680	0.696	0.712	0.724	0.744	0.759	0.773	0.786	0.797	0.808	0.818	0.827	0.836	0.844	0.857	0.867	0.871		
	26	0.420	0.447	0.475	0.505	0.541	0.586	0.631	0.669	0.705	0.742	0.775	0.802	0.821	0.839	0.858	0.872	0.895	0.914	0.930	0.945	0.957	0.970	0.982	0.992	1.002	1.011	1.026	1.038	1.044		
	27	0.315	0.333	0.357	0.381	0.413	0.451	0.485	0.530	0.560	0.593	0.626	0.652	0.678	0.697	0.714	0.727	0.748	0.766	0.780	0.793	0.805	0.816	0.826	0.836	0.845	0.853	0.867	0.877			
	28	0.306	0.324	0.352	0.378	0.411	0.436	0.467	0.503	0.538	0.564	0.591	0.620	0.645	0.670	0.689	0.703	0.727	0.748	0.765	0.779	0.791	0.803	0.813	0.823	0.832	0.840	0.853	0.864	0.871		
4 OVA/OVA Ctrls *i.n.*	29	0.212	0.228	0.246	0.266	0.289	0.314	0.335	0.361	0.380	0.401	0.417	0.432	0.448	0.462	0.476	0.487	0.506	0.521	0.534	0.545	0.554	0.563	0.571	0.579	0.586	0.592	0.604	0.613	0.617		
	30	0.321	0.352	0.385	0.409	0.439	0.470	0.499	0.523	0.544	0.563	0.579	0.594	0.606	0.615	0.624	0.633	0.647	0.660	0.671	0.681	0.691	0.699	0.707	0.715	0.722	0.729	0.740	0.745			
	31	0.234	0.251	0.268	0.288	0.304	0.322	0.335	0.351	0.367	0.381	0.395	0.406	0.417	0.426	0.434	0.441	0.452	0.462	0.470	0.477	0.484	0.490	0.496	0.501	0.506	0.511	0.519	0.526			
	32	0.379	0.401	0.420	0.439	0.470	0.504	0.527	0.555	0.582	0.606	0.625	0.640	0.655	0.668	0.679	0.690	0.707	0.723	0.735	0.746	0.757	0.767	0.777	0.786	0.795	0.803	0.818	0.830	0.834		
	33	0.334	0.348	0.366	0.399	0.424	0.445	0.474	0.504	0.532	0.556	0.582	0.607	0.627	0.645	0.662	0.675	0.697	0.717	0.732	0.745	0.757	0.769	0.779	0.788	0.797	0.806	0.822	0.835	0.844		
	34	0.302	0.334	0.366	0.413	0.458	0.500	0.536	0.576	0.610	0.647	0.677	0.705	0.728	0.749	0.765	0.779	0.801	0.820	0.838	0.853	0.867	0.879	0.891	0.901	0.910	0.919	0.936	0.948			
	35	0.240	0.261	0.286	0.314	0.335	0.358	0.382	0.403	0.421	0.441	0.457	0.470	0.482	0.492	0.501	0.509	0.522	0.533	0.544	0.553	0.561	0.569	0.576	0.583	0.589	0.596	0.605	0.613			
	36	0.278	0.291	0.303	0.319	0.338	0.358	0.389	0.423	0.446	0.470	0.494	0.519	0.536	0.554	0.568	0.580	0.599	0.615	0.627	0.638	0.648	0.657	0.665	0.673	0.680	0.687	0.700	0.710			
	37	0.264	0.293	0.322	0.351	0.380	0.405	0.433	0.457	0.477	0.497	0.514	0.530	0.543	0.555	0.565	0.573	0.587	0.600	0.611	0.621	0.630	0.638	0.646	0.653	0.660	0.667	0.678	0.684			
	38	0.304	0.336	0.359	0.390	0.423	0.454	0.477	0.503	0.528	0.555	0.577	0.597	0.613	0.626	0.637	0.645	0.662	0.675	0.688	0.699	0.708	0.718	0.726	0.734	0.742	0.749	0.762	0.769			
4 OVA/ Fluticasone propionate 2 mg/kg *i.n.*	39	0.303	0.330	0.357	0.387	0.418	0.445	0.472	0.501	0.528	0.554	0.577	0.599	0.616	0.632	0.644	0.655	0.672	0.687	0.700	0.711	0.722	0.732	0.742	0.750	0.758	0.766	0.778	0.782			
	40	0.256	0.277	0.304	0.326	0.352	0.371	0.392	0.419	0.443	0.463	0.483	0.502	0.523	0.537	0.551	0.563	0.582	0.597	0.609	0.620	0.630	0.639	0.647	0.655	0.662	0.668	0.679	0.688			
	41	0.344	0.372	0.402	0.435	0.473	0.506	0.534	0.561	0.591	0.619	0.644	0.664	0.680	0.695	0.708	0.718	0.737	0.752	0.765	0.776	0.787	0.797	0.806	0.814	0.822	0.830	0.844	0.851			
	42	0.368	0.372	0.377	0.381	0.386	0.392	0.397	0.402	0.406	0.410	0.415	0.419	0.424	0.429	0.434	0.438	0.446	0.455	0.464	0.471	0.478	0.484	0.490	0.495	0.500	0.505	0.514	0.520	0.523		
	43	0.405	0.429	0.450	0.473	0.506	0.540	0.572	0.599	0.624	0.653	0.679	0.700	0.717	0.732	0.745	0.755	0.774	0.790	0.804	0.817	0.829	0.840	0.850	0.860	0.869	0.877	0.892	0.896			
	44	0.304	0.337	0.383	0.431	0.488	0.536	0.592	0.643	0.679	0.719	0.754	0.782	0.809	0.832	0.851	0.869	0.894	0.918	0.939	0.957	0.975	0.990	1.004	1.018	1.030	1.042	1.062	1.077	1.087		
	45	0.320	0.352	0.386	0.427	0.458	0.492	0.529	0.562	0.594	0.626	0.654	0.681	0.702	0.718	0.732	0.746	0.767	0.784	0.799	0.813	0.825	0.836	0.845	0.854	0.862	0.870	0.883	0.891			
	46	0.328	0.354	0.382	0.415	0.441	0.480	0.512	0.545	0.574	0.603	0.630	0.654	0.675	0.693	0.706	0.719	0.743	0.760	0.775	0.788	0.800	0.811	0.823	0.832	0.842	0.850	0.864	0.874			
	47	0.362	0.381	0.407	0.440	0.472	0.517	0.547	0.582	0.616	0.651	0.676	0.695	0.715	0.732	0.747	0.759	0.779	0.795	0.808	0.821	0.832	0.843	0.853	0.862	0.870	0.878	0.892	0.901			
	48	0.301	0.322	0.344	0.372	0.405	0.439	0.474	0.512	0.538	0.581	0.613	0.633	0.658	0.680	0.697	0.710	0.733	0.750	0.764	0.778	0.791	0.802	0.812	0.821	0.830	0.837	0.850	0.861	0.869		

Appendix 8 F-V curve values in the OVA-induced asthma model

Group	Animal no	0.02	0.04	0.06	0.08	0.1	0.12	0.14	0.16	0.18	0.2	0.22	0.24	0.26	0.28	0.3	0.32	0.34	0.36	0.38	0.4	0.42	0.44	0.46	0.48	0.5
1 PBS/Saline Ctrls	1	9.435	15.116	19.319	22.592	25.329	27.640	29.581	31.152	32.470	33.513	34.299	34.893	35.259	35.492	35.487	35.316	34.982	34.465	33.810	32.976	32.024	30.932	29.726	28.484	27.165
	2	9.351	14.737	18.662	21.712	24.011	25.717	26.967	27.740	28.151	28.330	28.251	27.989	27.607	27.102	26.521	25.869	25.202	24.418	23.450	22.377	21.087	19.632	18.078	16.401	14.723
	3	9.324	14.753	18.779	21.915	24.274	25.918	26.921	27.402	27.443	27.140	26.472	25.705	24.795	23.744	22.661	21.648	20.625	19.534	18.605	17.670	16.712	15.885	15.101	14.280	13.617
	4	9.146	14.272	18.043	21.005	23.411	25.343	26.956	28.176	28.896	28.869	28.348	27.346	25.821	23.867	21.585	19.089	16.431	13.889	11.707	10.105	9.002	8.206	7.645	7.137	6.673
	5	8.916	13.129	15.496	16.791	17.383	17.504	17.342	17.065	16.703	16.323	15.945	15.626	15.271	14.896	14.570	14.154	13.780	13.414	13.095	12.832	12.654	12.364	12.152	11.880	11.640
	6	8.816	13.816	17.308	19.985	22.026	23.493	24.453	25.023	25.284	25.276	25.009	24.605	24.066	23.427	22.731	22.000	21.240	20.519	19.755	19.013	18.302	17.572	16.895	16.261	15.634
	7	9.285	14.177	16.984	18.767	19.698	20.252	20.473	20.401	20.074	19.669	19.268	18.838	18.477	18.018	17.428	16.913	16.389	15.856	15.330	14.812	14.312	13.876	13.434	13.030	12.647
	8	8.803	13.589	16.840	19.273	21.090	22.408	23.354	24.017	24.464	24.673	24.703	24.608	24.425	24.152	23.794	23.394	22.973	22.523	22.019	21.501	20.971	20.391	19.758	19.112	18.457
2 OVA/OVA Ctrls *p.o.*	9	6.768	9.070	9.791	9.666	9.111	8.472	7.753	7.006	6.269	5.627	5.134	4.738	4.431	4.106	3.858	3.599	3.361	3.171	2.954	2.823	2.658	2.503	2.353	2.245	2.133
	10	9.118	13.700	16.407	18.068	18.971	19.329	19.253	18.856	18.164	17.209	16.025	14.654	13.161	11.662	10.228	8.916	7.726	6.672	5.732	4.963	4.350	3.866	3.438	2.996	2.598
	11	9.402	14.932	18.903	21.817	23.858	25.165	26.006	26.468	26.569	26.402	26.032	25.517	24.899	24.188	23.460	22.713	21.987	21.277	20.556	19.871	19.180	18.513	17.827	17.092	16.141
	12	9.225	14.047	16.872	18.597	19.548	20.015	20.026	19.814	19.380	18.851	18.219	17.476	16.771	15.971	15.072	13.965	12.649	10.991	9.329	7.724	6.221	5.076	4.240	3.595	3.083
	13	8.810	13.414	16.551	18.756	20.351	21.515	22.340	22.859	23.235	23.429	23.490	23.442	23.276	23.079	22.844	22.572	22.274	21.941	21.570	21.180	20.716	20.225	19.670	19.057	18.444
	14	9.141	14.490	18.381	21.476	24.006	26.016	27.401	28.251	28.694	28.655	28.281	27.609	26.645	25.543	24.299	22.951	21.569	20.199	18.796	17.495	16.247	15.077	13.916	12.926	12.022
	15	8.210	12.509	15.406	17.490	18.957	19.966	20.519	20.658	20.462	19.954	19.173	18.198	17.083	15.963	14.715	13.498	12.314	11.203	10.092	9.133	8.273	7.516	6.783	6.231	5.733
	16	7.450	11.095	13.477	15.099	16.209	16.917	17.322	17.427	17.376	17.141	16.869	16.577	16.269	15.936	15.592	15.211	14.746	14.208	13.317	12.095	10.624	9.027	7.578	6.085	4.753
	17	9.224	14.617	18.603	21.792	24.417	26.654	28.499	29.997	31.174	31.902	32.335	32.420	32.203	31.744	31.019	30.084	29.016	27.776	26.377	24.858	23.255	21.624	19.966	18.247	16.632
	18	9.028	14.326	18.180	21.190	23.619	25.474	26.781	27.546	27.798	27.696	27.262	26.555	25.665	24.605	23.384	22.160	20.877	19.648	18.444	17.223	16.082	15.040	14.032	13.162	12.345
3 OVA/ Dexamethasone 3 mg/kg *p.o.*	19	8.554	13.473	17.042	19.610	21.361	22.533	23.286	23.698	23.828	23.730	23.495	23.133	22.717	22.263	21.755	21.224	20.729	20.216	19.677	19.155	18.630	18.119	17.595	17.169	16.619
	20	9.039	14.110	17.677	20.144	21.677	22.466	22.688	22.421	21.772	20.865	19.731	18.523	17.208	15.916	14.641	13.364	12.166	10.985	9.925	9.009	8.206	7.529	6.804	6.150	5.594
	21	9.090	14.181	17.902	20.701	22.735	24.160	25.119	25.654	25.793	25.694	25.402	24.948	24.388	23.671	22.934	22.175	21.397	20.600	19.811	19.017	18.232	17.455	16.665	15.918	15.247
	22	9.208	14.663	18.643	21.818	24.377	26.519	28.220	29.583	30.566	31.207	31.583	31.668	31.534	31.141	30.516	29.704	28.660	27.452	26.023	24.414	22.706	20.918	19.090	17.289	15.567
	23	8.801	13.392	16.312	18.283	19.570	20.321	20.733	20.857	20.760	20.517	20.147	19.738	19.247	18.735	18.212	17.681	17.070	16.459	15.810	15.121	14.417	13.781	13.133	12.517	11.880
	24	9.045	14.506	18.451	21.571	24.173	26.317	28.157	29.665	30.720	31.291	31.440	31.035	30.297	29.219	27.812	26.190	24.377	22.457	20.529	18.668	16.937	15.332	13.884	12.572	11.376
	25	8.841	14.076	17.697	20.583	22.942	24.711	26.043	27.041	27.722	27.930	27.962	27.812	27.447	26.927	26.321	25.632	24.859	24.051	23.251	22.420	21.572	20.736	19.923	19.090	18.244
	26	9.041	14.236	17.899	20.697	22.770	24.260	25.177	25.612	25.586	25.102	24.198	22.990	21.472	19.726	17.808	15.770	13.708	11.686	9.808	8.195	6.805	5.730	4.931	4.370	4.016
	27	8.542	13.163	16.512	19.026	20.965	22.494	23.730	24.716	25.485	26.144	26.551	26.819	27.021	27.150	27.186	27.179	27.136	27.053	26.903	26.745	26.450	25.875	24.935	23.697	22.234
	28	9.259	14.681	18.700	21.891	24.511	26.510	27.933	28.999	29.718	30.056	30.197	30.114	29.748	29.294	28.754	28.105	27.375	26.591	25.770	24.909	24.033	23.065	22.019	20.941	19.725
4 OVA/OVA Ctrls *i.n.*	29	8.529	13.213	16.306	18.323	19.383	19.713	19.531	18.941	18.032	16.935	15.754	14.576	13.320	12.171	11.126	10.157	9.298	8.559	7.809	7.189	6.576	5.953	5.284	4.640	3.867
	30	9.016	14.260	18.080	21.075	23.488	25.353	26.582	27.302	27.543	27.410	26.952	26.231	25.268	24.180	22.985	21.714	20.378	19.018	17.617	16.247	14.843	13.418	12.097	10.851	9.702
	31	8.926	13.935	17.356	19.512	20.618	20.922	20.595	19.794	18.641	17.214	15.723	14.176	12.671	11.274	9.738	8.293	6.978	5.823	4.797	3.996	3.206	2.416	1.552	0.723	0.472
	32	9.095	14.342	18.175	20.820	22.362	23.082	23.081	22.424	21.293	19.893	18.319	16.626	15.003	13.436	12.102	10.895	9.851	8.961	8.264	7.748	7.289	6.832	6.435	6.104	5.806
	33	6.575	9.056	10.282	10.822	10.997	10.939	10.772	10.525	10.236	9.908	9.572	9.189	8.814	8.482	8.109	7.799	7.461	7.134	6.831	6.566	6.331	6.090	5.879	5.765	5.571
	34	9.241	14.724	18.586	21.323	23.236	24.465	25.214	25.599	25.689	25.496	25.164	24.716	24.175	23.587	22.954	22.279	21.561	20.806	19.973	19.071	18.110	16.988	15.813	14.625	13.470
	35	8.706	12.950	15.592	17.113	17.958	18.363	18.416	18.264	17.939	17.418	16.736	15.950	14.905	13.712	12.327	10.837	9.398	8.066	6.939	5.999	5.304	4.710	4.183	3.638	3.120
	36	8.977	13.754	16.789	18.501	19.150	19.030	18.339	17.236	15.870	14.363	12.869	11.492	10.206	9.040	7.942	6.942	6.074	5.362	4.733	4.269	3.854	3.562	3.226	2.870	2.668
	37	8.490	12.793	15.345	16.810	17.528	17.598	17.227	16.529	15.575	14.541	13.453	12.272	11.117	9.953	8.676	7.452	6.296	5.367	4.618	3.981	3.480	3.182	2.874	2.590	2.465
	38	9.058	14.138	17.634	19.959	21.560	22.630	23.280	23.597	23.630	23.502	23.195	22.781	22.286	21.702	21.040	20.316	19.438	18.288	16.932	15.283	13.503	11.656	9.894	8.440	7.168
4 OVA/ Fluticasone propionate 2 mg/kg *i.n.*	39	9.069	14.406	18.075	20.611	22.259	23.216	23.534	23.421	22.999	22.309	21.462	20.479	19.393	18.323	17.254	16.196	15.208	14.241	13.300	12.407	11.557	10.835	10.211	9.721	9.188
	40	8.801	13.699	17.184	19.901	22.080	23.809	25.256	26.387	27.292	27.961	28.237	28.318	28.232	27.975	27.406	26.715	25.904	24.942	23.866	22.701	21.445	20.118	18.749	17.304	15.874
	41	8.281	12.910	16.299	18.956	21.078	22.820	24.249	25.382	26.079	26.453	26.508	26.245	25.599	24.707	23.646	22.412	20.980	19.585	18.177	16.788	15.459	14.251	13.165	12.160	11.245
	42	8.387	12.799	15.639	17.598	18.932	19.903	20.453	20.710	20.863	20.800	20.514	20.176	19.711	19.139	18.383	17.558	16.635	15.631	14.596	13.529	12.409	11.236	10.083	8.946	7.915
	43	7.673	11.645	14.341	16.309	17.773	18.903	19.730	20.334	20.786	21.088	21.266	21.387	21.445	21.482	21.505	21.504	21.487	21.433	21.351	21.210	21.009	20.755	20.397	19.956	19.425
	44	8.911	14.156	17.894	20.843	23.108	24.706	25.695	26.178	26.215	25.737	24.986	23.912	22.526	20.967	19.382	17.781	16.144	14.596	13.160	11.851	10.682	9.693	8.866	8.212	7.642
	45	9.245	14.671	18.697	21.918	24.555	26.827	28.693	30.297	31.663	32.559	33.109	33.319	33.181	32.792	32.088	31.180	30.089	28.846	27.462	25.973	24.450	22.936	21.418	19.894	18.434
	46	8.783	13.799	17.375	20.168	22.219	23.544	24.228	24.451	24.277	23.713	22.928	22.030	20.985	19.809	18.557	17.408	16.284	15.176	14.094	13.033	12.087	11.278	10.488	9.726	9.086
	47	8.946	14.267	17.829	20.129	21.613	22.441	22.755	22.709	22.397	21.879	21.239	20.533	19.780	19.009	18.271	17.516	16.785	16.060	15.309	14.629	13.917	13.344	12.752	12.215	11.747
	48	9.044	14.305	18.069	21.083	23.529	25.477	26.916	27.982	28.724	29.062	29.133	29.004	28.644	28.130	27.541	26.884	26.077	25.265	24.478	23.711	22.925	22.131	21.449	20.753	20.140

Group	Animal no	0.52	0.54	0.56	0.58	0.6	0.62	0.64	0.66	0.68	0.7	0.72	0.74	0.76	0.78	0.8	0.82	0.84	0.86	0.88	0.9	0.92	0.94	0.96	0.98	1
1 PBS/Saline Ctrls	1	25.800	24.437	23.088	21.848	20.559	19.377	18.232	17.137	16.038	14.935	13.860	12.837	11.834	10.941	10.072	9.279	8.485	7.704	6.890	6.031	5.139	4.335	3.725	3.258	2.802
	2	13.186	11.740	10.562	9.572	8.805	8.182	7.668	7.227	6.755	6.363	5.913	5.432	4.939	4.417	3.876	3.067	2.021	1.098	0.496						
	3	12.941	12.278	11.729	11.080	10.486	9.779	9.096	8.433	7.986	7.565	7.214	6.926	6.693	6.464	6.208	5.861	5.124	4.458	3.873	2.614	1.749	1.225	0.616	0.360	
	4	6.233	5.774	5.298	4.877	4.389	3.373	2.029	1.458	1.055	0.781	0.440														
	5	11.421	11.208	11.006	10.832	10.624	10.384	10.172	9.884	9.640	9.353	9.037	8.659	8.240	7.664	6.867	5.850	4.619	3.324	2.264	1.614	1.057	0.817	0.557		
	6	15.044	14.508	13.962	13.452	12.943	12.452	12.021	11.440	11.000	10.410	9.860	9.314	8.665	7.861	7.005	5.985	5.032	4.119	3.186	2.032	1.130	0.421			
	7	12.221	11.839	11.417	11.033	10.631	10.206	9.609	8.620	6.776	4.452	2.417	1.420	0.704												
	8	17.749	17.056	16.360	15.657	14.982	14.332	13.630	12.977	12.268	11.599	10.959	10.278	9.668	9.089	8.559	8.025	7.456	6.967	6.468	5.980	5.418	4.644	3.450	2.326	1.564
2 OVA/OVA Ctrls *p.o.*	9	2.043	1.930	1.861	1.778	1.729	1.691	1.682	1.664	1.653	1.688	1.631	1.587	1.566	1.545	1.497	1.438	1.411	0.820							
	10	2.211	1.743	1.299	0.950	0.719	0.458	0.393	0.373																	
	11	14.768	12.773	10.468	8.387	6.977	5.832	4.652	3.606	2.707	1.955	1.489	0.918	0.437	0.346											
	12	2.645	2.164	1.368	0.644	0.167																				
	13	17.862	17.153	16.447	15.703	14.869	13.893	12.798	11.411	9.925	8.409	7.149	6.101	5.271	4.585	3.985	3.499	2.986	2.471	2.037	1.522	1.048	0.862	0.756	0.634	0.481
	14	11.248	10.515	9.836	9.237	8.645	8.093	7.600	7.102	6.604	6.085	5.606	5.133	4.678	4.266	3.816	3.448	3.168	2.822	2.491	2.020	1.305	0.614	0.268		
	15	5.368	5.052	4.779	4.528	4.283	4.015	3.190	1.967	1.338	0.780	0.309	0.215													
	16	3.999	3.473	3.030	2.421	1.773	1.345	0.835	0.560	0.243																
	17	15.024	13.533	12.203	10.986	9.930	9.000	8.206	7.456	6.751	5.999	5.141	4.161	3.300	2.649	2.045	1.368	0.645	0.390							
	18	11.616	10.993	10.405	9.819	9.291	8.763	8.191	7.657	7.027	6.203	5.204	4.249	3.321	2.307	1.583	0.978	0.541	0.469							
3 OVA/ Dexamethasone 3 mg/kg *p.o.*	19	16.150	15.693	15.231	14.746	14.265	13.700	13.113	12.368	11.501	10.514	9.435	8.308	7.159	6.002	4.867	3.819	2.987	2.165	1.465	0.896	0.524	0.206			
	20	5.091	4.628	4.130	3.711	3.320	2.967	2.598	2.384	2.131	1.886	1.576	0.850	0.773												
	21	14.607	14.058	13.510	12.906	12.330	11.742	11.005	10.141	8.967	7.559	6.159	4.960	4.150	3.515	2.943	2.464	1.851	1.133	0.644	0.364	0.170				
	22	13.922	12.497	11.254	10.174	9.314	8.487	7.849	7.310	6.886	6.467	6.046	5.624	5.167	4.669	4.042	3.266	2.270	1.490	0.966	0.379	0.118				
	23	11.338	10.790	10.204	9.739	9.235	8.734	8.317	7.672	6.699	5.486	4.023	2.485	1.357	0.721	0.347	0.186									
	24	10.303	9.340	8.545	7.871	7.312	6.808	6.225	5.350	4.267	3.252	2.603	2.121	1.554	0.907	0.439	0.146									
	25	17.431	16.578	15.595	14.589	13.229	11.677	10.016	8.335	6.818	5.568	4.558	3.749	3.020	2.354	1.741	1.261	0.822	0.578	0.429						
	26	3.748	3.556	3.431	3.319	3.223	3.137	3.059	2.980	2.924	2.889	2.855	2.805	2.756	2.731	2.688	2.671	2.629	2.573	2.517	2.470	2.405	2.275	2.068	1.721	1.293
	27	20.545	18.675	16.756	14.876	13.141	11.638	10.414	9.417	8.546	7.698	6.814	5.899	5.038	4.177	3.355	2.509	1.716	1.113	0.514	0.275					
	28	18.478	17.183	15.844	14.543	13.409	12.354	11.368	10.548	9.800	9.127	8.519	8.021	7.553	6.864	5.446	3.579	2.400	1.739	1.088	0.573					
4 OVA/OVA Ctrls *i.n.*	29	2.990	2.084	1.388	0.947	0.647	0.289																			
	30	8.630	7.636	6.660	5.870	5.162	4.440	3.544	2.443	1.438	0.841	0.580	0.472													
	31																									
	32	5.530	5.222	4.890	4.606	4.262	3.890	3.574	3.294	3.044	2.814	2.548	2.278	1.976	1.723	1.514	1.282	1.063	0.861	0.507						
	33	5.476	5.385	5.301	5.192	5.091	4.985	4.902	4.812	4.704	4.610	4.524	4.449	3.816	2.177	0.991	0.421	0.180								
	34	12.260	11.033	9.985	9.078	8.307	7.661	7.159	6.722	6.334	6.091	5.810	5.572	5.328	5.081	4.821	4.456	3.964	3.140	2.265	1.357	0.693	0.437	0.174		
	35	2.563	2.013	1.447	0.918	0.583																				
	36	2.500	2.365	2.203	2.123	2.006	1.931	1.686	1.340	1.133	0.843	0.577	0.544	0.343												
	37	2.245	0.465																							
	38	6.261	5.504	4.864	4.292	3.830	3.334	2.826	2.286	1.807	1.240	0.853	0.439													
4 OVA/ Fluticasone propionate 2 mg/kg *i.n.*	39	8.730	8.302	7.831	7.401	6.920	6.304	5.381	4.106	2.978	2.222	1.753	1.309	0.818	0.461	0.175										
	40	14.424	12.904	11.457	9.901	8.315	6.726	5.052	3.402	1.914	0.795	0.601														
	41	10.414	9.657	8.983	8.322	7.653	7.060	6.525	6.024	5.589	5.219	4.856	4.519	4.148	3.839	3.503	3.126	2.672	1.721	0.811	0.290					
	42	7.021	6.209	5.522	4.676	3.557	2.938	2.269	2.086	1.425	0.563	0.481														
	43	18.814	18.126	17.378	16.540	15.728	14.880	14.008	13.128	12.274	11.387	10.294	9.118	7.704	6.197	4.677	3.470	2.597	1.879	1.231	0.623	0.333				
	44	7.206	6.847	6.575	6.348	6.125	5.917	5.711	5.528	5.344	5.124	4.883	4.464	3.813	3.140	2.676	2.324	2.090	1.919	1.643	1.296	0.974	0.645	0.416	0.263	
	45	17.077	15.813	14.600	13.522	12.565	11.777	11.033	10.407	9.710	8.915	7.893	6.799	5.749	4.879	4.140	3.483	2.944	2.375	1.761	1.124	0.323				
	46	8.510	7.950	7.400	6.833	6.269	5.735	5.319	4.948	4.558	4.159	3.552	3.065	2.723	2.147	1.746	1.643	1.521	1.391	0.719						
	47	11.251	10.769	10.276	9.815	9.380	8.957	8.557	8.106	7.712	7.305	6.887	6.476	6.020	5.498	4.628	3.289	1.802	1.107	0.858	0.627	0.357	0.204			
	48	19.523	18.921	18.362	17.769	17.287	16.700	16.066	15.254	14.202	12.980	11.596	10.209	8.749	7.372	6.023	4.826	3.776	2.919	2.092	0.994	0.337				

Appendix 9 Airway hyperresponsiveness test parameters

Group	Animal no	Resistance Rl(cm H2O*sec/ml)					Compliance Cdyn(ml/cm H2O)				
		PBS	0.625 mg/mL	2.5 mg/mL	5 mg/mL	12.5 mg/mL	PBS	0.625 mg/mL	2.5 mg/mL	5 mg/mL	12.5 mg/mL
1 PBS/Saline Ctrls	1	1.483	1.594	1.884	2.473	2.690	0.032	0.030	0.026	0.022	0.019
	2	1.279	1.352	1.660	2.409	2.516	0.031	0.029	0.026	0.019	0.013
	3	3.055	2.791	4.006	4.116	5.805	0.020	0.017	0.014	0.012	0.010
	4	1.319	1.719	2.371	4.068	5.274	0.030	0.026	0.020	0.016	0.014
	5	1.626	1.576	2.355	2.697	3.568	0.029	0.028	0.020	0.021	0.014
	6	1.639	1.816	2.355	2.684	3.960	0.026	0.024	0.022	0.020	0.014
	7	1.497	1.582	1.872	2.302	3.058	0.034	0.032	0.030	0.024	0.021
	8	1.383	1.388	1.532	1.867	2.464	0.032	0.029	0.028	0.025	0.021
2 OVA/OVA Ctrls *p.o.*	9	2.138	2.313	3.016	5.447	8.483	0.021	0.019	0.015	0.009	0.009
	10	2.856	3.750	3.278	7.928	10.849	0.032	0.024	0.022	0.011	0.005
	11	1.845	3.102	3.578	5.781	12.448	0.023	0.020	0.015	0.006	0.004
	12	1.544	1.863	3.163	5.990	10.108	0.022	0.019	0.016	0.009	0.004
	13	1.689	2.320	3.314	3.632	12.949	0.030	0.028	0.016	0.017	0.006
	14	1.551	2.014	4.614	3.893	3.697	0.027	0.020	0.014	0.011	0.010
	15	1.565	1.689	2.037	4.678	12.808	0.023	0.020	0.015	0.009	0.004
	16	died due to anaesthesia									
	17	1.894	2.028	4.409	4.390	5.467	0.018	0.015	0.010	0.008	0.008
	18	2.012	3.109	3.836	6.313	8.139	0.019	0.016	0.012	0.010	0.007
3 OVA/ Dexamethasone 3 mg/kg *p.o.*	19	1.538	1.516	2.230	3.791	5.733	0.024	0.022	0.018	0.012	0.007
	20	1.525	1.532	2.017	3.840	5.132	0.028	0.026	0.022	0.012	0.008
	21	1.712	1.777	2.450	3.170	4.510	0.021	0.019	0.014	0.013	0.009
	22	1.706	1.773	1.914	2.913	6.517	0.025	0.024	0.023	0.015	0.008
	23	3.445	3.893	3.636	6.400	8.005	0.014	0.009	0.012	0.008	0.014
	24	1.587	1.659	1.920	3.224	3.976	0.021	0.019	0.017	0.013	0.015
	25	1.453	1.504	1.793	3.082	6.611	0.025	0.024	0.021	0.014	0.005
	26	1.339	1.350	2.767	7.353	8.806	0.037	0.030	0.027	0.011	0.008
	27	1.539	1.569	1.670	2.054	2.907	0.024	0.021	0.020	0.018	0.017
	28	1.431	1.474	1.814	2.517	4.472	0.027	0.025	0.023	0.017	0.016
4 OVA/OVA Ctrls *i.n.*	29	1.847	2.038	4.309	5.200	9.407	0.018	0.014	0.014	0.011	0.006
	30	2.250	2.549	2.483	2.542	2.716	0.034	0.034	0.034	0.033	0.029
	31	1.686	1.833	2.191	3.814	5.287	0.019	0.016	0.014	0.012	0.007
	32	1.237	1.410	2.014	4.784	5.180	0.031	0.027	0.019	0.012	0.009
	33	1.391	1.695	2.954	4.151	6.437	0.037	0.029	0.017	0.011	0.007
	34	1.661	1.660	1.958	2.580	3.668	0.023	0.020	0.019	0.018	0.011
	35	1.603	1.648	1.987	3.415	10.144	0.026	0.024	0.019	0.012	0.005
	36	3.423	5.584	7.659	9.498	10.149	0.013	0.008	0.006	0.008	0.004
	37	5.175	5.941	8.374	12.424	12.222	0.010	0.004	0.004	0.003	0.002
	38	4.050	5.929	6.104	8.899	12.165	0.024	0.013	0.014	0.005	0.009
4 OVA/ Fluticasone propionate 2 mg/kg *i.n.*	39	2.473	2.466	2.427	2.454	2.489	0.046	0.044	0.046	0.047	0.041
	40	1.489	1.517	1.689	2.437	2.881	0.023	0.022	0.020	0.017	0.008
	41	1.470	1.488	1.734	2.190	3.385	0.027	0.025	0.023	0.019	0.013
	42	1.364	1.382	1.623	2.131	3.288	0.033	0.030	0.027	0.021	0.014
	43	3.350	3.993	4.084	5.682	11.213	0.044	0.039	0.023	0.025	0.008
	44	1.498	1.862	1.844	2.049	4.205	0.033	0.019	0.021	0.019	0.012
	45	1.484	1.525	1.605	2.255	4.567	0.026	0.024	0.023	0.018	0.011
	46	1.390	1.457	1.911	2.925	6.788	0.027	0.025	0.022	0.017	0.008
	47	1.525	1.491	1.618	1.871	2.643	0.032	0.030	0.028	0.024	0.018
	48	1.472	1.455	1.682	2.338	3.862	0.026	0.024	0.022	0.019	0.012

Appendix 10 F-V curve and parameters data post-Mch challenge

Group	Animal no	FVC (mL)	FEV100 (mL)	PEF (mL/sec)	MMEF (mL/sec)	FEV100/ FVC	0.02	0.04	0.06	0.08	0.10	0.12	0.14	0.16	0.18	0.20	0.22	0.24	0.26	0.28	0.30	0.32	0.34	0.36	0.38	0.40	0.42
1 PBS/Saline Ctrls	5	0.782	0.687	7.620	11.392	0.879	6.765	9.373	10.626	11.216	11.387	11.289	11.098	10.855	10.552	10.241	9.908	9.612	9.286	8.987	8.730	8.523	8.277	8.057	7.833	7.647	7.477
	6	0.903	0.764	9.767	16.917	0.846	8.436	12.293	14.520	15.819	16.529	16.828	16.890	16.770	16.579	16.375	16.013	15.714	15.352	14.992	14.582	14.212	13.834	13.424	13.045	12.667	12.311
	7	0.847	0.680	6.541	13.740	0.802	7.504	10.706	12.374	13.195	13.616	13.639	13.504	13.144	12.729	12.199	11.682	11.169	10.515	10.042	9.535	9.088	8.681	8.267	7.896	7.458	7.026
	8	1.042	0.340	1.368	7.122	0.326	5.584	6.923	7.066	6.817	6.450	5.950	5.286	4.772	4.320	3.887	3.548	3.271	3.002	2.761	2.517	2.279	2.169	1.953	1.877	1.766	1.666
2 OVA/OVA Ctrls *p.o.*	9	0.873	0.540	3.900	12.637	0.619	6.762	9.745	11.395	12.222	12.545	12.480	12.176	11.609	10.916	10.067	9.165	8.271	7.405	6.659	6.057	5.538	5.078	4.786	4.557	4.339	4.080
	10	0.471	0.251	1.263	6.144	0.532	5.275	6.098	5.703	4.972	4.190	3.496	2.902	2.457	2.040	1.756	1.519	1.340	1.142	1.091	0.958	0.825	0.658	0.617	0.643	0.573	0.498
	11	0.724	0.631	7.524	13.946	0.871	7.340	10.634	12.429	13.330	13.797	13.896	13.820	13.540	13.185	12.763	12.284	11.806	11.221	10.651	10.134	9.597	9.043	8.524	8.027	7.485	7.078
	12	0.517	0.369	3.100	10.140	0.714	6.480	8.755	9.873	10.119	9.842	9.244	8.480	7.565	6.677	6.140	5.539	4.676	3.880	3.070	2.620	2.330	2.078	1.810	1.498	1.281	1.043
	13	0.729	0.481	2.962	12.999	0.660	6.642	9.551	11.153	12.095	12.660	12.892	12.694	12.059	11.171	10.096	9.022	8.022	7.104	6.305	5.564	4.920	4.326	3.690	3.160	2.767	2.393
	14	0.697	0.553	5.739	12.032	0.794	6.386	9.021	10.456	11.282	11.786	11.959	11.951	11.789	11.527	11.122	10.656	10.250	9.738	9.033	8.253	7.635	7.100	6.566	5.998	5.466	4.875
	15	0.702	0.527	4.856	10.751	0.751	6.857	9.370	10.402	10.697	10.588	10.351	10.117	9.767	9.332	8.787	8.239	7.703	7.215	6.723	6.251	5.847	5.522	5.187	4.814	4.493	4.217
3 OVA/ Dexamethasone 3 mg/kg *p.o.*	19	0.617	0.571	7.263	13.475	0.925	7.373	10.399	12.054	12.935	13.335	13.450	13.310	13.052	12.631	12.223	11.656	11.043	10.299	9.456	8.578	7.721	6.935	6.287	5.735	5.225	4.814
	20	0.886	0.745	7.242	18.304	0.841	8.541	12.981	15.708	17.259	18.047	18.287	18.193	17.755	17.167	16.499	15.748	14.944	14.093	13.236	12.326	11.459	10.652	9.927	9.285	8.651	7.999
	21	0.646	0.633	11.263	15.855	0.980	8.210	11.920	13.987	15.093	15.656	15.833	15.790	15.595	15.287	14.965	14.611	14.159	13.640	13.123	12.610	12.138	11.597	11.070	10.545	9.957	9.389
	22	0.922	0.880	12.362	23.026	0.954	8.796	13.577	16.793	19.081	20.741	21.882	22.590	22.968	22.957	22.724	22.300	21.711	21.031	20.284	19.512	18.639	17.733	16.860	16.002	15.204	14.449
	23	0.820	0.686	7.189	11.919	0.836	6.696	9.383	10.793	11.535	11.817	11.903	11.803	11.552	11.289	10.953	10.608	10.199	9.747	9.397	9.138	8.772	8.420	8.124	7.900	7.663	7.455
	24	0.714	0.666	9.372	17.155	0.932	7.921	12.032	14.471	15.961	16.782	17.114	17.105	16.860	16.458	15.920	15.374	14.738	14.046	13.303	12.567	11.798	11.025	10.289	9.610	8.953	8.346
	25	0.768	0.377	1.434	10.592	0.491	7.144	9.432	10.301	10.263	9.755	8.986	7.983	6.775	5.528	4.560	3.938	3.489	3.097	2.846	2.617	2.409	2.186	1.889	1.627	1.418	1.202
4 OVA/OVA Ctrls *i.n.*	29	0.490	0.423	4.420	14.339	0.864	7.446	11.025	13.230	14.183	14.114	13.427	12.116	10.494	8.872	7.226	5.858	4.826	4.179	3.668	3.273	2.908	2.652	2.371	2.075	1.751	1.586
	21	0.669	0.624	13.063	22.115	0.933	7.969	12.296	15.300	17.546	19.171	20.358	21.150	21.686	21.995	22.070	21.898	21.474	20.805	19.980	18.965	17.800	16.493	15.075	13.641	12.252	10.909
	30	0.532	0.494	6.438	10.900	0.928	7.102	9.588	10.606	10.870	10.642	10.220	9.745	9.259	8.771	8.219	7.693	7.160	6.785	6.418	6.046	5.706	5.433	5.123	4.856	4.568	4.177
	31	0.898	0.693	6.132	15.451	0.771	7.506	11.480	13.805	15.055	15.401	15.127	14.501	13.684	12.781	11.917	11.060	10.285	9.547	8.915	8.444	8.032	7.692	7.339	7.016	6.755	6.562
	32	0.537	0.488	5.670	12.076	0.910	7.224	10.229	11.656	12.064	11.815	11.283	10.555	9.771	8.994	8.194	7.430	6.807	6.266	5.734	5.322	4.890	4.490	4.137	3.758	3.404	3.021
	33	0.524	0.459	6.465	15.122	0.874	8.028	11.642	13.606	14.602	15.025	15.089	14.828	14.395	13.786	12.969	11.982	10.780	9.361	7.786	6.300	5.020	4.109	3.474	2.933	2.423	1.773
	34	0.830	0.651	6.330	13.740	0.785	7.211	10.252	11.933	12.992	13.560	13.711	13.607	13.285	12.682	12.046	11.355	10.616	9.978	9.433	8.946	8.484	8.072	7.664	7.275	6.800	6.482
5 OVA/Fluticason propionate 100 mg/kg *i.n.*	39	0.783	0.648	6.957	15.413	0.828	8.048	11.625	13.611	14.696	15.211	15.336	15.247	15.029	14.694	14.241	13.748	13.157	12.421	11.638	10.825	10.007	9.196	8.432	7.713	7.099	6.546
	40	0.728	0.607	5.627	14.223	0.835	8.434	12.062	13.662	14.205	13.992	13.373	12.493	11.491	10.670	9.869	9.085	8.364	7.719	7.207	6.793	6.425	6.049	5.730	5.476	5.223	4.985
	41	1.294	1.058	10.066	20.782	0.818	8.885	13.522	16.444	18.320	19.542	20.287	20.660	20.766	20.725	20.490	20.212	19.879	19.493	19.036	18.574	18.056	17.524	16.982	16.383	15.844	15.317
	42	0.730	0.686	10.043	22.969	0.940	9.296	14.584	18.250	20.627	22.049	22.777	22.922	22.577	21.871	20.942	19.882	18.816	17.705	16.631	15.627	14.618	13.559	12.411	11.183	10.020	9.049
	43	0.755	0.410	2.351	8.611	0.543	6.213	8.082	8.576	8.412	7.957	7.308	6.705	6.242	5.820	5.442	5.035	4.605	4.139	3.621	3.212	2.873	2.593	2.351	2.233	2.130	2.056
	44	0.944	0.817	12.778	20.966	0.865	8.211	12.624	15.618	17.659	19.096	20.057	20.648	20.878	20.907	20.781	20.501	20.172	19.756	19.315	18.831	18.311	17.765	17.213	16.675	16.112	15.620
	45	0.787	0.647	7.080	17.743	0.822	8.257	12.175	14.556	16.072	16.978	17.445	17.667	17.735	17.574	17.301	16.976	16.516	15.945	15.282	14.462	13.496	12.458	11.210	10.021	8.846	7.779

Group	Animal no	0.44	0.46	0.48	0.50	0.52	0.54	0.56	0.58	0.60	0.62	0.64	0.66	0.68	0.70	0.72	0.74	0.76	0.78	0.80	0.82	0.84	0.86	0.88	0.90	0.92	0.94	0.96	0.98	1.00
1 PBS/Saline Ctrls	5	7.320	7.153	6.999	6.816	6.609	6.426	6.235	6.052	5.837	5.573	5.256	4.749	3.997	3.108	2.334	1.608	0.873	0.986	0.193										
	6	11.904	11.513	11.116	10.629	10.086	9.494	8.811	8.062	7.291	6.546	5.776	5.053	4.322	3.724	3.218	2.758	2.176	1.757	1.261	0.878	0.637	0.417	0.354	0.209	0.098				
	7	6.666	6.327	6.004	5.672	5.379	5.101	4.839	4.621	4.388	4.210	4.053	3.901	3.678	3.496	3.282	2.958	2.604	2.171	1.619	0.788	0.414	0.238							
	8	1.600	1.561	1.485	1.474	1.381	1.311	1.267	1.266	1.164	1.145	1.100	1.055	1.051	0.992	0.990	0.935	0.933	0.921	1.000	0.866	0.859	0.827	0.808	0.729	0.708	0.699	0.668	0.640	0.625
2 OVA/OVA Ctrls *p.o.*	9	3.892	3.902	3.694	3.575	3.490	3.331	3.159	2.980	2.741	2.584	2.480	2.380	2.260	2.123	1.980	1.812	1.603	1.408	1.252	1.046	0.795	0.505							
	10	0.346	0.269	0.131																										
	11	6.617	6.210	5.697	5.149	4.624	4.102	3.489	2.836	2.310	1.956	1.716	1.519	1.062	0.601	0.352														
	12	0.828	0.543	0.523	0.326	0.332	0.304																							
	13	2.078	1.909	1.826	1.696	1.551	1.335	1.162	1.000	0.842	0.617	0.578	0.527	0.389	0.302	0.283	0.309													
	14	4.377	3.950	3.577	3.256	2.949	2.682	2.417	2.149	1.901	1.670	1.410	1.139	0.703	0.702															
	15	3.936	3.663	3.343	3.036	2.676	2.286	1.827	1.437	1.124	0.839	0.648	0.497	0.317	0.179															
3 OVA/ Dexamethasone 3 mg/kg *p.o.*	19	4.485	4.149	3.787	3.458	3.047	2.442	1.602	0.843	0.551	0.339	0.155																		
	20	7.433	6.927	6.549	6.260	5.981	5.767	5.559	5.317	5.157	4.932	4.715	4.453	4.173	3.883	3.513	2.995	2.440	1.871	1.511	1.192	0.865	0.626	0.284						
	21	8.724	8.108	7.356	6.666	5.839	4.913	3.896	2.885	1.989	1.223	0.421																		
	22	13.725	13.074	12.484	11.910	11.355	10.839	10.306	9.829	9.404	8.974	8.591	8.177	7.747	7.359	6.967	6.541	6.095	5.653	5.157	4.189	2.962	2.090	1.424	0.751	0.250				
	23	7.290	7.041	6.842	6.634	6.370	5.963	5.490	5.063	4.700	4.339	3.909	3.389	2.986	2.548	2.061	1.662	1.197	0.757	0.649	0.306	0.128								
	24	7.803	7.282	6.710	6.271	5.700	5.107	4.466	3.881	3.372	2.920	2.281	1.359	0.803	0.387															
	25	1.142	1.071	1.040	0.956	0.927	0.856	0.813	0.778	0.692	0.658	0.610	0.535	0.517	0.460	0.314	0.239	0.183												
4 OVA/OVA Ctrls *i.n.*	29	1.274	0.864	0.377																										
	21	9.458	8.157	6.995	5.988	5.169	4.261	3.178	2.241	1.512	0.895	0.516	0.302	0.250																
	30	3.532	2.684	1.780	0.884	0.690	0.455																							
	31	6.323	6.108	5.888	5.733	5.534	5.334	5.179	5.007	4.832	4.683	4.500	4.345	4.183	4.005	3.819	3.638	3.461	3.256	2.996	2.471	1.682	1.005	0.417	0.218					
	32	2.543	2.001	1.599	1.699	1.208	0.972	0.340																						
	33	1.323	0.851	0.638	0.429	0.348	0.262																							
	34	6.235	5.863	5.537	5.265	5.086	4.868	4.651	4.502	4.343	4.138	3.916	3.672	3.429	3.190	2.918	2.734	1.841	1.035	0.649	0.325									
5 OVA/Fluticason propionate 100 mg/kg *i.n.*	39	6.101	5.657	5.261	4.980	4.707	4.449	4.172	3.926	3.527	3.260	2.965	2.780	2.581	2.398	2.208	4.023	3.730	2.537	1.074	0.648	0.283								
	40	4.808	4.637	4.409	4.234	4.056	3.842	3.622	3.330	2.961	2.562	2.102	1.753	1.247	0.636	0.091	0.143													
	41	14.730	14.337	13.876	13.466	13.058	12.638	12.253	11.834	11.500	11.111	10.751	10.444	10.120	9.803	9.509	9.190	8.938	8.680	8.297	8.115	7.871	7.616	7.399	7.206	6.969	6.750	6.538	6.293	6.061
	42	8.290	7.646	6.975	6.224	5.679	5.319	4.904	4.467	4.178	3.816	3.294	2.227	1.003	0.351	0.222														
	43	1.963	1.878	1.803	1.770	1.645	1.534	1.475	1.371	1.371	1.302	1.221	1.152	1.034	0.919	0.715	0.351	0.150												
	44	15.121	14.661	14.212	13.774	13.377	12.912	12.484	12.023	11.478	10.818	9.945	8.895	7.606	6.313	4.936	3.827	2.989	2.339	1.861	1.456	1.127	0.913	0.711	0.537	0.306	0.321	0.129		
	45	6.879	6.147	5.499	4.965	4.478	4.031	3.523	3.054	2.595	2.007	1.590	1.275	1.020	0.761	0.632	0.448	0.330	0.174											

Appendix 11 Total and differential cell count in BALF

Group	Animal no	Total cell count 10^9/L	Lymphocytes 10^9/L	Macrophages 10^9/L	Neutrophils 10^9/L	Eosinophils 10^9/L
1 PBS/Saline Ctrls	1	0.23	0.01	0.22	0	0
	2	0.31	0.02	0.29	0	0
	3	0.73	0.01	0.71	0.01	0.01
	4	0.38	0.01	0.37	0	0
	5	0.24	0.05	0.18	0.01	0.01
	6	0.15	0.02	0.13	0	0
	7	0.09	0	0.08	0.01	0.01
	8	0.27	0.03	0.24	0	0
2 OVA/OVA Ctrls *p.o.*	9	1.22	0.04	0.45	0.05	0.68
	10	1.23	0.04	0.41	0.04	0.74
	11	5.1	0.05	1.34	0.05	3.65
	12	2.13	0.06	0.68	0.01	1.37
	13	0.98	0.04	0.38	0.07	0.49
	14	Blood in sample				
	15	0.35	0.01	0.25	0.04	0.05
	16	No sample				
	17	Blood in sample				
	18	0.72	0.02	0.33	0.03	0.32
3 OVA/ Dexamethasone 3 mg/kg *p.o.*	19	0.38	0.02	0.25	0.08	0.02
	20	0.52	0.03	0.39	0.07	0.02
	21	0.33	0.01	0.26	0.05	0.01
	22	0.27	0.04	0.2	0.03	0
	23	0.21	0.01	0.16	0.04	0
	24	0.3	0.01	0.21	0.06	0.02
	25	0.12	0	0.09	0.03	0
	26	0.13	0	0.12	0.01	0
	27	0.29	0.02	0.21	0.05	0.01
	28	0.19	0	0.16	0.03	0
4 OVA/OVA Ctrls *i.n.*	29	1.21	0.03	0.56	0.1	0.51
	30	1.97	0.04	0.7	0.06	1.16
	31	Blood in sample				
	32	0.73	0.04	0.34	0.11	0.24
	33	0.63	0.02	0.38	0.05	0.18
	34	1.04	0.04	0.41	0.07	0.52
	35	0.35	0.02	0.28	0.01	0.03
	36	0.41	0.02	0.18	0.04	0.16
	37	Blood in sample				
	38	0.96	0.03	0.28	0	0.64
4 OVA/ Fluticasone propionate 2 mg/kg *i.n.*	39	0.27	0	0.22	0.04	0.01
	40	0.13	0.01	0.1	0.01	0.01
	41	0.41	0.01	0.38	0.01	0.01
	42	0.42	0.02	0.36	0.02	0.01
	43	0.35	0.02	0.28	0.04	0.01
	44	No sample				
	45	0.55	0.03	0.45	0.03	0.04
	46	0.36	0.02	0.26	0.07	0.01
	47	0.39	0.02	0.27	0.05	0.04
	48	0.34	0.04	0.27	0.02	0.01

Appendix 12 Immunoglobulin E and cytokines analysis in the BALF (pg/mL)

Group	Animal no	IL-4	IL-5	IL-13	IgE
1 PBS/Saline Ctrls	1	0	0	0	5.59
	2	0	0	0	2.74
	3	0	0	16.49	1.4
	4	10.74	0	13.7	2.01
	5	0	0	14.78	1.58
	6	7.08	11.83	46.4	9.03
	7	4.03	5.53	tech. error	tech. error
	8	0	4.82	40.88	6.06
2 OVA/OVA Ctrls *p.o.*	9	8.42	6.06	37.22	32.03
	10	12.79	5.93	52.97	36.78
	11	18.18	12.18	58.53	128.11
	12	8.94	6.2	31.35	123.07
	13	10.31	4.62	26.78	56.47
	14	0	0	0	0
	15	10.96	0	8.6	12.02
	16	no sample			
	17	2.52	0	48.28	103.01
	18	7	4.17	26.98	14.37
3 OVA/ Dexamethasone 3 mg/kg *p.o.*	19	0	0	13.05	15.54
	20	4.03	7.06	28.78	13.52
	21	0	3.91	28.18	27.1
	22	0	0	tech. error	tech. error
	23	0	0	0	tech. error
	24	0	0	0	39.7
	25	0	0	0	13.77
	26	0	0	0	11.52
	27	0	0	0	20
	28	0	0	0	12.22
4 OVA/OVA Ctrls *i.n.*	29	17.85	0	0	24.66
	30	2.61	0	17.33	tech. error
	31	23.05	15.9	43.36	95.47
	32	58.62	0	8.14	37.57
	33	0	0	13.05	20.79
	34	3.78	0	0	47.45
	35	0	0	0	6.78
	36	17.58	0	0	9.32
	37	6.92	0	37.22	103.84
	38	0	0	0	29.39
4 OVA/ Fluticasone propionate 2 mg/kg *i.n.*	39	0	0	9.06	40.9
	40	0	12.75	41.26	tech. error
	41	0	0	0	14.97
	42	6.08	8.97	28.78	18.8
	43	9.37	15.69	44.69	66.18
	44	no sample			
	45	0	0	0	11.77
	46	0	0	0	15.83
	47	0	0	0	39.93
	48	0	0	12.62	12.98

Appendix 13 Histology and immunohistochemical results in the BLM-induced pulmonary fibrosis model

Group	Animal no	Matsuse modified Ashcroft score	Positive segmented tissue area (mm²)	
			alpha SMA	COL1A1
1 PBS Ctrls	1	1	1.72	13.13
	2	1	2.27	11.48
	3	1	2.55	12.9
	4	1	5.15	15.93
	5	1	3.25	14.33
	6	1	2.14	7.43
	7	1	1.55	5.06
	8	1	2.58	8.61
	9	1	2.96	11.3
	10	1	3.6	7.1
2 BLM Ctrls	11	3.8	4.7	34.37
	12	3.7	4.37	27.76
	13	3.6	5	28.56
	14	3.8	4.04	32.75
	16	4.0	5.5	42.45
	17	2.6	3.89	24.67
	18	3.1	4.71	39.74
	20	2.6	3.32	21.72
	21	3	4.12	21.73
	22	3.1	15.34	32.26
	23	3	9.03	18.53
	24	3.3	4.81	14.19
	25	3.5	8.47	24.98
	26	3.2	7.27	19.26
	28	3.6	10.14	27.9
	30	3.3	4.51	26.04
3 BLM/ Nintedanib 60 mg/kg *p.o. bid*	31	1.5	2.7	12.15
	32	2.9	3.53	19.67
	34	2.2	4.43	19.21
	35	2.4	3.96	12.21
	36	3.3	7.24	28.06
	37	3.2	4.21	29.29
	38	2.1	9.03	14.23
	39	2.3	3	15.88
	40	2.2	5.57	15.39
	41	2.8	6.89	15.44
	42	2.4	2.69	18.86
	43	3.2	12.14	19.42
	44	3.1	3.91	24.24
	45	3	3.88	19.67
	46	3.0	3.42	20.94
	48	2.2	5.03	15.99
	49	3.2	4.55	18.53
	50	1.3	5.2	9.04
4 BLM/ Pirfenidone 100 mg/kg *p.o. bid*	51	2.7	3.57	15.44
	52	2.8	4.39	21.25
	53	2.2	3.53	13.07
	54	3.3	7.64	26.14
	55	2.0	4.35	14.17
	56	2.7	3.06	22.68
	57	3.2	3.86	27.03
	58	3.5	5.08	24.86
	59	2.5	4.08	19.6
	61	1.0	5.59	8.08
	62	3.3	5.79	30.04
	63	2.9	4.96	28
	64	2.2	4.2	7.63
	65	2.6	2.58	16.06
	67	3.0	2.49	12.34
	68	2.8	2.93	19.81
	69	1.6	3.22	9.89
	70	2.7	6.29	14.16

Appendix 14 Histology score and goblet cell metaplasia in the OVA-induced asthma model

Group	Animal no	Inflammation	Epithelial damage		Inflammation and epithelial score	Goblet cell metaplasia
			Bronchi	Alveoli		
1 PBS/Saline Ctrls	1	0	0	0	0	0.5
	2	0	0	0	0	0
	3	0	0	0	0	0.5
	4	0	0	0	0	0
	5	0	0	0	0	0.5
	6	0	0	0	0	0.5
	7	0	0	0	0	0
	8	0	0	0	0	0.5
2 OVA/OVA Ctrls *p.o.*	9	6	2	5	13	3.5
	10	10	2	9	21	3
	11	9	1	6	16	3
	12	6.5	1	5	12.5	3.5
	13	7.5	0	4	11.5	3
	14	7.5	2	4.5	14	3.5
	15	10.5	4.5	7	22	3
	16	6	1	2	9	3
	17	7.5	2	6	15.5	3.5
	18	6.5	1	2	9.5	3
3 OVA/ Dexamethasone 3 mg/kg *p.o.*	19	2	0	1	3	1.5
	20	1	0	1	2	1.5
	21	2.5	0	1.5	4	2.5
	22	3.5	3.5	3.5	10.5	1.5
	23	5.5	2.5	4.5	12.5	3
	24	4.5	1.5	2.5	8.5	2.5
	25	5	1	2	8	3
	26	3	0	2	5	2.5
	27	2	0	1.5	3.5	1.5
	28	2	0	1.5	3.5	1.5
4 OVA/OVA Ctrls *i.n.*	29	8.5	1.5	6.5	16.5	3.5
	30	8	1	5	14	3.5
	31	9	1	7	17	3.5
	32	6	0	4.5	10.5	3
	33	4.5	0	1.5	6	3.5
	34	10	2.5	6.5	19	3.5
	35	5.5	2	3	10.5	3.5
	36	6.5	1.5	3	11	3
	37	11	2	6.5	19.5	4
	38	9	1.5	4.5	15	3
4 OVA/ Fluticasone propionate 2 mg/kg *i.n.*	39	1.5	0	0	1.5	0.5
	40	2	0	0	2	1
	41	1.5	0	0	1.5	0.5
	42	2	0	0	2	1
	43	1	0	0	1	1
	44	2.5	0	2.5	5	1
	45	1.5	0	1	2.5	1
	46	0	0	0	0	0
	47	1	0	1	2	1
	48	2	0	1	3	1

10 BIOGRAPHY

Željka Anzulović Šanta, born on May 2nd, 1988, in Split, Croatia, completed her elementary and high school education in Jelsa, Hvar. In 2014, she earned her Doctor of Veterinary Medicine degree from the Faculty of Veterinary Medicine at the University of Zagreb. During her studies, she received the Rector's Award for her scientific work "Molecular Etiological Retrospective Study of Canine Infectious Haemolytic Anaemias.", presented, along with master's thesis, at the 6th International Congress of Veterinary Science and Profession.

Following the completion of her master's degree, Željka joined Fidelta Ltd. as an associate scientist in the in vivo team. Over the course of nine years with the company, she gained extensive experience as a study director and project leader in preclinical research. Her work encompassed various therapeutic areas, including inflammation, gastrointestinal diseases, and arthritis, with a particular emphasis on respiratory diseases such as pulmonary fibrosis, asthma, and chronic obstructive pulmonary disease. Throughout her career, she specialized in conducting ante mortem respiratory functional measurements.

Currently, Željka serves as the Lead Scientist-Pharmacologist in the In Vivo Pharmacology and Toxicology Department at Selvita Ltd., where she leads a small team of scientists. She is an active member of the Croatian Laboratory Animal Science Association (CroLASA) and has participated in numerous international conferences, meetings, and workshops. Additionally, she has made significant contributions to several scientific papers, either as a co-author or as the first author.

List of publications:

- ANZULOVIĆ ŠANTA, Ž., A. OGNJENOVIĆ, M. ANTOLIĆ, S. ČUŽIĆ, I. GLOJNARIĆ, B. HRVAČIĆ, F. BOŽIĆ (2023): Retrospective assessment of nintedanib in the mice model of pulmonary fibrosis: alignment with patient outcomes in idiopathic pulmonary fibrosis. Vet. Stan. 54, 395-406.
- BECK, A., D. HUBER, M. ANTOLIĆ, Ž. ANZULOVIĆ, I. REIL, A. POLKINGHORNE, G. BANETH, R. BECK (2019): Retrospective study of canine infectious haemolytic anaemia cases reveals the importance of molecular investigation in accurate postmortal diagnostic protocols. Comp. Immunol. Microb. 65, 81-87.
- HUBER, D., A. BECK, Ž. ANZULOVIĆ, D. JURKOVIĆ, A. POLKINGHORNE, G. BANETH, R. BECK (2017): Microscopic and molecular analysis of Babesia canis in archived and diagnostic specimens reveal the impact of anti-parasitic treatment and postmortem changes on pathogen detection. Parasite. Vector. 10, 495-495.

List of conferences:

- BECK, A., D. HUBER, M. ANTOLIĆ, Ž. ANZULOVIĆ, I. REIL, R. BECK (2014): Molecular retrospective study of canine infectious haemolytic anaemias. Proceedings of the Cutting Edge Pathology, 2nd Joint European Congress of the ESVP, ESTP and ECVP, Berlin, 2014; Journal of Comparative Pathology 152:1, pp. 53
- ANZULOVIĆ, Ž., R. BECK, D. HUBER, M. ANTOLIĆ, A. BECK (2015): Genotyping of piroplasms detected in canine stained peripheral blood smears and postmortem tissue imprints. Proceedings of the 8th International Congress of Veterinary Science and Profession, Zagreb, 2015.
- ANZULOVIĆ, Ž., B. HRVAČIĆ, I. GLOJNARIĆ, D. RELKOVIĆ (2016): Depression-Like Behaviour in Mice is Induced by the Chronic Inflammation and Systemic Immune Activation in the Model of Collagen Induced Arthritis. Proceedings of the 8th Croatian Congress of Pharmacology, Split, 2016.
- ANZULOVIĆ, Ž., M. ANTOLIĆ, S. ČUŽIĆ, I. GLOJNARIĆ, B. HRVAČIĆ, A. OGNJENOVIĆ, A. MARKOTA (2018): Digital localization and quantification of Wnt-3α signalling-edited target approach in a 21 day murine model of idiopathic pulmonary fibrosis // HDIR-5: Translating Science to Medicine - Targets and Therapeutics Zagreb, Croatia, 2018.
- ANZULOVIĆ ŠANTA, Ž., M. ANTOLIĆ, A. OGNJENOVIĆ, S. ČUŽIĆ, I. GLOJNARIĆ, B. HRVAČIĆ (2019): A translational value of pulmonary function tests in a mouse model of bleomycin-induced pulmonary fibrosis: effects of approved therapies Nintedanib and Pirfenidone. Proceedings at the ERS International Congress 2019, Madrid, Spain
- ANZULOVIĆ, Ž. (2017): Lung Function Evaluation in a Model of Mice Pulmonary Fibrosis" Proceedings of the DSI™ User Group Meeting, Reims France, 2017
- BRUIĆ, A, Ž. ANZULOVIĆ ŠANTA, F. BUJAN, A. MARKOTA, V. BENCETIĆ MIHALJEVIĆ, V. KELAVA, R. SUZUKI, A. BROWN, B. HRVAČIĆ, J. PADOVAN, V. ERAKOVIĆ HABER, I. GLOJNARIć (2019): Animal gastrointestinal function tests as a useful tool in preclinical drug development. Proceedings of the 9th Croatian Congress of Pharmacology, Zagreb, 2019.
- OGNJENOVIĆ, A., S. ČUŽIĆ, M. ANTOLIĆ, V. MILUTINOVIĆ, Ž. ANZULOVIĆ ŠANTA, B. HRVAČIĆ, I. GLOJNARIĆ (2023): WNT3a in a mouse model of bleomycin induced lung fibrosis. Proceedings of the 35th European Congress of Pathology in Dublin, 2023.